

BIOACTIVE COMPOUNDS FROM LICHEN *Usnea baileyi* (Stirt.) Zahlbr. AND USNIC ACID
DERIVATIVES



A Dissertation Submitted in Partial Fulfillment of the Requirements
for the Degree of Doctor of Philosophy in Chemistry

Department of Chemistry

Faculty of Science

Chulalongkorn University

Academic Year 2019

Copyright of Chulalongkorn University

สารออกฤทธิ์ทางชีวภาพจากไลเคน *Usnea baileyi* (Stirt.) Zahlbr. และอนุพันธ์กรดอูสนิก



วิทยานิพนธ์นี้เป็นส่วนหนึ่งของการศึกษาตามหลักสูตรปริญญาวิทยาศาสตรดุษฎีบัณฑิต

สาขาวิชาเคมี ภาควิชาเคมี

คณะวิทยาศาสตร์ จุฬาลงกรณ์มหาวิทยาลัย

ปีการศึกษา 2562

ลิขสิทธิ์ของจุฬาลงกรณ์มหาวิทยาลัย

Thesis Title BIOACTIVE COMPOUNDS FROM LICHEN *Usnea baileyi*
(Stirt.) Zahlbr. AND USNIC ACID DERIVATIVES

By Mr. Kieu Van Nguyen

Field of Study Chemistry

Thesis Advisor Assistant Professor WARINTHORN CHAVASIRI, Ph.D.

Accepted by the Faculty of Science, Chulalongkorn University in Partial
Fulfillment of the Requirement for the Doctor of Philosophy

..... Dean of the Faculty of Science
(Professor POLKIT SANGVANICH)

DISSERTATION COMMITTEE

..... Chairman
(Associate Professor VUDHICHAJ PARASUK, Ph.D.)

..... Thesis Advisor
(Assistant Professor WARINTHORN CHAVASIRI, Ph.D.)

..... Examiner
(Assistant Professor PANUWAT PADUNGROS, Ph.D.)

..... Examiner
(Associate Professor PREECHA PHUWAPRAISIRISAN, Ph.D.)

..... Examiner
(Assistant Professor SIWAPORN BOONYASUPPAYAKORN,
Ph.D.)

..... External Examiner
(Dr. Poonsakdi Ploypradith, Ph.D.)

ก๊อ แวน เหยียน : สารออกฤทธิ์ทางชีวภาพจากไลเคน *Usnea baileyi* (Stirt.) Zahlbr. และอนุพันธ์กรดอูสนิก. (BIOACTIVE COMPOUNDS FROM LICHEN *Usnea baileyi* (Stirt.) Zahlbr. AND USNIC ACID DERIVATIVES) อ.ที่ปรึกษาหลัก : ผศ.วรินทร์ ชวศิริ ดร.

จากการศึกษาองค์ประกอบทางเคมีของไลเคน *Usnea baileyi* (Stirt.) Zahlbr. แยกได้บีสแซนโทนใหม่สิบสาร (US1-3, 5-11) และเดซิโดนใหม่หนึ่งสาร (US4) ได้พิสูจน์ทราบโครงสร้างของสารโดยอาศัยหลักฐานทางสเปกโทรสโกปี HRESIMS, 1D และ 2D NMR และเปรียบเทียบข้อมูลจากเอกสารอ้างอิง ได้ศึกษาคอนฟิเกอเรนซ์แบบสัมบูรณ์ผ่านการวิเคราะห์ด้วย ECD, การคำนวณ DFT-NMR และศึกษาคะแนนจากความน่าจะเป็นแบบ DP4 ได้ศึกษาฤทธิ์ทางชีวภาพของบีสแซนโทนที่แยกได้ ได้แก่ ฤทธิ์ต้านพาราซิส ความเป็นพิษต่อเซลล์ (US1-3) ฤทธิ์ต้านแบคทีเรียและฤทธิ์ยับยั้งเอ็นไซม์ (ไทโรซิเนส และ α -กลูโคซิเดส) (US5-11) พบว่า สารไม่แสดงฤทธิ์หรือมีฤทธิ์น้อยต่อ *Plasmodium falciparum* (ฤทธิ์ต้านพาราซิส) และความเป็นพิษต่อเซลล์ไลน์เจ็ดชนิด US5 แสดงฤทธิ์ต้านแบคทีเรีย *Escherichia coli* ATCC25922 และ *Bacillus subtilis* ATCC6633 ที่ดี ด้วยค่า MIC 62.5 mg/mL US6 ซึ่งมีโครงสร้างแกนเหมือนกับ US5 แสดงฤทธิ์ต้าน *B. subtilis* ที่ดี (MIC 62.5 mg/mL) US10 และ US11 แสดงฤทธิ์ยับยั้ง α -กลูโคซิเดส ที่ดีกว่าสารเปรียบเทียบ, acarbose ด้วยค่า IC₅₀ 83, 64 และ 94 mM ตามลำดับ

นอกจากนี้ได้เตรียมอนุพันธ์ของกรดอูสนิกสิบเอ็ดชนิด จากปฏิกิริยาออกซิเดชัน Dakin (UD1-5) และเอสเทอร์ฟิเคชัน (UE1-6) พิสูจน์ทราบโครงสร้างและทดสอบฤทธิ์ยับยั้งไทโรซิเนสและ α -กลูโคซิเดส พบว่า UD2, UD5, UE5 และ UE6 แสดงฤทธิ์ยับยั้ง α -กลูโคซิเดสที่น่าสนใจ ด้วยค่า IC₅₀ 43, 91, 27, และ 69 μ M ตามลำดับ

สาขาวิชา เคมี
ปีการศึกษา 2562

ลายมือชื่อนิสิต

ลายมือชื่อ อ..... ที่ปรึกษาหลัก.

5972872023 : MAJOR CHEMISTRY

KEYWORD: Lichen, *Usnea baileyi*, bisxanthone, depsidone, tyrosinase, alpha-glucosidase, antibacterial, usnic acid

Kieu Van Nguyen : BIOACTIVE COMPOUNDS FROM LICHEN *Usnea baileyi* (Stirt.) Zahlbr. AND USNIC ACID DERIVATIVES. Advisor: Asst. Prof. WARINTHORN CHAVASIRI, Ph.D.

The investigation of chemical constituents of lichen *Usnea baileyi* (Stirt.) Zahlbr. led to the isolation of ten new bisxanthenes (US1–3, 5-11) and a new depsidone (US4). The structures were unambiguously established by the spectroscopic evidence including HRESIMS, 1D and 2D NMR, as well as comparison to literature data. Moreover, the absolute configurations were elucidated through ECD analyses, DFT-NMR calculations and subsequent DP4 probability score. The biological activities of isolated bisxanthenes were evaluated for antiparasitic, cytotoxic (US1-3), antibacterial, and enzymatic inhibitory (tyrosinase and α -glucosidase) (US5-11) activities. The results revealed null to mild bioactivities against *Plasmodium falciparum* (antiparasitic activity) as well as cytotoxic activity against seven cell lines. US5 exhibited good antibacterial activity against *Escherichia coli* ATCC25922 and *Bacillus subtilis* ATCC6633 (MIC 62.5 mg/mL for each bacteria). In addition, US6, the same co-structure as US5 revealed good activity against *B. subtilis* (MIC 62.5 mg/mL). US10 and US11 displayed better activity on α -glucosidase than a positive compound, acarbose with IC_{50} values 83, 64, and 94 mM, respectively.

Moreover, 11 derivatives of usnic acid derived from Dakin oxidation (UD1-5) and esterification (UE1-6) were prepared, characterized and evaluated for tyrosinase and α -glucosidase inhibitory activities. Interestingly, UD2, UD5, UE5, and UE6 displayed good anti- α -glucosidase activity with IC_{50} 43, 91, 27, and 69 μ M, respectively.

Field of Study: Chemistry Student's Signature

Academic Year: 2019 Advisor's Signature

ACKNOWLEDGEMENTS

There are many individuals without whom my thesis might not be possible to complete, and to whom I am greatly indebted.

Firstly, I wish to direct my earnest thankfulness to my advisor, Assistant Professor Dr. Warinthorn Chavasiri, Department of Chemistry, Faculty of Science, Chulalongkorn University for his knowledge, suggestion, support, guidance and encouragement throughout this research. I also thank the Center of Excellence in Natural Products Chemistry and all members of WC-lab for their kind help in the research.

In addition, I would like to thank Prof. Ek Sangvichien, Dr Duong Thuc Huy, Mrs Asshaima Paramita Devi, and Mr Pakarapon Poonsukkho for their recommendation, testing bio-assays and encouragement throughout this research.

Moreover, I would also like to acknowledge Associate Professor Dr. Vudhichai Parasuk, Associate Professor Dr. Preecha Phuwapraisirisan, Assistant Professor Dr. Panuwat Padungros, Assistant Professor Dr Siwaporn Boonyasuppayakorn and Dr. Poonsakdi Ploypradith for serving as the chairman and committees of my thesis, for their help on comments, discussions, and suggestions.

I am also thankful for the helping from Ms. Natwida Dangphui who identified the scientific name of my material (lichen *usnea baileyi*). Furthermore, I would also like to thank Mr. Nguyen Thang Lam's family Lam Dong province, Vietnam for enthusiastic supports during the time I collected the material.

I would like to thank the scholarship from the Graduate School, Chulalongkorn University to commemorate The 100th Anniversary Chulalongkorn University, the 90th Anniversary Chulalongkorn University Fund (Ratchadaphiseksomphot Endowment Fund) and the Overseas Research Experience Scholarship for Graduate Student for the financial supports. All kind support and opportunities supplied me to achieve my research goals.

Finally, I would like to express my gratitude to my family in Vietnam for their love, understanding and guidance that have given me strength and courage when I am far from home. I am also grateful my wife for her love, support and encouragement.

Kieu Van Nguyen

TABLE OF CONTENTS

	Page
ABSTRACT (THAI).....	iii
ABSTRACT (ENGLISH).....	iv
ACKNOWLEDGEMENTS	v
TABLE OF CONTENTS	vi
LIST OF FIGURES.....	xi
LIST OF TABLES.....	xviii
LIST OF SCHEMES.....	1
LIST OF ABBREVIATIONS	xxi
Chapter 1 INTRODUCTION	1
1.1 The lichen.....	1
1.2 Biological significance of lichen substances.....	1
1.3 Biological activities of lichen substances.....	3
1.4 Research scope.....	6
Chapter 2 CHEMICAL CONSTITUENTS FROM LICHEN USNEA BAILEYI.....	7
2.1 Introduction	7
2.1.1 <i>Usnea</i> genus secondary metabolites.....	7
2.1.2 <i>U.baileyi</i> and its chemical constituents.....	9
2.1.3 Objectives.....	13
2.2 Experimental.....	13
2.2.1 Instruments and materials	13
2.2.1.1 Instruments and chemicals.....	13

2.2.1.2	Lichen material <i>U.baileyi</i>	14
2.2.2	Extraction.....	15
2.2.3	Biological activities	16
2.2.3.1	Cytotoxicity and antiparasitic activity of US1-3	16
2.2.3.2	Biological activities of compounds US5-11.....	17
2.2.3.2.1	Antibacterial activity.....	17
2.2.3.2.2	Tyrosinase inhibitory	18
2.2.3.2.3	α -glucosidase inhibitory	19
2.3	Results and discussion.....	19
2.3.1	Extraction and fractionation of lichen <i>Usnea baileyi</i>	19
2.3.2	Separation of dichloromethane fraction.....	19
2.3.3	Structural elucidation of compounds from dichloromethane fraction.	23
2.3.3.1	Compound <i>US1</i>	23
2.3.3.2	Compound <i>US2</i>	31
2.3.3.3	Compound <i>US3</i>	36
2.3.3.4	Compound <i>US4</i>	42
2.3.3.5	Compound <i>US5</i>	44
2.3.3.6	Compound <i>US6</i>	49
2.3.3.7	Compound <i>US7</i>	52
2.3.3.8	Compound <i>US8</i>	55
2.3.3.9	Compound <i>US9</i>	57
2.3.3.10	Compound <i>US10</i>	59
2.3.3.11	Compound <i>US11</i>	64
2.4	Biological activities.....	65

2.4.1	Cytotoxicity and antiparasitic activity	65
2.4.2	Anti-bacterial.....	66
2.4.3	Enzyme inhibitory.....	68
2.5	Conclusion.....	69
2.5.1	Chemical constituents of lichen <i>usnea baileyi</i>	69
2.5.2	Biological activities.....	71
Chapter 3 SYNTHESIS OF USNIC ACID DERIVATIVES AND THEIR ENZYME INHIBITORY		
ACTIVITY.....		
3.1	Introduction	72
3.1.1	Usnic acid, usnic acid derivatives and biological activities.....	73
3.1.2	Objectives.....	76
3.2	Experimental.....	76
3.2.1	Instrument and equipment.....	76
3.2.2	General procedure.....	77
3.2.2.1	Dakin Oxidation of usnic acid	77
3.2.2.2	Acetylation and benzylation of usnic acid.....	79
3.3	Results and discussion.....	81
3.3.1	Isolation and elucidation usnic acid derivatives via Dakin oxidation	81
3.3.2	Characterization of the products from Dakin oxidation of usnic acid.....	83
3.3.2.1	Compound UD1	83
3.3.2.2	Compound UD2	85
3.3.2.3	Compound UD3	85
3.3.2.4	Compound UD4	85
3.3.2.5	Compound UD5	86

3.3.2.6 Mechanism aspect of the formation of UD1-5 from the usnic acid.	87
3.3.3 Characterization of the products from esterification of usnic acid	89
3.3.3.1 The reaction of usnic acid with acetyl chloride	89
3.3.3.1.1 Compound UE1.....	90
3.3.3.1.2 Compound UE2.....	90
3.3.3.1.3 Compound UE3.....	91
3.3.3.1.4 Compound UE4.....	91
3.3.3.2 The reaction of usnic acid and UE2 with benzoyl chloride	91
3.3.3.2.1 Compound UE5.....	92
3.3.3.2.2 Compound UE6.....	93
3.4 Biological activities of usnic acid derivatives	93
3.5 Conclusion.....	95
Chapter 4 CONCLUSIONS.....	95
4.2 Chemical constituents of lichen <i>Usnea baileyi</i>	95
4.2 Synthesis of usnic acid derivatives <i>via</i> oxidation and esterification reactions	96
REFERENCES	97
APPENDIX.....	98
VITA.....	220

LIST OF FIGURES

Figure 1. 1	Types of lichen	1
Figure 2. 1	Chemical constituents (1-22) from <i>Usnea</i> genus (continuous).....	9
Figure 2. 2	Chemical constituents (23-44) from <i>U. baileyi</i>	11
Figure 2. 3	The lichen <i>Usnea baileyi</i>	15
Figure 2.4	Key COSY, HMBC and ROESY correlations of compound US1	25
Figure 2. 5	Experimental ECD plot of US1	26
Figure 2. 6	Chemical structure of US2	34
Figure 2. 7	Key ROE correlations of compound US2	35
Figure 2. 8	Comparison of the experimental ECD spectrum of US2 and calculated ECD spectrum for the (aS, 5'R, 8a'R, 10'R, 5R, 6R, 10S) stereoisomer (UV shift = -12 nm)	35
Figure 2. 9	Selected COSY and HMBC correlations of compound US3	36
Figure 2. 10	Relative configuration for Eumitrin E (US3): DP4 probabilities of the two candidate diastereoisomers.....	39
Figure 2. 11	Comparison of the experimental ECD spectrum of US3 and usneaxanthone A [64].....	42
Figure 2. 12	Key HMBC correlations of US4	44
Figure 2. 13	Selected COSY, HMBC, and NOESY correlations of US5	47
Figure 2. 14	The ECD spectra of US5 , US6	47
Figure 2. 15	<i>Selected COSY, HMBC, and NOESY correlations of US6</i>	50
Figure 2. 16	<i>Chemical structure and selected COSY, HMBC, and NOESY correlations of US7</i>	55
Figure 2. 17	The ECD spectra of US7-9	55

Figure 2. 18 Chemical structure and selected COSY, HMBC, and NOESY correlation of US8	56
Figure 2. 19 Selected COSY, HMBC, and NOESY correlations of US9	57
Figure 2. 20 Selected COSY, HMBC, and NOESY correlations of US10	61
Figure 2. 21 The ECD spectra of US10-11	61
Figure 2.22 Selected COSY, HMBC, and NOESY correlations of US11	64
Figure 2. 23 Chemical structures of eleven new compounds US1-11	70
Figure 3. 1 Reported usnic derivatives	74
Figure 3. 2 Dakin oxidation of usnic acid	82
Figure 3. 3 Proposed Dakin reaction mechanism of usnic acid	88
Figure 3. 4 Acetylation of usnic acid with acetyl chlorides	89
Figure 3. 5 Esterification of usnic acid with acetyl and benzoyl chlorides.....	92
Figure A. 1 HRESIMS spectrum of US1	108
Figure A. 2 The ¹ H NMR (CDCl ₃ , 500 MHz) spectrum of US1	109
Figure A. 3 The ¹ H NMR (CDCl ₃ , 500 MHz) spectrum of US1 (1.0 to 3.0 ppm).....	110
Figure A. 4 The ¹³ C NMR (CDCl ₃ , 125 MHz) spectrum of US1	111
Figure A. 5 The COSY (CDCl ₃ , 500 MHz) spectrum of US1	112
Figure A. 6 The COSY (CDCl ₃ , 500 MHz) spectrum of US1 (1.25 to 4.0 ppm).....	113
Figure A. 7 The HSQC (CDCl ₃ , 500 MHz, 125 MHz) spectrum of US1	114
Figure A. 8 The HMBC (CDCl ₃ , 500 MHz, 125 MHz) spectrum of US1	115
Figure A. 9 The ROESY (CDCl ₃ , 500 MHz) spectrum of US1	116
Figure A. 10 The ROESY (CDCl ₃ , 500 MHz) spectrum of US1 (1.25 to 4.0 ppm).....	117
Figure A. 11 The HRESIMS spectrum of US2	118

Figure A. 12	The ^1H NMR (CDCl_3 , 500 MHz) spectrum of US2	119
Figure A. 13	The ^{13}C NMR (CDCl_3 , 125 MHz) spectrum of US2	120
Figure A. 14	The COSY (CDCl_3 , 500 MHz) spectrum of US2	121
Figure A. 15	The COSY (CDCl_3 , 500 MHz) spectrum of US2 (1.25 to 5.5 ppm).....	122
Figure A. 16	The HSQC (CDCl_3 , 500 MHz, 125 MHz) spectrum of US2	123
Figure A. 17	The HMBC (CDCl_3 , 500 MHz, 125 MHz) spectrum of US2	124
Figure A. 18	The ROESY (CDCl_3 , 500 MHz) spectrum of US2	125
Figure A. 19	The ROESY (CDCl_3 , 500 MHz) spectrum of US2 (1.25 to 8.0 ppm).....	126
Figure A. 20	The HRESIMS spectrum of US3	127
Figure A. 21	The ^1H NMR (CDCl_3 , 500 MHz) spectrum of US3	128
Figure A. 22	The ^{13}C NMR (CDCl_3 , 125 MHz) spectrum of US3	129
Figure A. 23	The COSY (CDCl_3 , 500 MHz) spectrum of US3	130
Figure A. 24	The COSY (CDCl_3 , 500 MHz) spectrum of US3 (1.2 to 5.2 ppm).....	131
Figure A. 25	The HSQC (CDCl_3 , 500 MHz, 125 MHz) spectrum of US3	132
Figure A. 26	The HMBC (CDCl_3 , 500 MHz, 125 MHz) spectrum of US3	133
Figure A. 27	The ROESY (CDCl_3 , 500 MHz) spectrum of US3	134
Figure A. 28	The ROESY (CDCl_3 , 500 MHz) spectrum of US3 (1.2 to 5.0 ppm).....	135
Figure A. 29	The ROESY (CDCl_3 , 500 MHz) spectrum of US3 (zoom into 8-OH and 8a-OH correlations).....	136
Figure A. 30	The HRESIMS spectrum of US4	137
Figure A. 31	The ^1H NMR (CDCl_3 , 500 MHz) spectrum of US4	138
Figure A. 32	The HSQC (CDCl_3 , 500 MHz, 125 MHz) spectrum of US4	139
Figure A. 33	The HMBC (CDCl_3 , 500 MHz, 125 MHz) spectrum of US4	140
Figure A. 34	The HRESIMS spectrum of US5	141

Figure A. 35	The ^1H NMR (CDCl_3 , 400 MHz) spectrum of US5	142
Figure A. 36	The ^{13}C NMR (CDCl_3 , 100 MHz) spectrum of US5	143
Figure A. 37	The COSY (CDCl_3 , 400 MHz) spectrum of US5	144
Figure A. 38	The HSQC (CDCl_3 , 400 MHz) spectrum of US5	145
Figure A. 39	The HMBC (CDCl_3 , 400 MHz) spectrum of US5	146
Figure A. 40	The NOESY (CDCl_3 , 400 MHz) spectrum of US5	147
Figure A. 41	The NOESY (CDCl_3 , 400 MHz) spectrum of US5	148
Figure A. 42	The HRESIMS spectrum of US6	149
Figure A. 43	The ^1H NMR (CDCl_3 , 400 MHz) spectrum of US6	150
Figure A. 44	The ^{13}C NMR (CDCl_3 , 100 MHz) spectrum of US6	151
Figure A. 45	The COSY (CDCl_3 , 400 MHz) spectrum of US6	152
Figure A. 46	The HSQC (CDCl_3 , 400 MHz) spectrum of US6	153
Figure A. 47	The HMBC (CDCl_3 , 400 MHz) spectrum of US6	154
Figure A. 48	The HMBC (CDCl_3 , 400 MHz) spectrum of US6	155
Figure A. 49	The NOESY (CDCl_3 , 400 MHz) spectrum of US6	156
Figure A. 50	The HRESIMS spectrum of US7	157
Figure A. 51	The ^1H NMR (CDCl_3 , 500 MHz) spectrum of US7	158
Figure A. 52	The ^{13}C NMR (CDCl_3 , 125 MHz) spectrum of US7	159
Figure A. 53	The HSQC (CDCl_3 , 500 MHz) spectrum of US7	160
Figure A. 54	The HMBC (CDCl_3 , 500 MHz) spectrum of US7	161
Figure A. 55	The NOESY (CDCl_3 , 500 MHz) spectrum of US7	162
Figure A. 56	The HRESIMS spectrum of US8	163
Figure A. 57	The ^1H NMR (CDCl_3 , 600 MHz) spectrum of US8	164
Figure A. 58	The ^{13}C NMR (CDCl_3 , 150 MHz) spectrum of US8	165

Figure A. 59	The COSY (CDCl ₃ , 600 MHz) spectrum of US8	166
Figure A. 60	The HSQC (CDCl ₃ , 600 MHz) spectrum of US8	167
Figure A. 61	The HMBC (CDCl ₃ , 600 MHz) spectrum of US8	168
Figure A. 62	The NOESY (CDCl ₃ , 600 MHz) spectrum of US8	169
Figure A. 63	The HRESIMS spectrum of US9	170
Figure A. 64	The ¹ H NMR (CDCl ₃ , 500 MHz) spectrum of US9	171
Figure A. 65	The ¹³ C NMR (CDCl ₃ , 125 MHz) spectrum of US9	172
Figure A. 66	The HSQC (CDCl ₃ , 500 MHz) spectrum of US9	173
Figure A. 67	The HMBC (CDCl ₃ , 500 MHz) spectrum of US9	174
Figure A. 68	The NOESY (CDCl ₃ , 500 MHz) spectrum of US9	175
Figure A. 69	The HRESIMS spectrum of US10	176
Figure A. 70	The ¹ H NMR (CDCl ₃ , 400 MHz) spectrum of US10	177
Figure A. 71	The ¹³ C NMR (CDCl ₃ , 100 MHz) spectrum of US10	178
Figure A. 72	The COSY (CDCl ₃ , 400 MHz) spectrum of US10	179
Figure A. 73	The HSQC (CDCl ₃ , 400 MHz) spectrum of US10	180
Figure A. 74	The HMBC (CDCl ₃ , 400 MHz) spectrum of US10	181
Figure A. 75	The NOESY (CDCl ₃ , 400 MHz) spectrum of US10	182
Figure A. 76	The HRESIMS spectrum of US11	183
Figure A. 77	The NMR (CDCl ₃ , 400 MHz) spectrum of US11	184
Figure A. 78	The ¹³ C NMR (CDCl ₃ , 100 MHz) spectrum of US11	185
Figure A. 79	The HSQC (CDCl ₃ , 400 MHz) spectrum of US11	186
Figure A. 80	The HMBC (CDCl ₃ , 400 MHz) spectrum of US11	187
Figure A. 81	The NOESY (CDCl ₃ , 400 MHz) spectrum of US11	188
Figure A. 82	The HRESIMS spectrum of UD1	189

Figure A. 83	The ^1H NMR (CDCl_3 , 500 MHz) spectrum of UD1	190
Figure A. 84	The ^{13}C NMR (CDCl_3 , 500 MHz) spectrum of UD1	191
Figure A. 85	The HSQC (CDCl_3 , 500 MHz) spectrum of UD1	192
Figure A. 86	The HMBC (CDCl_3 , 500 MHz) spectrum of UD1	193
Figure A. 87	The HRESIMS spectrum of UD2	194
Figure A. 88	The ^1H NMR (CDCl_3 , 500 MHz) spectrum of UD2	195
Figure A. 89	The ^{13}C NMR (CDCl_3 , 125 MHz) spectrum of UD2	196
Figure A. 90	The HMBC (CDCl_3 , 500 MHz) spectrum of UD2	197
Figure A. 91	The ^1H NMR (CDCl_3 , 500 MHz) spectrum of UD3	198
Figure A. 92	The ^{13}C NMR (CDCl_3 , 125 MHz) spectrum of UD3	199
Figure A. 93	The HMBC (CDCl_3 , 500 MHz) spectrum of UD3	200
Figure A. 94	The HRESIMS spectrum of UD4	201
Figure A. 95	The ^1H NMR (CDCl_3 , 500 MHz) spectrum of UD4	202
Figure A. 96	The ^{13}C NMR (CDCl_3 , 125 MHz) spectrum of UD4	203
Figure A. 97	The HRESIMS spectrum of UD5	204
Figure A. 98	The ^1H NMR (CDCl_3 , 500 MHz) spectrum of UD5	205
Figure A. 99	The HRESIMS spectrum of UE1	206
Figure A. 100	The ^1H NMR (CDCl_3 , 400 MHz) spectrum of UE1	207
Figure A. 101	The ^{13}C NMR (CDCl_3 , 100 MHz) spectrum of UE1	208
Figure A. 102	The ^1H NMR (CDCl_3 , 400 MHz) spectrum of UE2	209
Figure A. 103	The ^{13}C NMR (CDCl_3 , 100 MHz) spectrum of UE2	210
Figure A. 104	The ^1H NMR (CDCl_3 , 400 MHz) spectrum of UE3	211
Figure A. 105	The ^{13}C NMR (CDCl_3 , 100 MHz) spectrum of UE3	212
Figure A. 106	The ^1H NMR (CDCl_3 , 400 MHz) spectrum of UE4	213

Figure A. 107	The ^{13}C NMR (CDCl_3 , 100 MHz) spectrum of UE4	214
Figure A. 108	The ^1H NMR (CDCl_3 , 400 MHz) spectrum of UE5	215
Figure A. 109	The ^{13}C NMR (CDCl_3 , 100 MHz) spectrum of UE5	216
Figure A. 110	The HRESIMS spectrum of UE6	217
Figure A. 111	The ^1H NMR (CDCl_3 , 400 MHz) spectrum of UE6	218
Figure A. 112	The ^{13}C NMR (CDCl_3 , 100 MHz) spectrum of UE6	219



LIST OF TABLES

Table 1.1 Biological activities of some lichen substances [5-9].....	4
Table 2.1 ¹ H (500 MHz) NMR data of US1-3 (CDCl ₃).....	28
Table 2.2 ¹³ C (125 MHz) NMR data for US1-3 (CDCl ₃).....	29
Table 2.3 Tentative ¹ H (500 MHz) and ¹³ C (125 MHz) NMR chemical shift assignment for US4 (CDCl ₃).....	43
Table 2.4 Tentative ¹ H (400 MHz) NMR chemical shift assignment for US5-6 (CDCl ₃).....	48
Table 2.5 Tentative ¹³ C (400 MHz) NMR chemical shift assignment for US5-6 ..	51
Table 2.6 Tentative ¹ H (400 MHz) NMR chemical shift assignment for US7-9 (CDCl ₃).....	54
Table 2.7 Tentative ¹³ C NMR chemical shift assignment for US7-9 (CDCl ₃).....	58
Table 2.8 Tentative ¹ H (400 MHz) NMR chemical shift assignment for US10-11 (CDCl ₃).....	62
Table 2.9 Tentative ¹³ C (100 MHz) NMR chemical shift assignment for US10-11 (CDCl ₃).....	63
Table 2.10 IC ₅₀ values (μM) of US1-3 for antiplasmodial and cytotoxic activities tests.....	65
Table 2.11 MIC values (μg/mL) of US5-11 against <i>E. coli</i> , <i>P. aeruginosa</i> , <i>S. aureus</i> , <i>B. subtilis</i> , and <i>C. albicans</i>	67
Table 2.12 IC ₅₀ values (μM) of α-glucosidase and tyrosinase of US5-11	68
Table 3.1 Biological activities of usnic acid [6, 8, 9, 76].....	72
Table 3.2 The yields and characteristics of oxidation analogues of usnic acid (UD1-5).....	82

Table 3.3 Tentative 1D NMR (400 MHz) chemical shift assignment for UD1–2 (CDCl ₃)	84
Table 3.4 Tentative 1D NMR (400 MHz) chemical shift assignment for UD3–5 (CDCl ₃)	87
Table 3.5 The yields and characteristics of ester analogues (UE1-4) of usnic acid with acetyl chloride	89
Table 3.6 The yields and characteristics of UD5-6	92
Table 3.7 α -glucosidase and tyrosinase inhibitory of usnic acid derivatives	94



LIST OF SCHEMES

Scheme 2. 1	The separation scheme of the fractions of <i>U. baileyi</i>	16
Scheme 2. 2	Procedure for the fractionation of <i>U. baileyi</i>	20
Scheme 2.3	Procedure for the separation of DC fraction of <i>U. baileyi</i>	21



LIST OF ABBREVIATIONS

1D	One dimensional
2D	Two dimensional
Ac	Acetone
AcOH	Acetic acid
br	Broad
calcd	Calculated
CDCl ₃	deuterated chloroform
CC	Column chromatography
COSY	Homonuclear shift correlation spectroscopy
°C	degree of Celsius
d	Doublet
Dc	dichloromethane
dd	Doublet of doublets
DMSO	Dimethyl sulfoxide
DMSO-d ₆	Deuterated dimethyl sulfoxide
DPPH	2,2-diphenyl-1-picrylhydrazyl

ECD	Electronic Circular Dichroism
equiv	Equivalent (s)
EtOAc	Ethyl acetate
EtOH	Ethanol
g	gram (s)
h	hour (s)
hexane	<i>n</i> -Hexane
HMBC	Heteronuclear Multiple Bond Correlation
HRESIMS	High resolution electrospray ionization mass Spectroscopy
HSQC	Heteronuclear single quantum coherence
Hz	hertz
IC ₅₀	inhibition concentration 50%
K ₂ CO ₃	potassium carbonate
m	Multiplet
MeOH	Methanol
min	minute (s)
mg	milligram (s)

MHz	megahertz
mL	milliliter (s)
mM	millimolar (s)
μg	microgram (s)
μM	micromolar (s)
Na_2SO_4	sodium sulfate
NMR	Nuclear magnetic resonance
ppm	Parts per million (chemical shift value)
pTLC	Preparative thin-layer chromatography
q	Quartet
quint	Quintet
rt	room temperature
s	Singlet
t	Triplet
TLC	Thin-layer chromatography
UV	Ultraviolet

Chapter 1

INTRODUCTION

1.1 The lichen

Lichens are symbiotic association of fungal partner (mycobiont) and photosynthetic partner (photobiont) such as green algae or cyanobacteria. Lichens comprise over 25,000 species with around 98% Ascomycota fungal partners, and occur in a wide range of habitats like on or within rock, on soil, trees, shrubs, trucks, animal carapaces and on bricks, leather, wood[1]. Lichens are divided into three main types of thalli: crustose, foliose and fruticose (**Figure 1.1**) [2].



Xanthoria sp.
(Crustose)

Xanthoparmelia sp.
(Foliose)

Usnea sp.
(Fruticose)

Figure 1. 1 Types of lichen

1.2 Biological significance of lichen substances

Some of the biological meaning of the lichen metabolites were summarized by Huneck and Yoshimura [3] as follows:

Lichens are slow-growing organisms, so the lichen metabolites are antibiotic and active protective substances to protect against lower and higher plants by themselves. The algae will be protected against too intensive irradiation by absorbing

UV light of aromatic lichen substances. Symbiotic equilibrium promotion, which affects the cell wall permeability of photobionts. Lichen metabolites such as aliphatic and aromatic acids are strong chelating agents, which are very helpful for supplying the lichen with minerals from the substrate. Antifeedant activities which protect the lichen from insects and animals. Hydrophobic properties prevent the saturation of the medulla with water and to allow continuous gas exchange.

❖ The usage of lichens

In the lichen division, lichens are composed of at least 8 orders, 45 families, and 6,000 species [4].

Lichens have been used as folk and traditional medicine like traditional Indian medicine or traditional Chinese medicine. *Evernia furfuracea* (L.) Mann, in the Parmeliaceae was used as drug [4]. In Arabian medicine, *Alectoria usneoides* was used to treat enlarged spleen (splenomegaly) [4]. *Letharia vulpine* (L.) was used in stomach diseases in Northern California [4]. In India, *Parmelia chinense* was used as liniment for headache, and *P. sancti-angeli* was used to treat tinea. In Nepal, *P. nepalese* (Taylor) Hale ex Sipman was used in the treatment of toothache and sore throat [4]. *Usnea*, belonging to Parmeliaceae, is a fruticose lichen. *Usnea* generally grows by hanging from tree branches, resembling grey and greenish hair [4]. *Usnea* sp. was used in homeopathic system of medicine and traditional medicine in Pacific island, New Zealand and traditional Chinese medicine. Around 500 A.D., *U. diffracta*

Vain was used as medicine in China. *U. barbata* has been prescribed to use for uterine ailment by Hippocrates [4].

Lichens are used as basic material for perfume industry [3]. Up to 9,000 tons of two lichens: *Evernia prunastri* (L.) Ach. and *Pseudevernia furfuracea* (L.) Zopf. have been processed in Grasse, France. A typical “mossy” flavor from the ethanol extract of both lichens is used not only as a component in certain perfumes, but also as a fixative which keeps the flavor for a long time [3].

Moreover, lichens were used as basic material for dyes. In 1966, dyes from *Roccella* species and other lichens were published by Kok [3]. Today, litmus is a complex mixture of pigment prepared mainly from *Roccella* species [3].

1.3 Biological activities of lichen substances

The biological activities of lichen substances have been shown extensively including antibiotic, antimycobacterial, antifungal, antiviral, antipyretic, anti-inflammatory, analgesic, antiproliferative, antitumor and cytotoxic effects. The biological activities in some recent studies are summarized in **Table 1.1**.

Table 1.1 Biological activities of some lichen substances [5-9]

Antiviral activities	
Compounds	Viruses and viral enzymes
Depsidone: virensic acid and its derivatives	Human immunodeficiency virus.
Butyrolactone acid: protolichesterinic acid	HIV reverse transcriptase
(+)-Usnic acid and four orcinol depsides	Epstein-Barr virus (EBV)
Emodin, 7-chloroemodin, 7-chloro-1-O-methylemodin, 5,7-dichloroemodin, hypericin	HIV, cytomegalovirus and other viruses
Antibiotic and antifungal activities	
Compounds	Organisms
Usnic acid and its derivatives	Gram +ve bacteria, <i>Bacteroides</i> spp., <i>Clostridium perfringens</i> , <i>Bacillus subtilis</i> , <i>Staphylococcus aureus</i> , <i>Staphylococcus</i> spp., <i>Enterococcus</i> spp., <i>Mycobacterium</i> <i>aurum</i>
Methyl orsellinate, ethyl orsellinate, methyl β -orsellinate, methyl haematommate	<i>Epidermophyton floccosum</i> , <i>Microsporum canis</i> , <i>M. gypseum</i> , <i>Trichophyton rubrum</i> , <i>T. mentagrophytes</i> , <i>Verticillium achliae</i> , <i>Bacillus subtilis</i> , <i>Staphylococcus aureus</i> , <i>Pseudomonas aeruginosa</i> , <i>Escherichia</i> <i>coli</i> , <i>Candida albicans</i>

Protolichesterinic acid	<i>Helicobacter pylori</i>
Pulvinic acid and its derivatives	<i>Drechslera rostrata</i> , <i>Alternaria alternate</i> , <i>Aerobic and anaerobic bacteria</i>

Antitumour and antimutagenic activities

Compounds	Activities/cell types
(-)-Usnic acid	Antitumoral effect against Lewis Lung carcinoma, P388 leukaemia, mitotic inhibition, apoptotic induction, antiproliferative effect against human HaCaT keratinocytes
Scabrosin ester and its derivatives, euplectin	Cytotoxic effect against murine P815 mastocytoma and other cell lines
Hydrocarpone, salazinic acid, stictic acid	Apoptotic effect against primary culture of rat hepatocytes
Psoromic acid, chrysophanol, emodin and its derivatives	Antiproliferative effect against leukemia cells
Salazinic acid and stictic acid	Apoptotic effect against primary culture of rat hepatocytes

Enzyme inhibitory activities

Compounds	Enzymes
Atranorin	Trypsin, Pankreaselastase, Phosphorylase
Chrysophanol	Glutathione reductase
Confluentic acid, 2- <i>β</i> -O-methylperlatolic acid	Monoaminoxidase B
4-O-Methylcryptochlorophaeic	Prostata glandinsynthetase

acid	
(+)-Protolichesterinic acid	5-Lipoxygenase (HIV reverse transcriptase)
Vulpinic acid	Phosphorylase
Norsolorinic acid	Monoamino oxidase
Physodic acid	Arginine decarboxylase
Usnic acid	Ornithine decarboxylase

1.4 Research scope

In Vietnam, the tropical monsoon climate is very suitable for lichen development [10]. Vietnam has a number of diverse tropical lichen, but only a few species have been studied [10]. The chemical constituents of Vietnamese lichens are worth for further investigation in order to isolate novel compounds and/or biologically active compounds according to the diversity of Vietnamese lichens. Thus, the major purpose is to investigate the chemical constituents of Vietnamese lichen, *Usnea baileyi* (Stirt.) Zahlbr. collected in highland.

Chapter 2

CHEMICAL CONSTITUENTS FROM LICHEN USNEA BAILEYI

2.1 Introduction

2.1.1 *Usnea* genus secondary metabolites

Usnea, appeared on host trees as a shrub-like, generally grows hanging from tree branches, resembling grey and greenish hair (**Figure 1.1**). In the middle of the thallus, an elastic chord or axis running through that can be indicated by carefully pulling a filament apart from either end [11]. It is one of the largest genera in Parmeliaceae with more than 600 species [12]. Many secondary metabolites of *Usnea* genus have been reported.

Seven compounds-(+) :usnic acid (1), 2-hydroxy-4-methoxy-3,6-dimethylbenzoic acid (2), ethyl 2,4-dihydroxy-3,6-dimethylbenzoate (3), ethyl 2-hydroxy-4-methoxy-3,6-dimethylbenzoate (4), evernic acid (5), barbatic acid (6) and diffractaic acid (7) were isolated from *U. emidotteries* [13] (**Figure 2.1**)

In addition, Devehat and Boustie [14] isolated two new β -orcinol depsidones, depsidone 1 (8) and cryptostictinolide (9), together with thirteen known compounds : barbatic acid (6), atranorin (10), norstictic acid (11), stictic acid (12), fumarprotocetraric acid (13), constictic acid (14), cryptostictic acid (15), menegazziaic acid (16), peristictic acid (17), methyl β -orcinolcarboxylate (18), (+)-usnic acid (1) and ergosterol peroxide (19) from *U. articulata* collected in Indonesia (**Figure 2.1**).

Paranagama and Gunatilaka (2007) [15] isolated herbarin (20) and a heptaketide, 1-hydroxydehydroherbarin (21) from lichen *U. cavernosa* (Figure 2.1).

From lichen *U. alata* growing on trees in La Carbonera, state of Mérida, Venezuela, Keeton and Keogh (1973) [16], norstictic acid (11), stictic acid (12) and caperatic acid (22) were isolated (Figure 2.1).

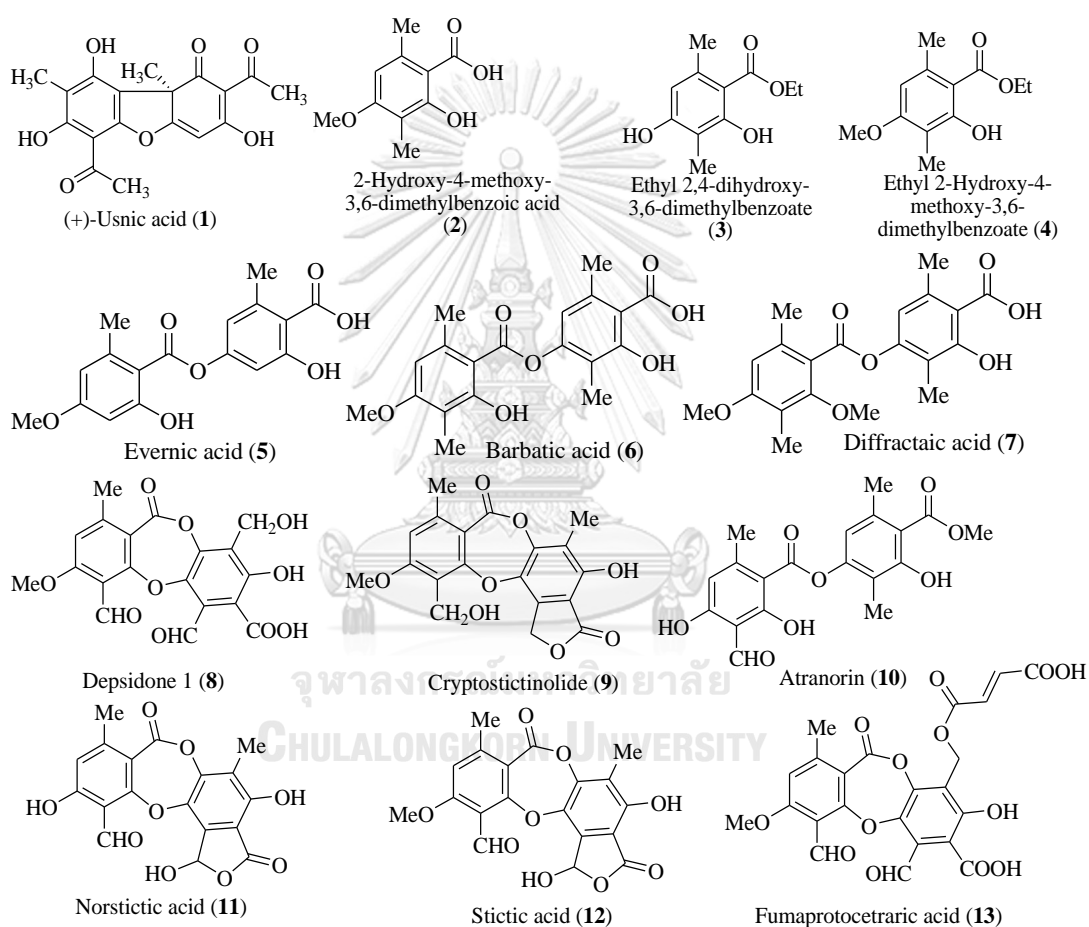


Figure 2. 1 Chemical constituents (1-22) from *Usnea* genus

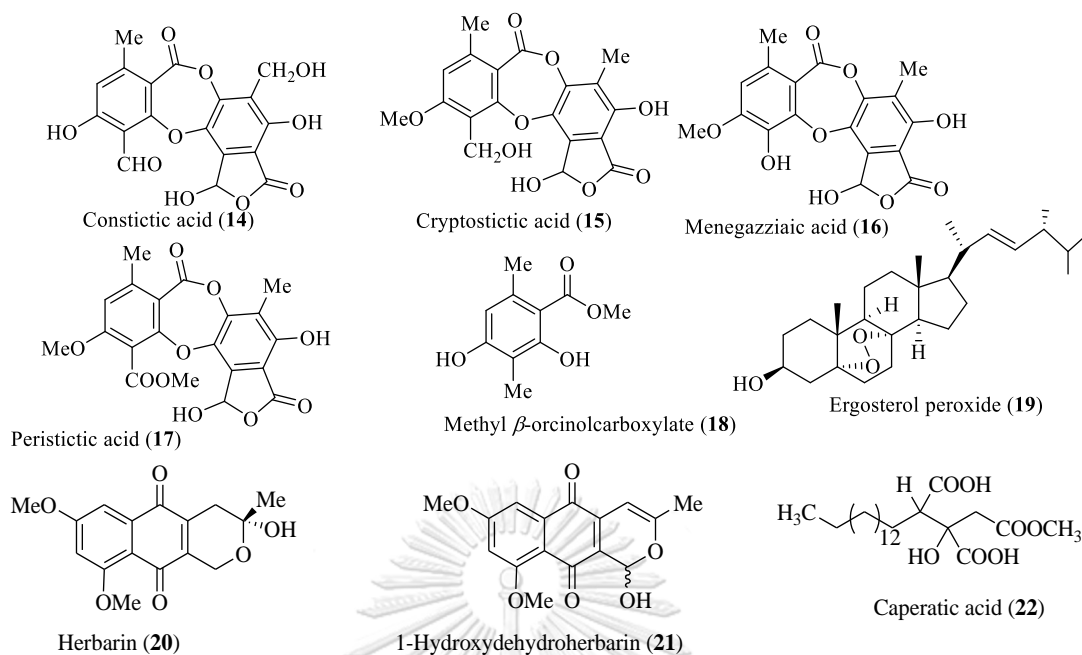


Figure 2. 1 Chemical constituents (1-22) from *Usnea* genus (continuous)

2.1.2 *U.baileyi* and its chemical constituents

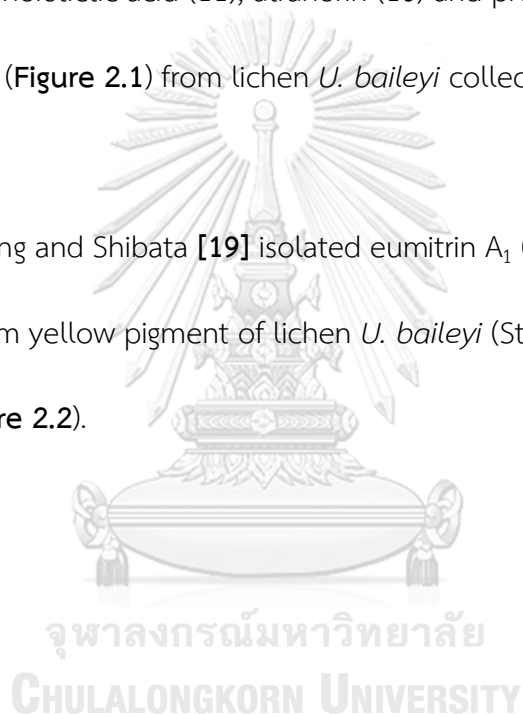
Several species of *Usnea* have been investigated; nonetheless, there are a few papers reporting for the constituents of *U. baileyi*.

Nguyen and co-workers [17] reported the chemical constituents of *U. baileyi* thalli collected on tree barks at Lam Dong province, Vietnam. Twenty seven metabolites (Figure 2.2) from a detailed chromatographic fractionation of the acetone extract, were elucidated as bailexanthone (23), bailesidone (24), stictic acid (12), constictic acid (14), cryptostictic acid (15), hypoconstictic acid (25), menegazzaic acid (16), 8'-*O*-methylconstictic acid (26), methylstictic acid (27), 8'-*O*-methylmenegazzaic acid (28), virensic acid (29), 9'-*O*-methylprotocetraric acid (30), protocetraric acid (31), barbatic acid (6), diffractaic acid (7), 4-*O*-demethylbarbatic acid

(32), atranorin (10), (20*R*, 24*R*)-ocotillone (33), (20*S*, 24*R*)-ocotillone (34), betulonic acid (35), usnic acid (1), dasypogalactone (36), 7-hydroxy-5-methoxy-6-methylphthalide (37), methyl 4-*O*-methylhaematomate (38), methyl orcinolcarboxylate (39), atranol (40), and eumitrin A₂ (41).

Moreover, in 2010, Din and Elix [18] reported the presence of usnic acid (1), salazinic acid (42), norstictic acid (11), atranorin (10) and protocetraric acid (31) as major compounds (Figure 2.1) from lichen *U. baileyi* collected in Bukit Larut, Taiping, Malaysia.

In 1973, Yang and Shibata [19] isolated eumitrin A₁ (43), eumitrin A₂ (41) and eumitrin B (44) from yellow pigment of lichen *U. baileyi* (Stirt.) Zahlbr collected at Yuriagehama (Figure 2.2).



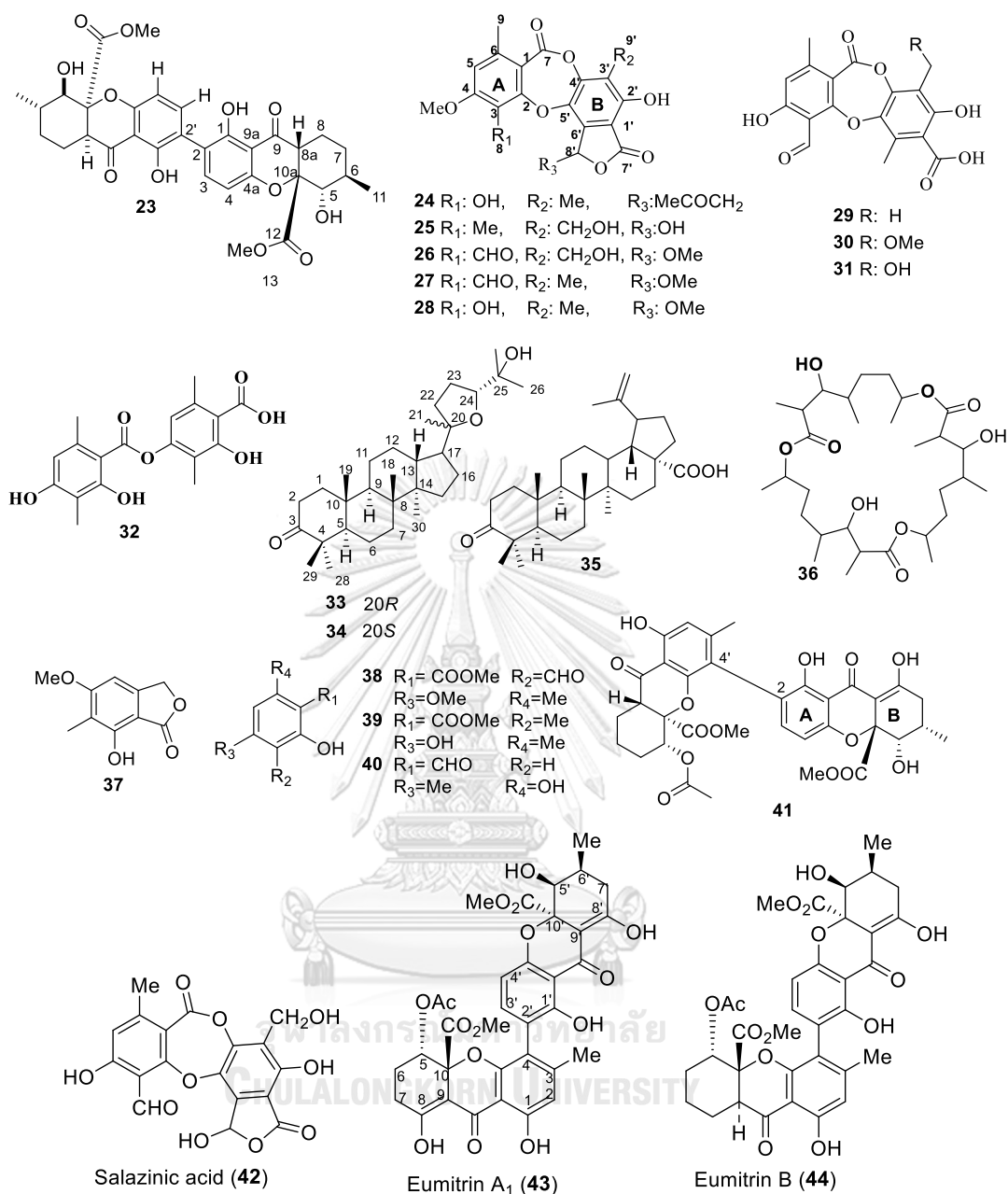


Figure 2. 2 Chemical constituents (23-44) from *U. baileyi*

Within this underexplored chemodiversity, a collection of structurally unique xanthenes were reported [20]. In addition, ergochrome dimers structurally related to the eumitrin [19] and secalonic acid series [21, 22] were scarcely reported from lichen source, in particular from *Usnea* species. Such dimeric xanthenes were

privileged structures since they were endowed with various and significant bioactivities [23]. Accordingly, secalonic acids exhibited a wide array of bioactivities including cytotoxic, antibacterial, antitumor, and anti-HIV properties [24, 25]. The structurally-related tetrahydroxanthone atropisomer phomoxanthone A from the mangrove-associated fungus *Phomopsis longicolla* also displayed promising antitumor properties [26], renewing the interest in isolating and synthesizing new derivatives from this structural class. Numerous xanthone dimers were axially chiral natural products and the preferred biaryl torsional angle (*i.e.* M- or P- helicity) plays a prevalent role in their pharmacological activities. Secalonic acids were also of utmost interest since they were reported to occur as mycotoxins with toxic, fetotoxic/teratogenic, and mutagenic properties [27].

The fruticose lichen *U. baileyi* has been phytochemically investigated by several authors and reported to contain depsides (barbatic and thamnolic acids), depsidones (protocetraric, norstictic, and salazinic acids), aliphatic and paraconic acids (caperatic and protolichesterinic acids), the dibenzofuran-related usnic acid, and xanthone dimers [19, 28]. As to this latter phytochemical group, the late Asahina first reported on the occurrence of yellow pigments within *U. baileyi*, the so-called eumitrins A1, A2, B, and T (Asahina, 1967). A few years later, Shibata and co-workers elucidated these eumitrins [19]. The HPLC-based chemical profiling of *U. baileyi* recently revealed the occurrence of a wider set of dimeric xanthenes, including eumitrins A3 and B2, which are still to be structurally elucidated [18]. Some other

unidentified dimeric xanthenes were also reported from different lichen sources, namely eumitrin U, X or Y [29-31].

In the search for new xanthone dimers from lichen source, our previous phytochemical investigation of the acetone extract of *U. baileyi* led to the isolation and structure elucidation of bailexanthone, along with a new depsidone, bailesidone [17].

2.1.3 Objectives

In Vietnam, the tropical monsoon climate is very suitable for lichen developing [10]. Vietnam has a number of diverse tropical lichens, but only a few species have been studied [10]. The chemical constituents of Vietnamese lichens are worth for further investigation in order to isolate novel compounds and/or biologically active compounds according to the diversity of Vietnamese lichens.

The major purpose of this study is the isolation, structure elucidation, synthesizing derivatives and evaluation biological activities of the chemical constituents of Vietnamese lichen, *U. baileyi* collected in highland .

2.2 Experimental

2.2.1 Instruments and materials

2.2.1.1 Instruments and chemicals

Specific rotations were obtained on a Perkin-Elmer 341 digital polarimeter. Electronic Circular Dichroism and corresponding UV-visible spectra were measured on

a Jasco J-815 spectropolarimeter. The IR spectra were acquired using a Shimadzu FTIR-8200 infrared spectrophotometer. 1D and 2D NMR spectra were acquired using a Bruker Advance 400 MHz or a Bruker AM-500 MHz spectrometer. Chemical shifts are referenced to the residual solvent signal (CDCl_3 : $\delta_{\text{H}} = 7.26$, $\delta_{\text{C}} = 77.1$). HR-ESI-MS data were recorded using a Bruker MicroTOF Q-II mass spectrometer. Open-column chromatography separations were performed on silica gel (40-63 μm , Himedia). TLC analyses were carried out on precoated silica gel 60 F254 or silica gel 60 RP-18 F254S plates (Merck), and spots were visualized by spraying with 10% H_2SO_4 solution followed by heating.

2.2.1.2 Lichen material *U.baileyi*

In June 2015, lichen *U. baileyi* (**Figure 2.3**) was collected from the barks of trees in Tam Bo mountain, Di Linh, Lam Dong, Vietnam where is 1000 m altitude. The scientific name of this lichen was identified by Ms. Natwida Dangphui and Assistant Professor Dr. Ek Sangvichien, Lichen Research Unit, Department of Biology, Faculty of Science, Ramkhamhaeng University, Bangkok, Thailand.

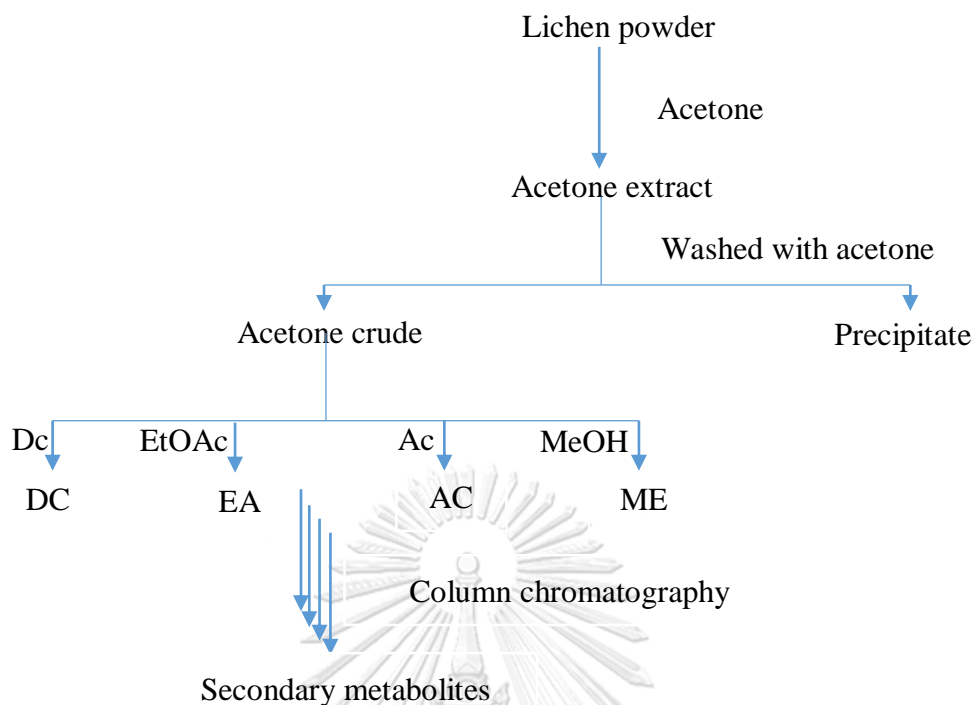


Figure 2. 3 The lichen *Usnea baileyi*

2.2.2 Extraction

Dried lichen *U. baileyi* was ground and extracted by maceration with acetone. The solvent was removed *in vacuo* using rotatory evaporator to get acetone crude extract which was applied to silica gel quick column eluting with dichloromethane (Dc, CH_2Cl_2), ethyl acetate (EtOAc), acetone (Ac) and methanol (MeOH) to obtain four fractions: DC, EA, AC, and ME, respectively.

Isolation and purification of secondary metabolites from the extracts of lichen *U. baileyi* was conducted by various methods such as column chromatography on each fraction as Scheme 2.1.



Scheme 2. 1 The separation scheme of the fractions of *U. baileyi*

2.2.3 Biological activities

2.2.3.1 Cytotoxicity and antiparasitic activity of US1-3

This activity was carried out by Structure Fédérative de Recherche BIOSIT, Université de Rennes 1. The cytotoxicity of **US1–3** was evaluated against a panel of 6 representative cell lines, namely Huh7 (differential hepatocellular carcinoma), Caco 2 (differentiating colorectal adenocarcinoma), MDA-MB-231 (breast carcinoma), HCT-116 (actively proliferating colorectal carcinoma), PC-3 (prostate carcinoma), NCI-H2 (lung carcinoma), and diploid skin fibroblasts as normal cell lines for control. Cells were grown as reported elsewhere and the inhibition of cell proliferation was determined as in Coulibaly *et al.*[32]. **US1–3** were also assayed for their antiparasitic activity

against the chloroquine-resistant strain of *Plasmodium falciparum* FcB1. The details of the experimental procedure for this bioassay are similar to those formerly reported [33].

2.2.3.2 Biological activities of compounds US5-11

2.2.3.2.1 Antibacterial activity

This activity was carried out by Lichen Research Unit and Lichen Herbarium, Department of Biology, Faculty of Science, Ramkhamhaeng University. The minimum inhibitory concentration (MIC) for each compound was determined by the broth micro-dilution method according to the recommendations of the Clinical and Laboratory Standards Institute (CLSI). (CLSI, 2015) [34].

Compounds **US5-11** were evaluated for their antimicrobial activities against *Bacillus subtilis* (ATCC 6633), *Staphylococcus aureus* (ATCC 25923), *Escherichia coli* (ATCC 25922), *Pseudomonas aeruginosa* (ATCC 27853), and *Candida albicans* (ATCC 10231) by micro-broth dilution method in 96-well culture plates. The test microorganisms were incubated at 37 °C for 24 h in Mueller-Hinton broth and the bacterial suspension were adjusted to 0.5 McFarLand unit. The inoculum was then diluted 100 times and 100 µL of inoculum was added to 96-well.

Stock solution of each compound was dissolved in 100% dimethylsulfoxide (DMSO) to a stock solution of 1 mg/mL. The compound was further two fold diluted in DMSO and tested at final concentrations between 500 to 0.98 µg/mL.

Chloramphenicol was used as a positive control. The growth was observed after 24 hours of incubation using visual reaction by addition color of idonitrotetrazolium (INT), wherereading +: growth color pink (growth) and reading – : growth color yellow (no growth)

2.2.3.2.2 Tyrosinase inhibitory

The tyrosinase inhibitory activity was performed using 96 well micro plate [35] with modification. Compounds were prepared in 10% DMSO in buffer and two fold dilutions were done to obtain various concentrations. 50 μL of sample solution in buffer were placed in 96 well plate, then 50 μL tyosinase enzyme from mushroom (250 U/mL) were added and the mixture was incubated for 5 minutes. 50 μL of 5 mM L-tyrosine was added later as a substrate; the mixtures were then incubated further for 30 minutes. The reaction was measured at 490 nm. Kojic acid was used as a positive control. The concentration range of extract used for the activity was 0-200 $\mu\text{g/mL}$. Percent of tyrosinase inhibition was calculated from the following equation (1) and IC_{50} was determined for each sample.

$$\% \text{ Tyrosinase inhibition} = \frac{\Delta A_{\text{control}} - \Delta A_{\text{sample}}}{\Delta A_{\text{control}}} \times 100 \quad (1)$$

Where " ΔA control" was the absorbance value at 490 nm without the test sample and " ΔA sample" was the absorbance value with mixture contained the sample.

2.2.3.2.3 α -glucosidase inhibitory

This inhibitory activity was evaluated according to [35].

Enzymatic activity was calculated by measuring absorbance at 405 nm (ALLSHENG micro plate reader AMR-100). All samples were analyzed in triplicate at various concentrations to obtain the IC_{50} value of each compound. The mean values and standard deviation were also identified.

2.3 Results and discussion

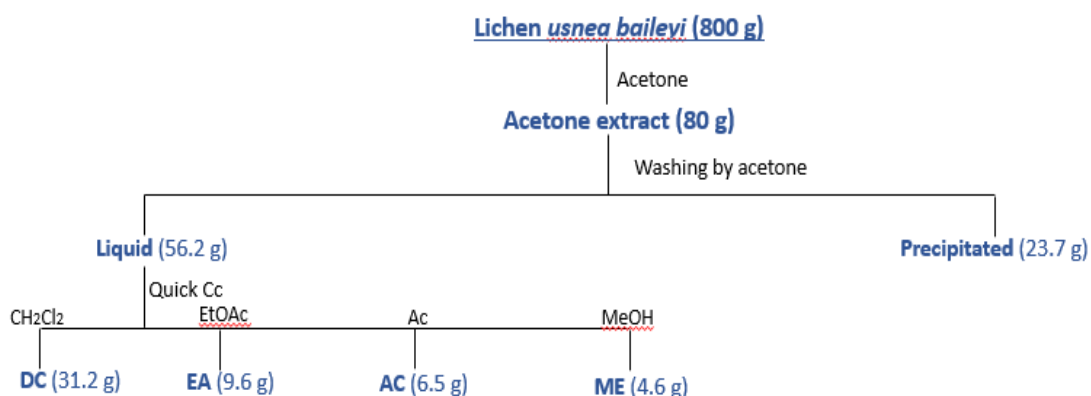
2.3.1 Extraction and fractionation of lichen *Usnea baileyi*

The air-dried lichen powder (800 g) was extracted with acetone at room temperature by maceration to get acetone extract (80 g) after evaporating acetone under reduced pressure. The acetone extract (80 g) was washed many times with acetone to obtain two parts: precipitate (23.7 g) and the acetone solution which was further evaporated to afford the acetone fraction (56.2 g). The acetone fraction (56.2 g) was applied to silica gel quick column eluting with CH_2Cl_2 , EtOAc, acetone and MeOH to obtain four fractions: **DC** (31.2 g), **EA** (9.6 g), **AC** (6.5 g) and **ME** (4.6 g).

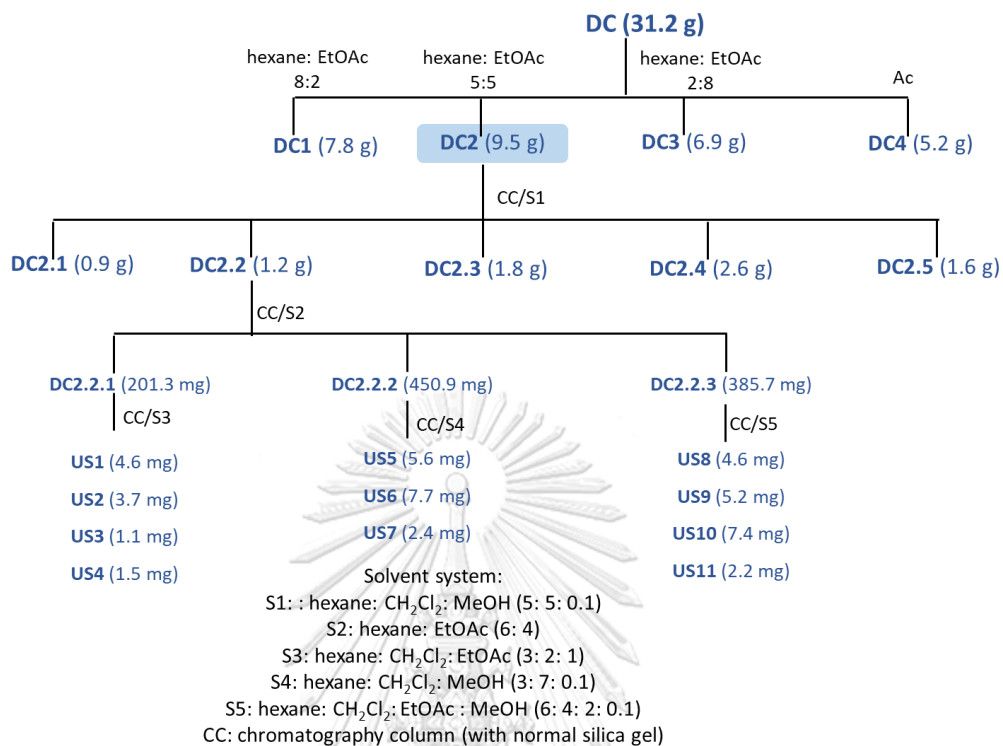
2.3.2 Separation of dichloromethane fraction

The dichloromethane fraction (**DC**, 31.2 g) was subjected to silica gel column chromatography using a solvent system of *n*-hexane/EtOAc (8:2 to 0:1) affording four subfractions **DC1** (7.8 g), **DC2** (9.5 g), **DC3** (6.9 g), and **DC4** (5.2 g) (**Scheme 2.2**). Subfraction **DC2** (9.5 g) was selected for further fractionation by silica gel column

chromatography using an isocratic mobile phase consisting of *n*-hexane/ CH_2Cl_2 /MeOH (5:5:0.1) to afford subfractions **DC2.1-5**: **DC2.1** (0.9 g), **DC2.2** (1.2 g), **DC2.3** (1.8 g), **DC2.4** (2.6 g), and **DC2.5** (1.6 g). Fraction **DC2.2** (1.2 g) was re-separated by open-air column chromatography using an isocratic elution solvent system consisting of *n*-hexane/EtOAc (6:4) to afford three fractions **DC2.2.1-3**. Further fractionation of **DC2.2.1** (201.3 mg) by silica gel column chromatography using *n*-hexane/ CH_2Cl_2 /EtOAc (3:2:1) solvent system to afford compounds **US1** (4.6 mg), **US2** (3.7 mg), **US3** (1.1 mg), and **US4** (1.5 mg). Further fractionation of **DC2.2.2** (450.9 mg) by silica gel column chromatography using *n*-hexane/ CH_2Cl_2 /MeOH (3:7:0.1) solvent system to afford compounds **US5** (5.6 mg), **US6** (6.7 mg), and **US7** (2.4 mg). **DC2.2.3** (385.7 mg) by silica gel column chromatography using *n*-hexane/ CH_2Cl_2 /EtOAc/MeOH (6:4:2:0.1) solvent system to afford compounds **US8** (4.6 mg), **US9** (5.2 mg), **US10** (7.4 mg), and **US11** (2.2 mg). The procedure for the fractionation of *U. baileyi* is summarized in **Schemes 2.2** and **2.3**.



Scheme 2. 2 Procedure for the fractionation of *U. baileyi*



Scheme 2.3 Procedure for the separation of DC fraction of *U. baileyi*

US1: yellow, amorphous solid. $[\alpha]_D^{20} + 28.00$ (c 0.02, MeOH) ; λ_{\max} (log ϵ)

205 (4.2), 249 (3.2), 339 (4.1) nm ; IR (KBr) ν_{\max} 3400, 2907, 1732, 1628, 1424, 1335, 1258, 1212 cm^{-1} ; HRESIMS m/z 623.1792 [M-H]⁻ (calcd. for C₃₂H₃₁O₁₃, 623.1770).

US2: yellow, amorphous solid. $[\alpha]_D^{20} - 114.70$ (c 0.02, MeOH) ; λ_{\max} (log ϵ)

205 (3.1), 278 (1.6), 336 (1.4) nm; IR (KBr) ν_{\max} 3455, 2959, 1746, 1628, 1453, 1368, 1218 cm^{-1} ; HRESIMS m/z 689.1820 [M+Na]⁺ (calcd. for C₃₂H₃₂O₁₃Na, 689.1841).

US3: yellow, amorphous solid. $[\alpha]_D^{20}$ - 57.00 (c 0.02, MeOH) ; λ_{\max} (log ϵ) 238 (2.7), 270 (1.2), 317 (0.9) nm ; IR (KBr) ν_{\max} : 3421, 3379, 1733, 1618, 1304 cm^{-1} ; HRESIMS m/z 667.1658 [M-H]⁻ (calcd. for $\text{C}_{33}\text{H}_{31}\text{O}_{15}$, 667.1663).

US4: white, amorphous solid. λ_{\max} (log ϵ) 253 (1.9), 306 (2.1) ; IR (KBr) ν_{\max} : 3424, 3291, 2951, 1749, 1736, 1729 cm^{-1} ; HRESIMS m/z 357.0614 [M-H]⁻ (calcd. for $\text{C}_{18}\text{H}_{13}\text{O}_8$, 357.0616).

US5: yellow, amorphous solid; $[\alpha]_D^{25}$ - 104.4 (c 0.02, MeOH); λ_{\max} (log ϵ) 232 (4.3), 269 (4.4), 371 (3.9) nm; HRESIMS m/z 633.1942 [M+Na]⁺ (calcd. for $\text{C}_{32}\text{H}_{34}\text{O}_{12}\text{Na}$, 633.1948).

US6: yellow, amorphous solid; $[\alpha]_D^{25}$ - 68.4 (c 0.02, MeOH); ; λ_{\max} (log ϵ) 236 (4.3), 266 (4.4), 365 (4.0) nm; HRESIMS m/z 633.1922 [M+Na]⁺ (calcd. for $\text{C}_{32}\text{H}_{34}\text{O}_{12}\text{Na}$, 633.1948).

US7: yellow, amorphous solid; $[\alpha]_D^{25}$ - 34.0 (c 0.02, MeOH); λ_{\max} (log ϵ) 207 (4.3), 266 (4.3), 367 (3.8) nm; HRESIMS m/z 647.1740 [M+Na]⁺ (calcd. for $\text{C}_{32}\text{H}_{32}\text{O}_{13}\text{Na}$, 647.1741).

US8: yellow, amorphous solid; $[\alpha]_D^{25}$ - 18.8 (c 0.02, MeOH); λ_{\max} (log ϵ) 236 (4.2), 267 (4.3), 373 (3.8) nm ; HRESIMS m/z 647.1766 [M+Na]⁺ (calcd. for $\text{C}_{32}\text{H}_{32}\text{O}_{13}\text{Na}$, 647.1741).

US9: yellow, amorphous solid; $[\alpha]_D^{25} + 258.8$ (c 0.02, MeOH); λ_{\max} (log ϵ) 235 (4.3), 267 (4.4), 364 (3.8) nm; HRESIMS m/z 647.1748 [M+Na]⁺ (calcd. for C₃₂H₃₂O₁₃Na, 647.1741).

US10: yellow, amorphous solid; $[\alpha]_D^{25} - 259.0$ (c 0.02, MeOH); λ_{\max} (log ϵ) 243 (4.5), 283 (4.5), 336 (4.6) nm; HRESIMS m/z 689.1824 [M+Na]⁺ (calcd. for C₃₄H₃₄O₁₄Na, 689.1846).

US11: yellow, amorphous solid; $[\alpha]_D^{25} - 264.8$ (c 0.02, MeOH); λ_{\max} (log ϵ) 214 (4.4), 241 (4.4), 319 (4.6) nm; HRESIMS m/z 687.1716 [M+Na]⁺ (calcd. for C₃₄H₃₂O₁₄Na, 687.1690).

2.3.3 Structural elucidation of compounds from dichloromethane fraction.

2.3.3.1 Compound US1

The molecular formula of **US1** could be established as C₃₂H₃₂O₁₃ based on ¹³C NMR and HRESIMS data, verifying the presence of 18 double-bond equivalents. Owing to molecular formula requirements and 30 protons being evident from ¹H NMR analysis, two protons were deduced to occur as aliphatic hydroxy groups. The ¹H and HSQC spectra revealed three hydrogen-bonded hydroxy groups at δ_H 13.77 (1H, s, OH-8), 11.88 (1H, s, OH-1) and 11.73 (1H, s, OH-1'); two pairs of *ortho*-oriented aromatic protons at δ_H 7.48 (2H, d, $J = 8.5$ Hz, H-3 and H-3') and 6.63 (2H, d, $J = 8.5$ Hz, H-4 and H-4'); two oxygenated methine signals at δ_H 3.93 (1H, d, $J = 11.5$ Hz, H-5) and 3.73 (1H, d, $J = 10.5$ Hz, H-5'); three methine signals at δ_H 2.98 (1H, dd, $J = 12.0$,

4.5 Hz), 2.42 (1H, m, H-6) and 1.83 (1H, m, H-6'); three diastereotopic pairs of methylene hydrogens at δ_{H} 2.74 (1H, dd, $J = 19.0, 6.0$ Hz, H-7) and 2.32 (1H, dd, $J = 19.0, 6.5$ Hz, H-7); at δ_{H} 2.20 and 2.15 (2H, m, H2-8') and at δ_{H} 1.95 (1H, m, H-7') and 1.21 (1H, m, H-7'); two methoxy signals at δ_{H} 3.70 (3H, s) and at δ_{H} 3.73 (3H, s); two methyl groups at δ_{H} 1.17 (3H, d, $J = 6.5$ Hz) and at 1.12 (3H, d, $J = 6.5$ Hz). The two methoxy groups could be straightforwardly defined as methyl ester moieties based on HMBC correlations from H3-13' to C-12' and from H3-13 to C-12. The ^{13}C NMR spectrum of **US1** revealed an apparent twinning for many carbon resonances, leading to infer that it might correspond to a dimeric structure with some slight differences between each subunit. The scaffold of each subunit could be determined to be a xanthone.

The first subunit was determined as a hexahydroxanthone based on the COSY spectrum which allowed the development of a spin system identified as H-5'/H-6'/(H3-11')/H2-7'/H2-8'/H-8a'. The chemical shift of C-5' (δ_{C} 80.3) was indicative of the ipso location of a first aliphatic hydroxy group. The C-10' location of the methyl ester group could be determined from the long-range heteronuclear correlation from both the oxymethine proton H-5' at δ_{H} 3.73 and the oxymethine proton H-8a' at δ_{H} 2.98 to C-12'. The chemical shift value of C-10' indicated that this carbon was oxygenated and the HMBC correlations from H-8' to C-9' and from H-8a' to C-4' and C-9a' defined a chromenone core. The second spin system in this monomer involved

two *ortho*-oriented aromatic protons and the connection of this phenyl ring to the γ -pyrone nucleus of the hexahydroxanthone could be deduced from long-range heteronuclear correlations from the aromatic protons H-3' at δ_{H} 7.48 and H-4' at δ_{H} 6.63 to C-4a' (δ_{C} 159.0) and C-9a' (δ_{C} 107.4). A phenol group could be assigned at C-1' as evidenced by HMBC correlations from the phenolic proton at δ_{H} 11.73 to C-1' (δ_{C} 159.5), C-2' (δ_{C} 118.2) and C-9a'. Due to C-2' being a quaternary carbon, it can be deemed that this specific site is linked to the other part of the compound. The key COSY, HMBC and ROESY correlations of **US1** are summarized as in **Figure 2.4**.

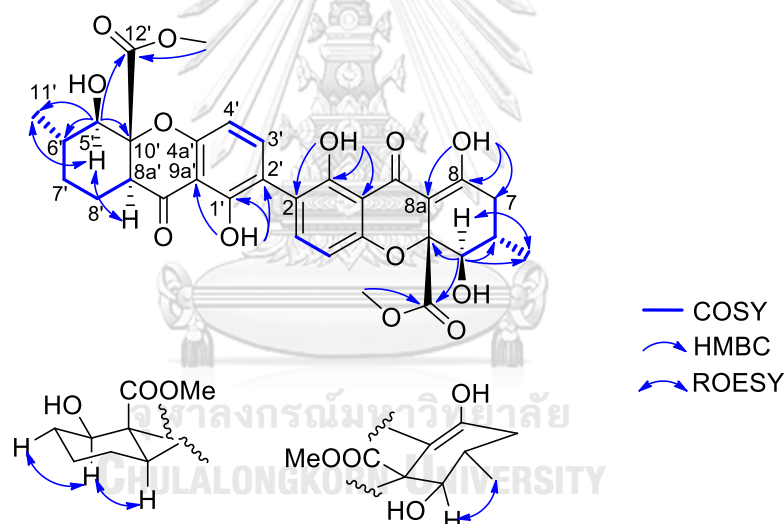


Figure 2.4 Key COSY, HMBC and ROESY correlations of compound **US1**

The second monomer, subunit II, was highly reminiscent of the first one. The most salient spectroscopic difference between the two sub-units being the intense downfield shift of C-8 and C-8a compared to their homologous positions in the first sub-unit (with respective δ_{C} values of 177.7 and 101.7 vs 20.4 and 51.2 ppm) that indicated the occurrence of an enolic moiety at these positions, as further backed up

by the HMBC cross-peaks between the hydrogen-bonded hydroxy group OH-8 at δ_C 13.77 and C-7 (δ_C 36.4), C-8 (δ_C 177.7) and C-8a (δ_C 101.7). The NMR signal patterns related to this subunit, including COSY and HMBC data, confirmed a similar gross structure of the rest of this monomer, compared to that of subunit I. Due to ^1H NMR resonances for two *ortho* oriented aromatic protons, the only remaining possibility for monomeric units linkage was a bond tethering C-2 with C-2' which was depicted in **Figure 2.4**. The tentative chemical shift assignments of **US1** are tabulated in **Tables 2.1** and **2.2**.

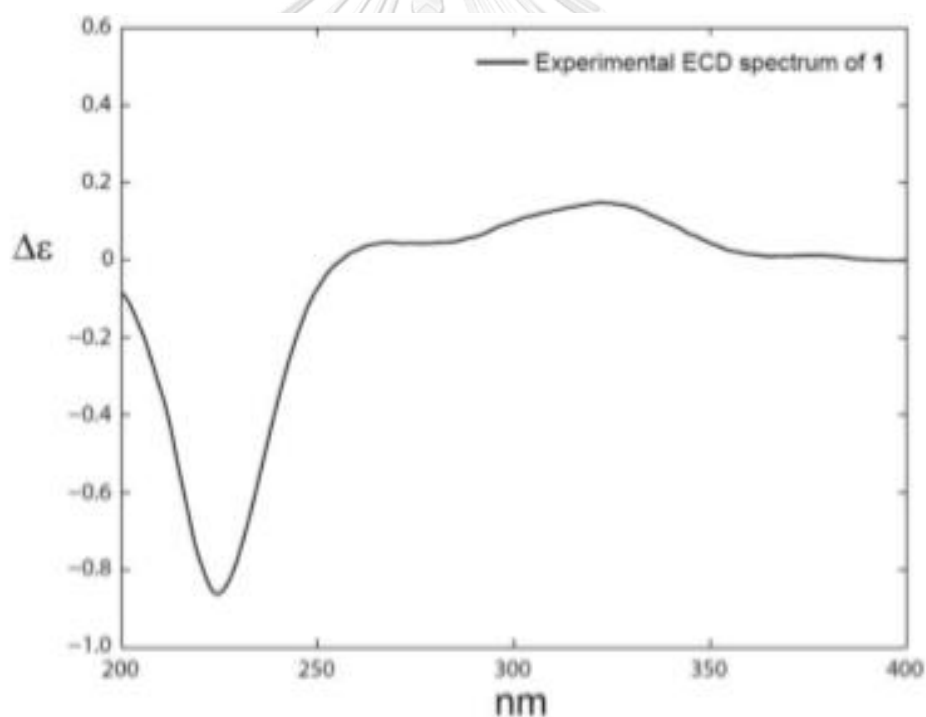


Figure 2. 5 Experimental ECD plot of **US1**



จุฬาลงกรณ์มหาวิทยาลัย
CHULALONGKORN UNIVERSITY

Table 2.1 ¹H (500 MHz) NMR data of US1-3 (CDCl₃)

No.	<u>Eumitrin C (US1)</u>	<u>Eumitrin D (US2)</u>	<u>Eumitrin E (US3)</u>
	δ_{H} , mult. (<i>J</i> in Hz)	δ_{H} , mult. (<i>J</i> in Hz)	δ_{H} , mult. (<i>J</i> in Hz)
3	7.48, 1H, d, 8.5	7.76, 1H, d, 8.5	7.85, 1H, d, 8.5
4	6.63, 1H, d, 8.5	6.58, 1H, d, 8.5	6.69, 1H, d, 8.5
5	3.93, 1H, d, 11.5	4.47, 1H, d, 3.5	4.37, 1H, d, 3.5
6	2.42, 1H, m	2.89, 1H, m	2.16, 1H, m
7	2.74, 1H, dd, 19.0, 6.0	2.95, 1H, dd, 17.0, 8.5	2.35, 1H, m
	2.32, 1H, dd, 19.0, 10.5	2.24, 1H, dd, 17.5, 4.0	2.16, 1H, m
8a		3.22, 1H, d, 17.0	
		3.10, 1H, d, 17.0	
11	1.17, 3H, d, 6.5	1.30, 3H, d, 7.0	1.22, 3H, d, 6.0
13	3.70, 3H, s	3.67, 3H, s	
1-OH	11.88, 1H, s	11.75, 1H, s	11.30, 1H, s
8-OH	13.77, 1H, s		7.09, 1H, br s
8a-OH			6.38, 1H, br s
2'		6.49, 1H, s	6.50, 1H, s
3'	7.48, 1H, d, 8.5		
4'	6.63, 1H, d, 8.5		
5'	3.73, 1H, d, 10.5	5.03, 1H, dd, 12.0, 5.0	5.01, 1H, dd, 12.0, 5.0
6'	1.83, 1H, m	1.66, 1H, m	1.80, 1H, m
		1.74, 1H, m	1.69, 1H, m
7'	1.95, 1H, m	1.86, 1H, m	1.89, 1H, m
	1.21, 1H, m	1.52, 1H, m	1.52, 1H, m
8'	2.15 - 2.20, 2H, m	1.86, 1H, m	1.89, 1H, m
		1.52, 1H, m	1.52, 1H, m
8a'	2.98, 1H, dd, 12.0, 4.5	2.97, 1H, dd, 12.0, 5.0	2.97, 1H, dd, 12.5, 4.5
11'	1.12, 3H, d, 6.5	2.13, 3H, s	2.13, 3H, s
13'	3.73, 3H, s	3.71, 3H, s	3.66, 3H, s
15'		2.00, 3H, s	1.94, 3H, s
1'-OH	11.73, 1H, s	11.47, 1H, s	11.48, 1H, s

Table 2.2 ^{13}C (125 MHz) NMR data for **US1-3** (CDCl_3).

No.	US1 δ_{C}	US2 δ_{C}	US3 δ_{C}	No.	US1 δ_{C}	US2 δ_{C}	US3 δ_{C}
1	159.0	159.5	161.4	1'	159.5	161.8	162.0
2	117.7	107.5	118.5	2'	118.2	111.4	111.4
3	140.4	143.1	145.4	3'	140.4	151.0	150.7
4	107.7	107.3	107.5	4'	107.7	115.5	115.0
4a	158.4	159.0	158.3	4a'	159.0	156.5	156.7
5	77.1	87.7	74.8	5'	80.3	72.6	72.6
6	29.4	30.1	29.8	6'	34.3	26.1	26.3
7	36.4	36.3	34.2	7'	31.2	22.4	22.4
8	177.7	175.4	108.9	8'	20.4	25.3	25.6
8a	101.7	39.9	73.6	8a'	51.2	48.7	48.8
9	187.3	194.4	195.0	9'	197.4	197.6	197.6
9a	107.3	117.3	106.7	9a'	107.4	104.9	104.9
10	84.9	84.6	84.6	10'	87.5	83.4	83.6
11	18.1	21.0	15.1	11'	18.4	21.2	21.9
12	169.3	168.9	165.5	12'	170.4	170.3	169.8
13	53.0	53.4		13'	53.4	53.4	53.4
				14'		169.8	170.4
				15'		20.9	20.8

The absolute configurations of 2,2'-secalonic acids and **US1** were similar and could be reliably determined from their $n\text{-}\pi^*$ ECD bands around 330 nm, that are correlated with the configurations of the C-10 and C-10' stereogenic centers [36, 37]. A positive $n\text{-}\pi^*$ ECD band at 333 nm determined C-10 R, C-10' R configuration and

also allowed the assignment of the other stereogenic centers based on the relative stereochemistry, in excellent agreement with literature data [38-40].

Accordingly, the magnitude of the vicinal coupling constant value of the oxymethine proton at H-5/H-5' bisects the dihedral angle of the adjacent proton(s). Regarding the currently described structure, the elevated coupling constant of H-5 and H-5' determined the axial position of both these oxymethine protons and established the C-5/C-6 and C-5'/C-6' *trans*-diaxial configuration, as in blennolide B or xantholepinone A among others ($^3J_{\text{H-5,H-6}}=11.5$ Hz and $^3J_{\text{H-5',H-6'}}=10.5$ Hz) [39]. This deduction was further supported by ROESY correlations between the oxymethine proton at δ_{H} 3.73 (H-5') and both the methyl group at δ_{H} 1.12 (H3-11') and the methine proton at δ_{H} 2.98 (H-8a') that determined the synfacial orientation of these substituents while the lack of ROE correlation with the contiguous methyl ester groups ascribed this latter functionality to the other face of the nucleus. The axial orientation of H-5 was diagnostic of a space arrangement identical to that of eumitrin A2 rather than that of eumitrin A1/eumitrin B [19] as further ascertained on various bisxanthone scaffolds [41-44]. The absolute stereostructure assignment of C-5 was proposed by the comparison of the NMR data of the long sought-after tetrahydroxanthone hemisecanolic acid monomers, blennolide B and its C-5 epimer, blennolide C, jointly determining a *5R*, *5'R'* configuration[39]. Thus, the (*5R*, *6R*, *10R*, *5'R*, *6'R*, *10'R*)-absolute configuration of **US1**, namely eumitrin C, was determined as

displayed in **Figure 2.4**. Conversely, the ECD spectra of dimeric xanthenes having a hindered rotation is indicative of their axial rather than central chiralities [45].

2.3.3.2 Compound US2

US2 was isolated as light yellow amorphous solid. Its molecular formula was determined to be $C_{34}H_{34}O_{14}$ based on the sodiated molecular ion peak at m/z 689.1820 (calcd for $C_{34}H_{34}O_{14}Na$, 689.1841). In spite of the closely related molecular formulae, the examination of the 1H and ^{13}C NMR spectra revealed some important structural differences with **US1** including the lack of the enolic signals that indicated the absence of a $\Delta^{8(9)}$ double bond and the occurrence of an acetoxycarbonyl group that could be located at C-5' based on the HMBC correlations from the acetoxycarbonyl protons at δ_H 2.00 (H3-15') to C-14' (δ_C 169.8) and C-5' (δ_C 72.6) as further backed up by the HMBC crosspeak between the oxymethine proton H-5' (δ_H 5.03) and C-14' (δ_C 169.8). Likewise, one of the methyl groups was downfield shifted to δ_H 2.13 indicating its aromatic nature, consistently with the disappearance of an aromatic proton signal and with the singlet status of the aromatic proton at δ_H 6.49 (H-2'). This methyl group was indeed located at C-3', based on the long-range heteronuclear correlations from these protons to C-2' (δ_C 111.4), C-3' (δ_C 151.0), and C-4' (δ_C 115.5). The COSY spectrum revealed the H-5'/H2-6'/H2-7'/H2-8'/H-8a' proton spin system, further supported by the full set of possible 2J and 3J correlations observed in the HMBC spectrum that established the hexahydroxanthone scaffold of

the first monomer. The *syn*facial orientation of the acetoxycarbonyl and of the methyl ester groups was established from the H3-13'/H3-15' ROE crosspeak while the key ROE effect between the oxymethine proton at δ_{H} 5.03 (H-5') and the methine proton at δ_{H} 2.97 (H-8a') ascribed these protons to the other face of the structure. As formerly observed for **US1**, the vicinal coupling constant value of the oxymethine proton H-5' determined its axial orientation and thus defined a 5'*R* configuration identical to that of blennolide B to define the structure of this first subunit as displayed in **Figure 2.6**.

The remaining signals were assigned to a hydrogen-bonded hydroxy proton at δ_{H} 11.75, *ortho*-oriented aromatic protons at δ_{H} 6.58 and 7.76, an oxygenated methine protons at δ_{H} 4.47, an aliphatic methane proton at δ_{H} 2.89, a diastereotopic methylene proton at δ_{H} 2.32/2.16 and a methyl group at δ_{H} 1.30. The thorough analysis of long-range heteronuclear correlations established a partially saturated γ -pyrone system annulated to an aromatic ring. The molecular formula of **US2** determined a double bond equivalent of 18, and the presence of the pentacyclic biaryl scaffold determined so far along with the five carbonyl carbons [δ_{C} 175.4 (C-8), 170.3 (C-12'), 169.8 (C-14'), and 168.9 (C-12)] accounted for 17 elements of unsaturation, thereby leaving one aliphatic ring system to be introduced in the remaining part of the molecule. Accordingly, the analysis of the COSY spectrum revealed the proton spin system of H-5/H-6/H3-11/H-7 which was cyclized to afford a β -methyl- γ -lactone moiety as deduced from HMBC correlations of the oxymethine

proton at δ_{H} 4.47 (H-5), the methine proton at δ_{H} 2.89 (H-6), and the diastereotopic methylene protons at δ_{H} 2.24 and 2.95 (H2-7) to C-8 (δ_{C} 175.4). The key HMBC correlations from the methylene protons H2-7 to C-5 (δ_{C} 87.7), C-9 (δ_{C} 194.4), C-10a (δ_{C} 84.6) and C-12 (δ_{C} 168.9) defined the connection between the chromone core and both the γ -butyrolactone moiety and the ester group, as depicted in **Figure 2.6**.

The planar structure of **US2** was obtained by connecting the two monomeric units *via* the linkage of hexahydroxanthone C-4' and chromanone C-2, evidenced by the HMBC correlation of the aromatic proton at δ_{H} 7.76 (H-3) to C-4' (δ_{C} 115.5) and from the aromatic methyl protons at δ_{H} 2.13 to C-4'. The oxymethine proton H-5 was coupled to the tertiary methine proton H-6 with a coupling constant of 3.6 Hz, characteristic of *trans*-oriented protons in such ring system [46], as further validated by ROE correlation between H-5 and CH₃-11. This deduction was supported by the long-range interunit H-3/H-11' ROE crosspeak, as earlier reported on dimeric tetrahydroxanthone neosartorin that displays the same relative configuration and axial chirality [47].

The structure of **US2** comprised a rotationally hindered biaryl axis, as evidenced by the axial chirality of compounds being similarly *ortho*-substituted to the stereogenic biaryl axis [47, 48]. Each monomer of **US2** revealed a benzoyl chromophore with a maximum UV absorption near 240 nm [41, 49]. Based on the blennolide series, it was demonstrated that the ECD Cotton effects at this wavelength did not split [39]. On the opposite, the axially linked dimers display

obviously split CE indicating that the chromophores interacted with each other, as revealed by their opposite but not mirror ECD spectra plots. In such structures, axial chiralities governed chromophore spatial position and the ECD spectrum [48, 50, 51]. Thus, the chromophores' rotary manners were identical to those of the CD Exciton Chirality Rule. The anticlockwise manner of the two benzoyl chromophores of **US2** could be deduced from the negative exciton couplet centered at around 240 nm; consistently with earlier reports on related structures [47, 48], as further backed up by the ROE correlation between H-3 and H3-11' (**Figure 2.7**). The absolute configuration of γ -butyrolactone ring was deduced by comparison between both predicted spectra with the experimental one, which revealed an excellent fit for a (*aS*, 5'*R*, 8*a'R*, 10'*R*, 5*R*, 6*R*, 10*S*) configuration (**Figure 2.6**).

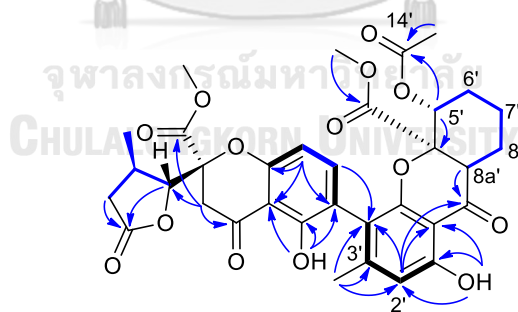


Figure 2. 6 Chemical structure of **US2**

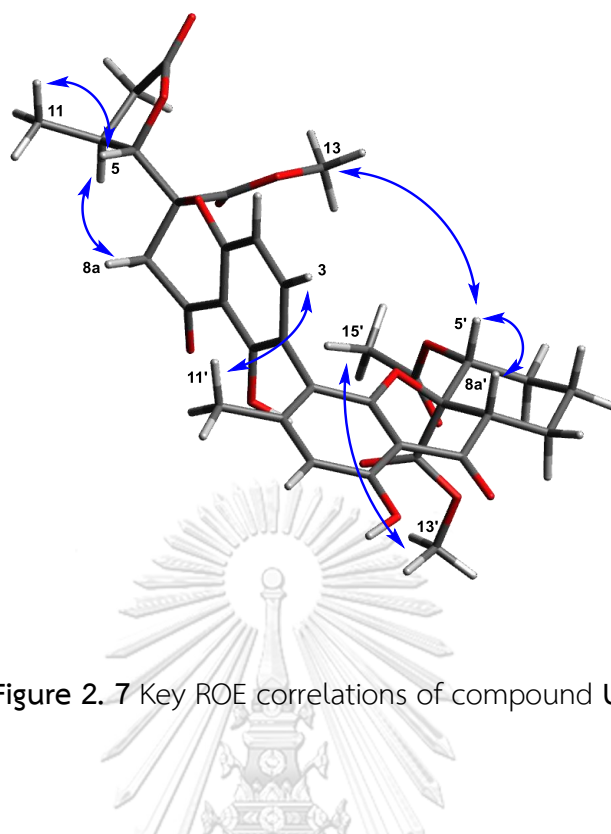


Figure 2. 7 Key ROE correlations of compound US2

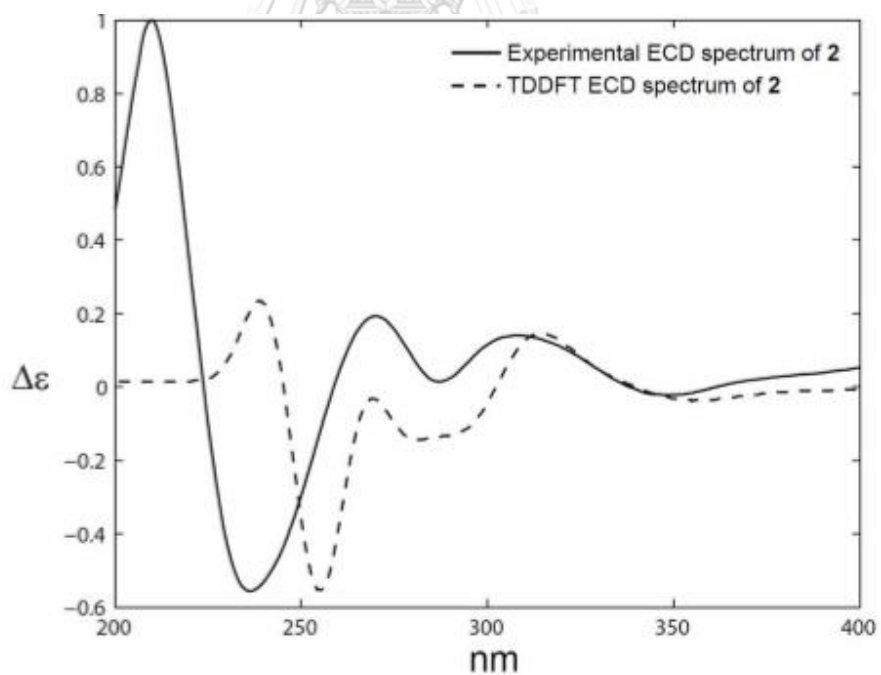


Figure 2. 8 Comparison of the experimental ECD spectrum of US2 and calculated ECD spectrum for the (aS, 5'R, 8a'R, 10'R, 5R, 6R, 10S) stereoisomer (UV shift = -12 nm)

2.3.3.3 Compound US3

US3 was obtained as light yellow amorphous solid. Its molecular formula was determined as $C_{33}H_{32}O_{15}$ based on HRESIMS measurements (m/z 667.1658 calcd for 667.1668 [M-H]⁻) and ^{13}C NMR data. The 1H NMR spectrum showed 30 protons, revealing the occurrence of **US3** supplementary aliphatic hydroxyl groups. The thorough analysis of the 2D NMR spectra determined a similar hexahydroxanthone monomeric building unit as in **US2**. As to the other subunit, the occurrence of a hydrogen-bonded hydroxy proton at δ_H 11.30 and the *ortho*-oriented aromatic protons at δ_H 7.85 and 6.69 determined the unchanged constitutions of A and B rings, as further supported by the key long-range heteronuclear correlations outlined in **Figure 2.9**.

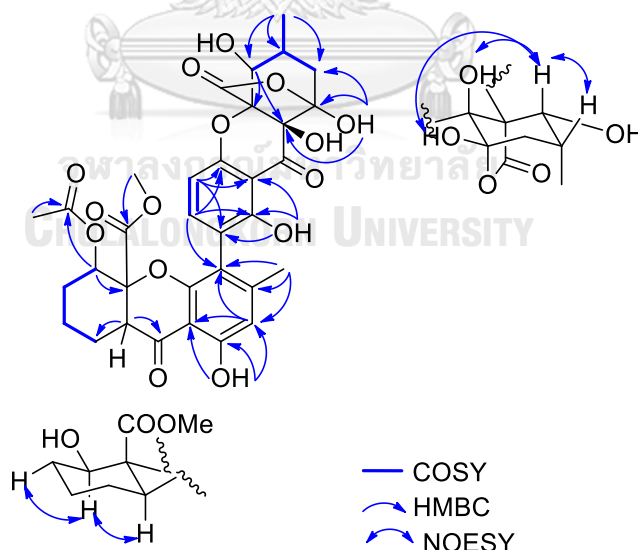


Figure 2. 9 Selected COSY and HMBC correlations of compound **US3**

The structural features elucidated account for 15 indices of hydrogen deficiency, leaving three more to be introduced, while five more oxygen atoms still

have to be incorporated into the structure. The COSY spectrum revealed the H₅/H₆/(H₃-11)/H₂-7 spin system, along with the HMBC correlations from the methyl protons at δ_{H} 1.22 to C-5 (δ_{C} 74.8), C-6 (δ_{C} 29.8), and C-7 (δ_{C} 34.0). An aliphatic hydroxyl group could be located at C-8 based on the long-range heteronuclear correlations from the hydroxyl proton at δ_{H} 7.09 to C-7, C-8 (δ_{C} 108.9), and C-8a (δ_{C} 73.6). The linkage of the OH group to the carbon resonating at δ_{C} 108.9 was determined based on the HMBC cross-peak between the oxymethine proton at δ_{H} 4.37 and C-8a. Owing to molecular formula requirements and to connectivity constraints, a bicyclic framework tethering C-8a with C-10 through a lactone could be determined, which was consistent with the resonating of C-8 at δ_{C} 108.9 that is indicative of a hemiketalic carbon. Likewise, the chemical shift of the tertiary carbon at δ_{C} 84.6 is in excellent agreement with earlier reports on molecules bearing a methyl ester group on this specific position [39, 41, 48].

Similar to **US2**, the aS axial chirality of **US3** could be determined based on the negative Exciton couplet at 240 nm [41, 49]. The (10*R*/10'*R*) absolute configurations could be determined based on the positive sign of the band *ca* 330 nm. The validity of this band to assign the absolute configurations of these stereogenic centers was demonstrated on both ester/ester (*e.g.* secalonic acid B), lactone/ester (*e.g.* ergochrysin B), and lactone/lactone (*e.g.* ergoflavine) xanthone dimers [43]. The null coupling constant value between H-5 and H-6 indicated their synfacial orientation [39, 52], as further validated by the ROE crosspeak between H-5

and H-6. This relative stereochemistry is in excellent agreement with ^{13}C NMR spectroscopic data of usneaxanthonones A–C [49]. Information regarding the relative stereochemistry of this subunit was also completed by the ROE correlation between both the hydroxyl at δ_{H} 6.38 (8a-OH) and at 7.09 (8-OH) and the oxygenated methine at δ_{H} 4.37 (H-5), ascribing these substituents to the same side of the cyclohexane nucleus. The relative stereochemistry of the lactone moiety could not be assigned based on ROESY spectrum. The comparison of the ^{13}C NMR data of the two candidate diastereoisomers with the observed chemical shifts of **US3** through Goodman and Smith DP4 parameter resulted in the prediction of the relative configuration with a 92.7% probability (**Figure 2.10**). This determined stereochemistry was further validated by the excellent agreement between the ECD plot of **US3** with that of the recently reported usneaxanthonone A, the absolute stereochemistry of which was unambiguously determined through single crystal X-ray diffraction analysis (**Figure 2.11**).

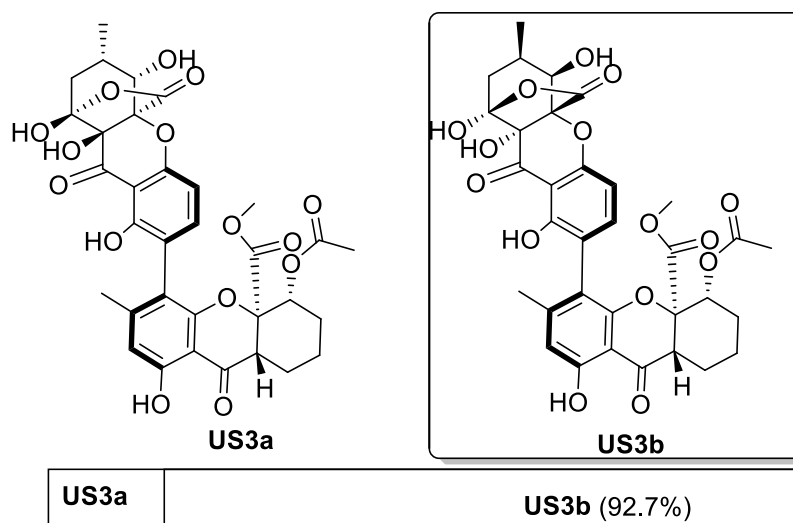
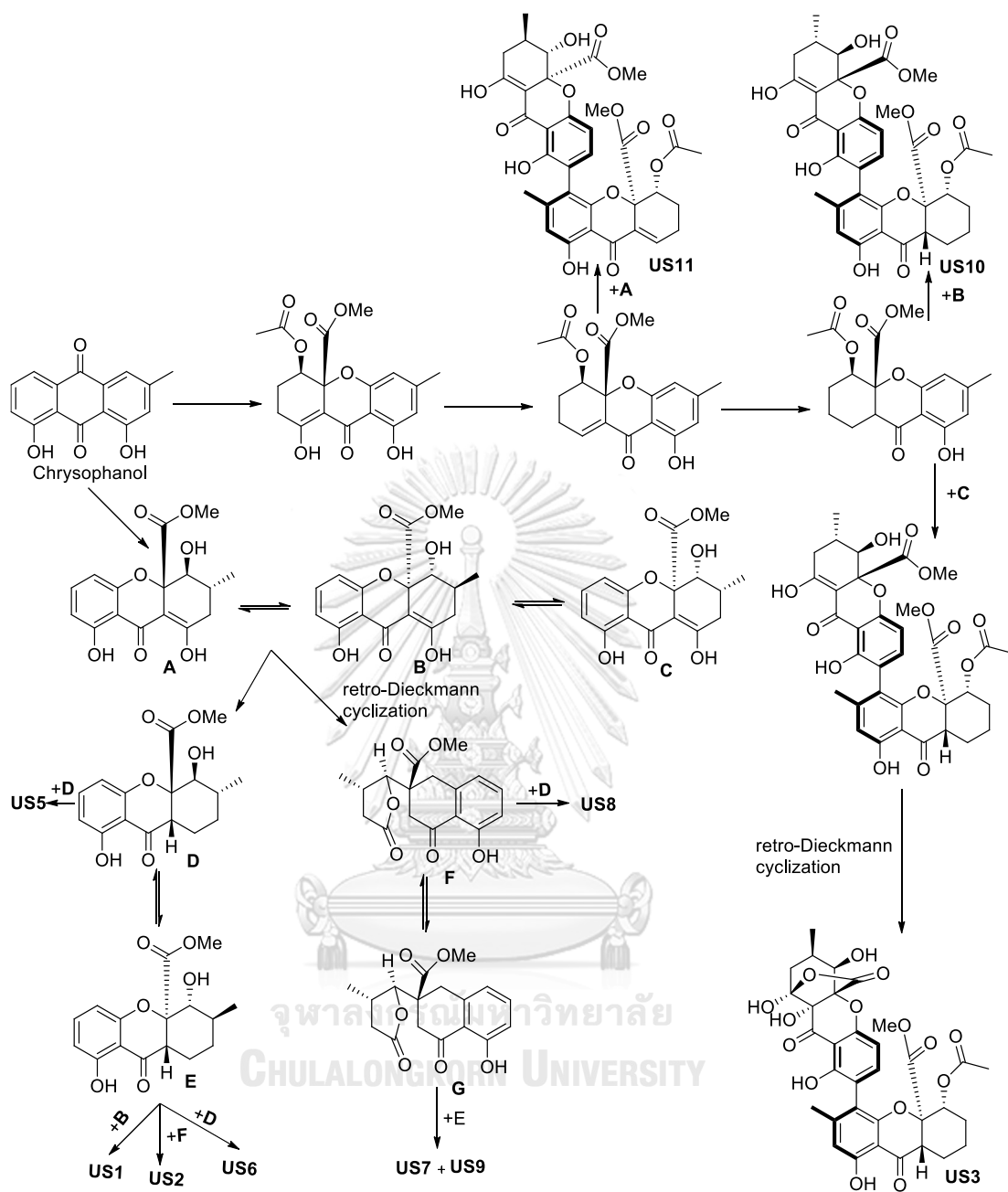


Figure 2. 10 Relative configuration for Eumitrin E (**US3**): DP4 probabilities of the two candidate diastereoisomers

The substitution patterns of the monomeric units are indicative of their origins from chrysophanol, following the so-called ravenelin pathway that leads to xanthenes displaying a methyl group at C-3 [20]. The understanding of the underlying biosynthetic pathways giving rise to xanthone dimers dramatically rose through a series of gene-deletion experiments carried out in the neosartorin-producing fungus *Aspergillus novofumigatus* [53]. The biosynthesis of the monomeric building blocks was proved to proceed from chrysophanol *via* Baeyer-Villiger monooxygenase, a methyltransferase, a reductase and an acetyltransferase. The heterodimerization would then involve p450 monooxygenase that most interestingly revealed sequence similarity with a p450 encoded upstream of the biosynthetic gene cluster of ergochrome xanthone dimers within *Claviceps purpurea* [54]. Despite being related to xanthone dimers being formerly reported to occur throughout literature, the newly described compounds display rather uncommon structural features. At first, eumitrin C stands among the rare tetrahydroxanthone/hexahydroxanthone dimers, a scaffold only being sustained so far by ergochromes AD and BD [42], and eumittrins A2 and B [19]. Xanthone monomers were already related to 2,2-disubstituted chroman-4-ones, particularly in fungi [23, 55]. The γ -butyrolactone ring of such chromanones results from a *retro*-Dieckmann cyclization, sometimes being accompanied by further ring cleavage intermediates such as the related γ -

hydroxybutyric acid derivatives and their corresponding methyl esters [41, 48]. Although being biogenetically related, xanthone/chromanone heterodimers are rare, being so far represented by related cases comprising blennolide G [39, 56], blennolides I and J [48, 57], gonytolides D and E [48], phomolactonexanthonones [58], and versixanthonones A-F [41]. Eumitrin D represents the first occurrence of xanthone dimer comprising a hexahydroxanthone and a chromanone. Lactone-comprising xanthone dimers were scarcely reported throughout literature with 5 such compounds being reported so far within this structural class, initially being reported as ergot pigments: the lactone/lactone ergoflavin [59] and the lactone/ester-based ergochrysin A and B [42], ergochrome CD [60], and ergoxanthin [61, 62] (**Scheme 2.3**). A suite of lactone/ester bisxanthonones, viz. usneaxanthonones A-C from *Usnea aciculifera*, very recently extended the number of compounds from this structural class, the structure elucidation of which was greatly aided by their having all crystallized [49]. The lactonic monomer of **US3** is unique due to C-8 hydroxylation that introduces an unprecedented hemiketalic function. Although unprecedented, the 8-OH group of the lactonic monomer of eumitrin E is also in line with the canonical substitution pattern of ravenelin-derived xanthonones [63]. The 2-4' biaryl linkage is shared with usneaxanthonones but not with lactone/ester xanthone heterodimers which was not reported so far within lactone/ester based xanthone dimers.



Scheme 2.3 Proposal biosynthesis of US1-3, US5-11.

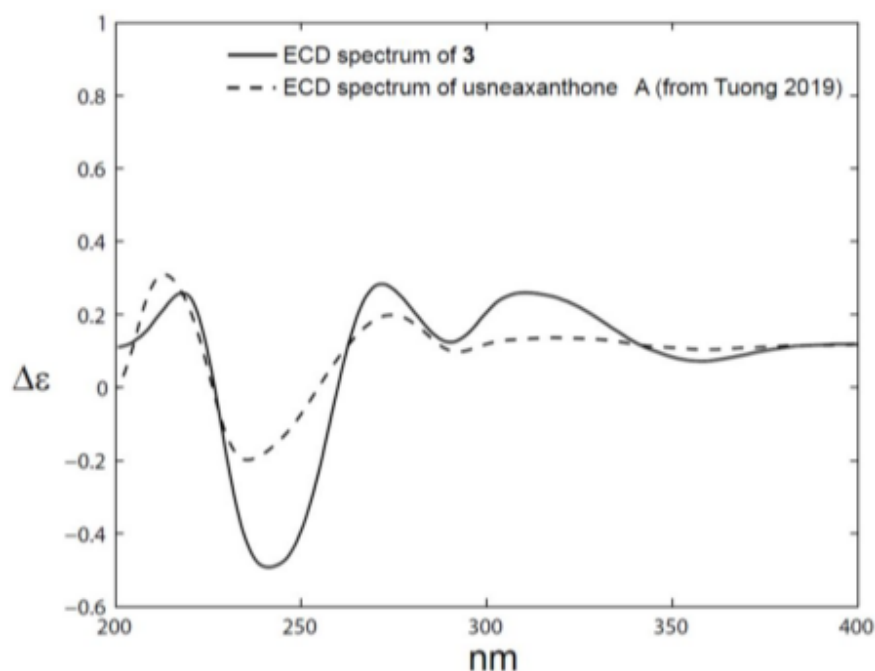


Figure 2.11 Comparison of the experimental ECD spectrum of **US3** and usneaxanthone A [64]

2.3.3.4 Compound US4

Compound **US4** was isolated as white amorphous solid and was assigned the molecular formula $C_{18}H_{14}O_8$ (12 indices of hydrogen deficiency) based on its negative-ion HRESIMS data which showed an $[M-H]^-$ peak at m/z 357.0614 (calcd. for $C_{18}H_{13}O_8$, 357.0616). The 1H NMR data revealed typical resonances of an aromatic methyl at δ_H 2.52 (3H, s), a methoxy group at δ_H 3.94 (3H, s), two oxygenated methylene [$(\delta_H$ 4.81, 2H, s) and $(\delta_H$ 5.69, 2H, s)], and two aromatic protons at δ_H 6.68 (1H, s) and 6.81 (1H, s). The small amount of **US4** precluded the acquisition of the ^{13}C NMR spectrum of convenient quality, but all of the chemical shifts could be deduced from inverse-detection heteronuclear NMR spectra (**Table 2.3**). The β -orcinol depsidone scaffold

was deduced by the near-identical 1D NMR data of **US4** to those of cryptostictinolide, as reported by Lohézic-Le Dévéhat *et al.* from *Usnea articulata* [14], and further backed up by 2D NMR correlations (**Figure 2.12**). The chemical shift value of C-3' (δ_C 108 ppm) is diagnostic of its being *ortho*-oriented to two oxygen functions, identifying **US4** as 3'-*O*-demethylcryptostictinolide, also evidenced by the HMBC correlations from the aromatic proton at δ_H 6.81 to C-1' (δ_C 109), C-2' (δ_C 151), C-4' (δ_C 151 ppm), and C-5' (δ_C 137).

Table 2.3 Tentative ^1H (500 MHz) and ^{13}C (125 MHz) NMR chemical shift assignment for **US4** (CDCl_3)

No.	δ_H , mult. (J in Hz)	δ_C	No.	δ_H , mult. (J in Hz)	δ_C
1		113.7	4-OMe	3.94, 3H, s	56.4
2		158.5	1'		107.5
3		117.2	2'		151.6
4		160.8	3'	6.81, 1H, s	108.8
5	6.68, 1H, s	111.1	4'		151.6
6		145.6	5'		138.3
7		nd	6'		138.3
8	4.81, 2H, s	53.8	7'		171.9
9	2.52, 3H, s	21.7	8'	5.69, 2H, s	68.7

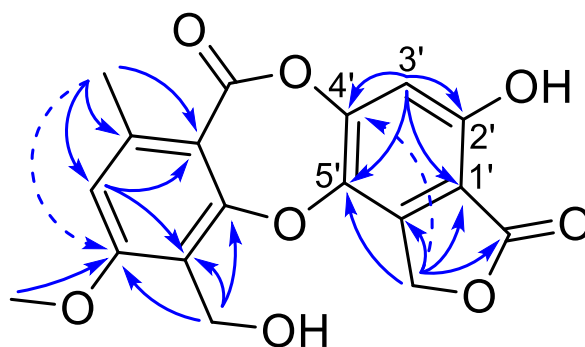


Figure 2. 12 Key HMBC correlations of **US4**

2.3.3.5 Compound **US5**

US5 was obtained as yellow powder. The HRESIMS of **US5** showed a sodiated ion peak at m/z 633.1942, consistent with a molecular formula of $C_{32}H_{34}O_{12}$ verifying the presence of 18 double-bond equivalents. Owing to molecular formula requirements and 16 protons being evident from 1H NMR analysis, one proton was deduced to occur as aliphatic hydroxy group. Altogether, the molecular formula and NMR of **US1** confirmed its homodimeric xanthone. The 1H NMR spectrum of **US5** shows the presence of one chelated hydroxy group (δ_H 12.21), two *ortho* aromatic protons at δ_H 7.48 and 6.58 with the coupling constant of 8.4 Hz, one oxymethine proton (δ_H 3.89, 1H, d, $J = 6.8$ Hz), one methoxy proton (δ_H 3.84, 3H, s), one doublet methyl proton (δ_H 1.11, 1H, d, $J = 6.4$ Hz) and six protons in the high-field range of 1.23-2.98 ppm. The ^{13}C NMR in accordance with the HSQC spectra of **US5** revealed the existence of 16 carbon signals, comprising of one conjugated ketone carbon (δ_C 198.7), one ester carbonyl carbon (δ_C 170.1), two aromatic methine carbons (δ_C 141.1 and 107.6), one methoxy group (δ_C 53.3), three methine carbons (δ_C 36.0, 46.4, and

74.0), two methylene carbons (δ_C 27.3 and 21.5), one methyl group (δ_C 17.7), and five quaternary carbons (δ_C 159.5, 157.3, 117.8, 106.8 and 85.6).

The first spin system was determined as a hexahydroxanthone based on the COSY spectrum which certified the development of a spin system identified as H-5/H-6/(H3-11)/H2-7/H2-8/H-8a. The chemical shift of C-5 (δ_C 74.0) was suggestive of the *ipso* location of an aliphatic hydroxy group. The oxygenated carbon C-10a location of the methyl ester group could be strong-minded from chemical shift value as well as the long-range correlation from both the oxymethine proton at δ_H 3.89 (H-5), the methine proton at δ_H 3.40 (H-8a), and methoxy proton at δ_H 3.70 (H3-13) to C-12 (δ_C 170.2). The HMBC correlations from H-8a to C-9 (δ_C 198.7) defined a chromenone system. The second spin system in this monomer involved two *ortho*-oriented aromatic protons and the connection of this phenyl ring to the γ -pyrone nucleus of hexahydroxanthone could be indicated from long-range heteronuclear correlations from the aromatic protons at δ_H 7.48 (H-3) and at δ_H 6.58 (H-4) to C-4a (δ_C 157.3) and C-9a (δ_C 106.8). A phenol group could be allocated at C-1 as evidenced by HMBC correlations from the phenolic proton at δ_H 11.73 to C-1 (δ_C 159.5), C-2 (δ_C 117.8) and C-9. Due to C-2 being a quaternary carbon, it can be supposed that this specific site is linked to another part of the compound.

The relative configuration of **US5** was recognized by extensive analysis of ^1H NMR (**Table 2.4**) and NOESY correlations (**Figure 2.13**). The coupling constant of H-5 (δ_H 3.89, d, $J = 6.8$ Hz) was inconsistent with the corresponding one reported in

secalonic acid A ($J = 11.3$ Hz) [20] or ergochrome BD ($J = 11.3$ Hz) [23] or bailexanthone ($J = 10.8$ Hz) [17]. In addition, the NOESY correlation of H-5 and H3-11 (**Figure 2.15**) designated the diaxial positions of H-5 and H-6 and further defining the *trans* configuration of 5-OH and H3-11 further sustained by NOESY correlations between the oxymethine proton at δ_{H} 3.89 (H-5) and the methyl group at δ_{H} 1.12 (H3-11).

The absolute assignment of C-5, C-6 was further proposed by the comparison of the NMR data of tetrahydroxanthone hemisecanolic acid monomers, blennolide G, dimeric secalonic B and its C-5 epimer, further supported the assigned *5S*, *6R* configuration [39]. The *antifacial* orientation of ester group at δ_{H} 3.84 (H3-13) and the methine proton at δ_{H} 3.40 (H-8a) with H-5 and H3-11 was supported by the disappearance of NOESY correlation of H-5 or H3-11 to H-8a or H3-13. Moreover, the coupling constants of H-8a (δ_{H} 2.98, t, $J = 4.8$ Hz) in **US1** were inconsistent with those of bailexanthone [17] led to define the equatorial position of H-8a. Furthermore, a negative $n\text{-}\pi^*$ ECD band (315 nm, $\Delta\epsilon = -2.6$) (**Figure 2.14**) determined C-10a *S*, C-10a' *S* configuration and also endorsed the assignment of the other chiral centers based on the relative stereochemistry, consistent with literature data [39]. Thus, the (*5S*, *6R*, *8aS*, *10aS*)-absolute configuration of **US5**, namely eumitrin F, was determined as displayed in **Figure 2.13**.

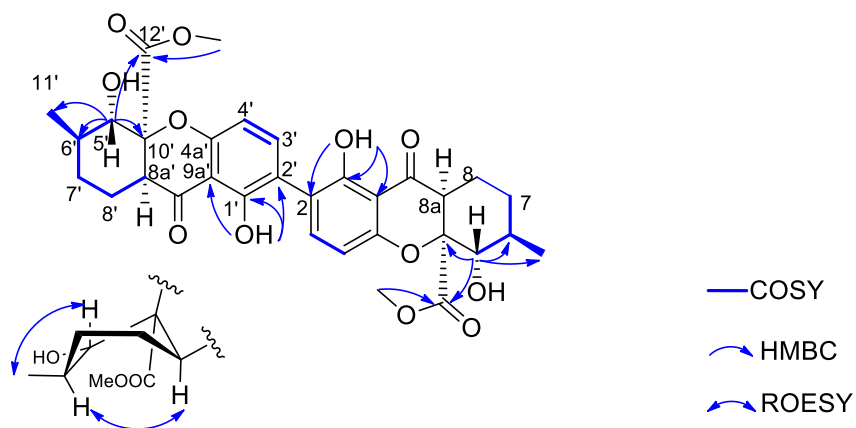


Figure 2. 13 Selected COSY, HMBC, and NOESY correlations of US5

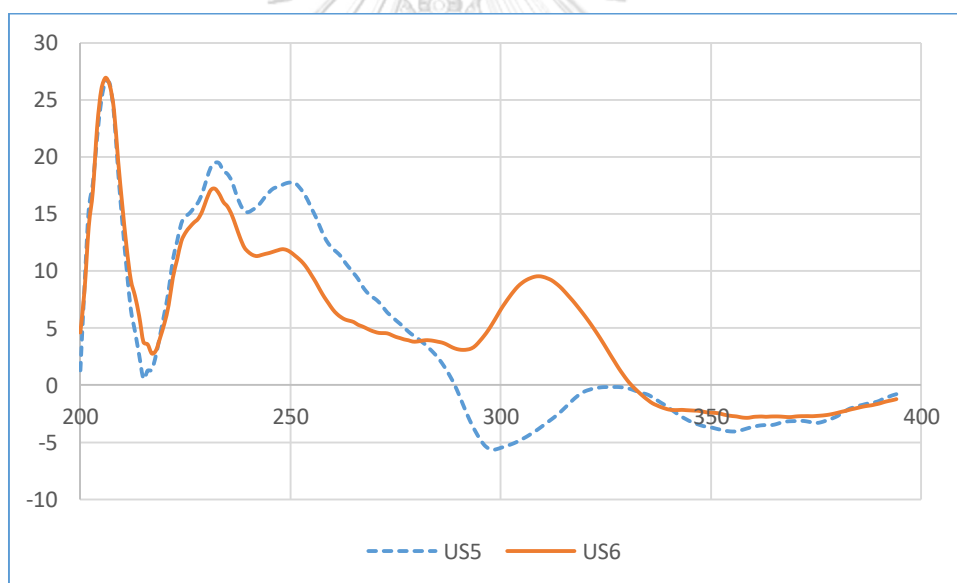


Figure 2. 14 The ECD spectra of US5, US6

Table 2.4 Tentative ^1H (400 MHz) NMR chemical shift assignment for **US5-6** (CDCl_3)

	US5	US6
	δ_{H}, J (Hz)	δ_{H}, J (Hz)
3	7.48, 1H, d, 8.4	7.47, 1H, d, 7.6
4	6.58, 1H, d, 8.4	6.58, 1H, d, 8.4
5	3.89, 1H, d, 6.8	3.89, 1H, d, 6.8
6	2.06, 1H, m	2.07, 1H, m
7	1.83, 1H, m	1.80, 1H, m
	1.29, 1H, m	1.29, 1H, m
8	2.24, 1H, m	2.20, 1H, m
	1.75, 1H, m	1.73, 1H, m
8a	3.40, 1H, s	3.39, 1H, m
11	1.11, 3H, d, 6.8	1.11, 3H, d, 6.6
13	3.84, 3H, s	3.83, 3H, s
1-OH	12.21, 1H, s	12.19, 1H, s
3'	7.48, 1H, d, 8.4	7.49, 1H, d, 8.0
4'	6.58, 1H, d, 8.4	6.62, 1H, d, 8.8
5'	3.89, 1H, d, 6.8	3.73, 1H, d, 10.4
6'	2.06, 1H, m	1.84, 1H, m
	1.83, 1H, m	1.96, 1H, m
7'	1.29, 1H, m	1.23, 1H, m
	2.24, 1H, m	
8'	1.75, 1H, m	2.17, 2H, m
8a'	3.40, 1H, s	2.99, 1H, dd, 11.6, 4.4
11'	1.11, 3H, d, 6.8	1.11, 3H, d, 6.6
13'	3.84, 3H, s	3.68, 3H, s
1'-OH	12.21, 1H, s	11.88, 1H, s

2.3.3.6 Compound US6

US6 was obtained as yellow powder. The HRESIMS of **US6** showed a sodiated molecular ion peak at m/z 633.1922, consistent with a molecular formula of $C_{32}H_{34}O_{12}$. The 1H NMR spectrum showed 30 protons, revealing the occurrence of two supplementary aliphatic hydroxyl groups. The exhaustive analysis of the 2D NMR spectra determined a similar hexahydroxanthone monomeric building unit as in **US5** with the C-2' as a quaternary carbon, a specific site is linked to the other monomeric of compound. As to the other monomeric, the occurrence of the chelated hydroxy group (δ_H 11.88), two *ortho* aromatic protons at δ_H 7.48 and 6.58 with the coupling constant of 8.4 Hz, one oxymethine (δ_H 3.89, 1H, d, $J = 6.8$ Hz), one methoxy (δ_H 3.83, 3H, s), one doublet methyl (δ_H 1.11, 1H, d, $J = 6.6$ Hz) and six protons in the high-field range of 1.23-2.98 ppm, determined the unchanged constitution of rings A, B and C, as further supported by the key correlations outlined in **Figure 2.15** with C-2 is a quaternary carbon for linking. Nonetheless, both methine, methoxy ester, and oxymethine protons were upfield shifted to δ_H 3.39 (H-8a), 3.83 (H3-13), and 3.89 (H-5), respectively, demonstrating the inconsistency of chirality stereochemistry of C-5, C-6, C-8a, and C-10a with those of **US5**.

The magnitude of the vicinal coupling constant of the oxymethine proton H-5 (δ_H 3.89, 1H, d, $J = 6.8$ Hz) determined its axial orientation and thus defined *5R* configuration identical to that of blennolide B to define the structure of this second subunit. Moreover, the *synfacial* orientation of the methyl group, methine proton,

and oxymethine proton was supported by the NOE correlation between H-5' to both of H3-11', and H-8a'. In addition, the coupling constants of H-8a' (δ_{H} 2.98, dd, $J = 11.6, 4.4$ Hz) in **US6** led to define the axial position of H-8a' identical with those of baileyxanthone [17], further supported by the positive $n-\pi^*$ ECD band (325 nm, $\Delta\epsilon = +4.5$) (**Figure 2.14**). Thus, the (5*S*, 6*R*, 8*aS*, 10*aS*, 5'*S*, 6'*R*, 8*aR*, 10*aR*)-absolute configuration of **US6**, namely eumitrin G, was determined as displayed in **Figure 2.15**.

^1H and ^{13}C NMR data of **US6** is presented in **Tables 2.4 and 2.5**.

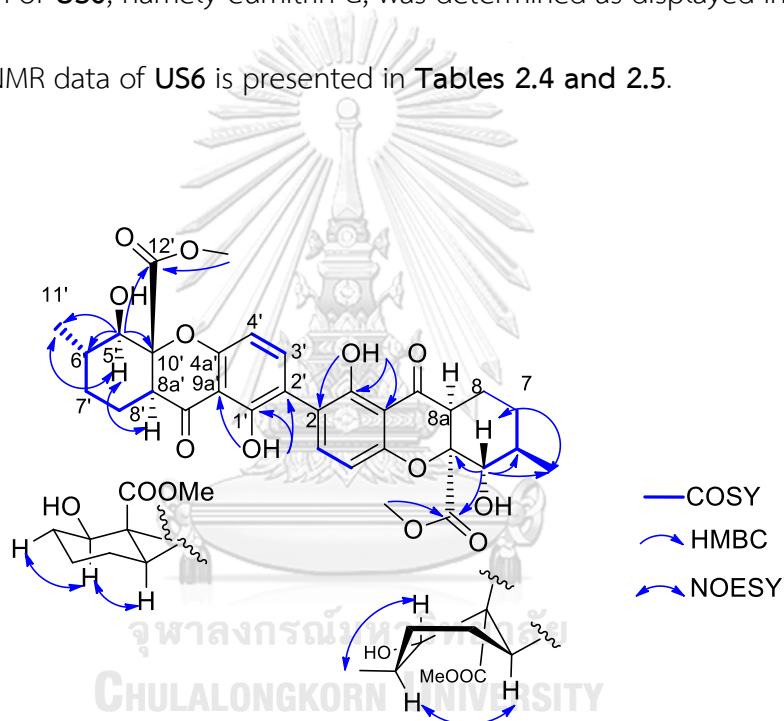


Figure 2.15 Selected COSY, HMBC, and NOESY correlations of **US6**

Table 2.5 Tentative ^{13}C NMR (400 MHz) NMR chemical shift assignment for **US5–6**

No.	US5	US6	No.	US5	US6
	δ_{C}	δ_{C}		δ_{C}	δ_{C}
1	159.5	159.6	1'	159.5	159.0
2	117.8	117.8	2'	117.8	117.6
3	141.1	141.0	3'	141.1	140.4
4	107.6	107.5	4'	107.6	107.4
4a	157.3	157.3	4a'	157.3	159.0
5	74.0	74.0	5'	74.0	80.3
6	36.0	36.0	6'	36.0	34.3
7	27.3	27.2	7'	27.3	31.2
8	21.5	21.4	8'	21.5	20.4
8a	46.4	46.3	8a'	46.4	51.2
9	198.7	198.7	9'	198.7	197.4
9a	106.8	106.8	9a'	106.8	107.6
10	85.6	85.6	10'	85.6	87.6
11	17.7	17.7	11'	17.7	18.4
12	170.1	170.2	12'	170.1	169.3
13	53.3	53.3	13'	53.3	53.0

2.3.3.7 Compound US7

US7 was isolated as light yellow gum. Its molecular formula was determined to be $C_{32}H_{32}O_{13}$ based on the sodiated ion peak at m/z 647.1740 (calcd for $C_{32}H_{32}O_{13}Na$, 647.1741). In spite of the closely related molecular formula, the examination of the 1H and ^{13}C NMR spectra revealed some important structural differences with **US6** including the lack of the methine signals at δ_H 3.40 and the occurrence of a carbonyl carbon δ_C 175.0 (C-8') and a methylene group at δ_H 3.27 (1H, d, $J = 17.5$ Hz) and 3.22 (1H, d, $J = 17.0$ Hz) that could be C-8a' based on the HMBC correlations from the methylene protons at δ_H 3.27 and 3.20 (H2-8a') to C-9' (δ_C 194.1), C-12' (δ_H 169.1), C-10a' (δ_C 84.2) and C-5' (δ_C 82.7), indicated the formation of a β -methyl- γ -lactone moiety as deduced from HMBC correlations of the oxymethine proton at δ_H 4.81 (H-5'), the methine proton at δ_H 2.97 (H-6'), and the diastereotopic methylene protons at δ_H 2.71 and 2.48 (H2-7') to C-8' (δ_C 175.0). The key HMBC correlations from the methylene protons H2-8' to C-5', C-10a' and C-12' also well-defined the connection between the chromone core and both γ -butyrolactone moiety and ester group, as showed in **Figure 2.16**. The planar structure of **US7** was obtained by connecting the two monomeric units *via* the linkage of hexahydroxanthone C-2' and chromanone C-2, supported by the HMBC correlation of the aromatic proton at δ_H 7.53 (H-3) to C-2' (δ_C 117.3) and 7.48 (H-3') to C-2 (δ_C 118.0).

The relative configuration of **US7** was recognized by extensive analysis of ^1H NMR (**Table 2.6**) and NOESY correlations (**Figure 2.16**). In the hexahydroxanthone monomer, the diaxial configuration of H-5 and H-6 was established by the NOE correlation of H-5 (δ_{H} 3.73) to both of H3-11 (δ_{H} 1.12), H-8a (δ_{H} 3.00), (**Figure 2.16**) designated the diaxial positions of H-5 and H-6 as well as the *synfacial* orientation of these substituents while the lack of ROE correlation with the contiguous methyl ester groups ascribed this latter functionality to the other face of the nucleus. Moreover, in the β -methyl- γ -lactone moiety, the oxymethine proton H-5' and the tertiary methine proton H-6', with a coupling constant of 6.5 Hz, specific of *trans*-oriented protons in such ring system [46], as further confirmed by ROE correlation between H-5' and H3-11'. The comparison of the NMR data with those of eumitrin D (**US2**) or versixanthone [41] led to the absolute assignment of C-5', C-6', and C-10a', further supported the assigned C-5'*R*, C-6'*R*, and C-10a'*R* configuration while the absolute assignment of C-5, C-6, C-8a and C-10a were further reinforced by the comparison of the NMR data as well as ECD spectroscopy of eumitrin C-D that further supported the assigned 5*S*, 6*R*, 8a*S*, and 10a*R* configuration. Thus, the (5*S*, 6*R*, 8a*S*, 10a*R*, 5'*R*, 6'*R*, 10a'*R*)-absolute configuration of **US7**, namely eumitrin H, was determined as displayed in **Figure 2.16**. ^1H and ^{13}C NMR data of **US7** is presented in **Tables 2.6 and 2.7**.

Table 2. 6 Tentative ^1H (400 MHz) NMR chemical shift assignment for **US7–9** (CDCl_3)

	US7	US8	US9
	δ_{H}, J (Hz)	δ_{H}, J (Hz)	δ_{H}, J (Hz)
3	7.48, 1H, d, 8.5	7.48, 1H, d, 8.4	7.65, 1H, d, 8.5
4	6.61, 1H, d, 8.5	6.58, 1H, d, 8.4	6.64, 1H, d, 8.5
5	3.73, 1H, d, 10.5	3.88, 1H, d, 13.2	3.74, 1H, d, 11.0
6	1.82, 1H, m	1.81, 1H, m	1.86, 1H, m
7	1.95, 1H, m	2.05, 1H, m	1.95, 1H, m
	1.19, 1H, m	1.29, 1H, M	1.28, 1H, m
8	2.20, 1H, m	2.26, 1H, m	2.19, 2H, m
	2.14, 1H, m	2.18, 1H, m	
8a	3.00, 1H, dd, 11.5, 5.0	3.41, 1H, dd, 7.2, 4.8	3.05, 1H, dd, 11.0, 5.5
11	1.12, 3H, d, 6.5	1.12, 3H, d, 7.2	1.12, 3H, d, 6.5
13	3.77, 3H, s	3.77, 3H, s	3.76, 3H, s
1-OH	11.91, 1H, s	12.21, 1H, s	11.79, 1H, s
3'	7.53, 1H, d, 8.5	7.53, 1H, d, 8.4	7.55, 1H, d, 8.5
4'	6.63, 1H, d, 8.5	6.63, 1H, d, 8.4	6.64, 1H, d, 8.5
5'	4.81, 1H, d, 6.5	4.81, 1H, d, 7.2	4.66, 1H, d, 7.5
6'	2.96, 1H, m	2.98, 1H, m	2.88, 1H, m
7'	2.70, 1H, dd, 8.5, 17.0	2.71, 1H, dd, 8.4, 17.4	2.20, 1H, dd, 8.5, 17.0
	2.48, 1H, dd, 11.5, 17.0	2.48, 1H, dd, 7.8, 17.4	2.28, 1H, dd, 11.5, 17.5
8a'	3.27, 1H, d, 17.5	3.28, 1H, d, 17.4	3.27, 1H, d, 17.5
	3.22, 1H, d, 17.0	3.21, 1H, d, 17.4	3.16, 1H, d, 17.5
11'	1.33, 3H, d, 7.0	1.34, 3H, d, 7.2	1.23, 3H, d, 7.0
13'	3.68, 3H, s	3.84, 3H, s	3.69, 3H, s
1'-OH	11.89, 1H, s	11.92, 1H, s	11.62, 1H, s

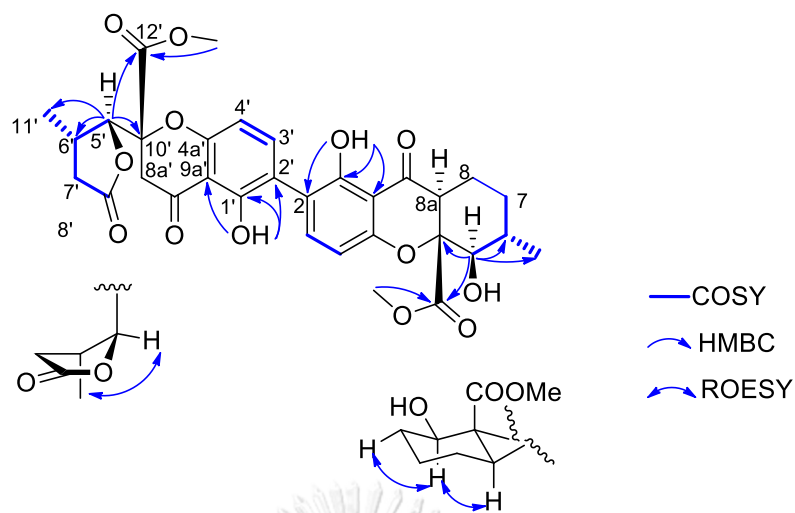


Figure 2. 16 Chemical structure and selected COSY, HMBC, and NOESY correlations of US7.

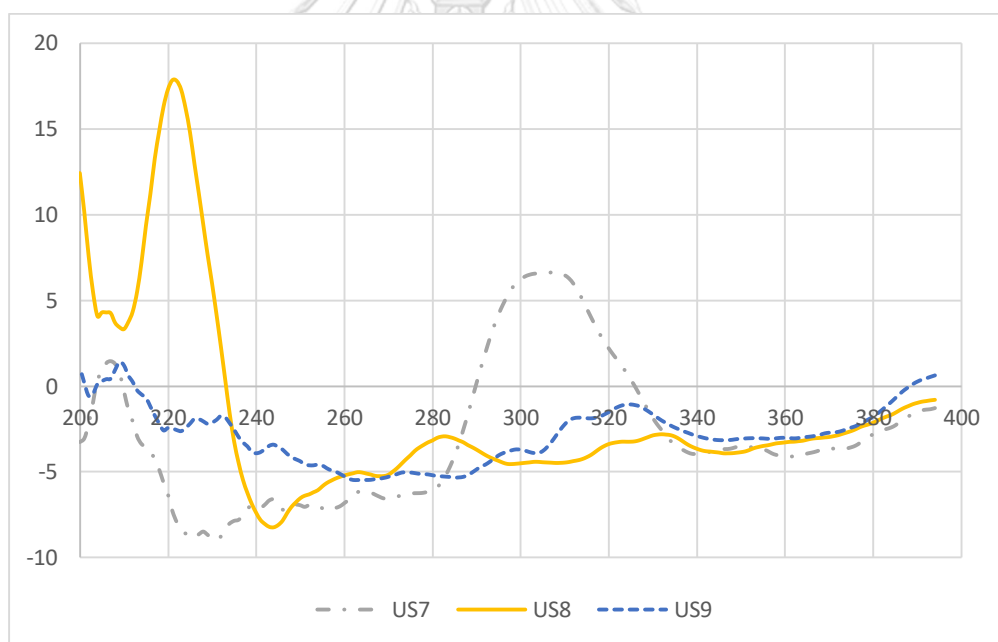


Figure 2. 17 The ECD spectra of US7-9

2.3.3.8 Compound US8

US8 was isolated as light yellow gum. Its molecular formula was determined to be $C_{32}H_{32}O_{13}$ based on the sodiated ion peak at m/z 647.1766 (calcd for

$C_{32}H_{32}O_{13}Na$, 647.1741). The creased resonances in the 1D NMR spectra, especially in the ^{13}C NMR spectrum, suggested that it be dimeric xanthone the same as **US7**. Similarly to **US7**, **US8** was also formed from hexahydroxanthone and chromanone monomers, with the same linkage patterns. The 2–2' linkage of two monomers was established by the HMBC correlation of the aromatic proton at δ_H 7.53 (H-3) to C-2' (δ_C 117.3) and 7.48 (H-3') to C-2 (δ_C 118.0). The examination of the 1H and ^{13}C NMR spectra revealed some important structural differences from **US7** including the lack of the methine signals at δ_H 3.00 and the occurrence of a methine signal at δ_H 3.40, belonging to H-8a implied the opposite stereochemistry at C-8a. Thus, (5*S*, 6*R*, 8a*R*, 10a*S*, 5'*R*, 6'*R*, 10a'*R*)-absolute configuration of **US8**, namely eumitrin I was determined as shown in **Figure 2.18**.

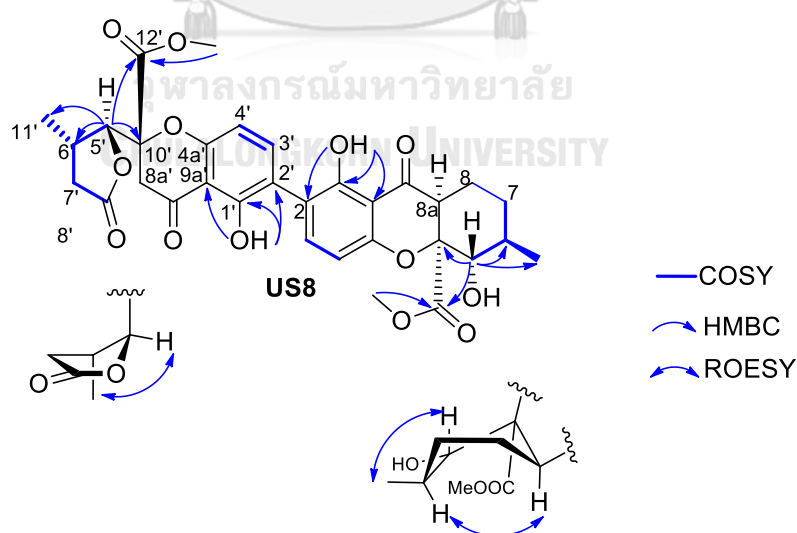


Figure 2. 18 Chemical structure and selected COSY, HMBC, and NOESY correlation of **US8**

2.3.3.9 Compound US9

Similar to **US7**, **US9** was also constructed from hexahydroxanthone and chromanone monomers, with different linkage pattern. In **US9**, namely eumitrin I, the linkage C2-C4' of two monomers was established by HMBC correlations of H-3 to C-4' and of H-3' to C-2, along with 1'-OH to C-2'. However, the negative $n-\pi^*$ ECD band (338 nm, $\Delta\epsilon = -1.5$) (Figure 2.17) incontract with those of **US7** suggested 10a'S configuration as shown in Figure 2.19. ^1H and ^{13}C NMR data of **US9**, namely eumitrin J are displayed in Tables 2.6 and 2.7.

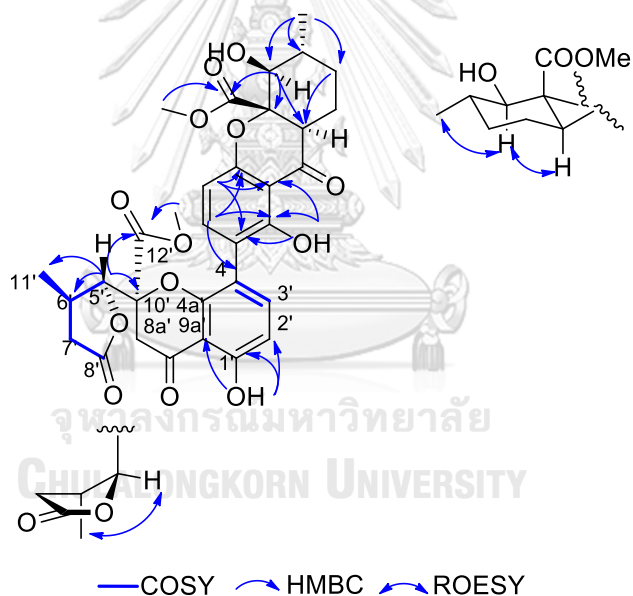


Figure 2. 19 Selected COSY, HMBC, and NOESY correlations of **US9**.

Table 2.7 Tentative ^{13}C NMR chemical shift assignment for **US7-9** (CDCl_3)

No	US7 ^a	US8 ^b	US9 ^a	No.	US7 ^a	US8 ^b	US9 ^a
	δ_{C}	δ_{C}	δ_{C}		δ_{C}	δ_{C}	δ_{C}
1	159.1	159.5	159.4	1'	159.3	159.3	159.1
2	117.4	117.5	117.2	2'	118.1	118.1	110.5
3	140.3	141.0	141.7	3'	141.4	141.4	140.7
4	107.4	107.6	108.1	4'	107.4	107.7	115.5
4a	158.5	158.5	158.7	4a'	159.0	157.4	158.7
5	80.3	74.1	82.5	5'	82.9	82.8	80.1
6	34.2	27.3	34.1	6'	33.6	36.1	34.1
7	31.2	33.7	35.6	7'	36.9	36.9	31.2
8	20.4	21.5	20.4	8'	175.0	175.0	174.8
8a	51.2	46.4	40.1	8a'	39.9	39.9	51.2
9	197.4	198.7	194.1	9'	194.2	194.2	197.7
9a	107.6	106.8	108.0	9a'	107.6	107.5	107.7
10	87.5	85.6	86.0	10'	84.6	84.6	87.7
11	18.5	17.8	14.8	11'	15.0	15.0	18.5
12	169.2	170.1	169.3	12'	169.2	169.2	168.9
13	53.8	53.4	53.0	13'	53.0	53.9	53.8

2.3.3.10 Compound US10

US10 was isolated as light yellow amorphous solid. Its molecular formula was determined to be $C_{34}H_{34}O_{13}$ based on the sodiated ion peak at m/z 689.1824 (calcd for $C_{34}H_{34}O_{14}Na$, 689.1846). In spite of their closely related molecular formulas, the 1H and ^{13}C NMR spectra displayed some important structural differences from **US5** and **US6** including the occurrence of an acetoxycarbonyl group that could be located at C-5' based on the HMBC correlations from both the methyl at δ_H 1.98 (H3-15') and oxygenated methine proton at δ_H 5.02 (H-5') and to C-14' (δ_C 169.0). Moreover, one of the methyl groups was downfield shifted to δ_H 2.16 (H3-11') indicating its aromatic nature, placed at C-3', based on the long-range heteronuclear correlations from these protons to C-2' (δ_C 111.4), C-3' (δ_C 151.2), and C-4' (δ_C 115.9), consistently with the disappearance of an aromatic proton signal and with the singlet status of the aromatic proton at δ_H 6.50 (H-2'). The COSY spectrum as well as the full set of 2J and 3J correlations in the HMBC spectrum revealed the H-5'/H2-6'/H2-7'/H2-8'/H-8a' proton spin system, established the hexahydroxanthone scaffold of the first monomer. The synfacial orientation of the methyl ester groups and of the acetoxycarbonyl was designed from the H3-13'/H3-15' ROE crosspeak while the key ROE effect between the oxymethine proton at δ_H 5.02 (H-5') and the methine proton at δ_H 2.98 (H-8') shown these protons to the other face of the structure. As formerly observed for **US7**, the magnitude of the vicinal coupling

constant of the oxymethine proton H-5' ($J = 11.2, 4.2$ Hz) determined its axial orientation and thus defined 5'*R* configuration identical to that of blennolide B to define the structure of this first subunit as displayed in **Figure 2.20**. The second monomer, subunit II, was highly reminiscent of those of **US5** and **US6**. The most noticeable spectroscopic difference being the intense downfield shift of C-8 and C-8a compared to their homologous positions in the second sub-unit of **US5** (with respective δ_C values of 179.8 and 100.2 vs 21.5 and 46.4 ppm, respectively) that indicated the occurrence of an enolic moiety at these positions. The NMR signal patterns related to this monomer, including COSY and HMBC data, confirmed a similar gross structure of the rest of this subunit, compared to that of **US5**. The HMBC correlations from both of H-2' and H-3 (with respective δ_H value of 6.50 and 7.68) to C-4', the monomeric units linkage was a bone tethering C-2 with C4'.

The axial orientation of H-5', determined a space arrangement identical to that of eumitrin A2 rather than that of eumitrin A1/eumitrin B [19]. However, the ROE correlations between the oxymethine proton at δ_H 4.14 (H-5) and the methyl group at δ_H 1.12 (H3-11') led to the determination of *synfacial* orientation of these substituents, strong-suggested for a (5*R*, 6*S*, 10a*R*, 5'*R*, 8a'*S*, 10a'*R*)-absolute configuration. Moreover, the anticlockwise manner of the two benzoyl chromophores of **US10** as a*S* could be deduced from the negative exciton couplet centered at around 240 nm; consistently with earlier reports on related structures

[47, 48]. Thus, the structure of **US10**, namely eumitrin K, was established as shown in

Figure 2.20. ^1H and ^{13}C NMR data of **US10** is presented in **Tables 2.8** and **2.9**.

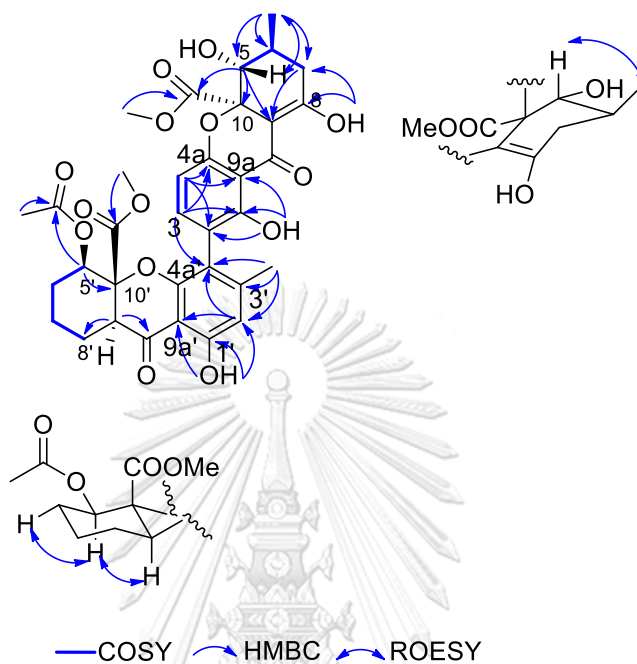


Figure 2. 20 Selected COSY, HMBC, and NOESY correlations of **US10**

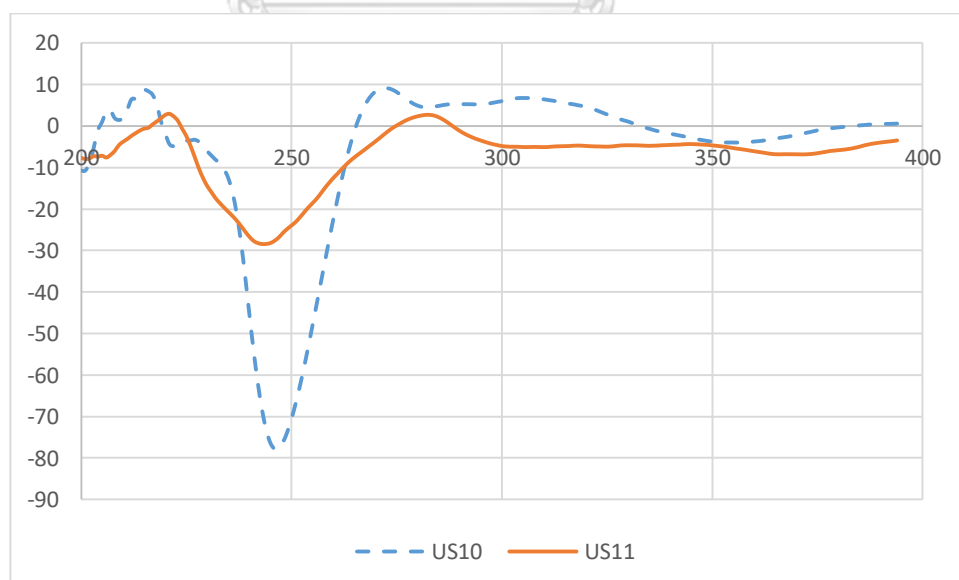


Figure 2. 21 The ECD spectra of **US10-11**

Table 2.8 Tentative ^1H (400 MHz) NMR chemical shift assignment for **US10–11**
(CDCl_3)

	US10	US11
	δ_{H}, J (Hz)	δ_{H}, J (Hz)
3	7.68, 1H, d, 8.4	7.27, 1H, d, 8.0
4	6.58, 1H, d, 8.4	6.61, 1H, d, 8.0
5	4.14, 1H, brs	4.18, 1H, brs
6	2.13, 1H, m	2.18, 1H, m
7	2.55, 1H, dd, 22.8, 11.2	2.54, 1H, dd, 18.4, 11.2
	2.41, 1H, dd, 22.8, 6.0	2.40, 1H, dd, 16.4, 4.0
11	1.19, 3H, d, 6.4	1.19, 3H, d, 6.4
13	3.65, 3H, s	3.70, 3H, s
1-OH	11.62, 1H, s	11.60, 1H, s
8-OH	13.97, 1H, s	-
2'	6.50, 1H, s	6.50, 1H, s
5'	5.02, 1H, dd, 11.2, 4.2	5.44, 1H, brs
6'	1.68, 2H, m	2.01, 2H, m
7'	1.87, 1H, m	2.54, 1H, m
	1.52, 1H, m	2.40, 1H, m
8'	1.87, 1H, m	7.30, 1H, brs
	1.52, 1H, m	
8a'	2.98, 1H, dd, 11.6, 3.6	
11'	2.16, 3H, s	2.08, 3H, s
13'	3.66, 3H, s	3.78, 3H, s
15'	1.98, 3H, s	1.82, 3H, s
1'-OH	11.45, 1H, s	12.01, 1H, s

Table 2.9 Tentative ^{13}C (100 MHz) NMR chemical shift assignment for **US10-11**
(CDCl_3)

No.	US10	US11	No.	US10	US11
	δ_{C}	δ_{C}		δ_{C}	δ_{C}
1	159.4	159.5	1'	161.7	162.3
2	117.9	117.9	2'	111.4	111.4
3	141.5	140.3	3'	151.2	150.5
4	107.6	108.0	4'	115.9	115.8
4a	157.4	157.5	4a'	156.5	156.2
5	71.5	71.5	5'	72.7	66.3
6	28.8	28.7	6'	26.2	23.6
7	32.7	32.8	7'	22.4	22.0
8	179.0	179.7	8'	25.3	141.7
8a	100.2	100.4	8a'	48.7	129.1
9	188.0	188.1	9'	197.5	184.9
9a	107.1	107.2	9a'	104.9	105.8
10	83.4	85.0	10'	85.1	81.0
11	17.6	17.7	11'	21.3	21.3
12	170.1	169.9	12'	171.4	171.4
13	53.2	53.7	13'	53.4	53.8
			14'	169.0	169.2
			15'	20.8	20.5

2.3.3.11 Compound US11

US11 was isolated as yellow oil. The molecular formula $C_{34}H_{32}O_{14}$ was established by the sodiated ion peak at m/z 687.1716 (calcd for $C_{34}H_{34}O_{14}Na$, 687.1690). The examination of the 1H and ^{13}C NMR spectra discovered some important structural differences from **US10** including the lack of the methine proton H-8a and the occurrence of aromatic proton at δ_H 7.30 that indicated the appearance of a $\Delta 8(9)$ double bond, that further supported by COSY correlation spin H-5'/H2-6'/H2-7'/H-8'. Moreover, the appearance of the methine proton H-5' at δ_H 5.44 suggested the similar of C-5' with eumitrin A1 [19]. Additionally, 10aS configuration was identified by the negative $n-\pi^*$ ECD band (327 nm, $\Delta\epsilon = -4.9$) further supported from the comparison with those of **US10**. Moreover, the aS axial chirality of **US11** could be determined based on the negative Exciton couplet at 240 nm similar to **US10**. Thus, the structure of **US11**, eumitrin L, was established as shown in **Figure 2.22**.

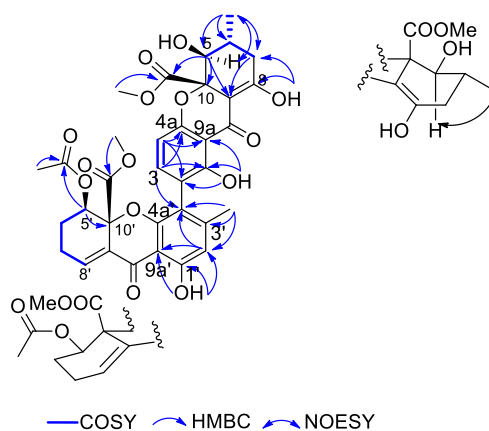


Figure 2.22 Selected COSY, HMBC, and NOESY correlations of **US11**

❖ These newly reported structures of bixanthenes may correspond to the sought-after eumitrins A3 and B2, reported from *U. baileyi* as well, that were named but not yet structurally elucidated, or also to either eumitrin U, X or Y. Nevertheless, since the authors cannot prove that these metabolites match of any of these former descriptions, it was rather decided to name the new dimer xanthenes with unprecedented designations.

2.4 Biological activities

2.4.1 Cytotoxicity and antiparasitic activity

The purified xanthone dimers **US1-3** were evaluated *in vitro* for their antiparasitic activity against the chloroquine-resistant strain of *Plasmodium falciparum* FcB1 and for cytotoxic activity against a panel of 7 representative cell lines. The results are presented in **Table 2.10**.

Table 2.10 IC₅₀ values (μM) of **US1-3** for antiplasmodial and cytotoxic activities tests

compound	<i>P. falciparum</i> FcB1	HuH 7	Caco-2	MDA -MB- 231	HCT11 6	PC3	MDA -MB- 468	MCF7	Fibroblasts
US1	96.5 ± 3.5	> 50	> 50	> 50	> 50	> 50	> 50	> 50	> 50
US2	73.0 ± 1.0	35	44	> 50	> 50	42	> 50	12	> 50
US3	>100	> 50	> 50	> 50	> 50	>50	> 50	>50	> 50
Chloroquine	0.05 ± 0.02	-	-	-	-	-	-	-	-
Roscovitine	-	12.5	17	17	9	11	16	10	> 50
Paclitaxel	-	0.01	0.04	0.02	0.01	0.01	0.01	0.01	> 50
Doxorubicin	-	0.06	0.05	0.03	0.08	0.04	0.04	0.08	> 50

Bisxanthenes **US1-3** revealed weak (**US1-2**) or no (**US3**) antiparasitic activity. For cytotoxicity assays, only **US2** exerted a moderate effect against the tested cell lines. MCF-7 cell line resulted slightly more susceptible with IC_{50} value of 12 μ M. Even though some bisxanthenes, such as the well-known phomoxanthone A [26], were associated with extensive cytotoxicity against a variety of cell lines, bisxanthenes comprising a γ -butyrolactone-related chromanone and a xanthone subunit tethered with either a 2,4'- or 4,2'-linkage were reported to exhibit quite selective potent cytotoxicity with low-micromolar IC_{50} values [41] or even none [58].

2.4.2. Anti-bacterial

Seven isolated bisxanthenes were investigated on antibacterial activity against five bacterial pathogens including *E. coli*, *P. aeruginosa*, *S. aureus*, *B. subtilis*, *C. albicans*.

E. coli can cause serious food poisoning when having contaminated food or drinking fouled water [65]. *P. aeruginosa* is a gram-negative pathogen on human [66, 67] as a multidrug resistant pathogen [68-70]. *S. aureus* is a pathogen found on the skin and in the nose. It is a causative agent of food poisoning, skin infections and hospital-acquired infections [71]. *C. albicans* is the most frequently met pathogenic human fungal species and normally colonizes swarm mucosal and soaking skin surfaces [72], but under conditions of immune dysfunction, it can rapidly conversion

from commensal to pathogen, affecting an group of infections ranging from localized mucosal to severe systemic infections with high morbidity and mortality rates [73-75].

The results of antibacterial activity of seven new isolated compounds were reported as collected in **Table 2.11**.

Table 2.11 MIC values ($\mu\text{g/mL}$) of **US5–11** against *E. coli*, *P. aeruginosa*, *S. aureus*, *B. subtilis*, and *C. albicans*

Sample	MIC ($\mu\text{g/mL}$)				
	<i>E. coli</i> ATCC25922	<i>P. aeruginosa</i> ATCC27853	<i>S. aureus</i> ATCC25923	<i>B. subtilis</i> ATCC6633	<i>C. albicans</i> TISTR
US5	62.5	250	500	62.5	250
US6	125	250	500	62.5	125
US7	450	450	900	450	450
US8	N.i	N.i	N.i	N.i	250
US9	350	350	700	250	250
US10	125	250	500	N.i	250
US11	250	250	125	N.i	250
*Chloramphenicol	9.76	31.25	19.53	4.88	250

N.i: No inhibition

All new bisxanthenes exhibited antibacterial activity, especially **US5** could possibly good activity against *E. coli* and *B. subtilis* (62.5 $\mu\text{g/mL}$ for each bacteria). In addition, **US6**, the same co-structure as **US5** also expressed good activity against *B.*

subtilis (62.5 $\mu\text{g/mL}$), but displayed weaker activity against *E. coli* than those of **US5**, relating to the opposite stereochemistry of C-8a.

This result embarks the interesting point to develop these bioactive compounds as anti-infectious agents.

2.4.3 Enzyme inhibitory

Seven new bixanthonones (**US5-11**) were further studied on α -glucosidase inhibitory and on tyrosinase inhibitory assay. The results are presented in **Table 2.12**.

Table 2.12 IC₅₀ values (μM) of α -glucosidase and tyrosinase of **US5-11**

No.	Compound	IC ₅₀ (μM)	
		α -glucosidase	tyrosinase
1	US5	>200	>200
2	US6	>200	>200
3	US7	>200	148.5 \pm 0.75
4	US8	>200	>200
5	US9	>200	>200
6	US10	83.4 \pm 0.94	>200
7	US11	64.2 \pm 0.51	>200
8	Acabose	93.6 \pm 0.49	>200
9	Kojic acid		36.1 \pm 1.07

All tested compounds exhibited enzyme inhibitory including α -glucosidase and tyrosinase inhibitory. Especially **US10** and **US11** not only showed good activity on α -glucosidase but also better activity than arcabose with IC_{50} values 83.4, 64.2, and 93.6 μ M, respectively. About tyrosinase enzyme, only **US7** exerted a moderate effect with IC_{50} 148 μ M.

2.5 Conclusion

2.5.1 Chemical constituents of lichen *usnea baileyi*

The chemical investigation of *U. baileyi* collected in Lam Dong, Vietnam led to the isolation of eleven new compounds including ten new bisxanthones **US1-3**, **US5-11** and a new depsidone **US4** as shown in **Figure 2.23**. The chemical structures of isolated compounds were elucidated by 1D, 2D NMR, ECD spectroscopy, ECD/DP4 calculation as well as compared to NMR data from the literatures.

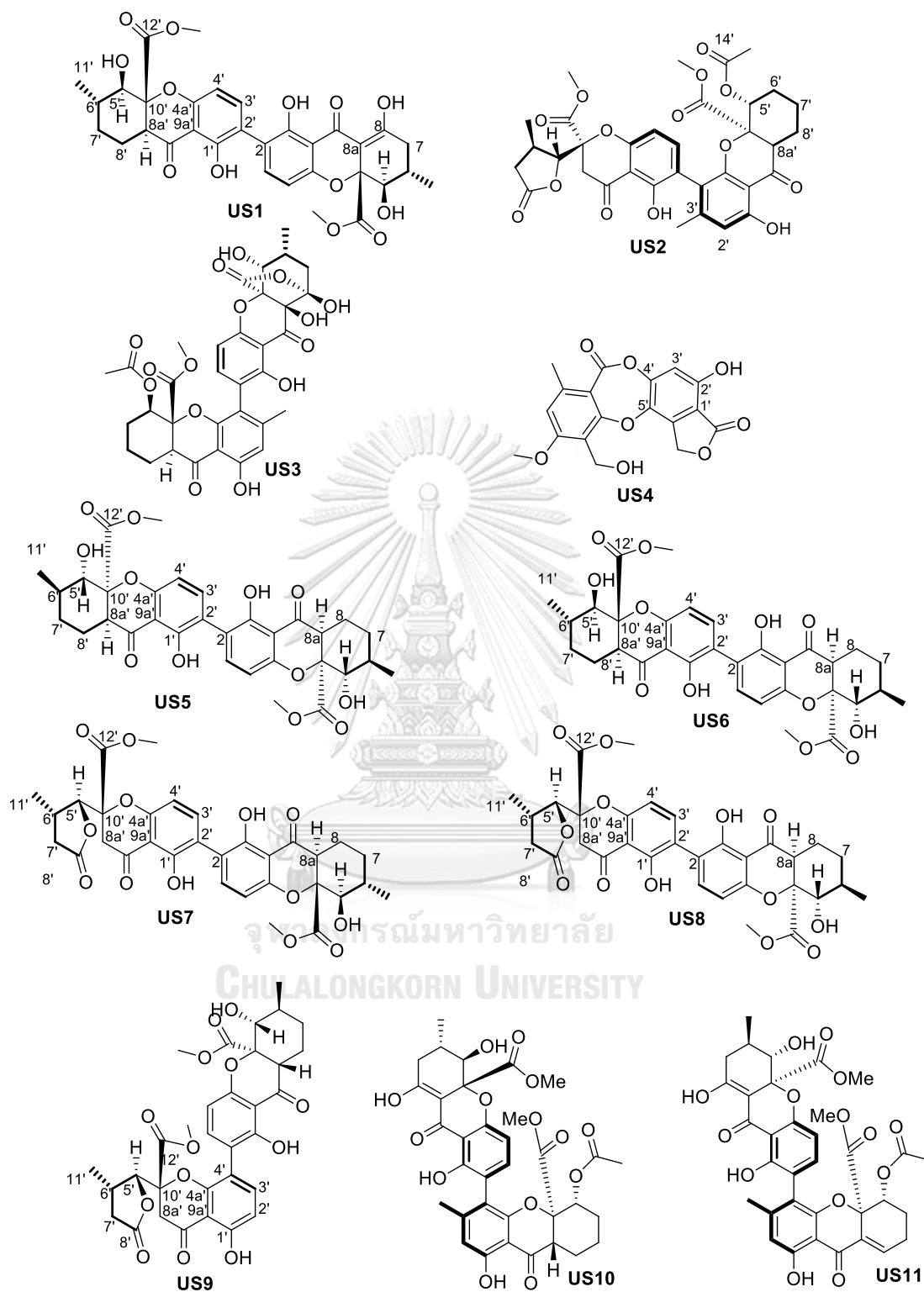


Figure 2. 23 Chemical structures of eleven new compounds US1-11

2.5.2 Biological activities

Ten new bisxanthenes were submitted to test for biological activity including cytotoxicity (only for **US1-3**), antibacterial, and enzyme inhibitory including tyrosinase and α -glucosidase (**US5-11**). In the enzyme inhibitory assays, **US10** and **US11** showed good activity on α -glucosidase with IC_{50} values 83.4 and 64.2, respectively, while **US7** revealed moderate effect on tyrosinase. **US5** and **US6** displayed good activity against *E. coli* with MIC 62.5 $\mu\text{g/mL}$. In addition, **US5** also exhibited good activity against *B. subtilis* (62.5 $\mu\text{g/mL}$). For cytotoxicity, **US2** showed good selectivity against tested cell lines with the highest activity against MCF7 of 12 μM .



Chapter 3

SYNTHESIS OF USNIC ACID DERIVATIVES AND THEIR ENZYME INHIBITORY ACTIVITY

3.1 Introduction

Usnic acid (C₁₈H₁₆O₇), a natural dibenzofuran which is a major constituent in *U. baileyi* exhibited anti-Gram positive bacteria [9], antiviral, anti-protozoal, anti-proliferative, anti-inflammatory, analgesic activity [76], and strong cytotoxicity on human cell lines [6, 9] (**Table 3.1**).

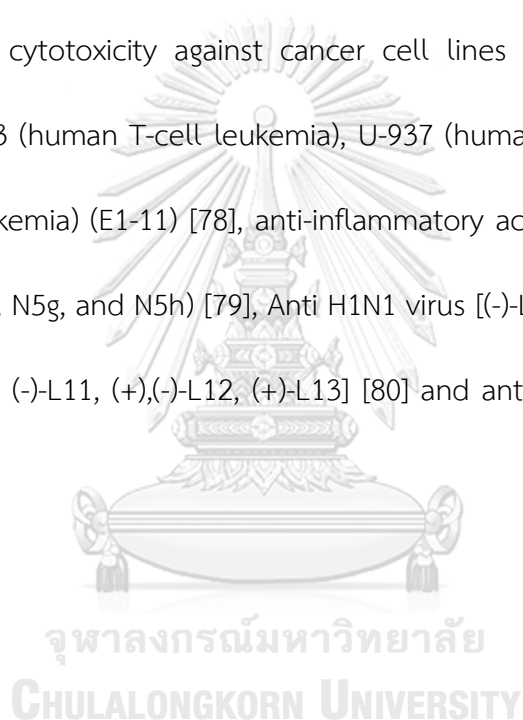
Table 3.1 Biological activities of usnic acid [6, 8, 9, 76]

Antimicrobial activity	Gram positive bacteria	<i>Enterococcus faecalis</i> , <i>Enterococcus faecium</i> , <i>Staphylococcus aureus</i> , <i>Streptococcus mutans</i> , <i>Streptococcus pyogenes</i> .
	Anaerobic bacteria	<i>Bacteroides fragilis</i> , <i>Bacteroides ruminicola</i> ssp. <i>brevis</i> , <i>Bacteroides thetaiotaomicron</i> , <i>Bacterioides vulgatus</i> , <i>Clostridium perfringens</i> , <i>Propionibacterium acnes</i> .
	Mycobacteria	<i>M. aurum</i> , <i>M. avium</i> , <i>M. smegmatis</i> , <i>M. tuberculosis</i> var. <i>bovis</i> , <i>M. tuberculosis</i> var. <i>hominis</i> .
Antiviral activity	(+) - usnic acid: inhibit herpes simplex type 1 and polio type 1 viruses, and <i>Epstein-Barr</i> virus.	
Antiproliferative activity	(-) - usnic acid: exhibit P388 leukaemia, L1210 cells. (+) - usnic acid: inhibit K-562 leukemic, endometrial carcinoma cell lines, against HaCaT.	
Cytotoxicity	Cytotoxic activity on cancer cell lines: 3LL, L1210, DU145, MCF7, K-562, U251, MDA-MB-231, H1299. Significant cytotoxicity against MM98 malignant mesothelioma cells, A431 vulvar carcinoma cells.	

However, the use of usnic acid in cytotoxicity treatment was limited because of its water insolubility. Thus, the synthesis of usnic acid derivatives to enhance their utilization is an interesting research.

3.1.1 Usnic acid, usnic acid derivatives and biological activities

Lately, many pharmacological aspects of usnic derivatives have been explored (**Figure 3.1**). Usnic acid derivatives showed a wide range of biological activities such as cytotoxicity against cancer cell lines (**A1-9**) [77] against L1210 (leukemia), CEM-13 (human T-cell leukemia), U-937 (human monocyte tumor), MT-4 (human T-cell leukemia) (E1-11) [78], anti-inflammatory activity (N2a, N2b, N3a, N3b, N4f, N4g, N4h, N5f, N5g, and N5h) [79], Anti H1N1 virus [(-)-L1, (+)-L3, (+)-L4, (+)-L5a, (-)-L6, (+)-L7, (+)-L8, (-)-L11, (+),(-)-L12, (+)-L13] [80] and antiproliferative activities (2D-53D) [81].



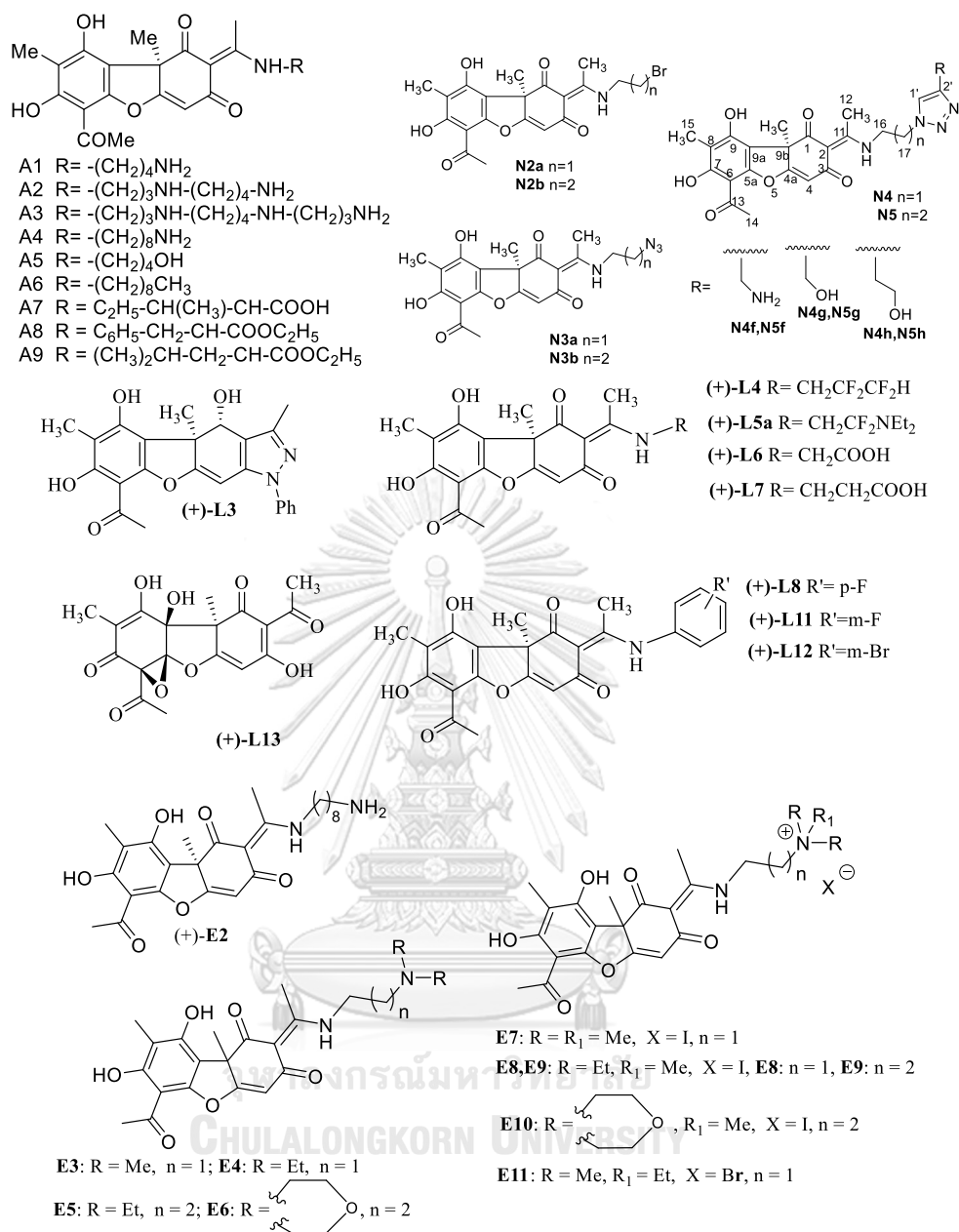
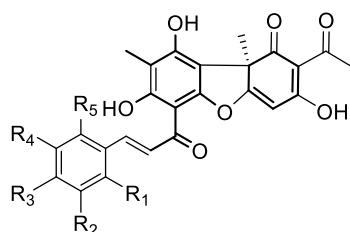
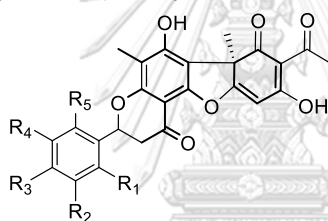


Figure 3. 1 Reported usnic derivatives



- 2D:** R₁= H, R₂= H, R₃=H, R₄= H, R₅= H
4D: R₁= H, R₂= H, R₃=Cl, R₄= H, R₅= H
5D: R₁= H, R₂= Cl, R₃=H, R₄= H, R₅= H
7D: R₁= Cl, R₂= H, R₃=Cl, R₄= H, R₅= H
9D: R₁= Cl, R₂= H, R₃=H, R₄= H, R₅= Cl
11D: R₁= H, R₂= Cl, R₃=H, R₄= Cl, R₅= H
13D: R₁= H, R₂= H, R₃=F, R₄= H, R₅= H
15D: R₁= F, R₂= H, R₃=H, R₄= H, R₅= H
16D: R₁= H, R₂= F, R₃=H, R₄= H, R₅= H
17D: R₁= F, R₂= H, R₃=H, R₄= H, R₅= F
18D: R₁= H, R₂= F, R₃=H, R₄= F, R₅= H
19D: R₁= H, R₂= H, R₃=Br, R₄= H, R₅= H
20D: R₁= H, R₂= H, R₃= COOH, R₄= H, R₅= H
22D: R₁= H, R₂= H, R₃= CH₃, R₄= H, R₅= H
24D: R₁= H, R₂= H, R₃= tBU, R₄= H, R₅= H
26D: R₁= H, R₂= H, R₃= OMe, R₄= H, R₅= H
28D: R₁= H, R₂= OMe, R₃= OMe, R₄= OMe, R₅= H
29D: R₁= H, R₂= OMe, R₃= OMe, R₄= H, R₅= H
30D: R₁= H, R₂= H, R₃= OEt, R₄= H, R₅= H
32D: R₁= OEt, R₂= H, R₃= H, R₄= H, R₅= H
34D: R₁= H, R₂= H, R₃= OBU, R₄= H, R₅= H
36D: R₁= H, R₂= H, R₃= ⁱPent, R₄= H, R₅= H
37D: R₁= H, R₂= H, R₃= SMe, R₄= H, R₅= H
38D: R₁= H, R₂= H, R₃= SEt, R₄= H, R₅= H
39D: R₁= H, R₂= H, R₃= Ph, R₄= H, R₅= H
40D: R₁= H, R₂= H, R₃= 4-F-Ph, R₄= H, R₅= H
41D: R₁= H, R₂= H, R₃= OPh, R₄= H, R₅= H
43D: R₁= H, R₂= H, R₃= O-4-F-Ph, R₄= H, R₅= H
45D: R₁= H, R₂= H, R₃= O-2-Cl-5-F-Ph, R₄= H, R₅= H
47D: R₁= H, R₂= CF₃, R₃= H, R₄= H, R₅= H
48D: R₁= H, R₂= H, R₃= CF₃, R₄= H, R₅= H
50D: R₁= H, R₂= CF₃, R₃= H, R₄= CF₃, R₅= H
52D: R₁= H, R₂= H, R₃= OCF₃, R₄= H, R₅= H



- 3D:** R₁= H, R₂= H, R₃=H, R₄= H, R₅= H
6D: R₁= H, R₂= Cl, R₃=H, R₄= H, R₅= H
8D: R₁= Cl, R₂= H, R₃=Cl, R₄= H, R₅= H
10D: R₁= Cl, R₂= H, R₃=H, R₄= H, R₅= Cl
14D: R₁= H, R₂= H, R₃=F, R₄= H, R₅= H
21D: R₁= H, R₂= H, R₃= COOH, R₄= H, R₅= H
23D: R₁= H, R₂= H, R₃= CH₃, R₄= H, R₅= H
25D: R₁= H, R₂= H, R₃= tBU, R₄= H, R₅= H
27D: R₁= H, R₂= OMe, R₃= H, R₄= H, R₅= H
31D: R₁= H, R₂= H, R₃= OEt, R₄= H, R₅= H
33D: R₁= OEt, R₂= H, R₃= H, R₄= H, R₅= H
35D: R₁= H, R₂= H, R₃= OBU, R₄= H, R₅= H
42D: R₁= H, R₂= H, R₃= OPh, R₄= H, R₅= H
44D: R₁= H, R₂= H, R₃= O-4-F-Ph, R₄= H, R₅= H
46D: R₁= H, R₂= H, R₃= O-2-Cl-5-F-Ph, R₄= H, R₅= H
49D: R₁= H, R₂= H, R₃= CF₃, R₄= H, R₅= H
53D: R₁= H, R₂= H, R₃= OCF₃, R₄= H, R₅= H

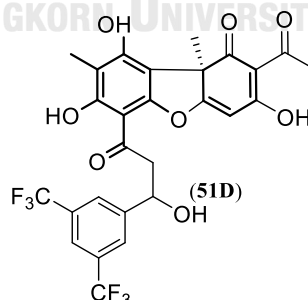
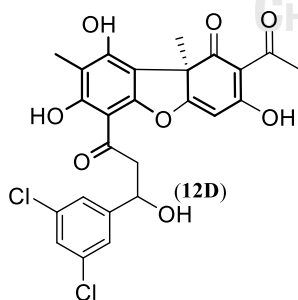


Figure 3.1 Reported usnic derivatives (continued)

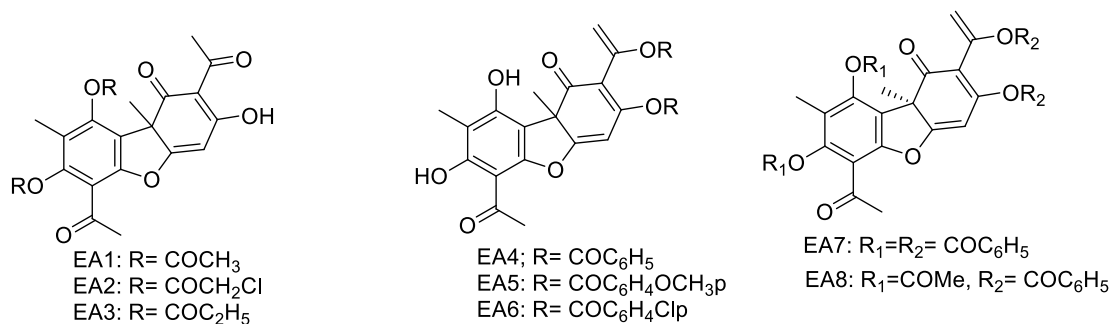


Figure 3.1 Reported usnic derivatives (continued)

Moreover, the esterification between usnic acid and acyl chlorides including acetyl, chloroacetyl, proionyl, benzoyl, 4-methoxybenzoyl, and 4-chlorobenzoyl chlorides to yield ester/vinyl ester derivatives (**EA1-8**) [82] was reported only for chemical transformation without biological activity evaluation. Thus, these derivatives are interesting to be re-synthesized for evaluating biological activities.

3.1.2 Objectives

Usnic acid derivatives were synthesized from esterification and oxidation reaction with full structural characterization through spectroscopic means. The evaluation on enzyme inhibitory including α -glucosidase and tyrosinase inhibition of those synthesized compounds was carried out.

3.2 Experimental

3.2.1 Instrument and equipment

All solvents used in this research were distilled prior to use except those which were reagent grades. 1D and 2D NMR spectra were acquired using a Bruker

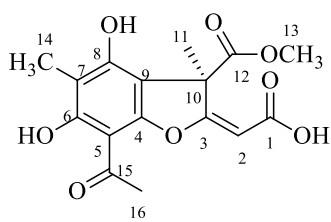
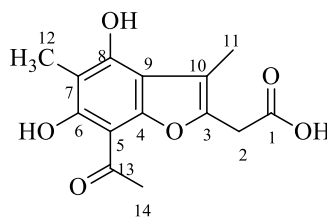
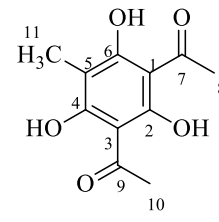
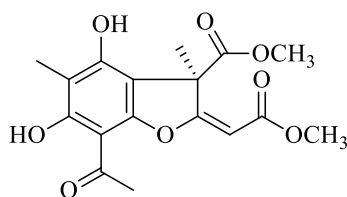
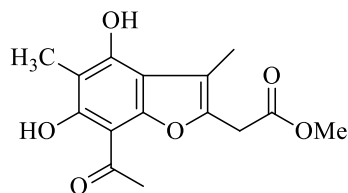
Advance 400 MHz, a Bruker AM-500 MHz or a JNM-ECA 600 MHz (JEOL, Tokyo, Japan) spectrometer. Chemical shifts are referenced to the residual solvent signal (CDCl_3 : δ_{H} = 7.26, δ_{C} = 77.1). HRESIMS data were recorded using a Bruker MicroTOF Q-II mass or MALDI-TOF-MS (SHIMADZU AXIMA-Resonance) spectrometer. Open-column chromatography separations were performed on silica gel (40-63 μm , Himedia). TLC analyses were carried out on precoated silica gel 60 F254 or silica gel 60 RP-18 F254S plates (Merck), and spots were visualized by spraying with 10% H_2SO_4 solution followed by heating.

3.2.2 General procedure

3.2.2.1 Dakin Oxidation of usnic acid

(+)-Usnic acid [$[\alpha]_{\text{D}}^{25} + 487.4$ (c 0.02, CHCl_3)], (1.0 g, 1.9 mmol) and K_2CO_3 (1.6 g, 11.6 mmol) were dissolved in MeOH (200 μL). 890 μL of H_2O_2 30% (8.7 mmol) was added while stirring at room temperature for 10 h. The reaction was quenched by adding acidic solution, HCl 1 M followed by extraction with EtOAc: H_2O (1:1) (v/v) 3 times and evaporated under vacuum. The purification using chromatography was proceeded using CH_2Cl_2 :EtOH: H_2O (8:0.2:0.01) to obtain the desired derivatives, **UD1-**

5.

**UD1****UD3****UD5****UD2****UD4**

UD1 Light yellow powder, yield: 25.2%; ^1H NMR (acetone- d_6 , 500 MHz) δ_{H} 13.52 (1H, s), 5.82 (1H, s), 3.57 (3H, s), 2.63 (3H, s), 1.95 (3H, s), 1.74 (3H, s). ^{13}C NMR (acetone- d_6 , 125 MHz) δ_{C} 200.9, 174.7, 169.0, 166.7, 162.4, 157.9, 154.7, 108.3, 105.9, 99.8, 96.7, 54.1, 52.2, 30.9, 19.9, 7.9. HRESIMS m/z [M-H] calcd for $\text{C}_{16}\text{H}_{15}\text{O}_8$: 335.0767; found 335.0797.

UD2: Light yellow powder, yield: 2.4%; ^1H NMR (CDCl_3 , 500 MHz) δ_{H} 13.33 (1H, s), 5.89 (1H, s), 3.76 (3H, s), 3.73 (3H, s), 2.69 (3H, s), 2.05 (3H, s), 1.93 (3H, s). ^{13}C NMR (CDCl_3 , 125 MHz) δ_{C} 201.4, 179.8, 172.1, 165.2, 163.5, 156.8, 151.1, 109.2, 103.6, 100.1, 96.8, 61.8, 53.9, 51.7, 31.4, 21.6, 7.4. HRESIMS m/z [M-H] calcd for $\text{C}_{17}\text{H}_{17}\text{O}_8$: 349.0923; found 349.0945.

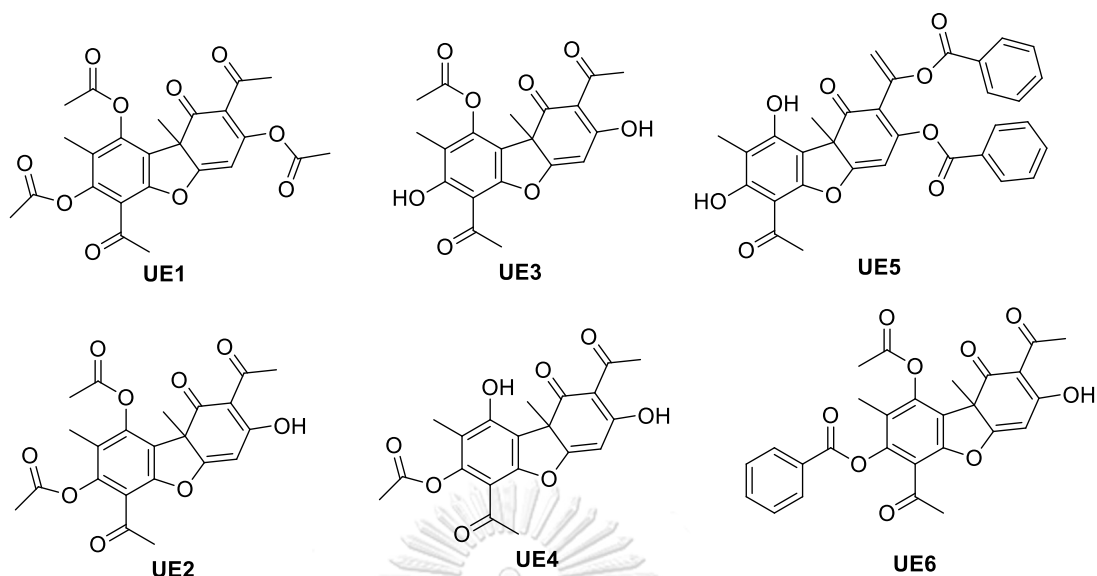
UD3: Light yellow powder, yield: 15.0%; ^1H NMR (CDCl_3 , 500 MHz) δ_{H} 13.33 (1H, s), 3.80 (2H, s), 2.72 (3H, s), 2.32 (3H, s), 2.14 (3H, s). ^{13}C NMR (CDCl_3 , 125 MHz) δ_{C} 201.3, 170.6, 163.2, 157.5, 154.3, 145.4, 113.4, 112.3, 105.8, 102.2, 32.3, 30.9, 9.8, 7.8.

UD4 : Light yellow powder, yield: 1.0%; ^1H NMR (CDCl_3 , 500 MHz) δ_{H} 13.78 (1H, s), 3.77 (2H, s), 3.77 (3H, s), 2.79 (3H, s), 2.36 (3H, s), 2.15 (3H, s). ^{13}C NMR (CDCl_3 , 125 MHz) δ_{C} 201.1, 169.8, 162.3, 154.8, 153.8, 143.3, 112.9, 110.6, 104.4, 102.2, 52.6, 32.2, 31.1, 9.8, 7.1.

UD5 : Light yellow powder, yield: 1.2%; ^1H NMR (CDCl_3 , 500 MHz) δ_{H} 2.72 (6H, s, 2XCH₃), 2.06 (3H, s). HRESIMS m/z [M-H] calcd for $\text{C}_{24}\text{H}_{23}\text{O}_{10}$: 223.0606; found 223.0627.

3.2.2.2 Acetylation and benzylation of usnic acid

A mixture of (+)-usnic acid (0.25 g, 0.725 mmol) in CHCl_3 (5 mL) was stirred at room temperature for 5 minutes. Acetyl chloride (4.35 mmol) was added, followed by pyridine (4.35 mmol) and stirred at room temperature for 6 h. Then, the organic layer was extracted with water and saturated aqueous NaHCO_3 , respectively, and dried over anhydrous Na_2SO_4 , filtered, and evaporated using rotatory vacuum evaporator. The products, **UE1-4** were purified by subjecting to silica gel column. Moreover, benzoyl chloride was also used for esterification with usnic acid and **UE3** to yield **UE5** and **UE6**, respectively.



UE1: Light yellow powder, yield: 10.4%; ^1H NMR (CDCl_3 , 400 MHz) δ_{H} 6.38 (1H, s), 2.65 (3H, s), 2.40 (3H, s), 2.35 (3H, s), 2.23 (3H, s), 2.22 (3H, s), 2.19 (3H, s), 2.02 (3H, s). ^{13}C NMR (CDCl_3 , 100 MHz) δ_{C} 203.0, 202.9, 195.0, 169.1x2, 168.4, 151.2, 147.8, 145.7, 145.5, 144.5, 121.5, 120.3, 115.5, 113.7, 108.5, 47.0, 31.8, 29.5, 21.1, 20.7, 20.5, 9.7, 9.1. HRESIMS m/z $[\text{M}+\text{H}]$ calcd for $\text{C}_{24}\text{H}_{23}\text{O}_{10}$: 471.1291; found 471.1297

UE2: Light yellow powder, yield: 15.2%; ^1H NMR (CDCl_3 , 400 MHz) δ_{H} 13.22 (1H, s), 5.91 (1H, s), 2.74 (3H, s), 2.54 (3H, s), 2.45 (3H, s), 2.03 (3H, s), 1.78 (3H, s). ^{13}C NMR (CDCl_3 , 100 MHz) δ_{C} 201.9, 198.4, 193.3, 190.9, 178.1, 168.6, 163.3, 155.7, 151.5, 117.7, 111.1, 106.3, 105.4, 98.8, 59.4, 32.0, 31.2, 26.0, 21.4, 9.3.

UE3: Light yellow powder, yield: 34.0%; ^1H NMR (CDCl_3 , 400 MHz) δ_{H} 5.90 (1H, s), 2.60 (3H, s), 2.54 (3H, s), 2.46 (3H, s), 2.33 (3H, s), 1.99 (3H, s), 1.82 (3H, s). ^{13}C NMR (CDCl_3 , 100 MHz) δ_{C} 198.6, 195.0, 192.8, 190.9, 177.8, 168.9, 168.8, 153.7, 149.0, 148.5, 123.6, 118.9, 116.1, 106.2, 98.8, 59.5, 32.1, 31.1, 26.2, 21.4, 20.8, 10.4.

UE4: Light yellow powder, yield: 17.5%; ^1H NMR (CDCl_3 , 400 MHz) δ_{H} 11.97 (1H, s), 5.97 (1H, s), 2.66 (3H, s), 2.57 (3H, s), 2.35 (3H, s), 2.06 (3H, s), 1.80 (3H, s). ^{13}C NMR (CDCl_3 , 100 MHz) δ_{C} 202.0, 197.8, 194.0, 191.8, 179.3, 169.2, 155.5, 154.2, 149.7, 117.4, 110.0, 105.4, 98.5, 59.1, 32.4, 32.0, 28.0, 20.9, 9.0.

UE5: Light yellow powder, yield: 80.6%; ^1H NMR (CDCl_3 , 400 MHz) δ_{H} 13.32 (1H, s), 10.52 (1H, s), 8.50-7.00 (10H, m), 6.04 (1H, s), 5.43 (1H, d, 1.2), 5.24 (1H, d, 1.2), 2.65 (3H, s), 2.12 (3H, s), 1.88 (3H, s). ^{13}C NMR (CDCl_3 , 100MHz) δ_{C} 201.0, 200.5, 174.0, 165.1, 164.5, 164.0, 163.0, 157.5, 156.4, 143.5, 134.6, 133.7, 133.6, 130.7, 130.3, 130.1, 129.1, 128.9, 128.6, 128.5, 128.0, 114.6, 109.8, 109.2, 104.0, 101.9, 96.6, 60.7, 31.3, 31.1, 7.7.

UE6: Light yellow powder, yield: 70.9%; ^1H NMR (CDCl_3 , 600 MHz) δ_{H} 8.18 (2H, m), 7.66 (1H, m), 7.53 (2H, m), 5.92 (1H, s), 2.60 (3H, s), 2.56 (3H, s), 2.49 (3H, s), 2.04 (3H, s), 1.85 (3H, s). ^{13}C NMR (CDCl_3 , 150 MHz) δ_{C} 202.6, 198.7, 195.0, 190.9, 177.9, 168.9, 164.6, 153.5, 148.9, 148.5, 134.2, 130.6, 128.9, 128.7, 119.1, 116.7, 114.5, 114.0, 98.9, 59.6, 32.0, 29.9, 26.2, 21.5, 10.6. HRESIMS m/z $[\text{M}+\text{Na}]$ calcd for $\text{C}_{27}\text{H}_{22}\text{O}_9\text{Na}$: 513.1162; found 513.1122.

3.3 Results and discussion

3.3.1 Isolation and elucidation usnic acid derivatives via Dakin oxidation

The Dakin oxidation of usnic acid yielded 5 products, namely **UD1-5**. Among them, novel structures of **UD1-2** were elucidated by 1D, 2D NMR, and HRESIMS

spectroscopy, while the known products **UD3-5** were readily confirmed on the basis of ^1H and ^{13}C NMR spectra or HRESIMS (**UD5**).

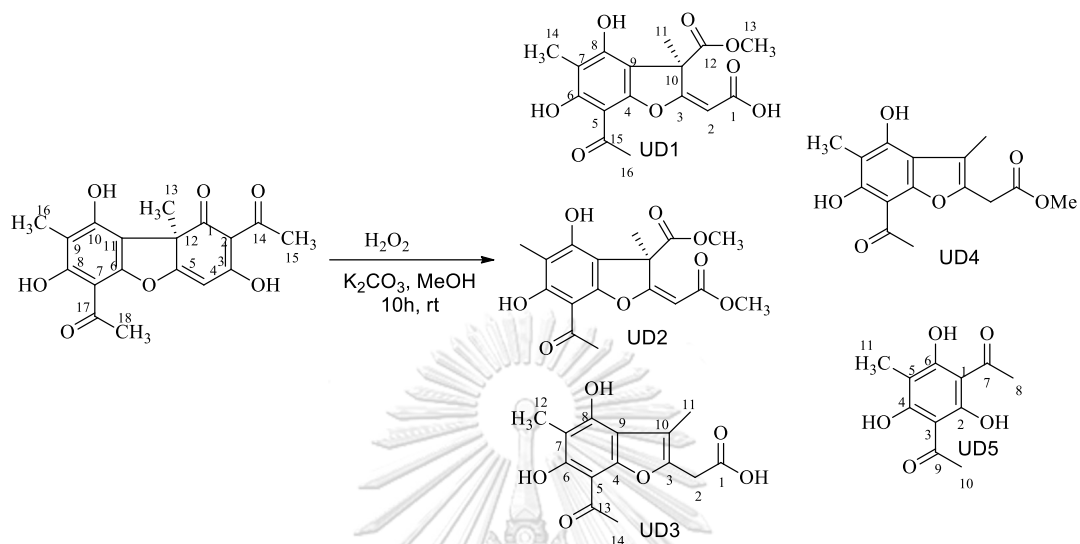


Figure 3. 2 Dakin oxidation of usnic acid

After purification by silica gel column, the desired products were obtained as shown in **Table 3.2**.

Table 3.2 The yields and characteristics of oxidation analogues of usnic acid (**UD1-5**)

oxidation analogues	Appearance	% Yield	Remarks
UD1	White powder	25.2	Novel
UD2	White powder	2.4	Novel
UD3	Brown powder	15.0	Known
UD4	Brown powder	1.0	Known
UD5	White powder	1.2	Known

3.3.2 Characterization of the products from Dakin oxidation of usnic acid

3.3.2.1 Compound UD1

The ^1H NMR spectrum of **UD1** showed a singlet of hydroxy chelated signal at δ_{H} 13.52, an olefin proton at δ_{H} 5.82, one methoxy group at δ_{H} 3.57, and three methyl groups at δ_{H} 2.63, 1.95 and 1.74 ppm. The ^{13}C NMR spectrum of **UD1** showed sixteen carbon signals, including one ketone carbon at δ_{C} 200.9 ppm, two carboxyl carbons at δ_{C} 174.7 and 169.0, eight olefin carbons in the range of δ_{C} 165.0-99.0, one methoxy carbon at δ_{C} 52.2 representing $-\text{COOMe}$, one tertiary carbon at δ_{C} 54.1 and three methyl groups at δ_{C} 30.8, 19.9, and 7.9. According to HSQC and HMBC spectroscopy, signals at δ_{H} 13.52, 5.82, 1.95, and 7.9 ppm representing 6-OH, H-2, H3-14, and H3-11 respectively, indicated the maintaining of starting material benzofuran which was further supported by comparison with those of usnic acid [17]. ^1H and ^{13}C NMR of **UD1** were distributed in **Table 3.3**.

Table 3.3 Tentative 1D NMR (400 MHz) chemical shift assignment for **UD1-2** (CDCl₃)

	UD1		UD2	
	δ_{H}	δ_{C}	δ_{H}	δ_{C}
1		166.7		165.2
2	5.82, 1H, s	96.7	5.89, 1H, s	96.8
3		174.7		179.8
4		154.7		151.1
5		99.8		100.1
6		162.4		163.5
7		105.9		103.6
8		157.9		156.8
9		108.3		109.2
10		54.1		53.9
11	1.74, 3H, s	19.9	1.93, 3H, s	21.6
12		169.0		172.1
13	3.57, 3H, s	52.2	3.76, 3H, s	51.7
14	1.95, 3H, s	7.86	2.05, 3H, s	7.4
15		200.9		201.4
16	2.63, 3H, s	30.9	2.69, 3H, s	31.4
1-OMe			3.73, 3H, s	61.8
6-OH	13.52, 1H, s		13.33, 1H, s	

The lack of 10-OH and H3-15 in usnic acid indicated the oxidation reaction occurred at C-1 and C-4, further supported by the correlation from both H3-11 and H3-13 (δ_{H} 3.57) to C-1 (δ_{C} 169.0) and from H-4 to C-1 (δ_{C} 174.7). Thus, the structure of **UD1** is elucidated as shown in **Figure 3.2**.

3.3.2.2 Compound UD2

The examination of the ^1H and ^{13}C NMR spectra revealed some important structural differences from **UD1** including the occurrence of a methoxy group that could be located at C-1 based on the HMBC correlations from the methoxy protons at δ_{H} 3.73 to C-1 (δ_{C} 166.2). Thus, the structure of **UD2** is a methyl ester of **UD1**.

3.3.2.3 Compound UD3

The ^1H NMR spectrum of **UD3** showed a singlet hydroxy chelated signal at δ_{H} 13.85, one methylene group at δ_{H} 3.80, and three methyl groups at δ_{H} 2.72, 2.33 and 2.14 ppm. The ^{13}C NMR spectrum of **UD4** exhibited sixteen carbon signals, including one ketone carbon at δ_{C} 201.3, one carboxyl carbon at δ_{C} 170.6, eight olefin carbons in the range of δ_{C} 165.0-102.0, one methylene carbon at δ_{C} 32.3, and three methyl groups at δ_{C} 30.9, 9.8, and 7.8. Compared **UD3** with those of usnetic acid [83], the structure of **UD3** is elucidated as shown in **Figure 3.2**.

3.3.2.4 Compound UD4

The examination of the ^1H and ^{13}C NMR spectra revealed some important structural differences from **UD3** including the occurrence of a methoxy group at δ_{H} 3.77 that could be located at C-1 based on the HMBC correlations from the methoxy protons at δ_{H} 3.77 to C-1 (δ_{C} 169.8). Thus, the structure of **UD4** is a methyl ester of **UD3**.

3.3.2.5 Compound UD5

The ^1H and ^{13}C NMR spectra exhibited the presence of three methyl groups with symmetric type of aromatic ring at δ_{H} 2.72 (6H, s, 2x-COCH₃), and 2.06 (3H, Ar-CH₃). Furthermore, the molecular formula of **UD5** was determined to be C₁₂H₁₃O₅ based on the deprotonated ion peak at m/z 223.0627 (calcd for C₁₂H₁₂O₅, 223.0606). The structure of **UD5** was confirmed as presented in **Figure 3.2**. The tentative ^1H NMR chemical shift assignment for **UD5** is displayed in **Table 3.4**.



Table 3.4 Tentative 1D NMR (400 MHz) chemical shift assignment for **UD3–5** (CDCl₃)

	UD3		UD4		UD5
	δ_{H}	δ_{C}	δ_{H}	δ_{C}	δ_{H}
1		170.6		169.8	
2	3.8 (2H, s)	32.3	3.77 (2H, s)	32.2	
3		145		143.3	
4		154.3		153.8	
5		102		102.2	
6		163		162.3	
7		105		104.4	
8		157		154.7	2.72 (3H, s)
9		113.4		112.9	
10		112.3		110.6	2.72 (3H, s)
11	2.3 (3H, s)	9.8	2.35 (3H, s)	9.8	2.06 (3H, s)
12	2.1 (3H, s)	7.8	2.15 (3H, s)	7.1	
13		201.3		201.1	
14	2.7 (3H, s)	30.9	2.79 (3H, s)	31.1	
1-			3.77 (3H, s)	52.6	
OMe					
6-OH	13.8 (1H, s)		13.8 (1H, s)		

3.3.2.6 Mechanism aspect of the formation of UD1-5 from the usnic acid.

With various conditions investigated, a mechanism for the formation **UD1-5** from the oxidation of usnic acid is proposed as presented in **Figure 3.3**.

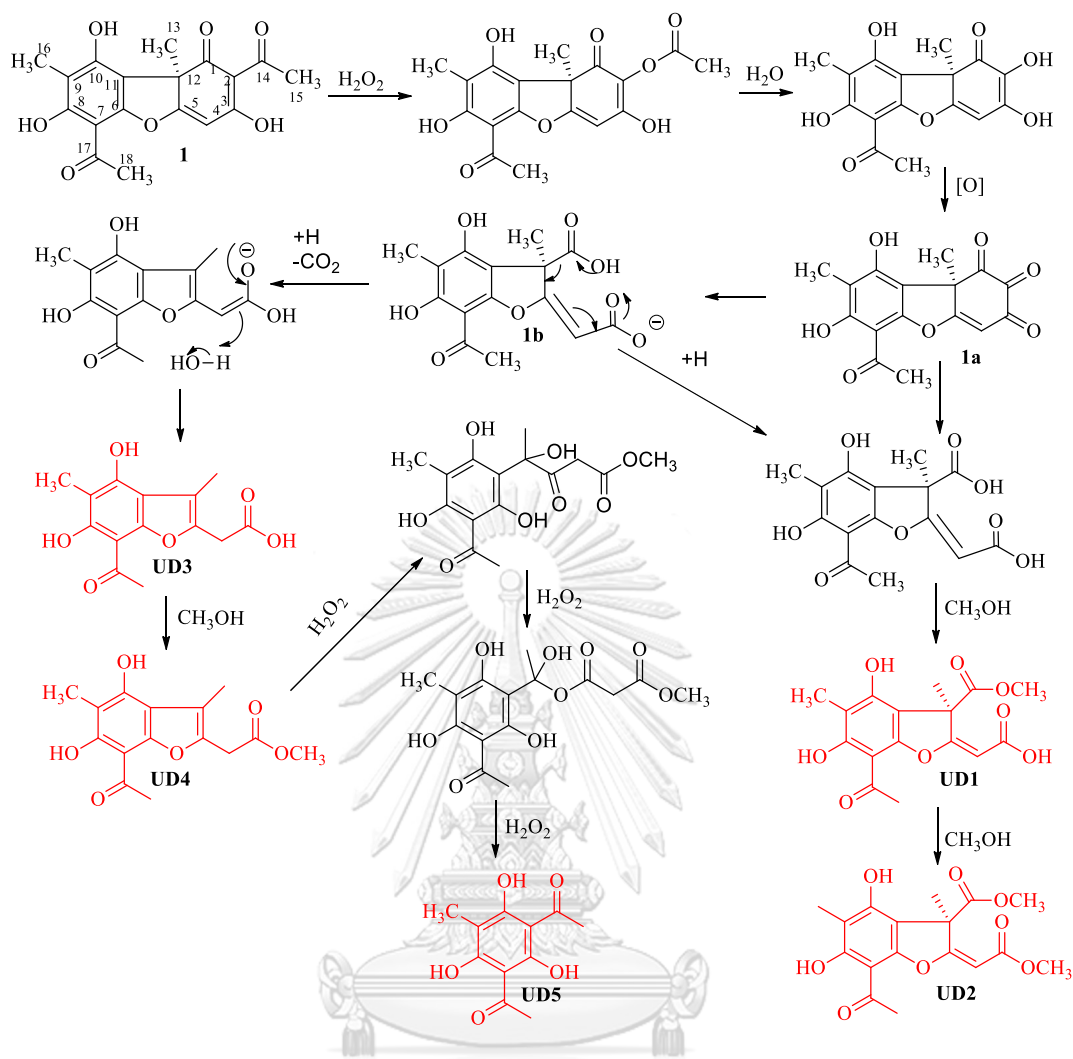


Figure 3. 3 Proposed Dakin reaction mechanism of usnic acid

The mechanism was believed to involve initial oxidation of usnic acid (1) at the ketone of the diketone (C-14) to give a hydroxyl at C-2 that was further oxidized to yield the corresponding triketone **1a**. The oxidation of ketone C-1 and C-3 led to the construction of a diacid **1b**. The methoxylation of **1b** led to the formation of **UD1**, that was further methoxylated to yield **UD2**. On the other hand, decarboxylation of **1b** led to the formation of **UD3** that was further methoxylated to obtain **UD4**. Finally, the oxidation of furan ring in **UD4** led to the creation of **UD5**.

3.3.3 Characterization of the products from esterification of usnic acid

3.3.3.1 The reaction of usnic acid with acetyl chloride

Four products, **UE1-4** were obtained from the esterification of usnic acid and acetyl chloride. A new chemical structure of **UE1** was elucidated by ^1H and ^{13}C NMR, along with HRESIMS spectroscopy, while the known products **UE2-4** were readily elucidated on the basis of their ^1H and ^{13}C NMR spectra.

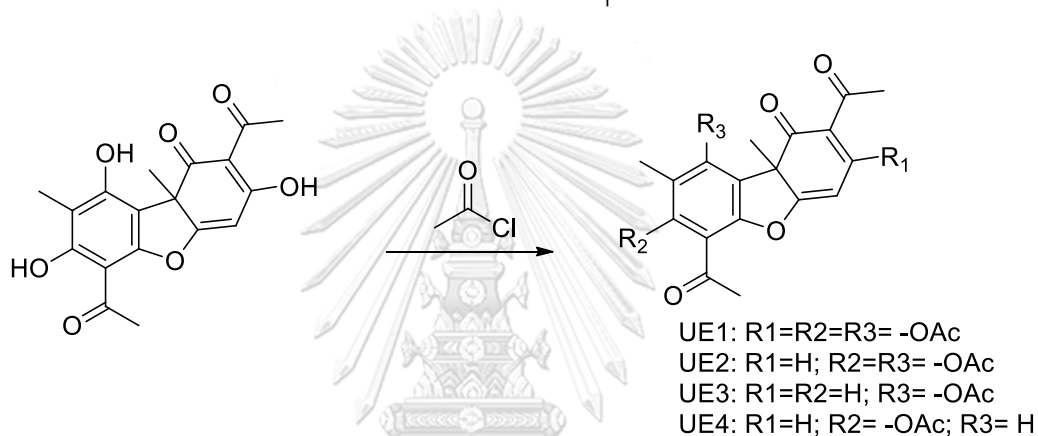


Figure 3. 4 Acetylation of usnic acid with acetyl chlorides

After purification by silica gel column, the desired products were obtained as shown in **Table 3.5**.

Table 3.5 The yields and characteristics of ester analogues (**UE1-4**) of usnic acid with acetyl chloride

Ester analogues	Appearance	% Yield	Remarks
UE1	Yellow powder	10.4	New
UE2	Yellow powder	15.2	Known
UE3	Yellow powder	34.0	Known
UE4	Yellow powder	17.5	Known

3.3.3.1.1 Compound UE1

The ^1H NMR spectrum of **UE1** showed an olefin proton at δ_{H} 6.38, and seven methyl groups at δ_{H} 2.65, 2.40, 2.35, 2.24, 2.22, 2.19 and 2.02. The ^{13}C NMR spectrum of **UE1** displayed twenty-three carbon signals, including three ketone carbons at δ_{C} 203.0, 202.9 and 195.0, three carboxyl carbons at δ_{C} 169.1x2 and 168.4, ten olefin carbons in the range of δ_{C} 155.0-100.0, one tertiary carbon at δ_{C} 47.0 and seven methyl carbons at δ_{C} 31.8, 29.5, 21.1, 20.7, 20.5, 9.7 and 9.2. The lack of 8- and 10-OH in usnic acid [17] along with the appearance of seven methyl groups indicated the esterification reaction occurred on 3-, 8-, and 10-OH of usnic acid. Thus, **UE1** is established as 3,8,10-triacetoxyusnic acid.

3.3.3.1.2 Compound UE2

The ^1H NMR spectrum of **UE2** showed a singlet of hydroxy chelated signal at δ_{H} 13.22, an olefin proton at δ_{H} 5.81, and five methyl groups at δ_{H} 2.74, 2.54, 2.45, 2.03, and 1.78. The ^{13}C NMR spectrum of **UE2** displayed sixteen carbon signals including four ketone carbons at δ_{C} 201.9, 198.4, 193.3, and 190.9, two carboxyl carbons at δ_{C} 178.1, ten olefin carbons in the range of δ_{C} 170.0-95.0, one tertiary carbon at δ_{C} 59.4 and five methyl carbons at δ_{C} 32.0, 31.2, 26.0, 21.4, and 9.2. The lack of 10-OH in usnic acid [17] along with the appearance of one acetoxycarbonyl group (δ_{H} 2.03, δ_{C} 178.1 and 21.4) indicated the esterification reaction occurred on

10-OH of usnic acid. Thus, the structure of **UE2**, 10-*O*-acetylusnic acid [82, 84], is elucidated as shown in **Figure 3.4**.

3.3.3.1.3 Compound UE3

The ^1H NMR spectrum of **UE3** showed an olefin proton at δ_{H} 5.90, and six methyl groups at δ_{H} 2.60, 2.54, 2.46, 2.33, 2.03 and 1.78. The lack of both of 10-OH and 13-OH in usnic acid [17] along with the appearance of two acetoxycarbonyl groups (δ_{H} 2.33 and 2.03) indicated the esterification reaction occurred on both of 10-OH and 13-OH of usnic acid. Thus, the structure of **UE3**, 8,10-*O*-diacetylusnic acid [82, 84], is elucidated as shown in **Figure 3.4**.

3.3.3.1.4 Compound UE4

The examination of the ^1H and ^{13}C NMR spectra revealed the similar spectra to those of **UE3**, excepted for the lack of 8-OH and the occurrence of 10-OH that indicated the reaction occurred at 8-OH. **UE4**, 8-*O*-acetylusnic acid [82, 84], is established as shown in **Figure 3.4**.

3.3.3.2 The reaction of usnic acid and UE2 with benzoyl chloride

UE5 and **UE6** were yielded from the esterification of benzoyl chloride with usnic acid and **UE3**, respectively. The elucidation of chemical structure was based on ^1H and ^{13}C NMR spectroscopy, further supported by HREISMS for new product (**UE6**).

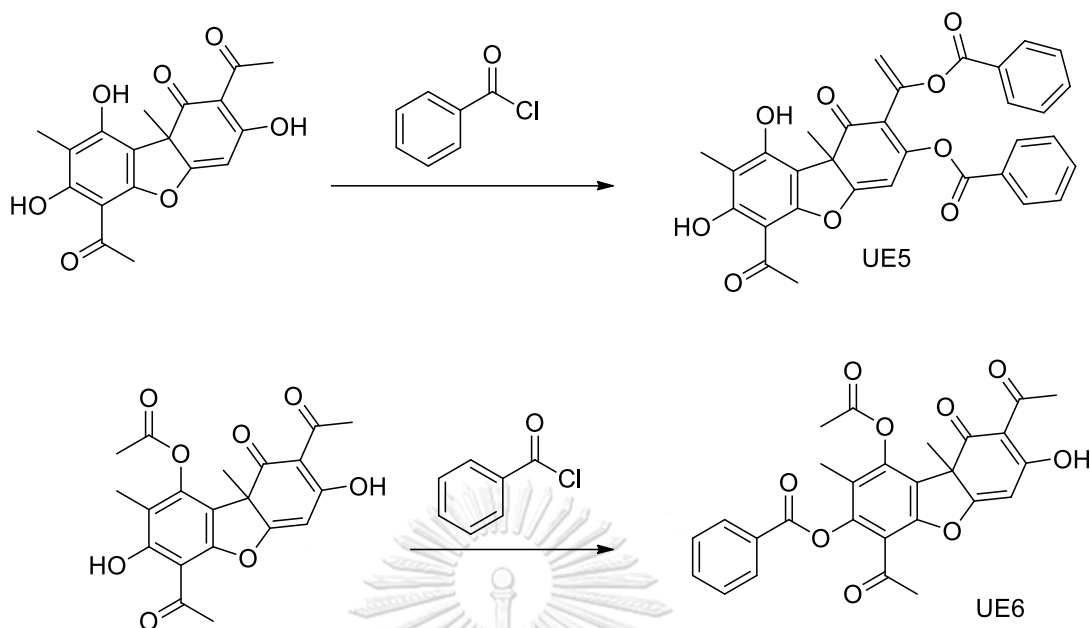


Figure 3. 5 Esterification of usnic acid with acetyl and benzoyl chlorides

Table 3.6 The yields and characteristics of UD5-6

Ester analogues	Appearance	% Yield	Remarks
UE5	Yellow powder	80.6	Known
UE6	Yellow powder	70.9	New

3.3.3.2.1 Compound UE5

The ^1H NMR of **UE5** displayed the presence of two chelated hydroxyl groups at δ_{H} 13.32 and 10.52, ten aromatic protons at δ_{H} 7.00-8.50, three olefin protons at δ_{H} 6.03, 5.43, and 5.24, and three methyl groups at δ_{H} 2.65, 2.12, 1.88. Comparison with those of usnic acid indicated the hydroxyl groups at δ_{H} 13.32 and 10.52 belonging to 8-OH and 10-OH, respectively. Moreover, the appearance of ten aromatic protons at δ_{H} 7.00-8.50 ppm along with a couple gem olefin proton at δ_{H} 5.43 (1H, d, $J = 1.2$ Hz) and 5.24 (1H, d, $J = 1.2$ Hz) implied the disubstitution on C-14

and C-3. Finally, **UE5** is established as benzoic acid 1-(6-acetyl-3-benzoyloxy-7,9-dihydroxy-8,9b-dimethyl-1-oxo-1,9b-dihydro-dibenzofuran-2-yl)-6inyl ester [84].

3.3.3.2.2 Compound UE6

The ^1H NMR spectrum of **UE6** showed five aromatic protons at δ_{H} 8.5-7.5, that implied mono benzoyl chloride reacted with **UE2**. A singlet signal at δ_{H} 5.86 (1H, s), belonging to H-4 in starting material, and five methyl groups at δ_{H} 2.60, 2.56, 2.48, 2.04 and 1.85. The examination of the ^{13}C NMR spectrum revealed some important structural differences from **UE2** including the occurrence of five aromatic carbons at δ_{C} 134.2, 130.6 x2 and 128.9x2 confirmed the addition of mono benzoyl chloride. Moreover, the lack of chelated hydroxyl proton 8-OH at δ_{H} 13.22 (**UE2**) identified that the reaction occurred at 8-OH. Finally, the structure of **UE6** is established as shown in **Figure 3.5**.

3.4 Biological activities of usnic acid derivatives

Eleven usnic acid derivatives including 5 products from Dakin reaction (**UD1-5**) and 6 esterification products (**UE1-6**) were further tested with α -glucosidase and tyrosinase inhibitory activities. From the results, all derivatives exhibited the same or higher activity comparing with starting material (usnic acid: >200 μM and no activity (NA) for α -glucosidase and tyrosinase, respectively). Especially, **UD2**, **UD5**, **UE5**, and **UE6** showed excellent α -glucosidase activity with IC_{50} 42.6 \pm 1.30, 90.8 \pm 0.32, 26.7 \pm 0.57, and 68.8 \pm 0.15 μM , respectively. These compounds not only displayed

higher activity than that of usnic acid, but also with that of a positive control, acarbose (IC_{50} : $93.6 \pm 0.49 \mu\text{M}$) as shown in **Table 3.3**. In this case, **UE5** displayed the strongest activity (IC_{50} : $26.7 \pm 0.57 \mu\text{M}$).

Table 3. 7 α -glucosidase and tyrosinase inhibitory of usnic acid derivatives

	Compounds	α -glucosidase IC_{50} (μM)	Tyrosinase IC_{50} (μM)
1	UD1	>200	NA
2	UD2	42.6 ± 1.30	NA
3	UD3	>200	>200
4	UD4	>200	>200
5	UD5	90.8 ± 0.32	NA
6	UE1	>200	NA
7	UE2	>200	>200
8	UE3	>200	NA
9	UE4	>200	>200
10	UE5	26.7 ± 0.57	>200
11	UE6	68.8 ± 0.15	NA
12	Uronic acid	>200	NA
13	Acarbose	93.6 ± 0.49	
14	Kojic acid		36.1 ± 1.07

3.5 Conclusion

From usnic acid, eleven derivatives were synthesized from Dakin oxidation (**UD1-5**) and esterification reactions (**UE1-6**). Their chemical structures were elucidated by 1D, 2D, and HRESIMS as well as comparison with those from literature. Among them, **UD1-2** was reported as novel compounds and **UE1** and **UE6** as new compounds. Interestingly, all products displayed the same or higher biological activity than the starting material, usnic acid when evaluated against α -glucosidase and tyrosinase. In the α -glucosidase assay, **UD2**, **UD5**, **UE5**, and **UE6** showed excellent activity (IC_{50} 42.6 ± 1.30 , 90.8 ± 0.32 , 26.7 ± 0.57 , and 68.8 ± 0.15 μ M, respectively). On the other hand, all tested compounds revealed weak or no inhibitory activity in the tyrosinase assay.

Chapter 4

CONCLUSIONS

4.2 Chemical constituents of lichen *Usnea baileyi*

In conclusion, eleven new compounds including ten new bisxanthenes (**US1-3**, **US5-11**), along with a new depsidone **US4** as shown in **Figure 2.21** were successfully isolated from DC fraction. The chemical structures of isolated compounds were elucidated by NMR, and also compared to the NMR data of those in literatures. In addition, antiparasitic, cytotoxicity (only for **US1-3**), antibacterial, and enzyme inhibitory including tyrosinase and α -glucosidase (**US5-11**) were performed.

The results revealed weak (**US1-2**) or no (**US3**) antiparasitic activity, and only **US2** exerted a moderate effect against MCF-7 cell line resulted slightly more susceptible with an IC_{50} value of 12 μ M.

On the other hand, the antibacterial activity of seven compounds (**US5-11**) resulted good activity against *E. coli* with MIC 62.5 μ g/mL for **US5-6** and *B. subtilis* with MIC 62.5 μ g/mL for **US5**, while all seven bisxanthenes (**US5-11**) displayed weak activity against tyrosinase and α -glucosidase.

The possible future research would be connected to the chemical constituents from the remaining dichloromethane fraction of *U. baileyi*. Furthermore, the synthesis of some derivatives from other major compounds as stictic acid, protocetraric acid or diffractaic and babartic acid should be studied. Other biological activities such as anticancer and some inhibitory activities such as α -glucosidase

(molecular docking, orthogonal assay, SAR for potential compounds), acetylcholinesterase should be examined on isolated compounds or derivatives.

4.2 Synthesis of usnic acid derivatives via oxidation and esterification reactions

Further structural modification of the parent compound, usnic acid isolated from *U. baileyi*, employed Dakin oxidation and esterification as key methods to accomplish eleven derivatives including five oxidation products, **UD1-5** and six ester analogues, **UE1-6**. Three compounds, **UD1-2**, **UE1**, and **UE6** were identified as new compounds. All derivatives were subsequently evaluated for α -glucosidase inhibitory activity. Interestingly, some candidates exhibited better activity than the parent compound or the control. In Dakin oxidation series, **UD2** displayed the most potent inhibition with IC_{50} value of 42.6 ± 1.30 and **UE5** showed the most potent in ester series with IC_{50} $26.7 \pm 0.57 \mu\text{M}$.

Further experiments should also be planned to investigate the influence of pH as well as different oxidants to clarify the oxidation mechanism. In esterification reaction, the products formed from usnic acid and benzoyl chloride revealed the strongest activity. Further experiments should study on other benzoyl chloride derivatives with different substituents on the aromatic ring.

In addition, study on the mode of inhibition in perspective of structure activity relationship should be focused.

REFERENCES



จุฬาลงกรณ์มหาวิทยาลัย
CHULALONGKORN UNIVERSITY

- [1] Yousuf, S., Choudhary, M. I., Atta ur, R. Chapter 7 - Lichens: Chemistry and Biological Activities. Study in Natural Products Chemistry (2014): 223-259.
- [2] Ranković, B. and Kosanić, M. Lichens as a Potential Source of Bioactive Secondary Metabolites. in Ranković, B. (ed.)Lichen Secondary Metabolites: Bioactive Properties and Pharmaceutical Potential, pp. 1-26. Cham: Springer International Publishing, 2015.
- [3] Huneck, S. and Yoshimura, I. Introduction. in Identification of Lichen Substances, pp. 1-9. Berlin, Heidelberg: Springer Berlin Heidelberg, 1996.
- [4] Malhotra, S., Subban, R., Singh, A. Lichens- Role in Traditional Medicine and Drug Discovery. 5 (2007): 1-6.
- [5] Boustie, J. and Grube, M. Lichens—a promising source of bioactive secondary metabolites. Plant Genetic Resources 3(2) (2005): 273-287.
- [6] Boustie, J., Tomasi, S., and Grube, M. Bioactive lichen metabolites: alpine habitats as an untapped source. Phytochemistry Reviews 10(3) (2011): 287-307.
- [7] Huneck, S. The Significance of Lichens and Their Metabolites. Naturwissenschaften 86(12) (1999): 559-570.
- [8] Micheletti, A.C., et al. Constituintes químicos de Parmotrema lichexanthonicum Eliasaro & Adler: isolamento, modificações estruturais e avaliação das atividades antibiótica e citotóxica. Química Nova 32 (2009): 12-20.
- [9] Müller, K. Pharmaceutically relevant metabolites from lichens. Applied Microbiology and Biotechnology 56(1) (2001): 9-16.
- [10] Le, D.H., Takenaka, Y., Hamada, N., Mizushina, Y., and Tanahashi, T. Polyketides from the Cultured Lichen Mycobiont of a Vietnamese Pyrenula sp. Journal of Natural Products 77(6) (2014): 1404-1412.
- [11] Brodo, I.M., Sharnoff, S.D., Sharnoff, S., and Nature, C.M.o. Lichens of North America. Yale University Press, 2001.
- [12] Wirtz, N., Printzen, C., Sancho, L.G., and Lumbsch, H.T. The Phylogeny and Classification of Neuropogon and Usnea (Parmeliaceae, Ascomycota) Revisited. Taxon 55(2) (2006): 367-376.

- [13] Rawat, M.S.M., Shukla, V., Negi, S., and Pant, G. Chemical study on Garhwal Himalayan lichen, *Usnea emidotteries*. 45B (2006): 2566-2570.
- [14] Lohézic-Le Dévéhat, F., et al. Stictic Acid Derivatives from the Lichen *Usnea articulata* and Their Antioxidant Activities. *Journal of Natural Products* 70(7) (2007): 1218-1220.
- [15] Paranagama, P.A., et al. Heptaketides from *Corynespora* sp. Inhabiting the Cavern Beard Lichen, *Usnea cavernosa*: First Report of Metabolites of an Endolichenic Fungus. *Journal of Natural Products* 70(11) (2007): 1700-1705.
- [16] Keeton, J.F. and Keogh, M.F. Caperatic acid from *Usnea alata*. *Phytochemistry* 12(3) (1973): 721-722.
- [17] Van Nguyen, K., Duong, T.-H., Nguyen, K.P.P., Sangvichien, E., Wonganan, P., and Chavasiri, W. Chemical constituents of the lichen *Usnea baileyi* (Stirt.) Zahlbr. *Tetrahedron Letters* 59(14) (2018): 1348-1351.
- [18] Din, L.B., Zakaria, Z., Samsudin, M.W., and Elix, J.A. Chemical profile of compounds from Lichens of Bukit Larut, Peninsular Malaysia. *Sains Malaysiana* 39(6) (2010): 901-908.
- [19] Yang, D.-M., Takeda, N., Iitaka, Y., Sankawa, V., and Shibata, S. The structures of eumitrins A1, A2 and B. *Tetrahedron* 29(3) (1973): 519-528.
- [20] Le Pogam, P. and Boustie, J. Xanthonones of Lichen Source: A 2016 Update. *Molecules* 21(3) (2016): 294.
- [21] YOSIOKA, I., NAKANISHI, T., IZUMI, S., and KITAGAWA, I. Structure of a lichen pigment entothein and its identity with secalonic acid A, a major ergot pigment. *Chemical and Pharmaceutical Bulletin* 16(10) (1968): 2090-2091.
- [22] Millot, M., Tomasi, S., Studzinska, E., Rouaud, I., and Boustie, J. Cytotoxic constituents of the lichen *Diploicia canescens*. *Journal of natural products* 72(12) (2009): 2177-2180.
- [23] Wezeman, T., Bräse, S., and Masters, K.-S. Xanthone dimers: a compound family which is both common and privileged. *Natural Product Reports* 32(1) (2015): 6-28.
- [24] Hu, Z., et al. Phytochemical and chemotaxonomic studies on *Phyllanthus urinaria*. *Biochemical Systematics and Ecology* 56 (2014): 60-64.

- [25] Qin, T. and Porco Jr, J.A. Total syntheses of secalonic acids A and D. Angewandte Chemie International Edition 53(12) (2014): 3107-3110.
- [26] Frank, M., et al. Phomoxanthone A-from mangrove forests to anticancer therapy. Current medicinal chemistry 22(30) (2015): 3523-3532.
- [27] Ehrlich, K.C., Lee, L., Ciegler, A., and Palmgren, M. Secalonic acid D: natural contaminant of corn dust. Appl. Environ. Microbiol. 44(4) (1982): 1007-1008.
- [28] Nuno, M. On the isolation of chemical ingredients of *Usnea bayleyi* (Stirt.) Zahlbr. Journal of Japanese botany (1971).
- [29] Bungartz, F., Elix, J.A., and Nash III, T.H. The genus *Buellia* sensu lato in the Greater Sonoran Desert Region: saxicolous species with one-septate ascospores containing xanthones. Bryologist (2004): 459-479.
- [30] Giralt, M. New morphological and chemical data for *Buellia imshaugii*. The Lichenologist 42(6) (2010): 763-765.
- [31] Lendemer, J.C., Sheard, J.W., Göran, T., and TØNSBERG, T. *Rinodina chrysiata*, a new species from far eastern Asia and the Appalachian Mountains of North America. The Lichenologist 44(2) (2012): 179-187.
- [32] Coulibaly, W.K., et al. Prospective study directed to the synthesis of unsymmetrical linked bis-5-arylidene rhodanine derivatives via “one-pot two steps” reactions under microwave irradiation with their antitumor activity. Medicinal Chemistry Research 24(4) (2015): 1653-1661.
- [33] Otogo N’Nang, E., et al. Theionbrunonines A and B: Dimeric Vobasine Alkaloids Tethered by a Thioether Bridge from *Mostuea brunonis*. Organic Letters 20(20) (2018): 6596-6600.
- [34] Clinical and Institute, L.S. Performance Standards for Antimicrobial Susceptibility Testing: Twenty-Fifth Informational Supplement, M07-A10. 2015, Wayne, PA, USA: CLSI.
- [35] Ramadhan, R. and Phuwapraisiran, P. New arylalkanones from *Horsfieldia macrobotrys*, effective antidiabetic agents concomitantly inhibiting α -glucosidase and free radicals. Bioorganic & medicinal chemistry letters 25(20) (2015): 4529-4533.

- [36] Steyn, P.S. The isolation, structure and absolute configuration of secalonic acid D, the toxic metabolite of *Penicillium oxalicum*. Tetrahedron 26(1) (1970): 51-57.
- [37] Andersen, R., Buechi, G., Kobbe, B., and Demain, A.L. Secalonic acids D and F are toxic metabolites of *Aspergillus aculeatus*. The Journal of organic chemistry 42(2) (1977): 352-353.
- [38] Franck, B., Gottschalk, E.M., Ohnsorge, U., and Hüper, F. Mutterkorn-Farbstoffe, XII. Trennung, Struktur und absolute Konfiguration der diastereomeren Secalonsäuren A, B und C. Chemische Berichte 99(12) (1966): 3842-3862.
- [39] Zhang, W., et al. New Mono- and Dimeric Members of the Secalonic Acid Family: Blennolides A–G Isolated from the Fungus *Blennoria* sp. Chemistry–A European Journal 14(16) (2008): 4913-4923.
- [40] Yamazaki, H., Ukai, K., and Namikoshi, M. Asperdichrome, an unusual dimer of tetrahydroxanthone through an ether bond, with protein tyrosine phosphatase 1B inhibitory activity, from the Okinawan freshwater *Aspergillus* sp. TPU1343. Tetrahedron Letters 57(7) (2016): 732-735.
- [41] Wu, G., et al. Versixanthonones A–F, cytotoxic xanthone–chromanone dimers from the marine-derived fungus *Aspergillus versicolor* HDN1009. Journal of natural products 78(11) (2015): 2691-2698.
- [42] Franck, B. and Baumann, G. Mutterkorn-Farbstoffe, XIV. Isolierung, Struktur und absolute Konfiguration der Ergochrome AD, BD, CD und DD. Chemische Berichte 99(12) (1966): 3875-3883.
- [43] Franck, B. and Baumann, G. Mutterkorn-Farbstoffe, XIII. Isolierung, Struktur und absolute Konfiguration der Ergochrysin A und B. Chemische Berichte 99(12) (1966): 3863-3874.
- [44] Franck, B., Gottschalk, E.-M., Ohnsorge, U., and Hüper, F. Mutterkorn-Farbstoffe, XII. Trennung, Struktur und absolute Konfiguration der diastereomeren Secalonsäuren A, B und C. Chemische Berichte 99(12) (1966): 3842-3862.

- [45] Elsässer, B., et al. X-ray structure determination, absolute configuration and biological activity of phomoxanthone A. European journal of organic chemistry 2005(21) (2005): 4563-4570.
- [46] Napolitano, J.G., Gavín, J.A., García, C., Norte, M., Fernández, J.J., and Hernández Daranas, A. On the Configuration of Five-Membered Rings: A Spin-Spin Coupling Constant Approach. Chemistry–A European Journal 17(23) (2011): 6338-6347.
- [47] Ola, A.R.B., et al. Absolute configuration and antibiotic activity of neosartorin from the endophytic fungus *Aspergillus fumigatiaffinis*. Tetrahedron Letters 55(5) (2014): 1020-1023.
- [48] Li, T.-X., et al. Unusual dimeric tetrahydroxanthone derivatives from *Aspergillus lentulus* and the determination of their axial chiralities. Scientific Reports 6 (2016): 38958.
- [49] Tuong, T.L., Aree, T., Do, L.T., Nguyen, P.K., Wonganan, P., and Chavasiri, W.J.F. Dimeric tetrahydroxanthones from the lichen *Usnea aciculifera*. 137 (2019): 104194.
- [50] Zhang, H.-J., Zhang, Y.-M., Luo, J.-G., Luo, J., and Kong, L.-Y. Anti-inflammatory diterpene dimers from the root barks of *Aphanamixis grandifolia*. Organic & Biomolecular Chemistry 13(27) (2015): 7452-7458.
- [51] Harada, N. and Nakanishi, K. Exciton chirality method and its application to configurational and conformational studies of natural products. Accounts of Chemical Research 5(8) (1972): 257-263.
- [52] Szwalbe, A.J., et al. Characterisation of the biosynthetic pathway to agnestins A and B reveals the reductive route to chrysophanol in fungi. Chemical Science 10(1) (2019): 233-238.
- [53] Matsuda, Y., Gotfredsen, C.H., and Larsen, T.O. Genetic Characterization of Neosartorin Biosynthesis Provides Insight into Heterodimeric Natural Product Generation. Organic Letters 20(22) (2018): 7197-7200.

- [54] Neubauer, L., Dopstadt, J., Humpf, H.-U., and Tudzynski, P. Identification and characterization of the ergochrome gene cluster in the plant pathogenic fungus *Claviceps purpurea*. Fungal Biology and Biotechnology 3(1) (2016): 2.
- [55] Masters, K.-S. and Bräse, S. Xanthonenes from Fungi, Lichens, and Bacteria: The Natural Products and Their Synthesis. Chemical Reviews 112(7) (2012): 3717-3776.
- [56] Cai, S., King, J.B., Du, L., Powell, D.R., and Cichewicz, R.H. Bioactive Sulfur-Containing Sulochrin Dimers and Other Metabolites from an *Alternaria* sp. Isolate from a Hawaiian Soil Sample. Journal of Natural Products 77(10) (2014): 2280-2287.
- [57] El-Elimat, T., et al. Biosynthetically Distinct Cytotoxic Polyketides from *Setophoma terrestris*. European Journal of Organic Chemistry 2015(1) (2015): 109-121.
- [58] Ding, B., et al. New Dimeric Members of the Phomoxanthone Family: Phomolactonexanthonenes A, B and Deacetylphomoxanthone C Isolated from the Fungus *Phomopsis* sp. Marine Drugs 11(12) (2013): 4961-4972.
- [59] McPhail, A.T., Sim, G.A., Asher, J.D.M., Robertson, J.M., and Silverton, J.V. Fungal metabolites. Part IV. The structure of ergoflavin: X-ray analysis of tetra-O-methylergoflavin di-p-iodobenzoate. Journal of the Chemical Society B: Physical Organic (0) (1966): 18-30.
- [60] Franck, B. Structure and Biosynthesis of the Ergot Pigments. Angewandte Chemie International Edition in English 8(4) (1969): 251-260.
- [61] Aberhart, D.J. and de Mayo, P. Mould metabolites—V: The constitution of ergoxanthin. Tetrahedron 22(7) (1966): 2359-2366.
- [62] Hooper, J.W., Marlow, W., Whalley, W.B., Borthwick, A.D., and Bowden, R. The chemistry of fungi. Part LXV. The structures of ergochrysin A, isoergochrysin A, and ergoxanthin, and of secalonic acids A, B, C, and D. Journal of the Chemical Society C: Organic (0) (1971): 3580-3590.
- [63] Hill, J.G., Nakashima, T.T., and Vederas, J.C. Fungal xanthone biosynthesis. Distribution of acetate-derived oxygens in ravenelin. Journal of the American Chemical Society 104(6) (1982): 1745-1748.

- [64] Tuong, T.L., Aree, T., Do, L.T., Nguyen, P.K., Wonganan, P., and Chavasiri, W. Dimeric tetrahydroxanthones from the lichen *Usnea aciculifera*. Fitoterapia 137 (2019): 104194.
- [65] Vogt, R.L. and Dippold, L. *Escherichia coli* O157: H7 outbreak associated with consumption of ground beef, June–July 2002. Public health reports 120(2) (2005): 174-178.
- [66] Menegário, A.A., Silva, A.J., Pozzi, E., Durrant, S.F., and Abreu Jr, C.H. On-line determination of Sb (III) and total Sb using baker's yeast immobilized on polyurethane foam and hydride generation inductively coupled plasma optical emission spectrometry. Spectrochimica Acta Part B: Atomic Spectroscopy 61(9) (2006): 1074-1079.
- [67] Tuzen, M., Saygi, K.O., Usta, C., and Soylak, M. *Pseudomonas aeruginosa* immobilized multiwalled carbon nanotubes as biosorbent for heavy metal ions. Bioresource Technology 99(6) (2008): 1563-1570.
- [68] Livermore, D.M. Multiple mechanisms of antimicrobial resistance in *Pseudomonas aeruginosa*: our worst nightmare? Clinical infectious diseases 34(5) (2002): 634-640.
- [69] Magiorakos, A.P., et al. Multidrug-resistant, extensively drug-resistant and pandrug-resistant bacteria: an international expert proposal for interim standard definitions for acquired resistance. Clinical microbiology and infection 18(3) (2012): 268-281.
- [70] Falagas, M.E., Koletsis, P.K., and Bliziotis, I.A. The diversity of definitions of multidrug-resistant (MDR) and pandrug-resistant (PDR) *Acinetobacter baumannii* and *Pseudomonas aeruginosa*. Journal of medical microbiology 55(12) (2006): 1619-1629.
- [71] Shahdordizadeh, M., Taghdisi, S.M., Ansari, N., Langroodi, F.A., Abnous, K., and Ramezani, M. Aptamer based biosensors for detection of *Staphylococcus aureus*. Sensors and Actuators B: Chemical 241 (2017): 619-635.
- [72] Cannon, R.D. and Chaffin, W. Colonization is a crucial factor in oral candidiasis. Journal of dental education 65(8) (2001): 785-787.

- [73] de Repentigny, L., Lewandowski, D., and Jolicoeur, P. Immunopathogenesis of oropharyngeal candidiasis in human immunodeficiency virus infection. Clinical microbiology reviews 17(4) (2004): 729-759.
- [74] Perlroth, J., Choi, B., and Spellberg, B. Nosocomial fungal infections: epidemiology, diagnosis, and treatment. Medical mycology 45(4) (2007): 321-346.
- [75] Schlecht, L.M., et al. Systemic Staphylococcus aureus infection mediated by Candida albicans hyphal invasion of mucosal tissue. Microbiology 161(Pt 1) (2015): 168.
- [76] Ingoldsdottir, K. Usnic acid. Phytochemistry 61(7) (2002): 729-736.
- [77] Bazin, M.-A., et al. Synthesis and cytotoxic activities of usnic acid derivatives. Bioorganic & medicinal chemistry 16(14) (2008): 6860-6866.
- [78] Luzina, O., et al. Synthesis and biological activity of usnic acid enamine derivatives. Chemistry of natural compounds 51(4) (2015): 646-651.
- [79] Vanga, N.R., Kota, A., Sistla, R., and Uppuluri, M. Synthesis and anti-inflammatory activity of novel triazole hybrids of (+)-usnic acid, the major dibenzofuran metabolite of the lichen Usnea longissima. Molecular diversity 21(2) (2017): 273-282.
- [80] Sokolov, D.N., et al. Anti-viral activity of (-)-and (+)-usnic acids and their derivatives against influenza virus A (H1N1) 2009. Bioorganic & medicinal chemistry letters 22(23) (2012): 7060-7064.
- [81] Ebrahim, H.Y., Akl, M.R., Elsayed, H.E., Hill, R.A., and El Sayed, K.A. Usnic acid benzylidene analogues as potent mechanistic target of rapamycin inhibitors for the control of breast malignancies. Journal of natural products 80(4) (2017): 932-952.
- [82] Takai, M., Uehara, Y., and Beisler, J.A.J.J.o.m.c. Usnic acid derivatives as potential antineoplastic agents. Journal of medicinal chemistry 22(11) (1979): 1380-1384.

- [83] Kutney, J.P., Leman, J.D., Salisbury, P.J., Yee, T., and Sánchez, I.H. Studies in the usnic acid series. IX. The biodegradation of (+)-usnic acid by *Mucor globosus*. Canadian journal of chemistry 62(2) (1984): 320-325.
- [84] Erba, E., Pocar, D., and Rossi, L.M.J.I.f. New esters of R-(+)-usnic acid. IL Farmaco 53(10-11) (1998): 718-720.



APPENDIX



จุฬาลงกรณ์มหาวิทยาลัย
CHULALONGKORN UNIVERSITY

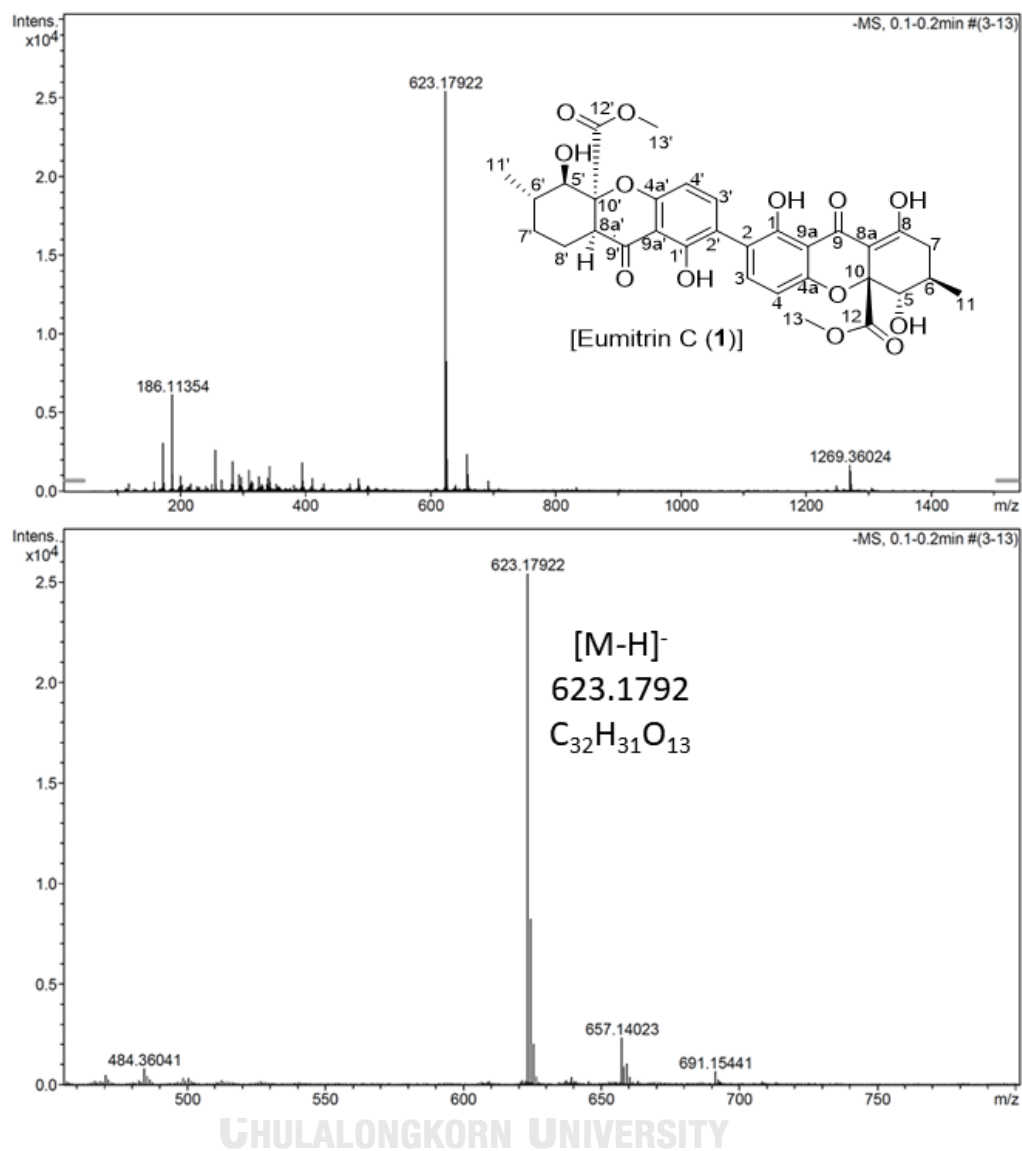


Figure A. 1 HRESIMS spectrum of US1

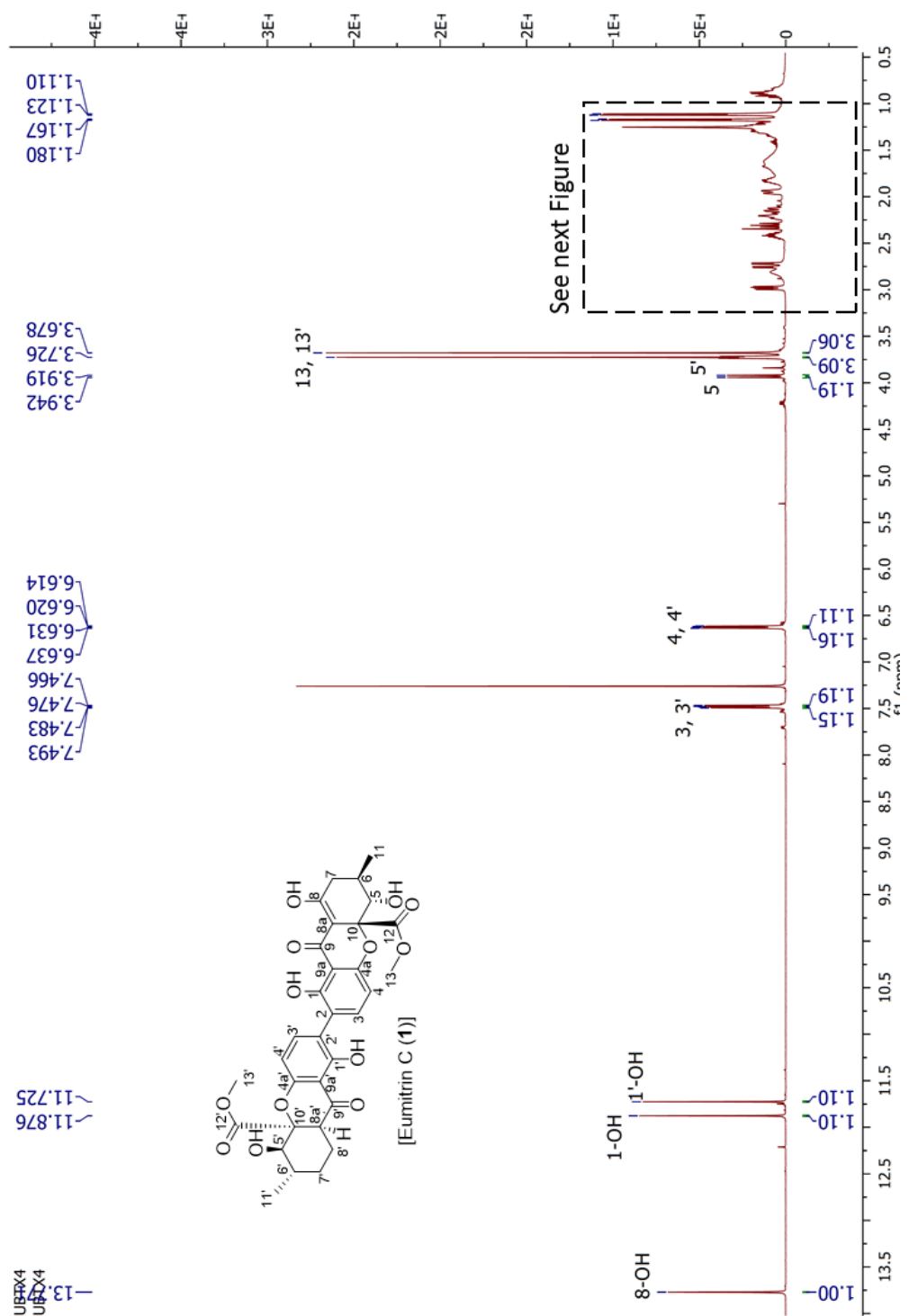


Figure A. 2 The ^1H NMR (CDCl_3 , 500 MHz) spectrum of **US1**

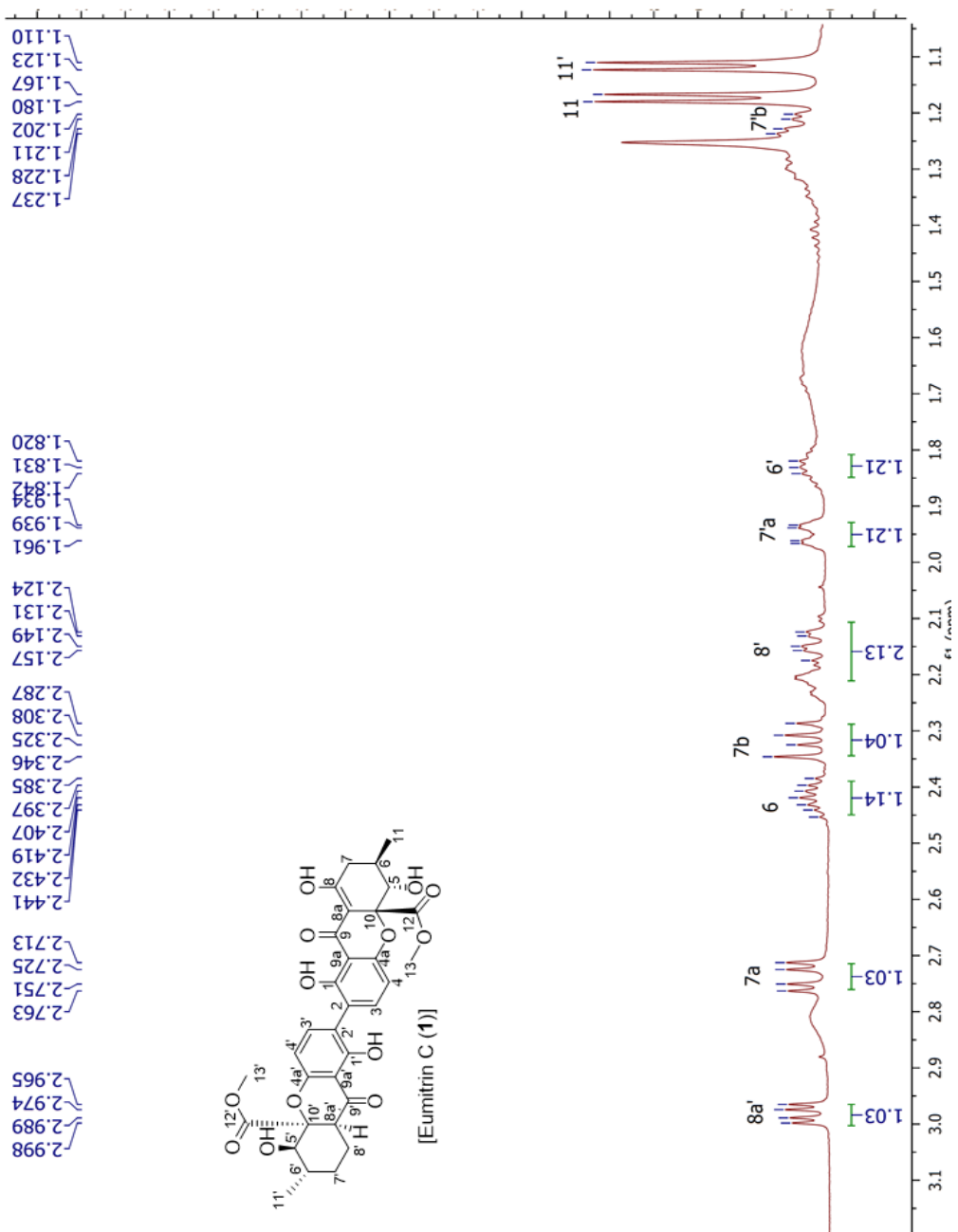


Figure A. 3 The ^1H NMR (CDCl_3 , 500 MHz) spectrum of **US1** (1.0 to 3.0 ppm)

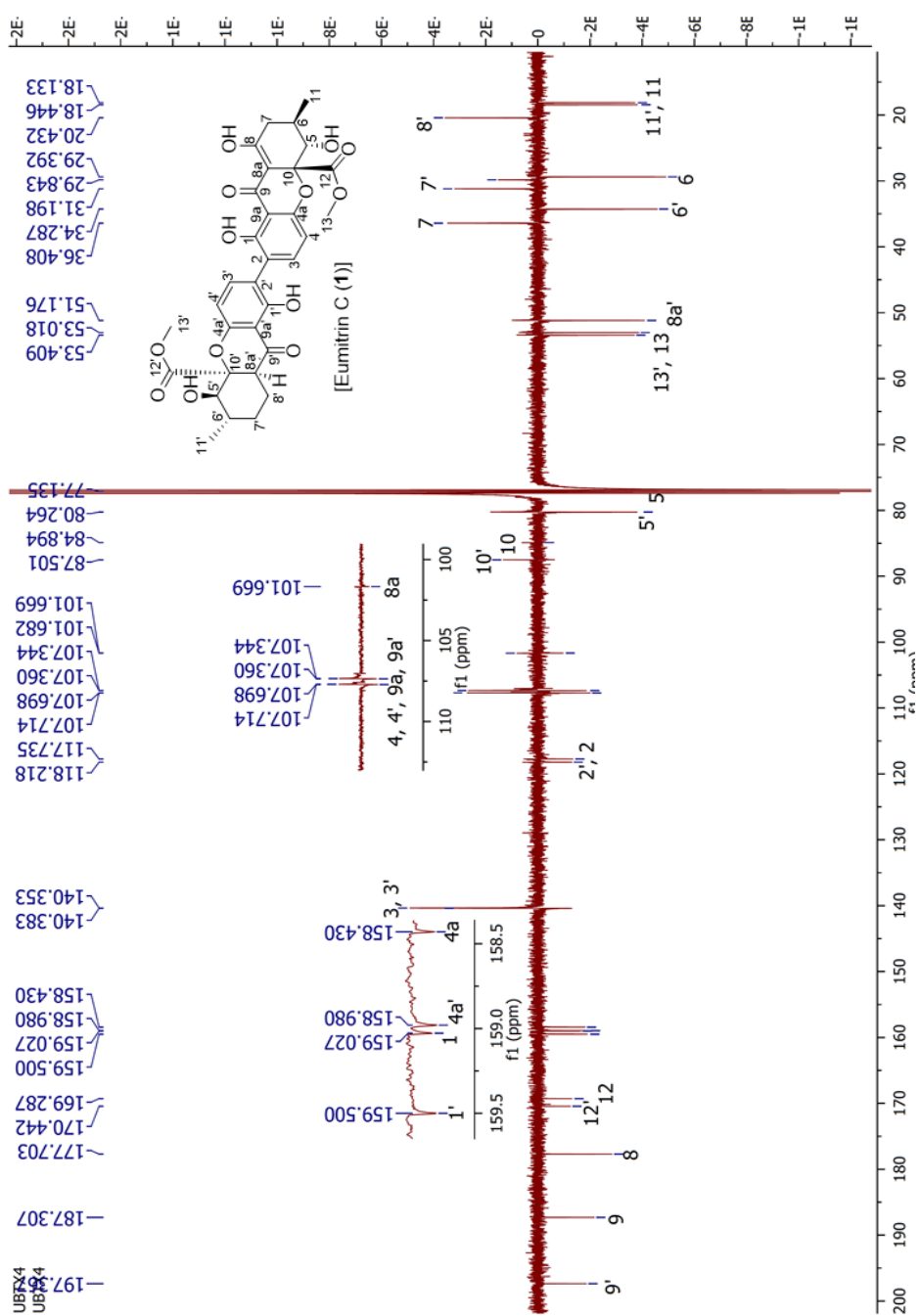


Figure A. 4 The ¹³C NMR (CDCl₃, 125 MHz) spectrum of US1

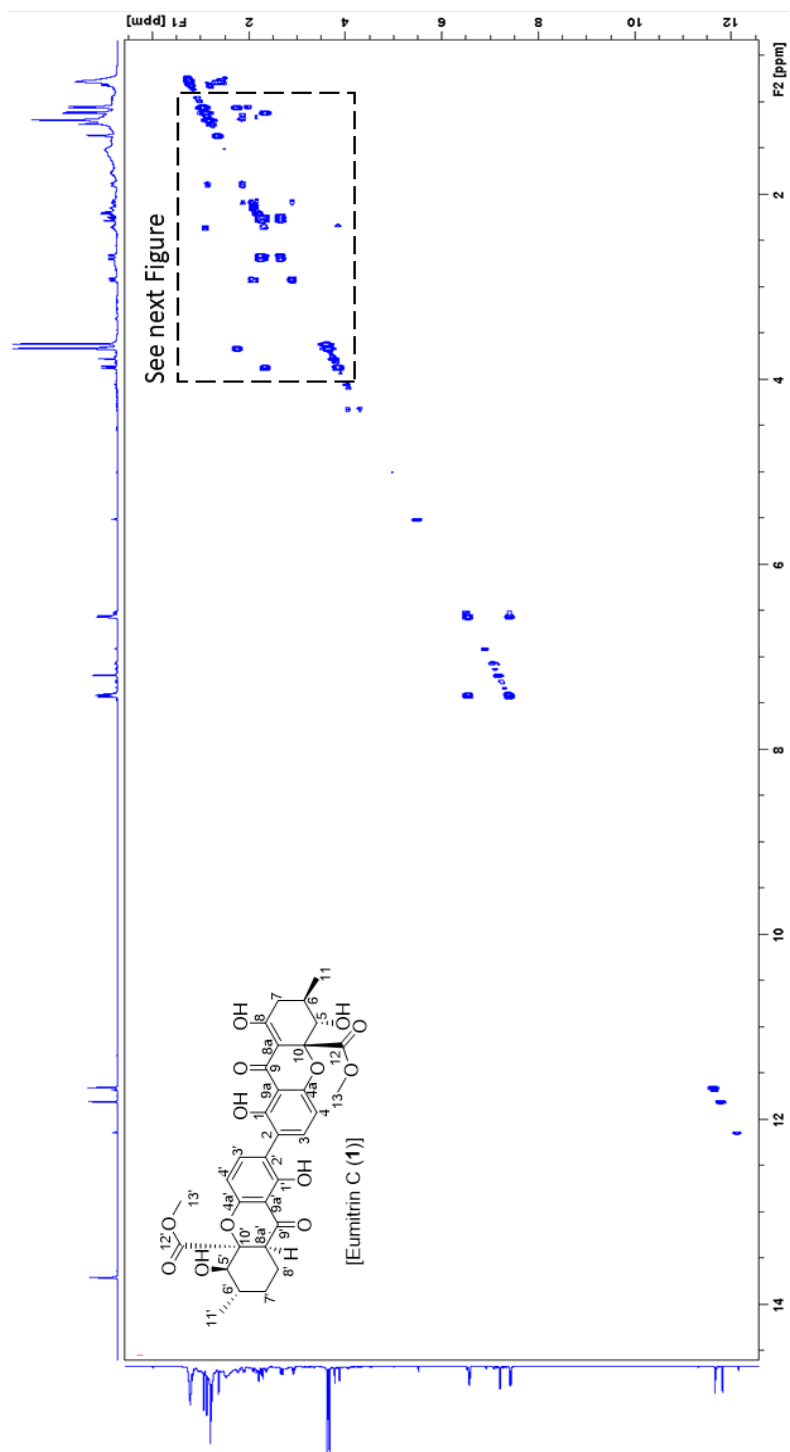


Figure A. 5 The COSY (CDCl₃, 500 MHz) spectrum of US1

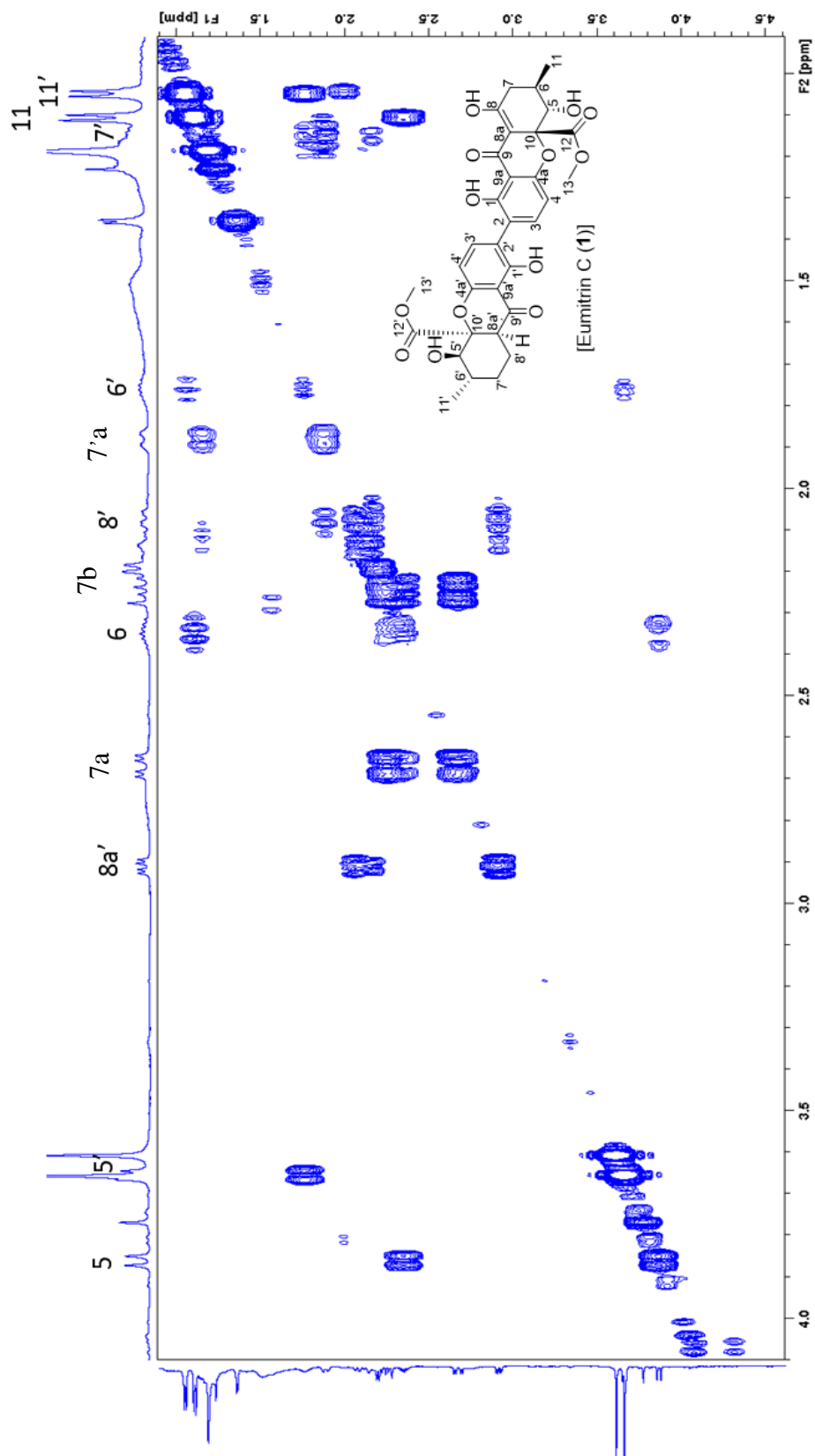


Figure A. 6 The COSY (CDCl₃, 500 MHz) spectrum of **US1** (1.25 to 4.0 ppm).

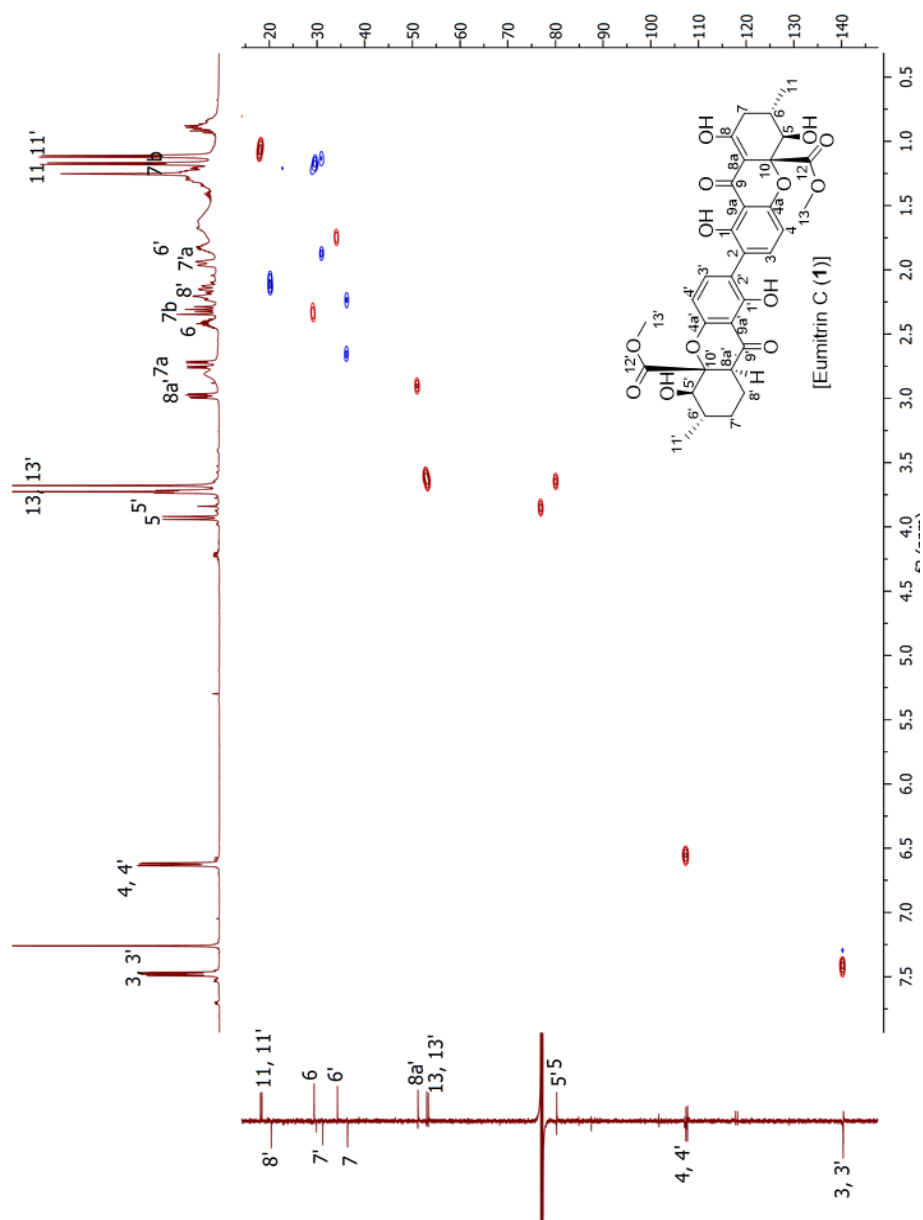


Figure A. 7 The HSQC (CDCl_3 , 500 MHz, 125 MHz) spectrum of US1

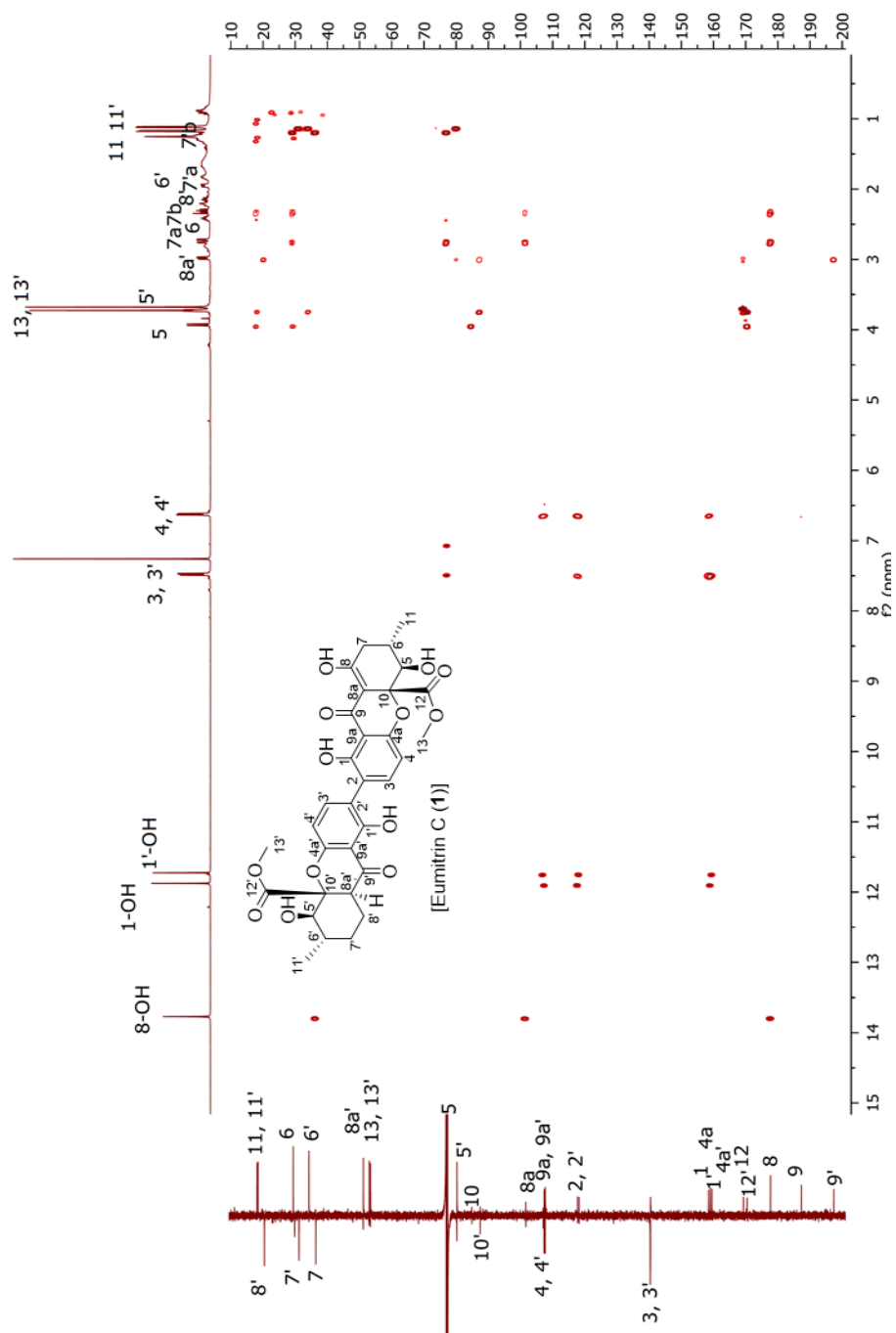


Figure A. 8 The HMBC (CDCl_3 , 500 MHz, 125 MHz) spectrum of **US1**

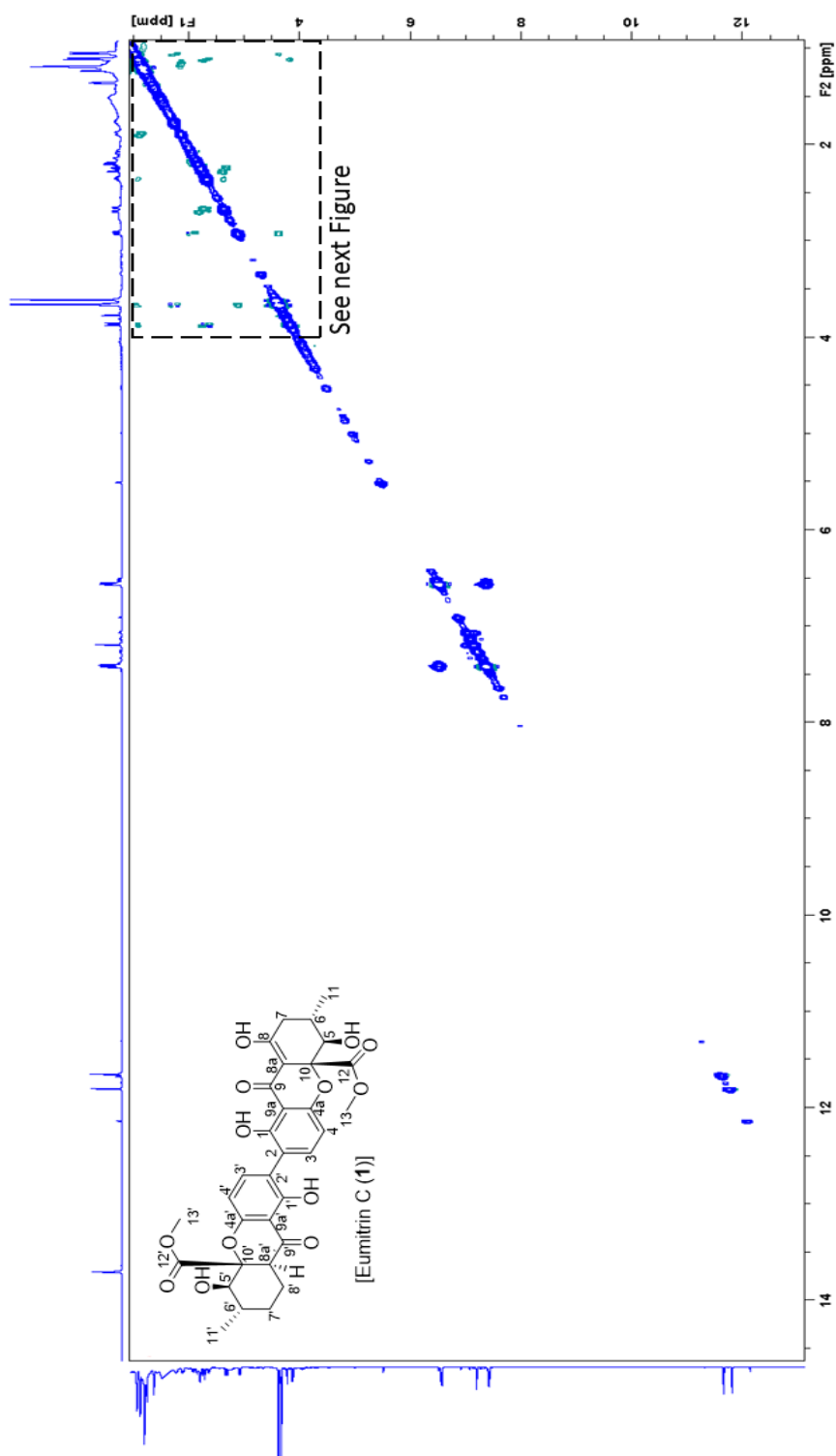


Figure A. 9 The ROESY (CDCl₃, 500 MHz) spectrum of US1

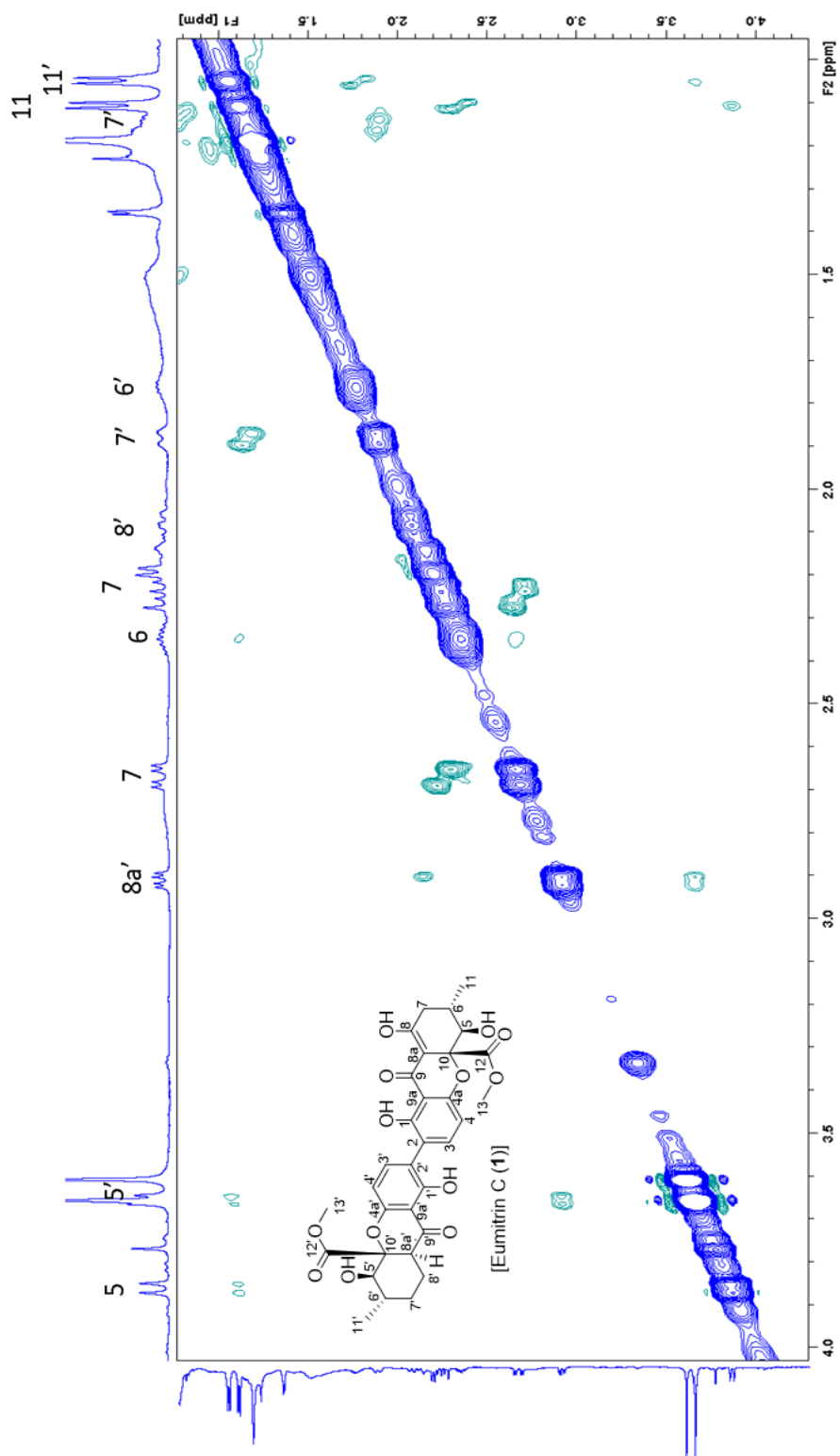


Figure A. 10 The ROESY (CDCl₃, 500 MHz) spectrum of US1 (1.25 to 4.0 ppm)

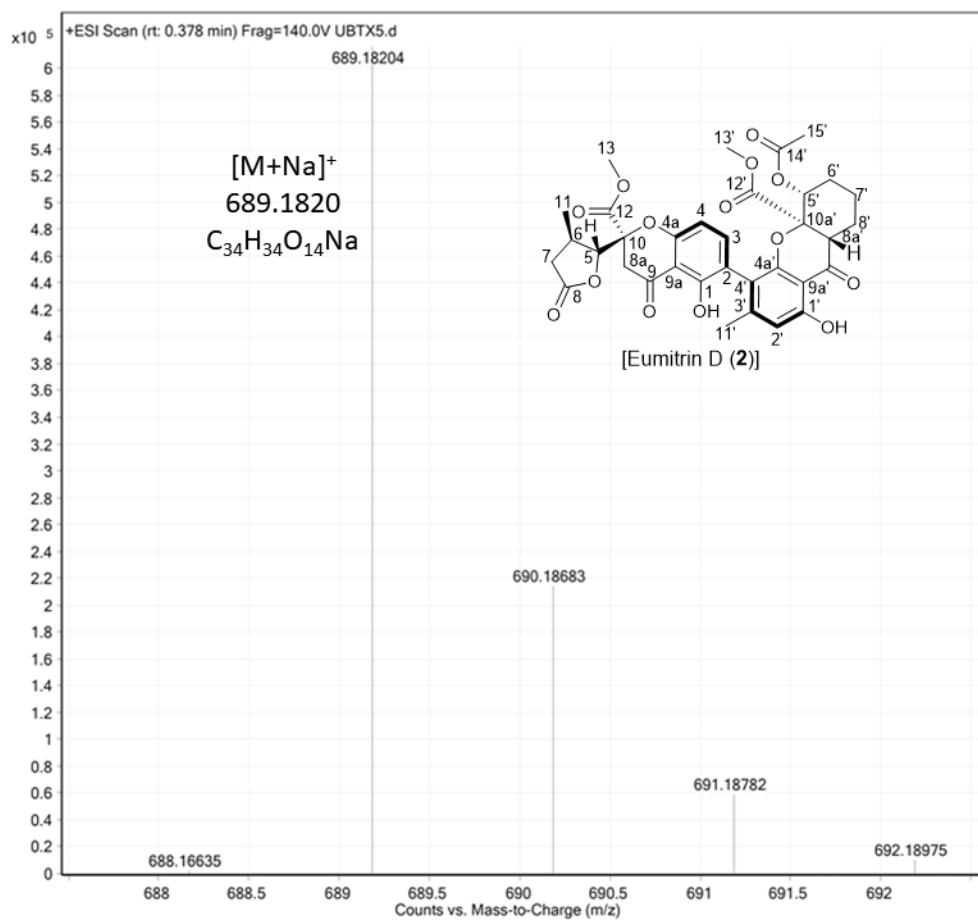


Figure A. 11 The HRESIMS spectrum of US2

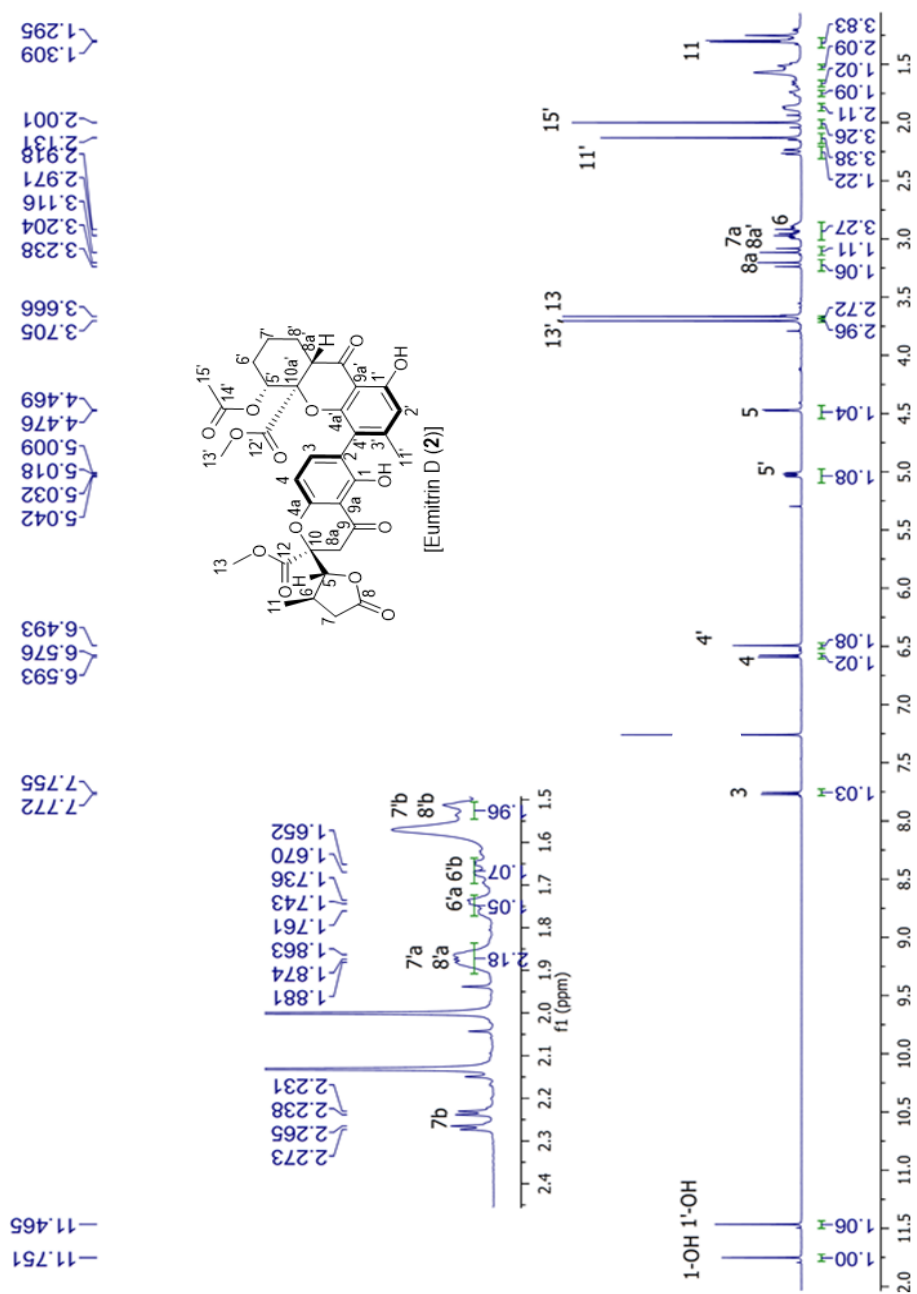


Figure A. 12 The ^1H NMR (CDCl_3 , 500 MHz) spectrum of **US2**

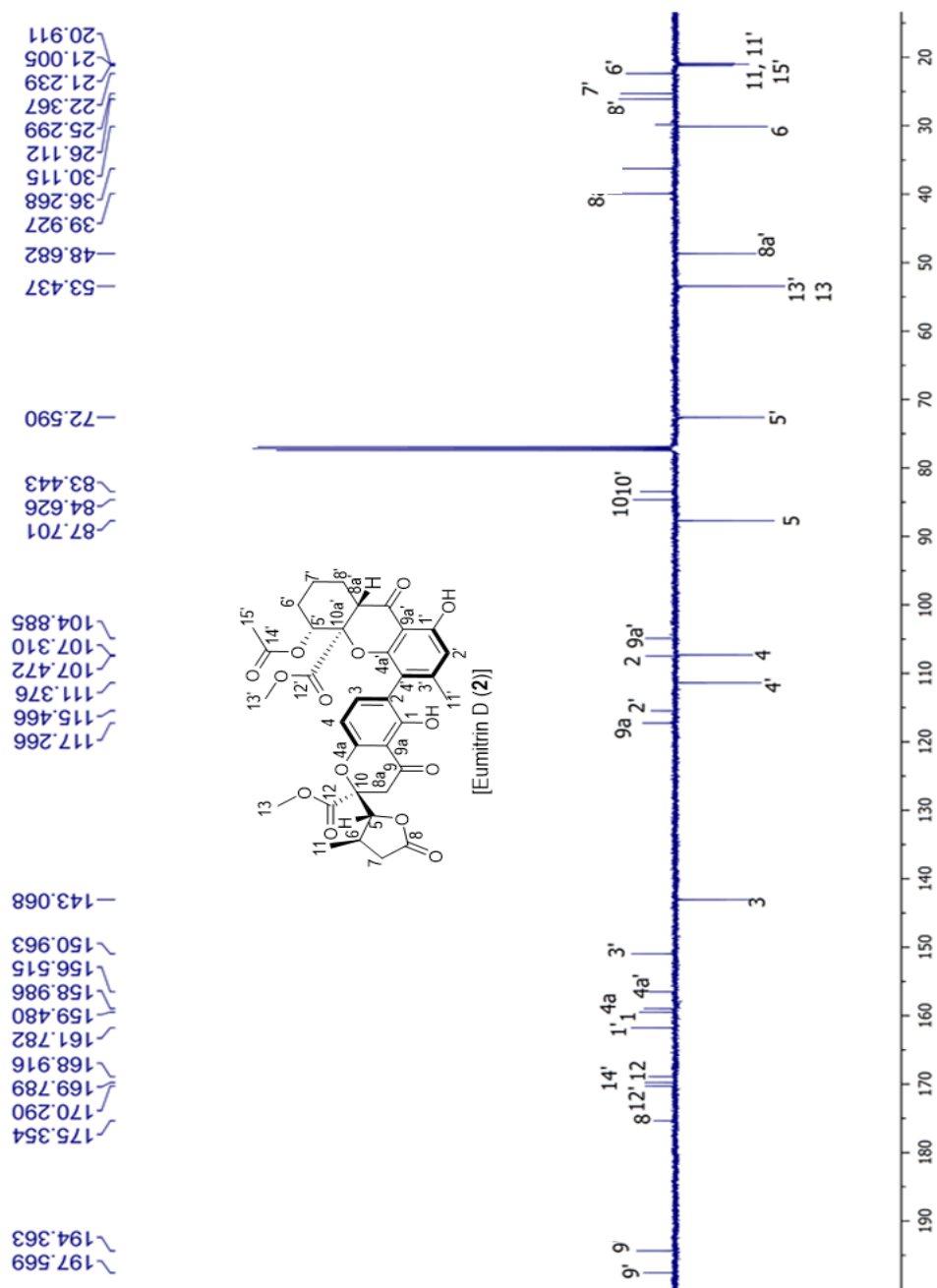


Figure A. 13 The ^{13}C NMR (CDCl_3 , 125 MHz) spectrum of US2

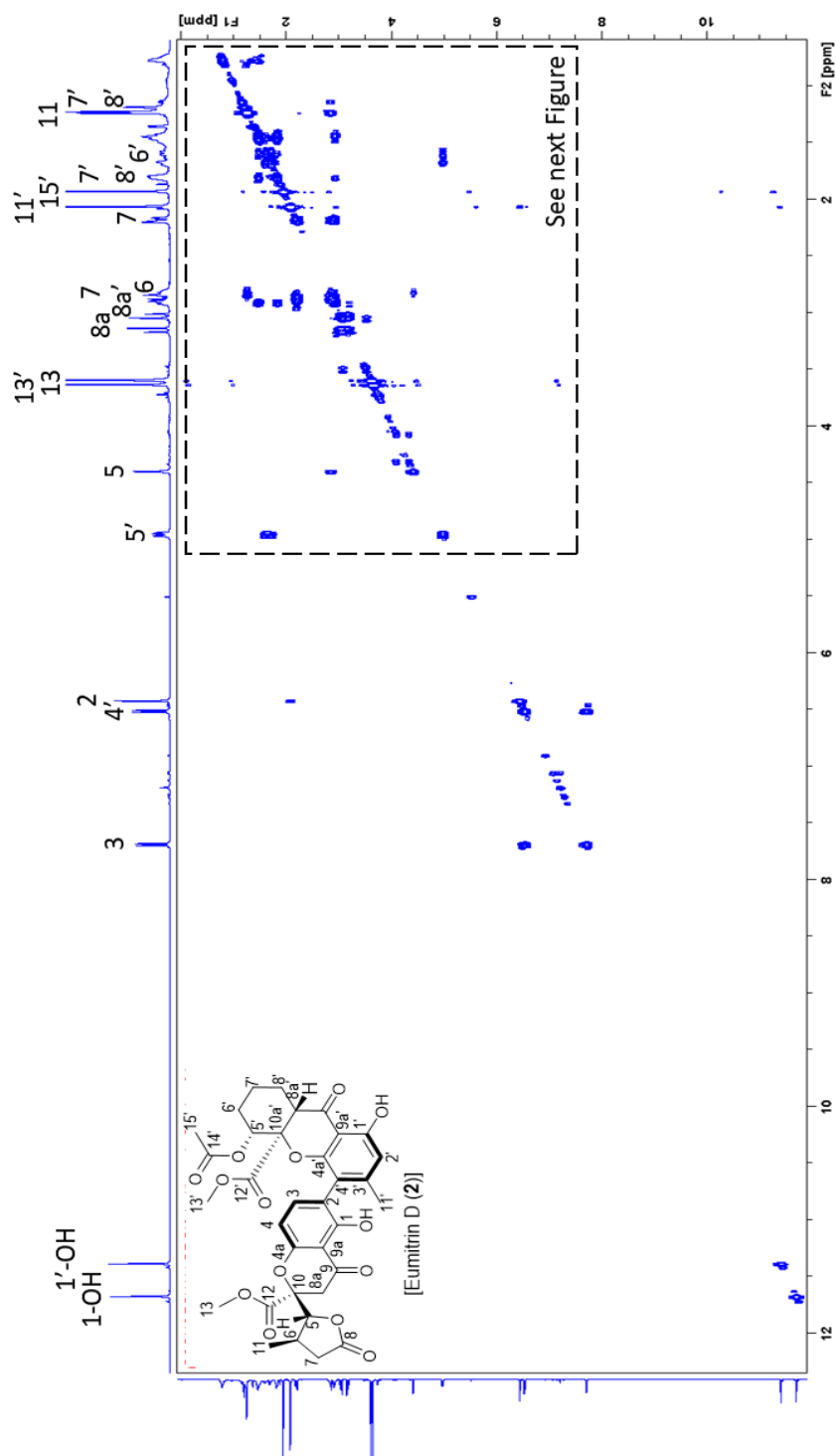


Figure A. 14 The COSY (CDCl_3 , 500 MHz) spectrum of US2

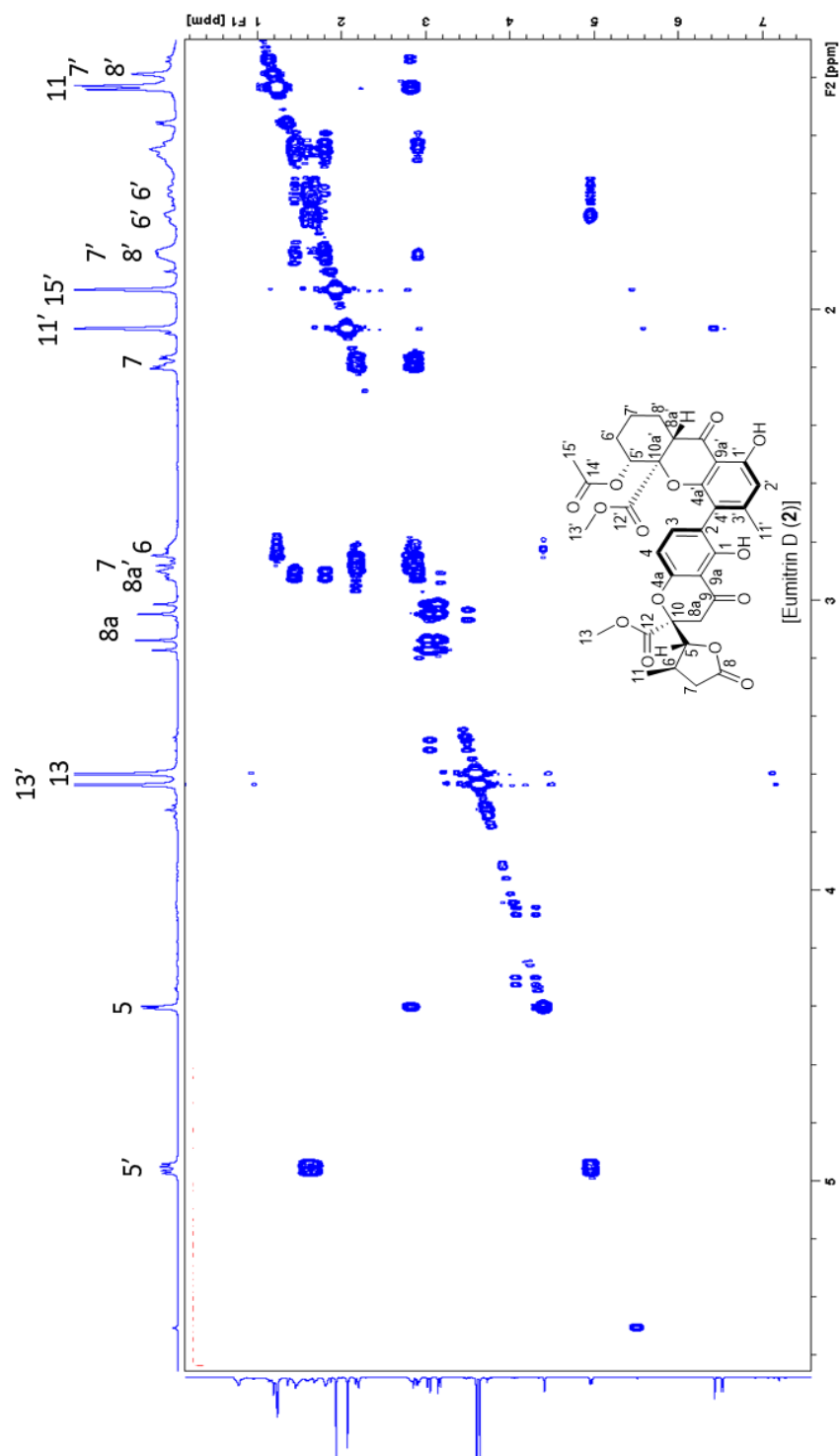


Figure A. 15 The COSY (CDCl₃, 500 MHz) spectrum of US2 (1.25 to 5.5 ppm)

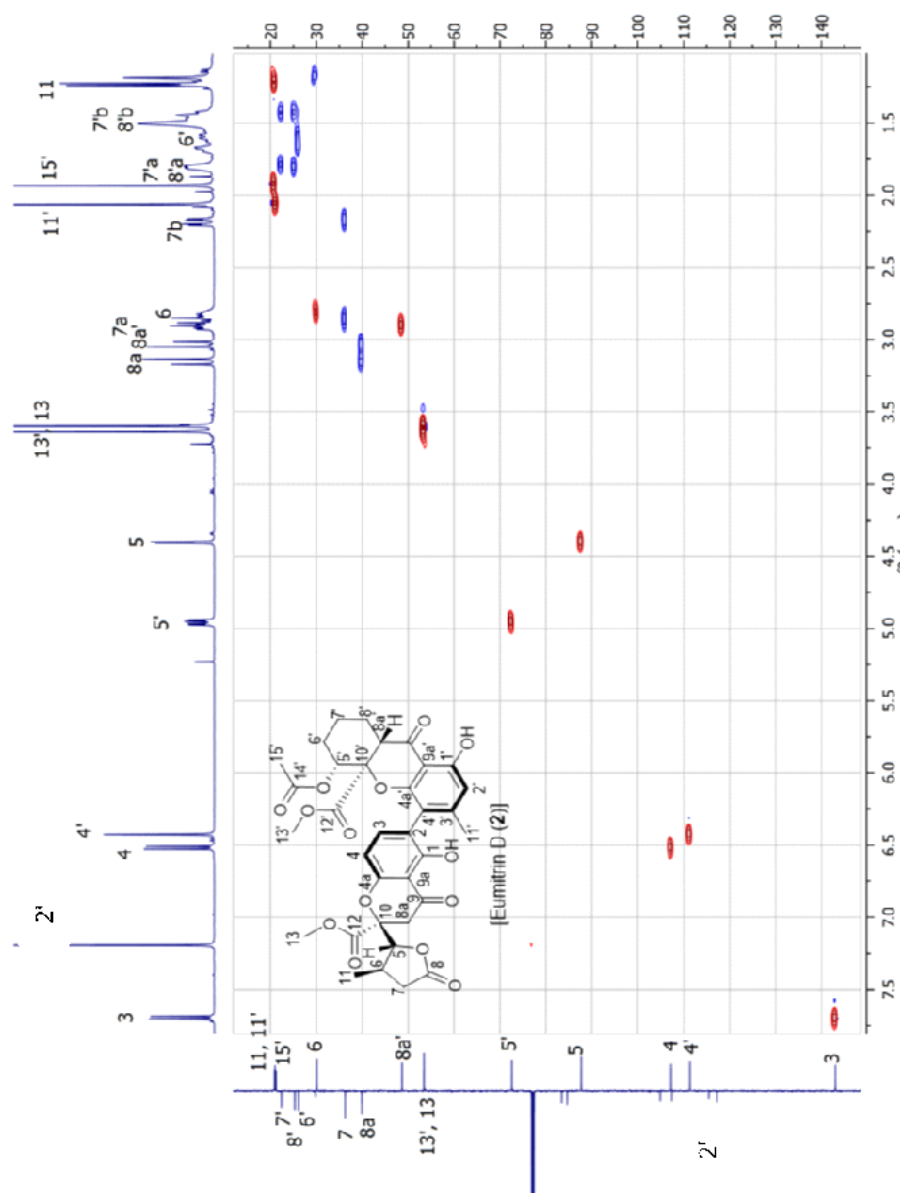


Figure A. 16 The HSQC (CDCl_3 , 500 MHz, 125 MHz) spectrum of US2

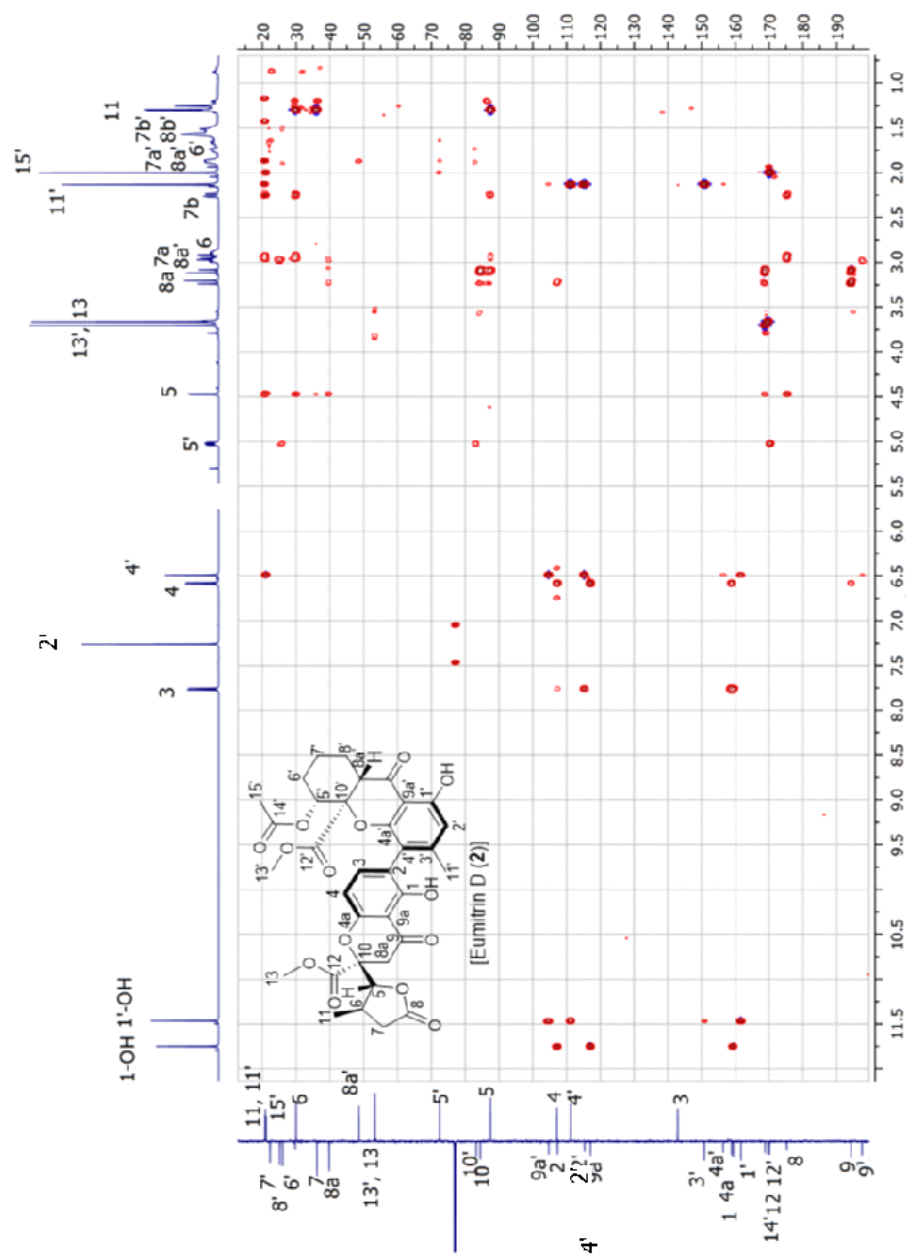


Figure A. 17 The HMBC (CDCl₃, 500 MHz, 125 MHz) spectrum of US2

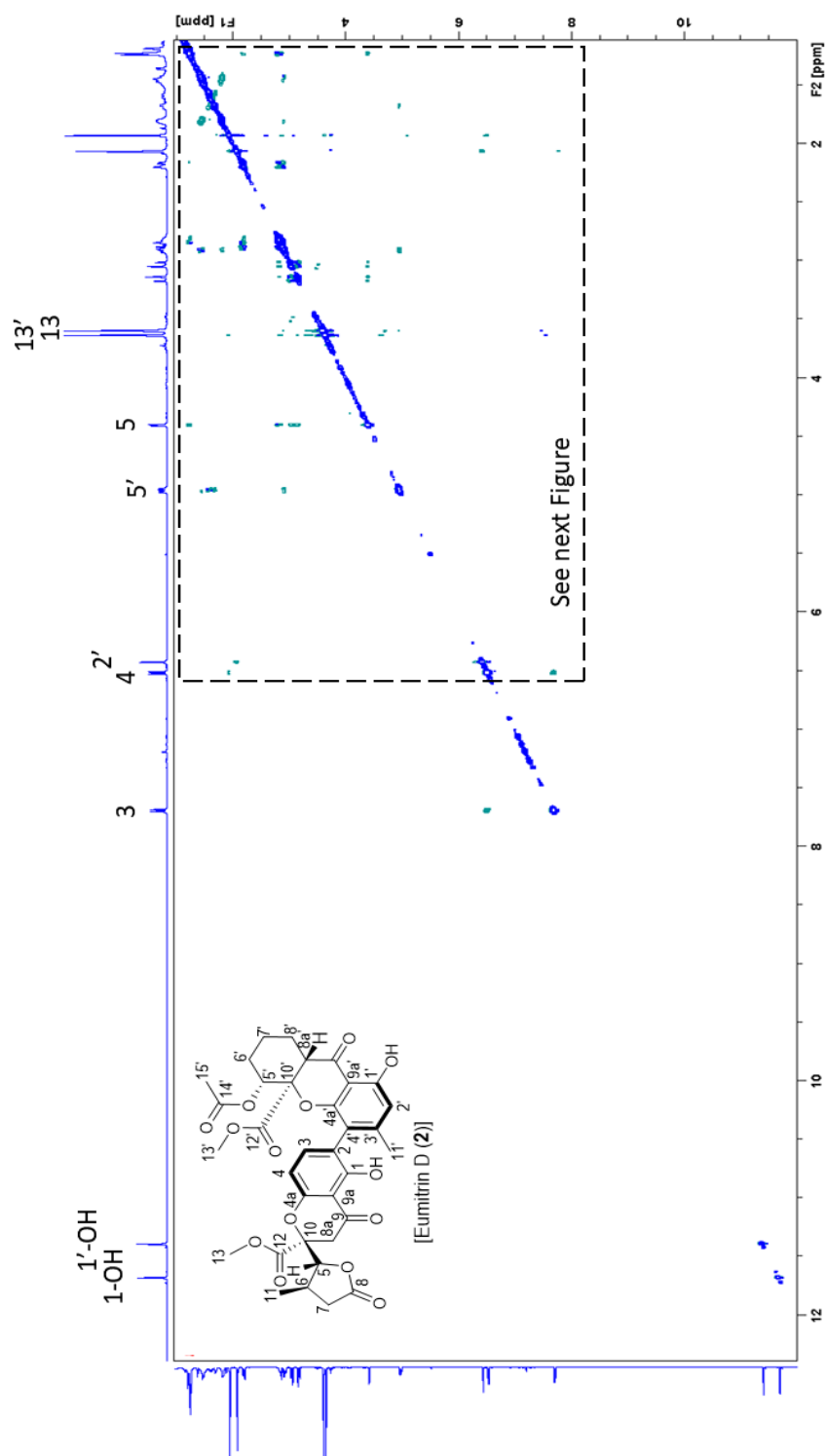


Figure A. 18 The ROESY (CDCl_3 , 500 MHz) spectrum of **US2**

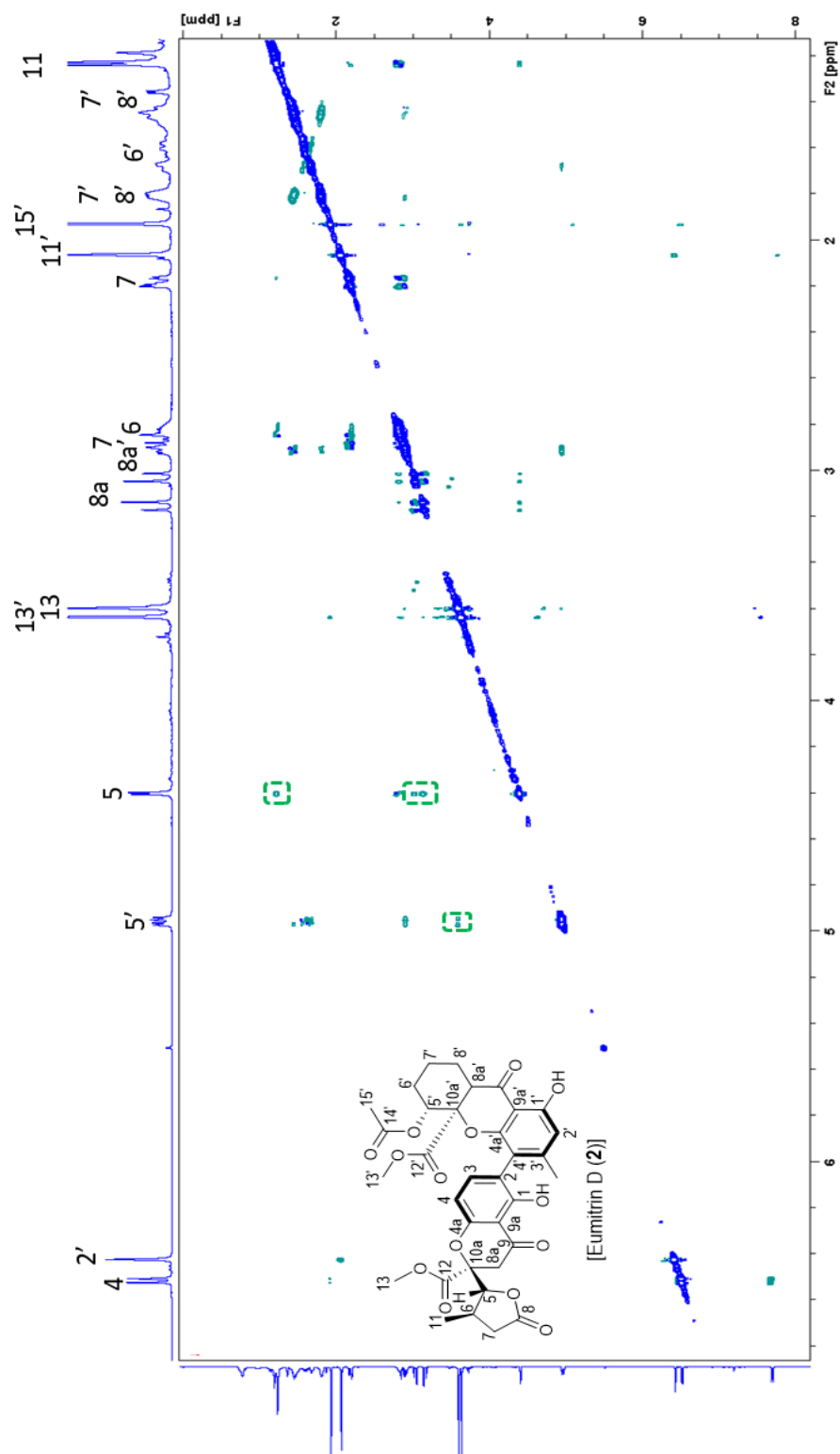


Figure A. 19 The ROESY (CDCl₃, 500 MHz) spectrum of US2 (1.25 to 8.0 ppm)

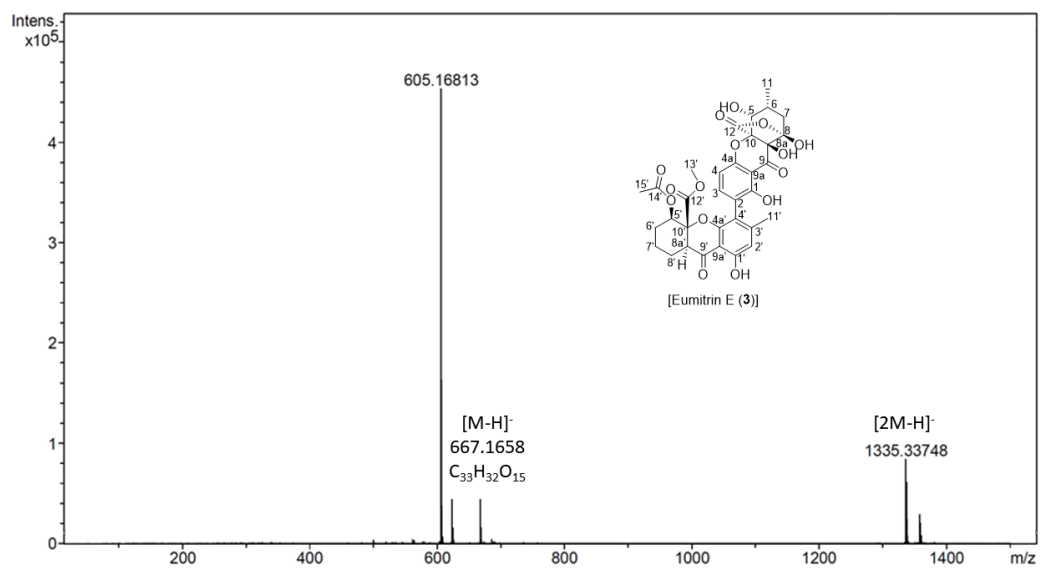
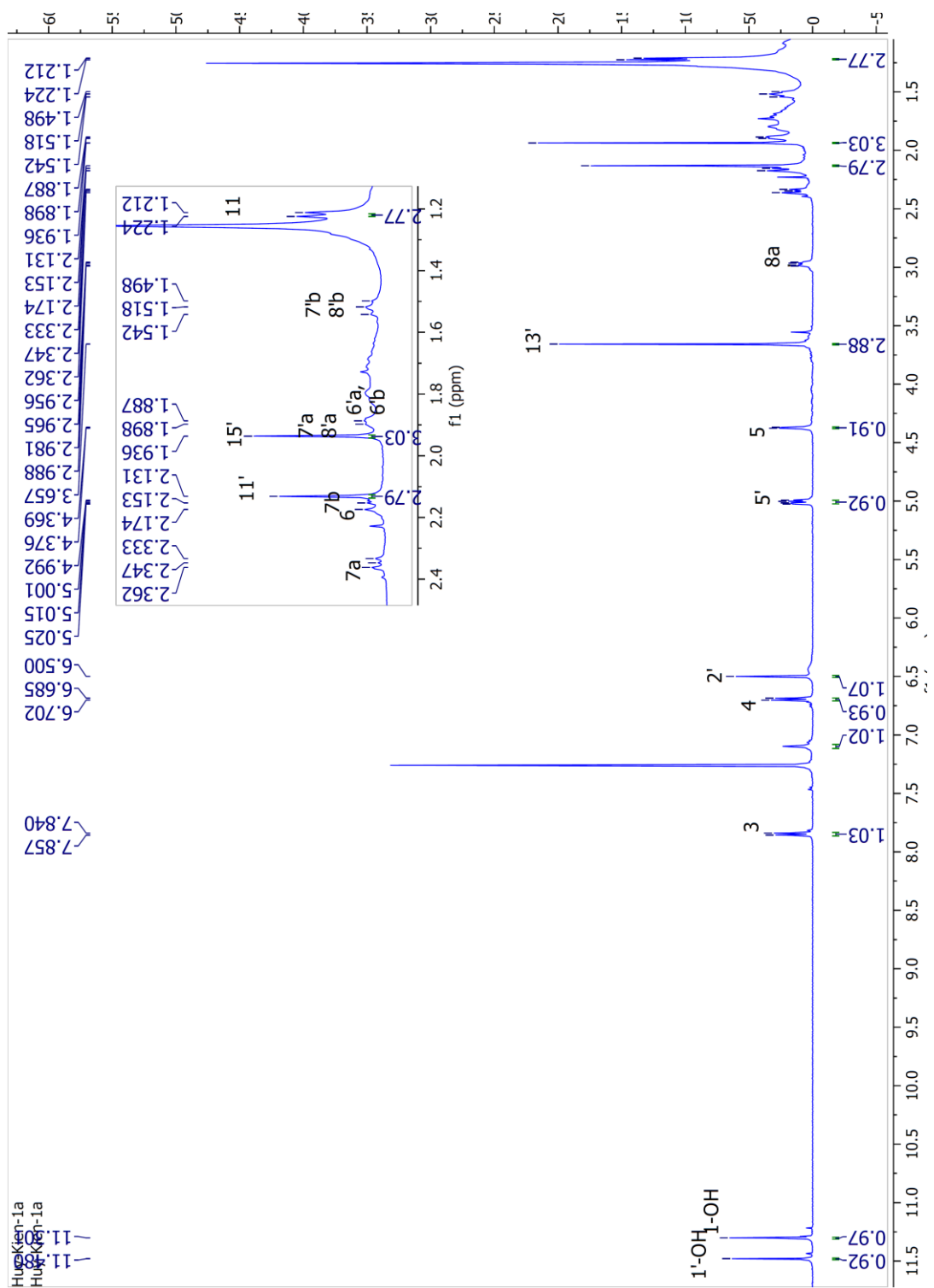


Figure A. 20 The HRESIMS spectrum of US3





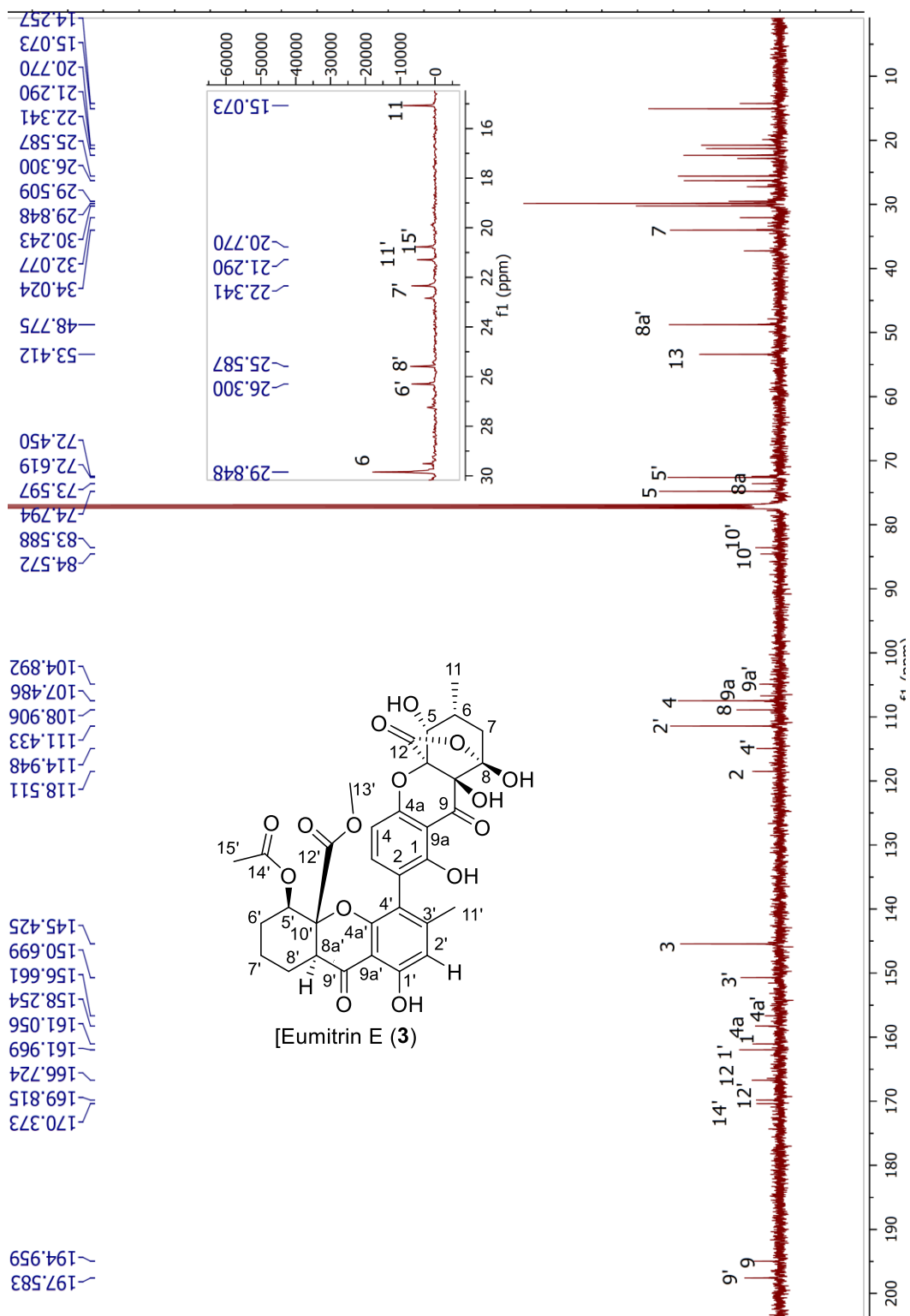


Figure A. 22 The ¹³C NMR (CDCl₃, 125 MHz) spectrum of US3

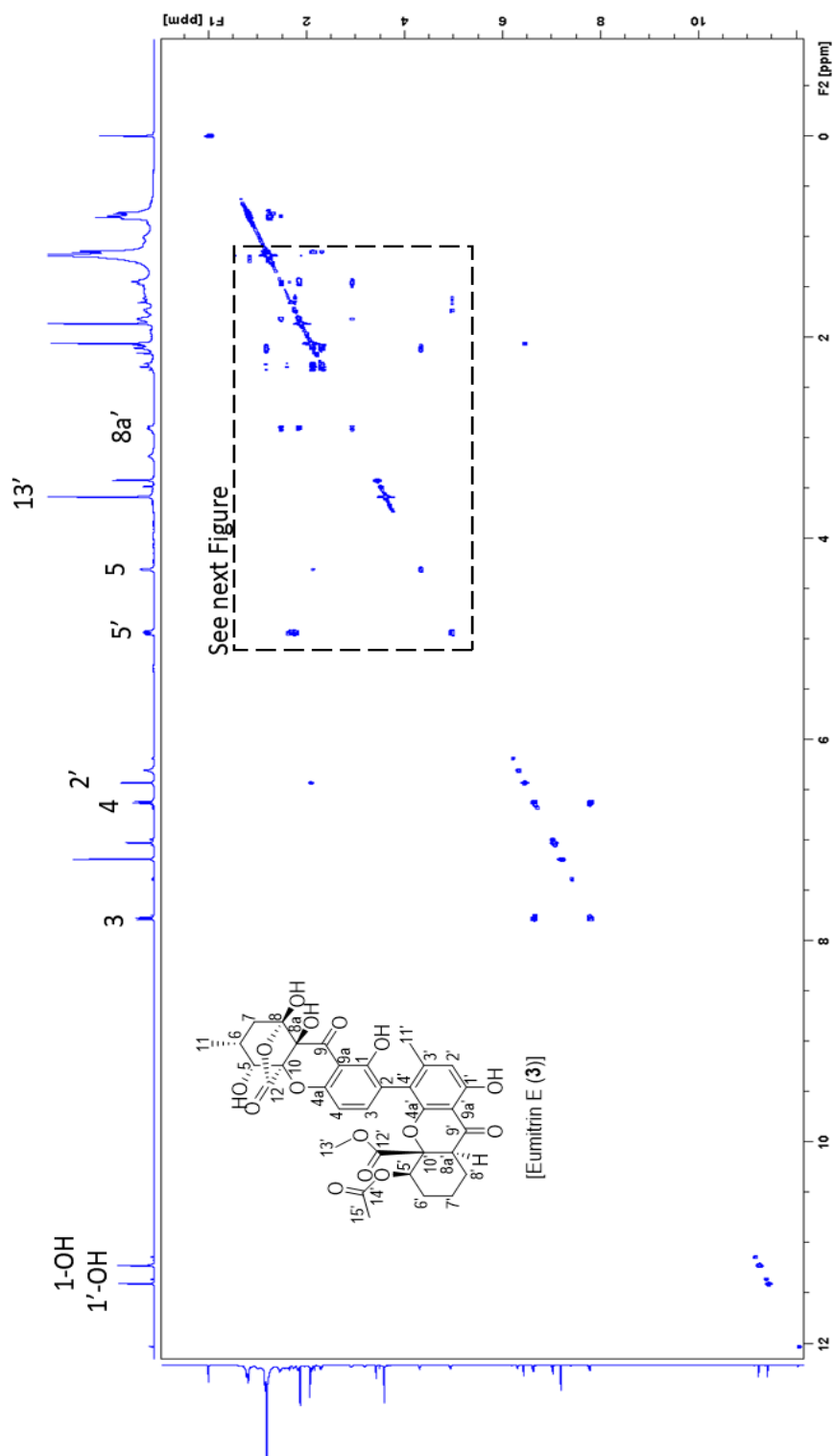


Figure A. 23 The COSY (CDCl₃, 500 MHz) spectrum of US3

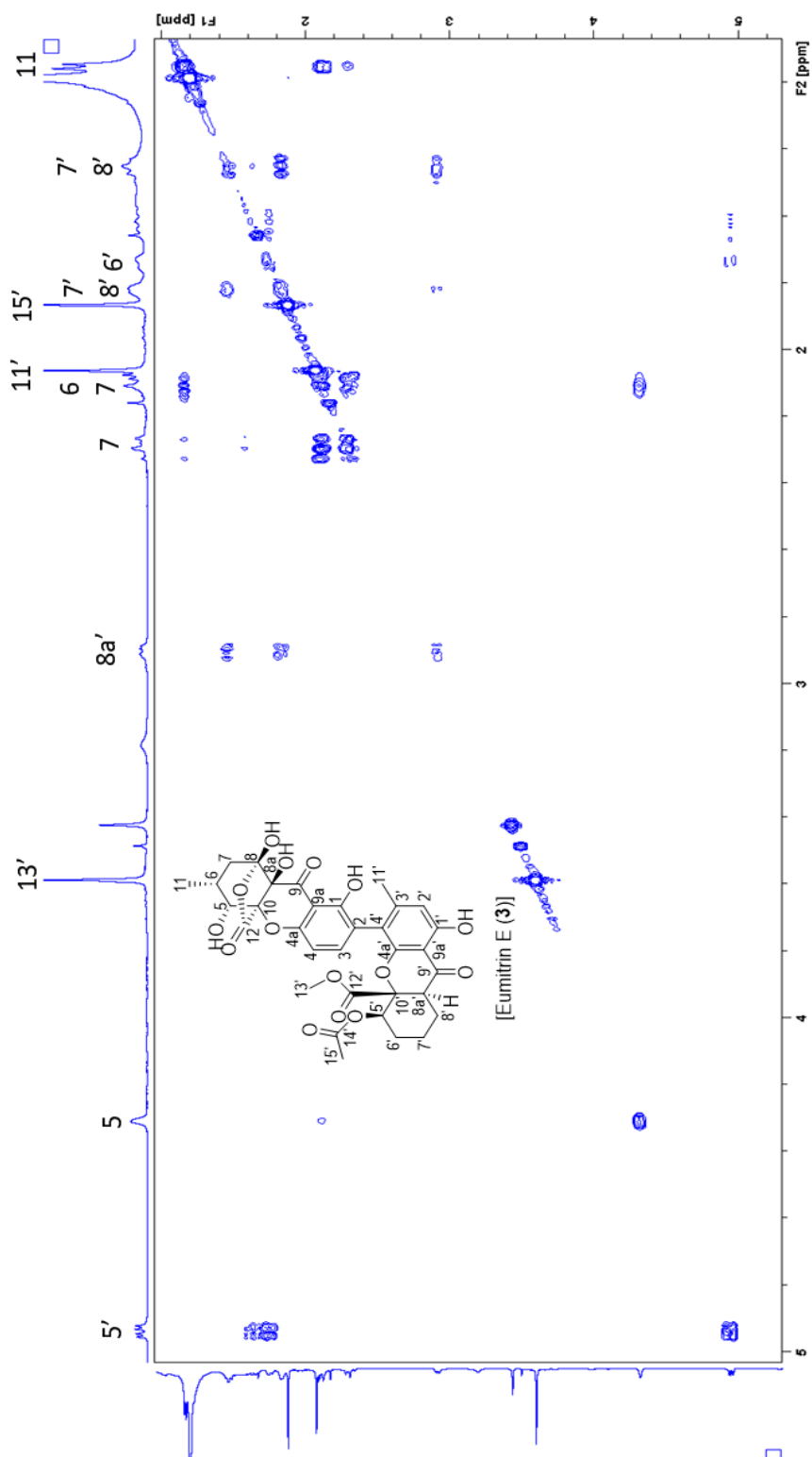


Figure A. 24 The COSY (CDCl₃, 500 MHz) spectrum of **US3** (1.2 to 5.2 ppm)

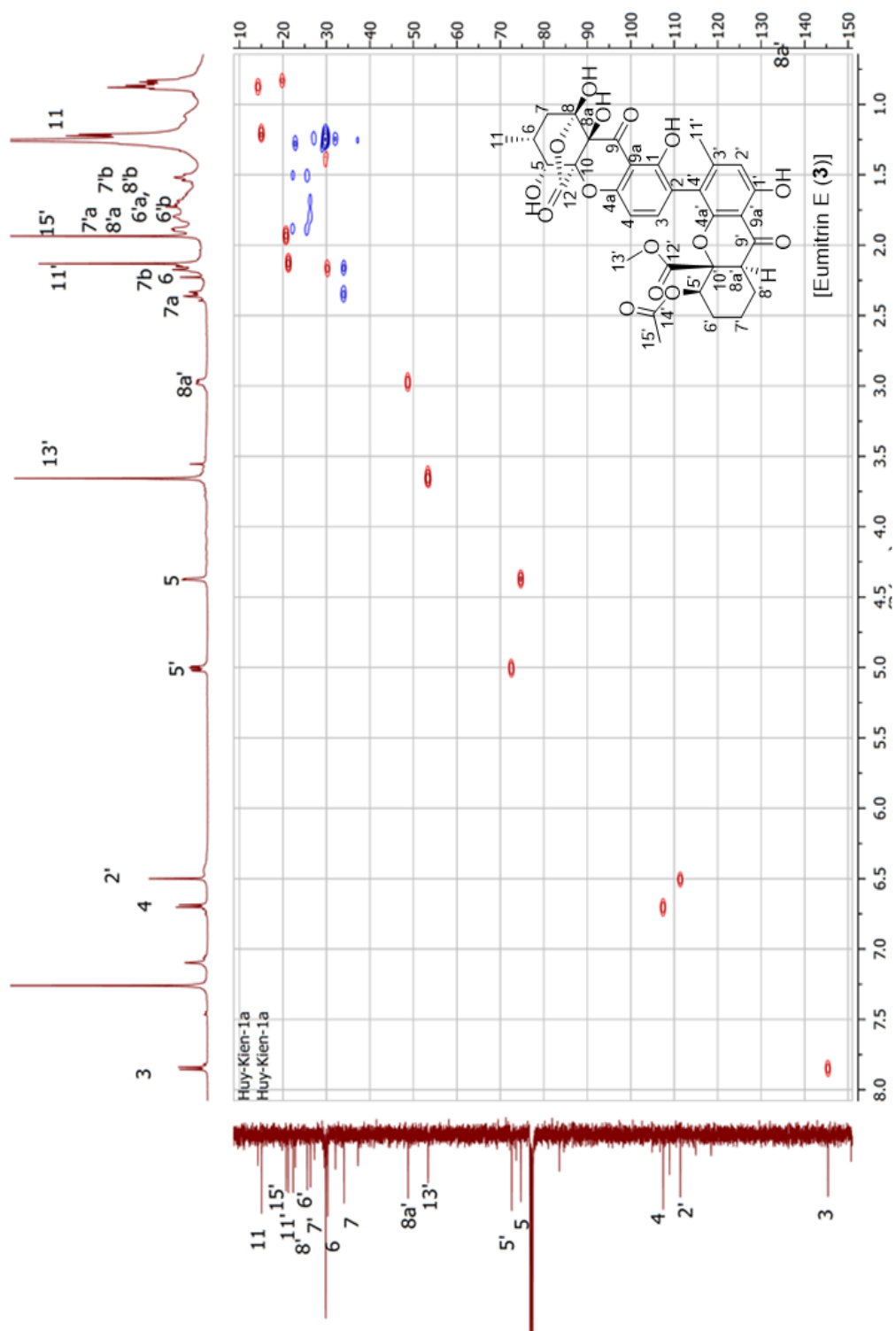


Figure A. 25 The HSQC (CDCl₃, 500 MHz, 125 MHz) spectrum of US3

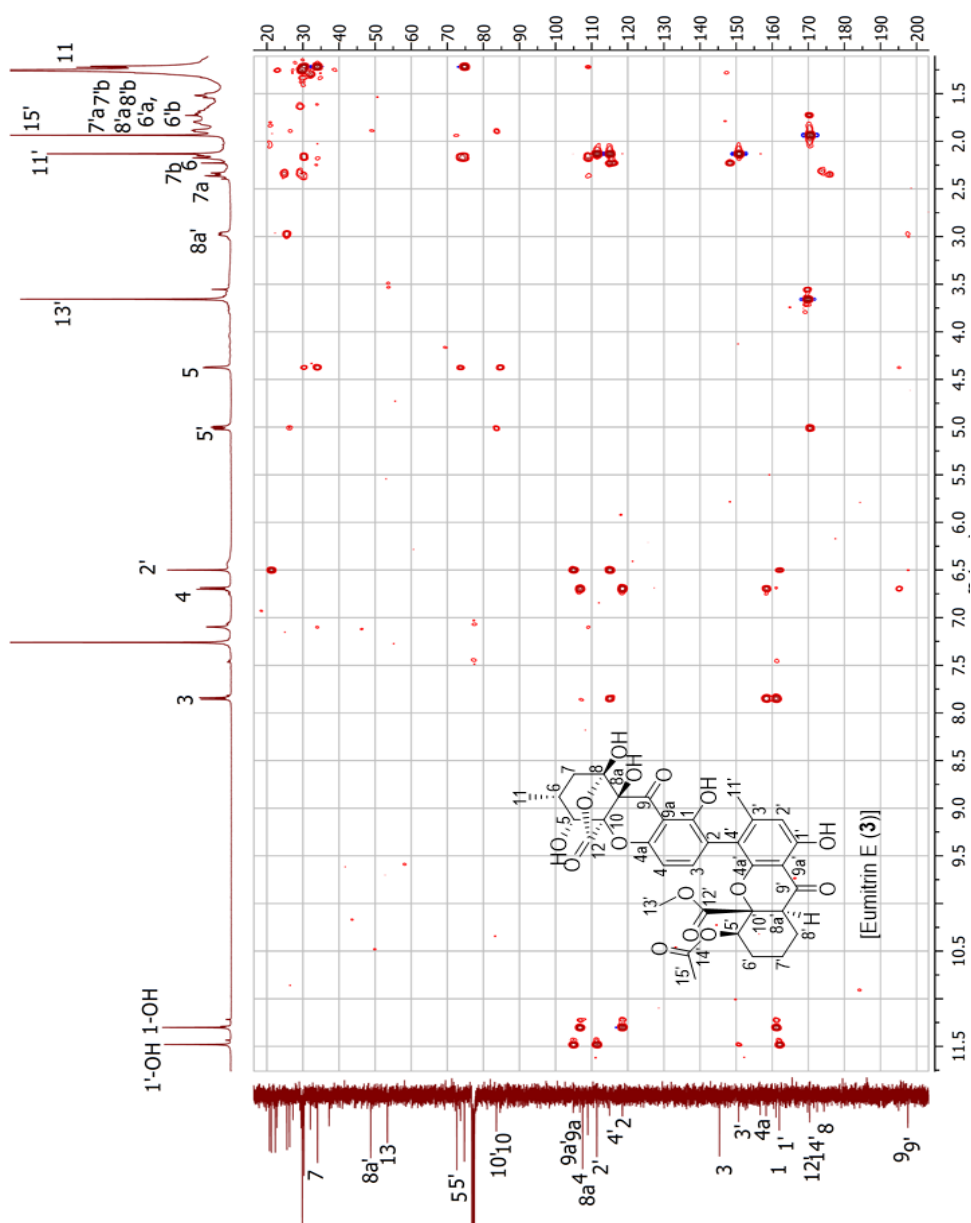
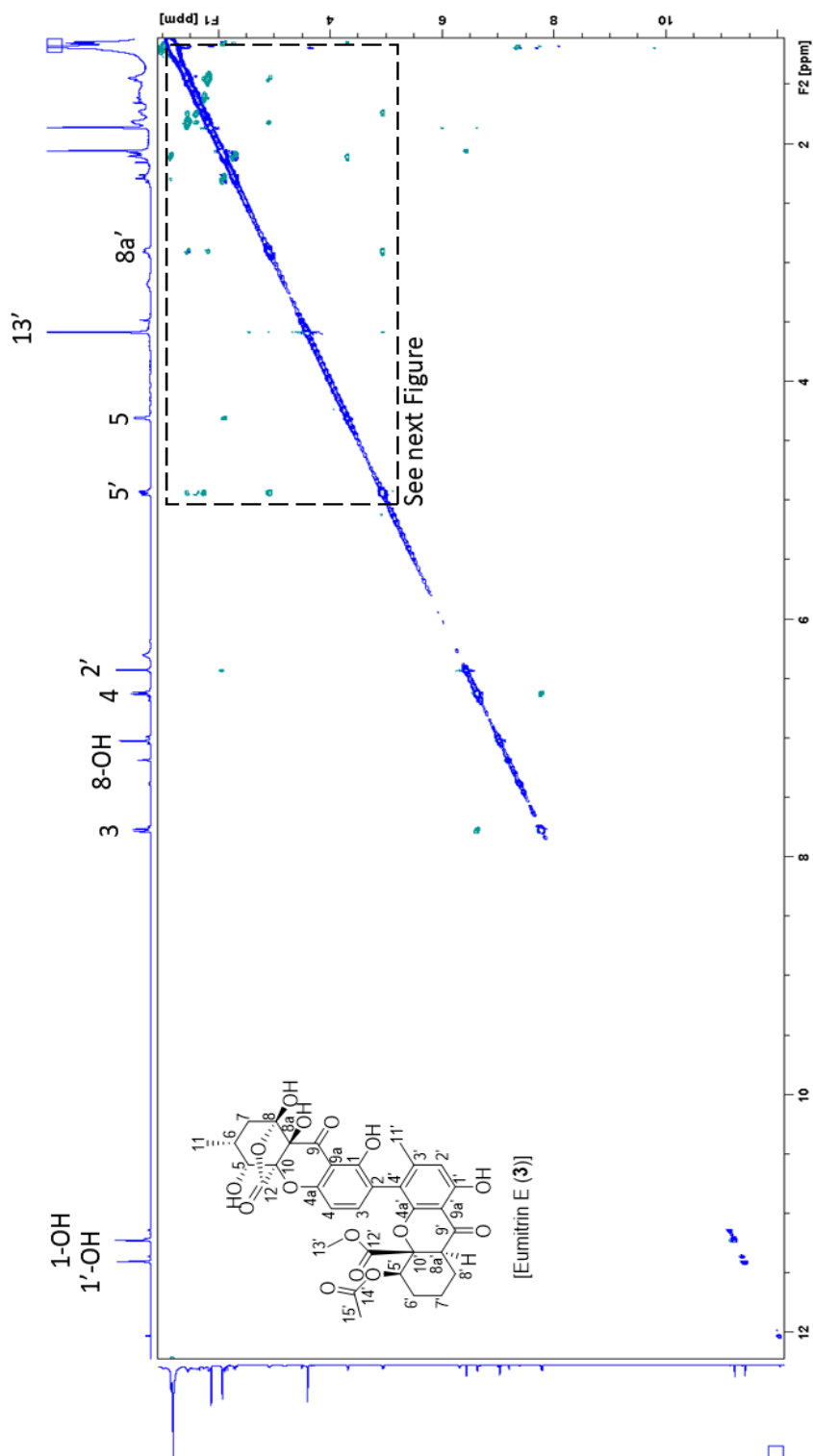


Figure A. 26 The HMBC (CDCl_3 , 500 MHz, 125 MHz) spectrum of US3

Figure A. 27 The ROESY (CDCl₃, 500 MHz) spectrum of US3

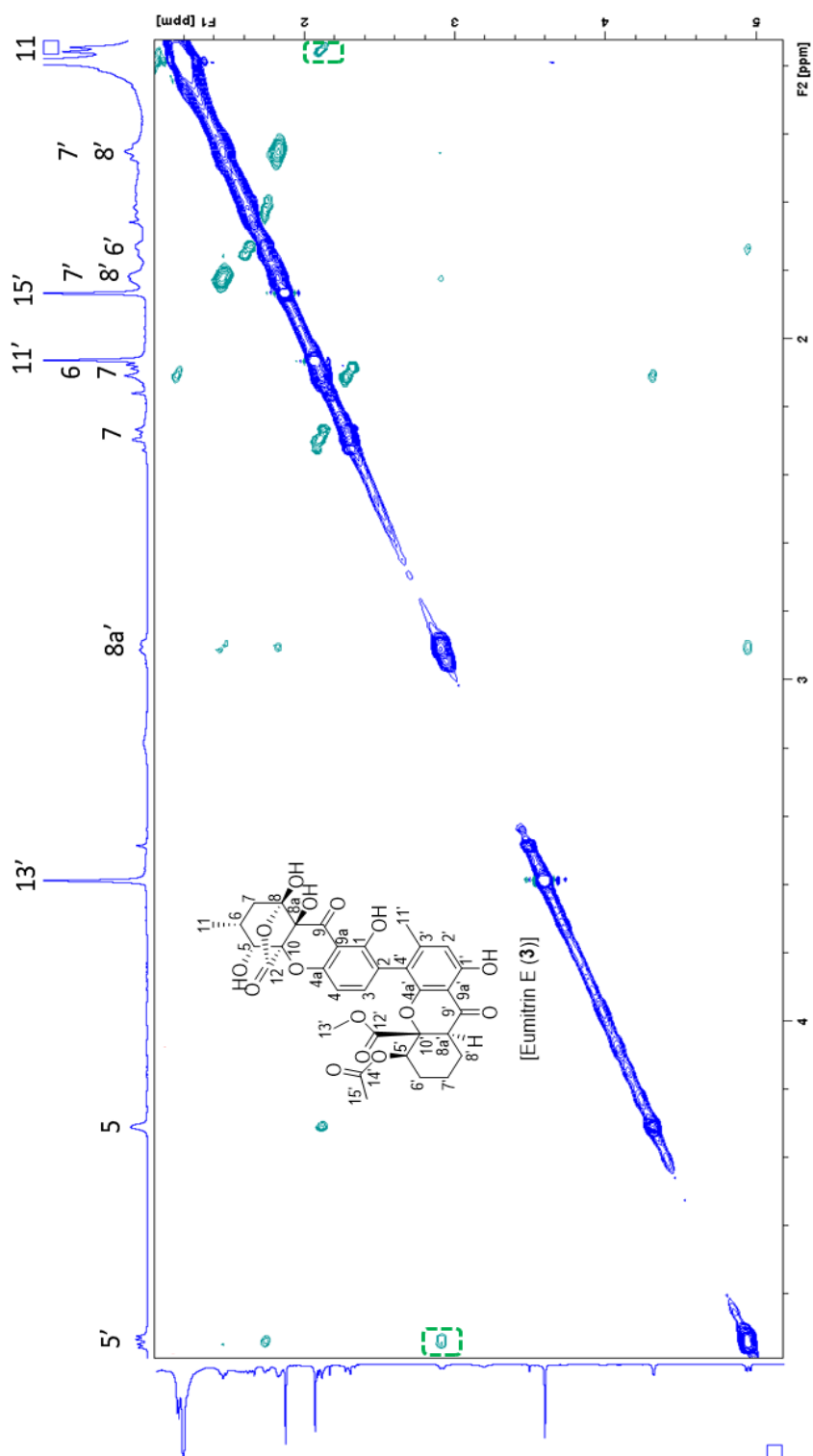


Figure A. 28 The ROESY (CDCl₃, 500 MHz) spectrum of **US3** (1.2 to 5.0 ppm)

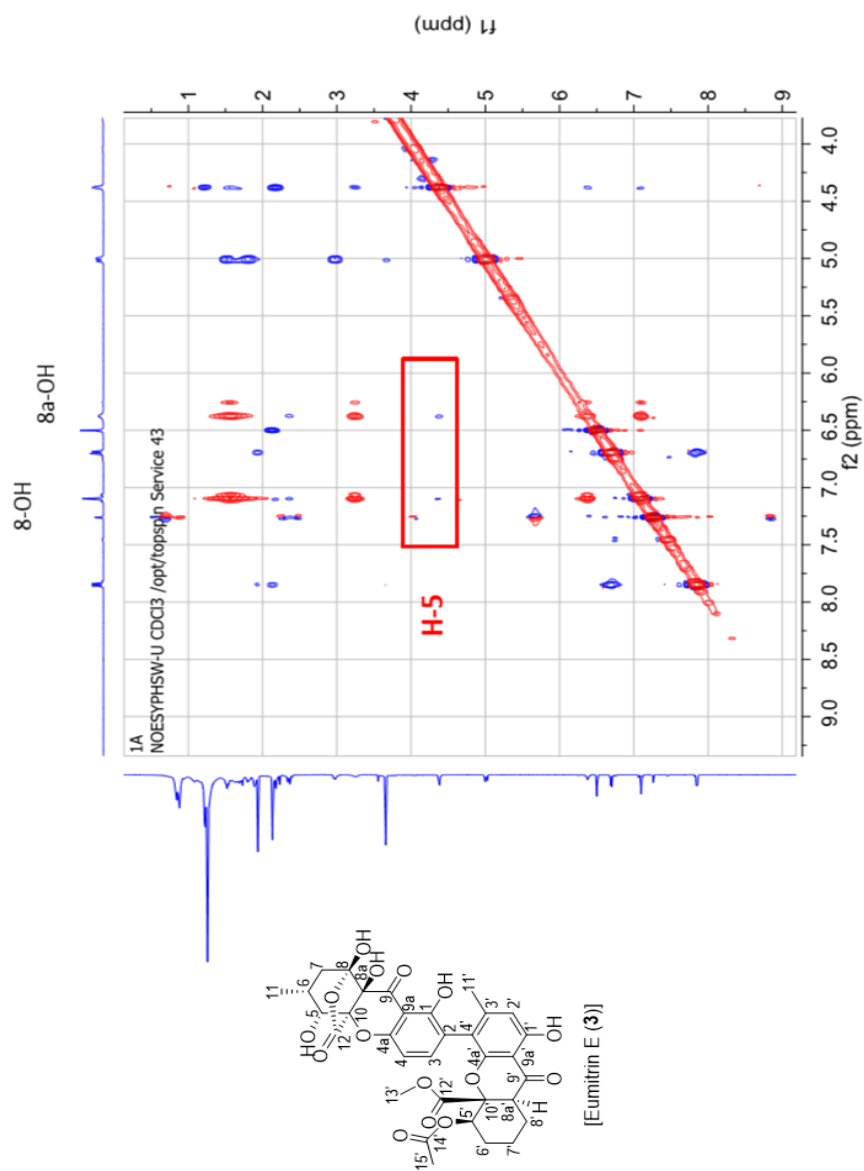


Figure A. 29 The ROESY (CDCl₃, 500 MHz) spectrum of **US3** (zoom into 8-OH and 8a-OH correlations)

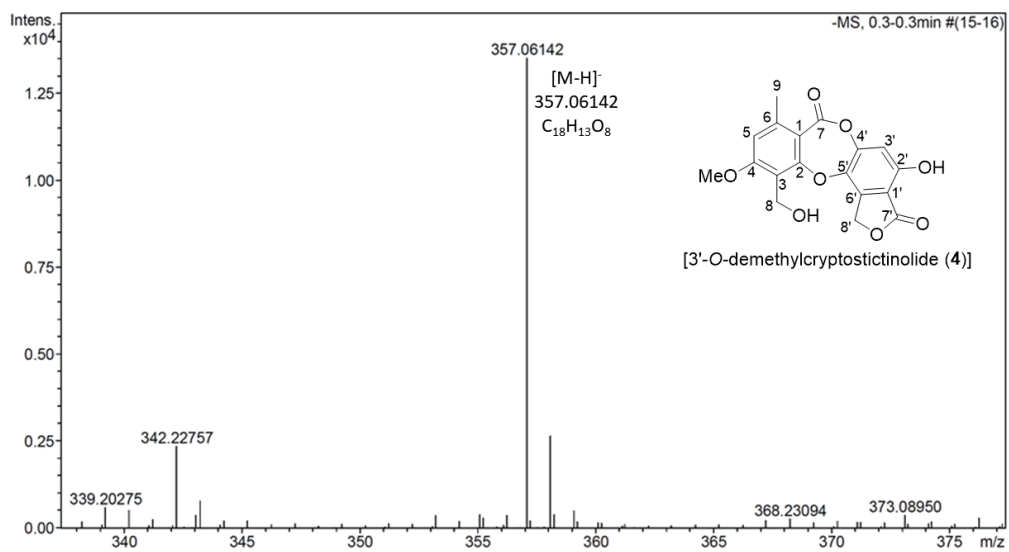


Figure A. 30 The HRESIMS spectrum of US4



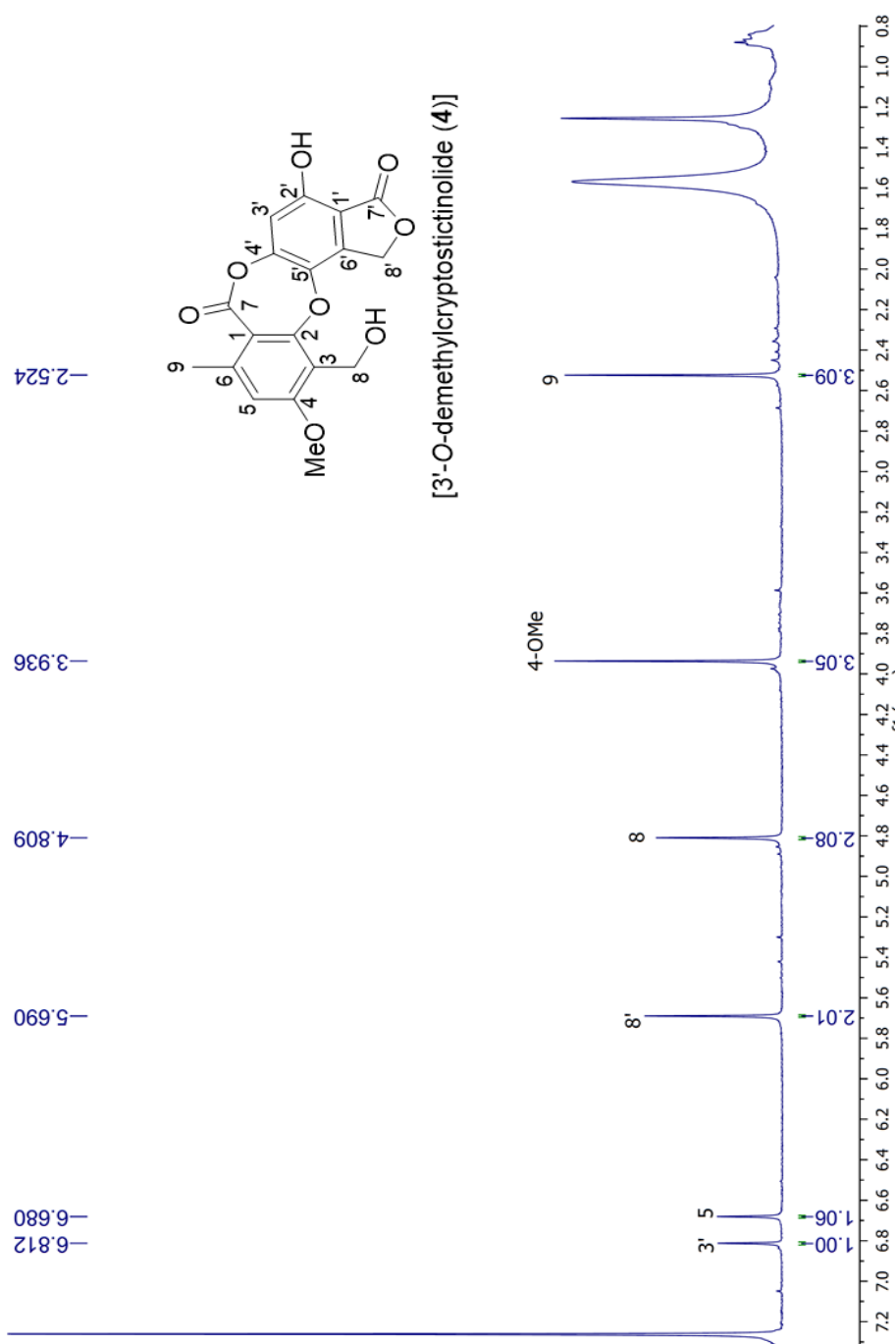


Figure A. 31 The ^1H NMR (CDCl_3 , 500 MHz) spectrum of US4

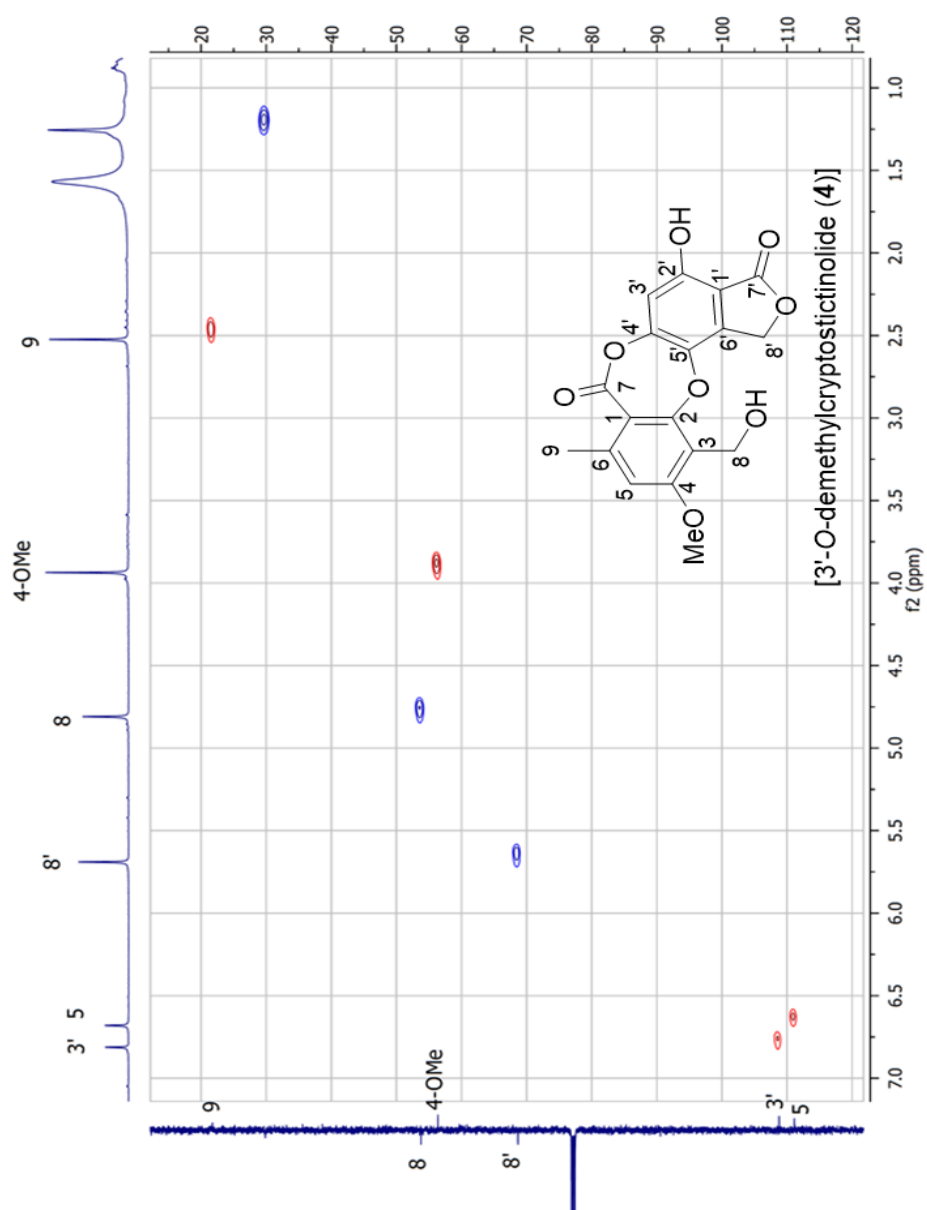


Figure A. 32 The HSQC (CDCl₃, 500 MHz, 125 MHz) spectrum of US4

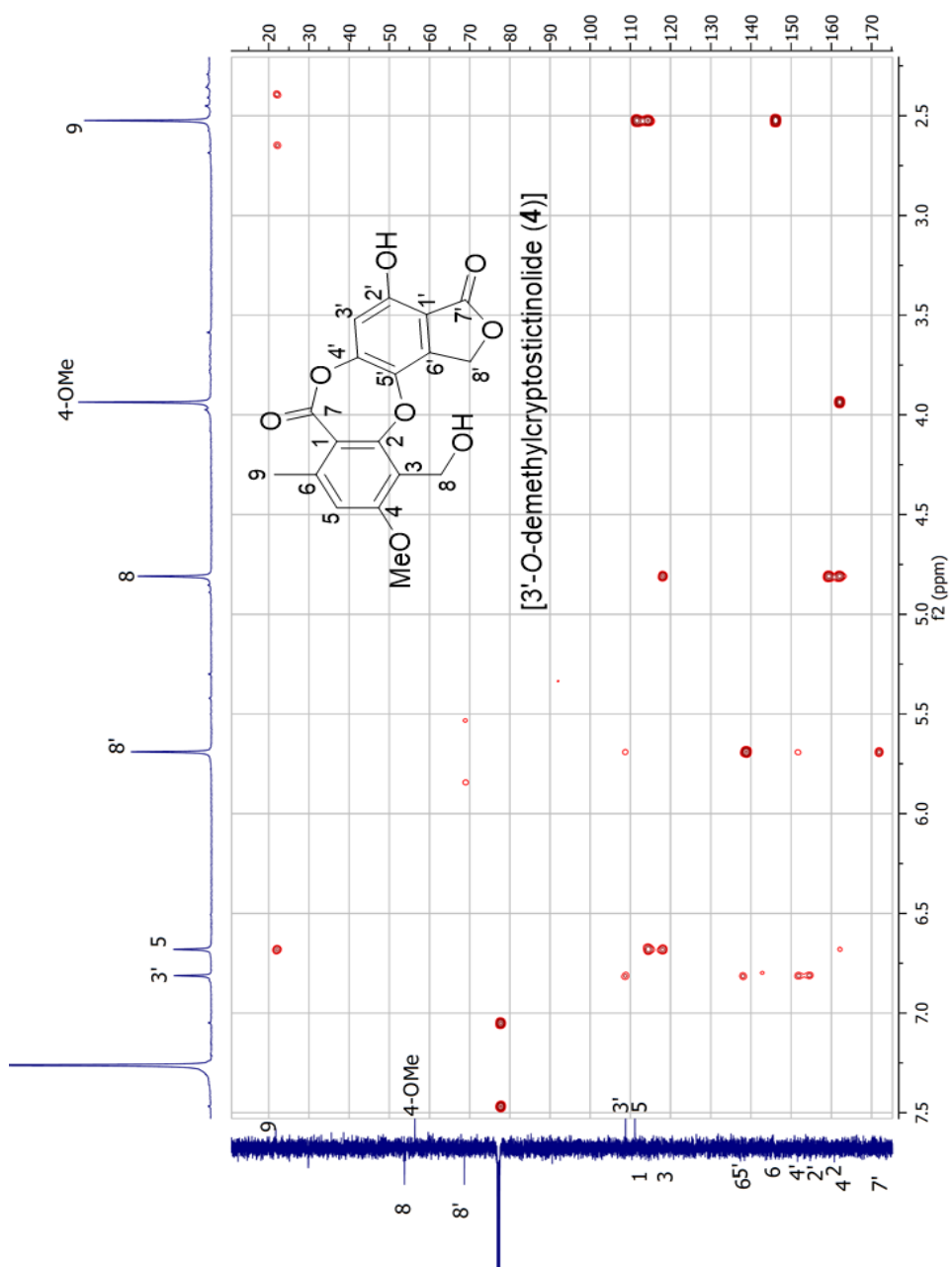


Figure A. 33 The HMBC (CDCl_3 , 500 MHz, 125 MHz) spectrum of US4

Generic Display Report

Analysis Info

Analysis Name D:\Data\Data Service\190325\XK9.5_RA7_01_2361.d
Method nv_pos_5min_profile_190214.m
Sample Name XK9.5
Comment

Acquisition Date 3/25/2019 4:41:41 PM

Operator CU.
Instrument micrOTOF-Q II

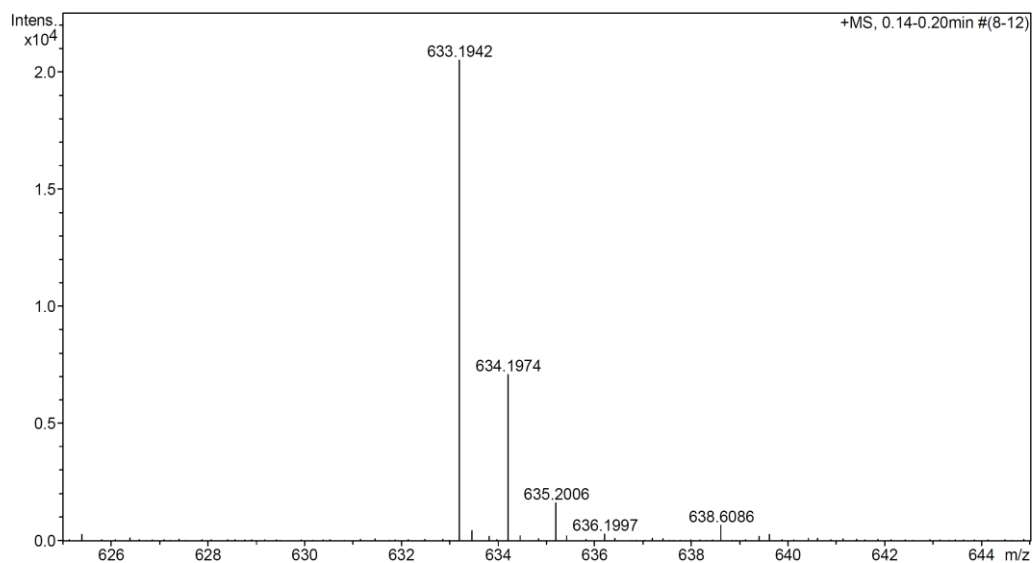
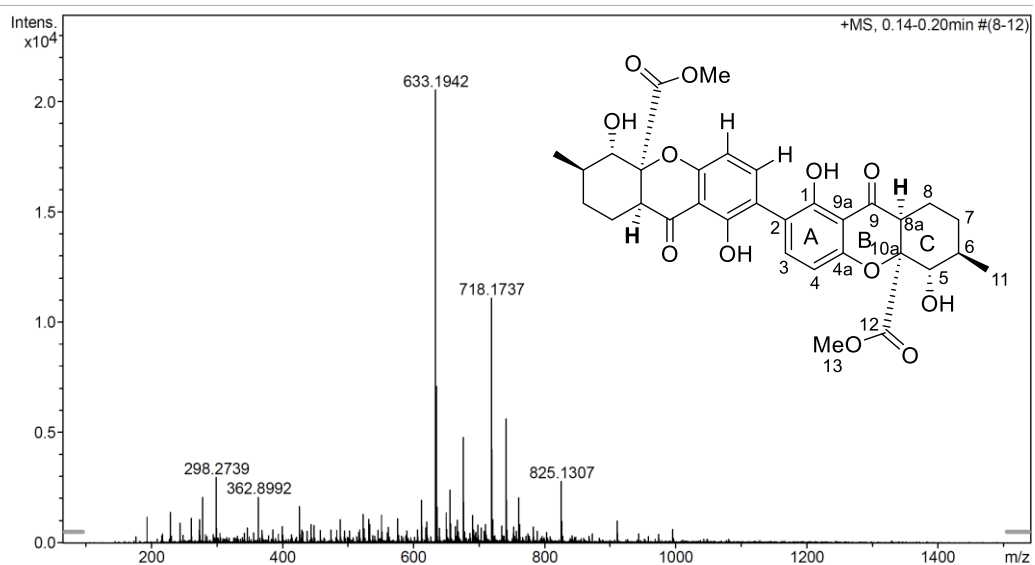


Figure A. 34 The HRESIMS spectrum of US5

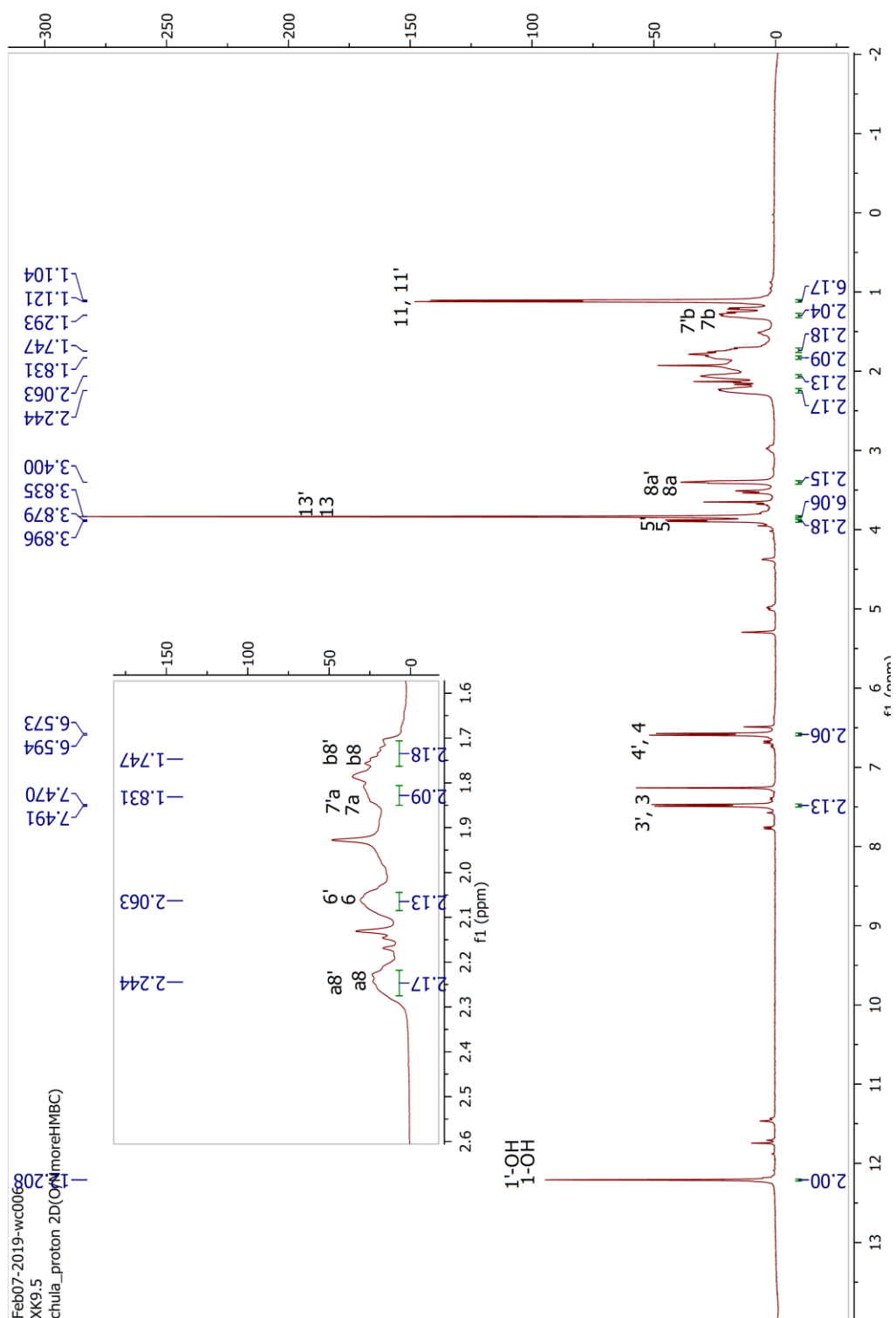


Figure A. 35 The ^1H NMR (CDCl_3 , 400 MHz) spectrum of US5

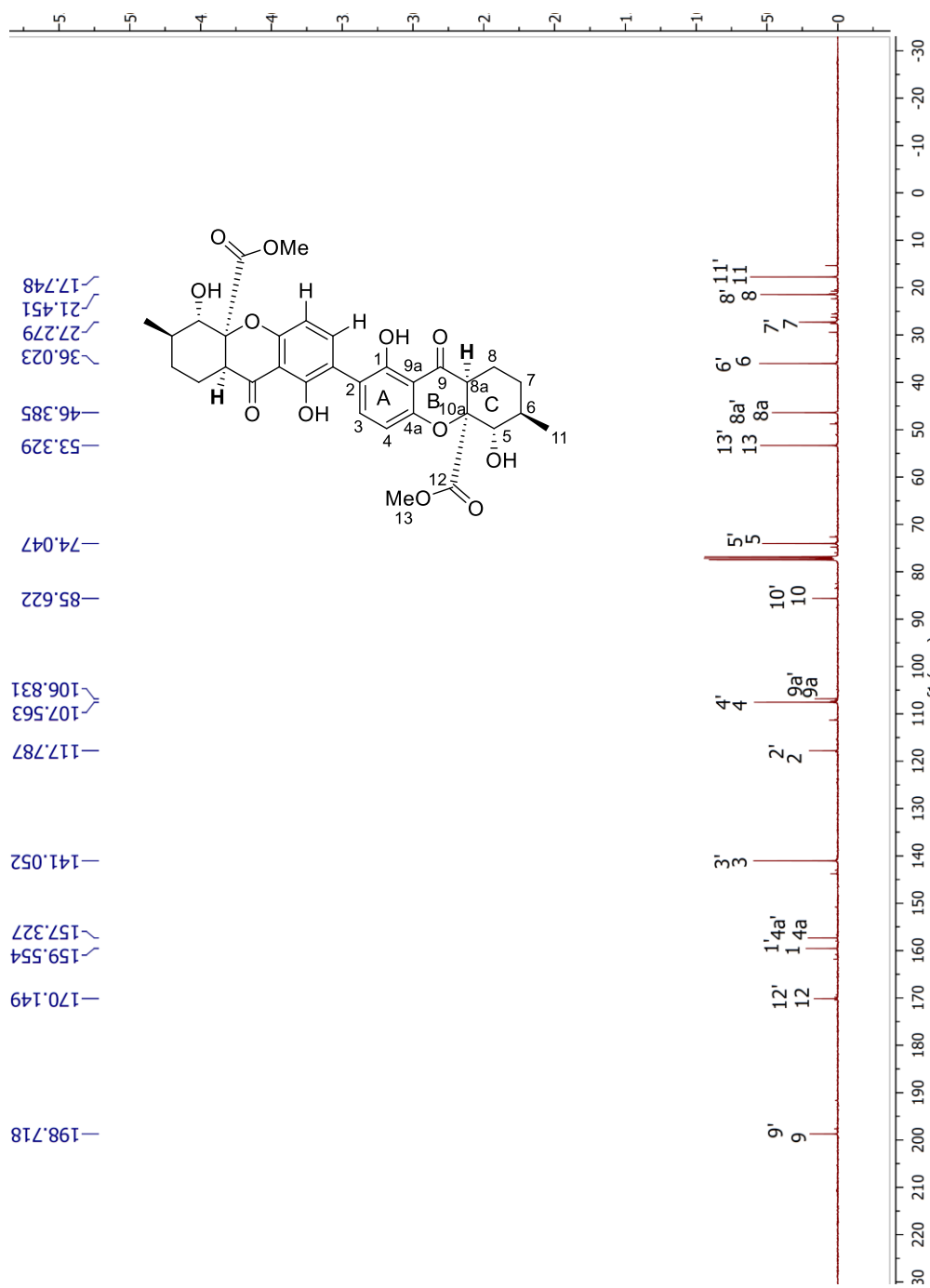


Figure A. 36 The ^{13}C NMR (CDCl_3 , 100 MHz) spectrum of US5

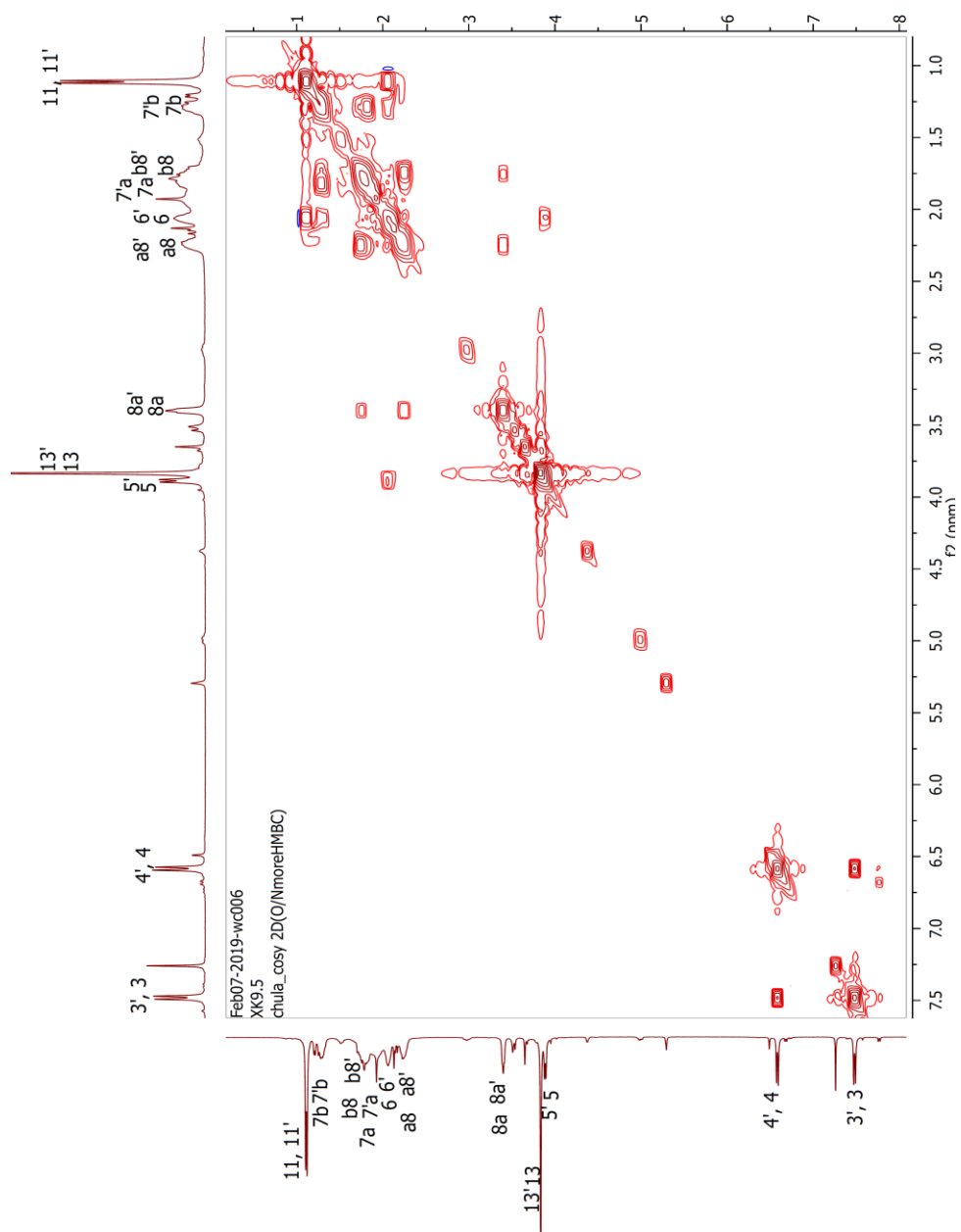


Figure A. 37 The COSY (CDCl₃, 400 MHz) spectrum of US5

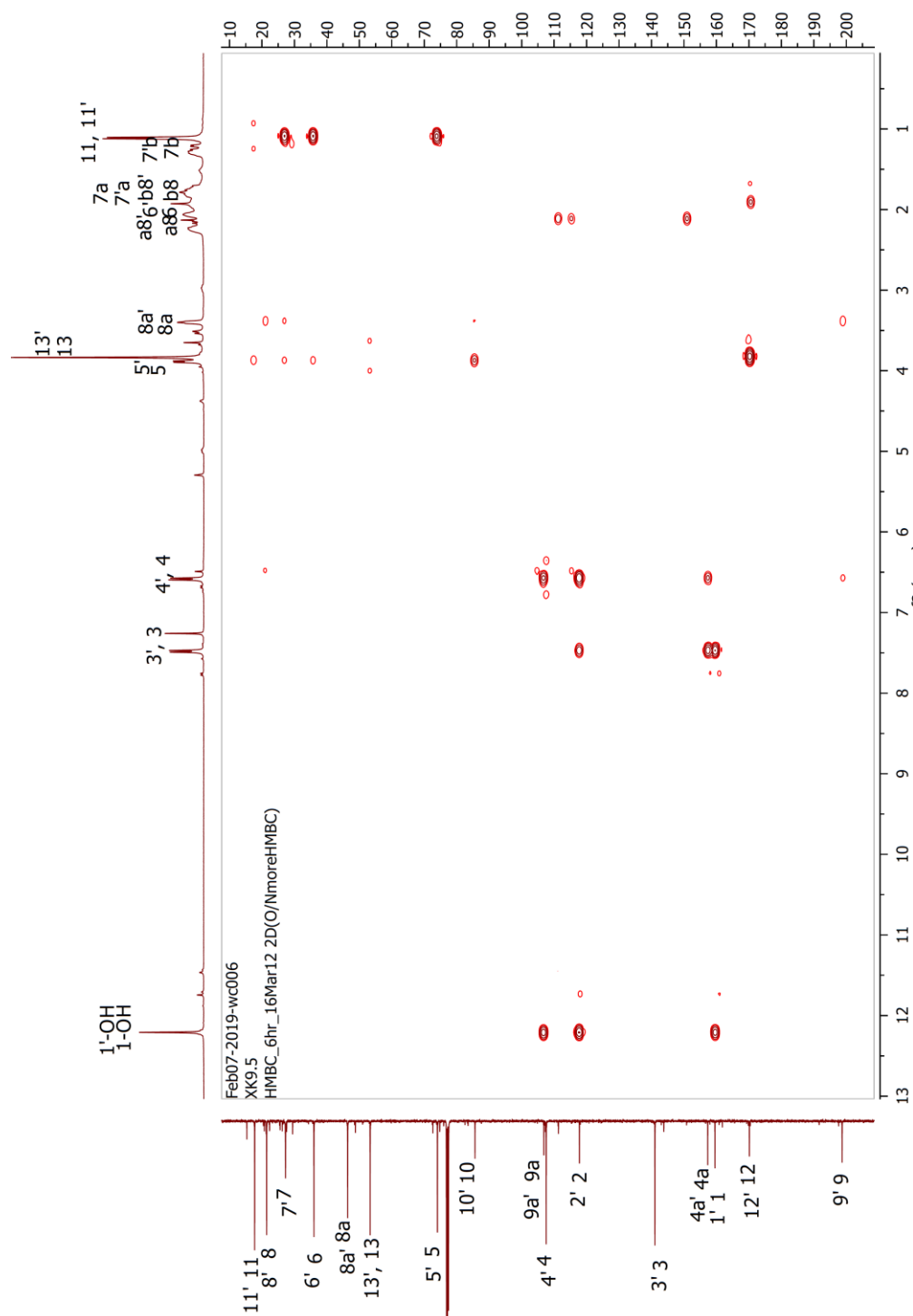


Figure A. 39 The HMBC (CDCl₃, 400 MHz) spectrum of US5

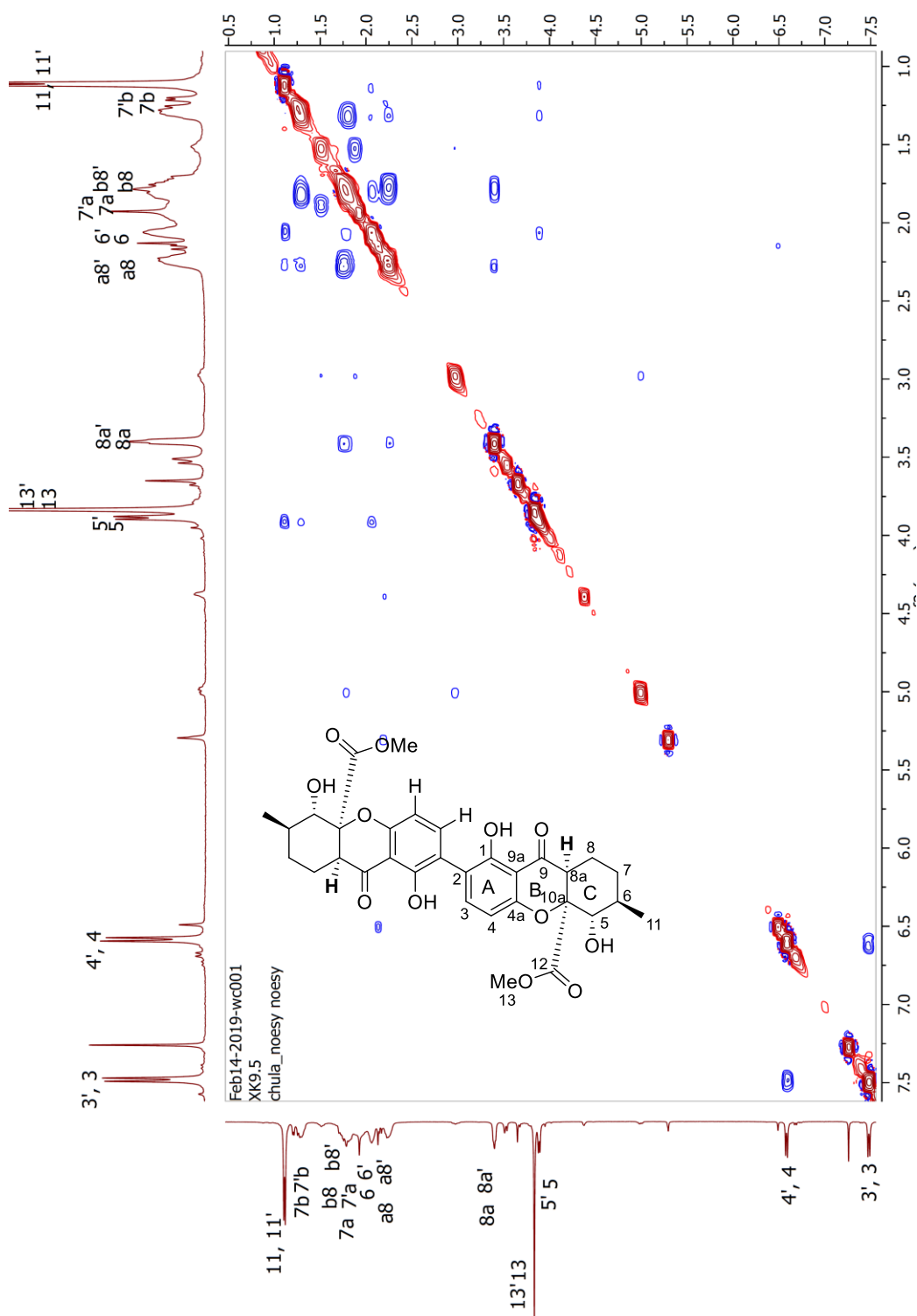


Figure A. 41 The NOESY (CDCl_3 , 400 MHz) spectrum of US5

Generic Display Report

Analysis Info

Analysis Name D:\Data\Data Service\190325\XK9.4_RB4_01_2366.d
Method nv_pos_5min_profile_190214.m
Sample Name XK9.4
Comment

Acquisition Date 3/25/2019 5:13:41 PM

Operator CU.
Instrument micrOTOF-Q II

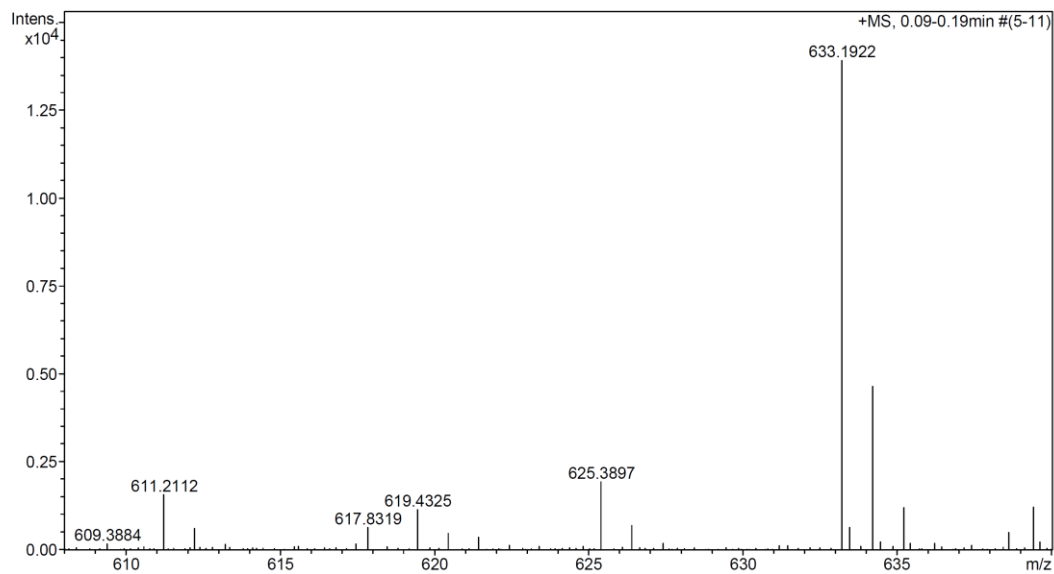
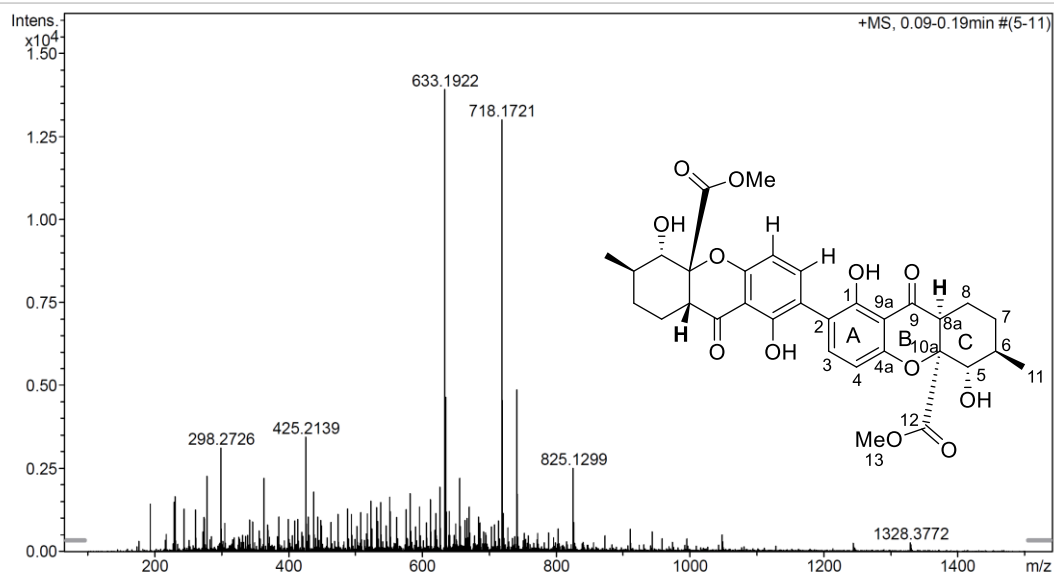


Figure A. 42 The HRESIMS spectrum of US6

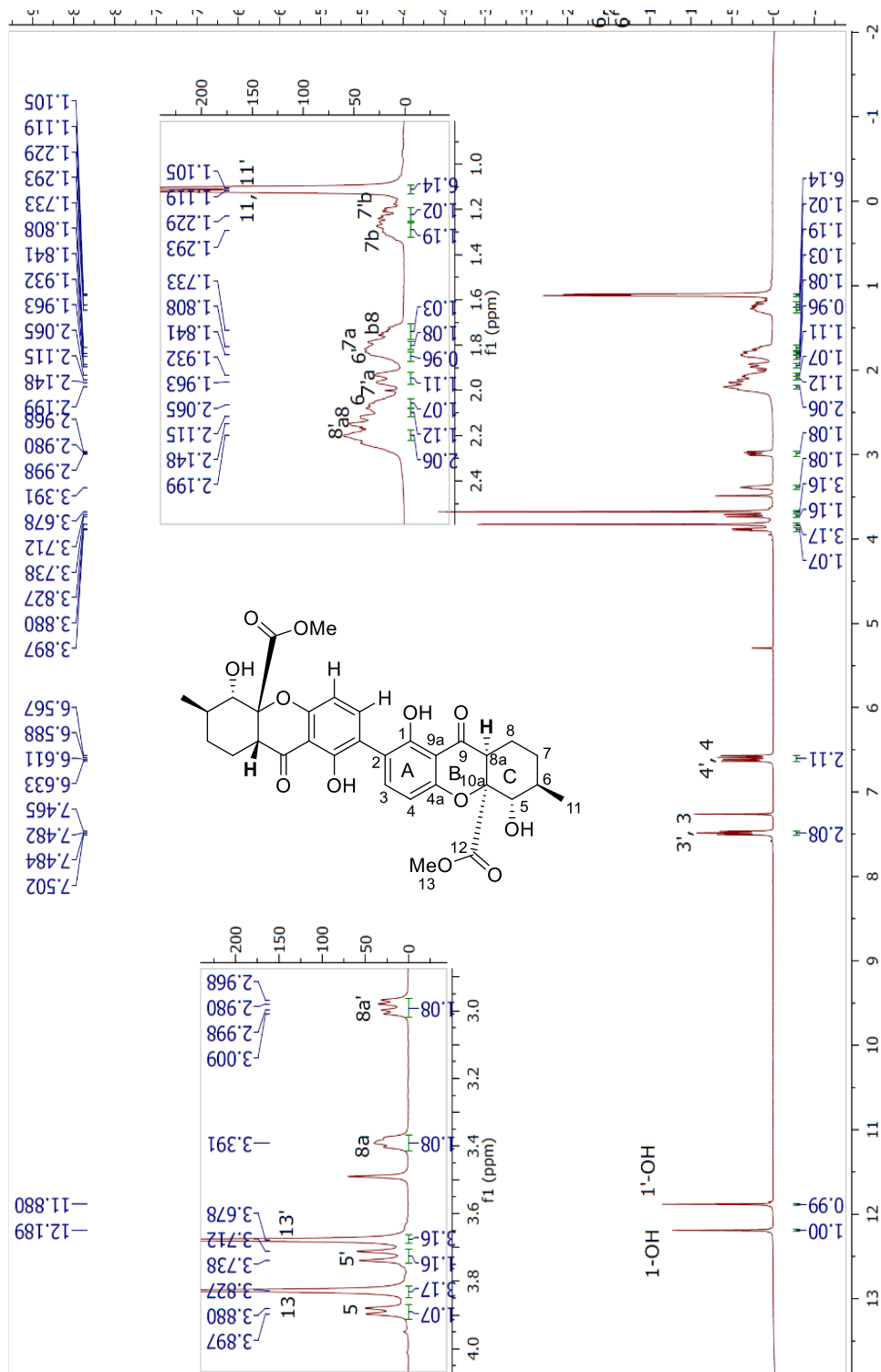


Figure A. 43 The ^1H NMR (CDCl_3 , 400 MHz) spectrum of US6

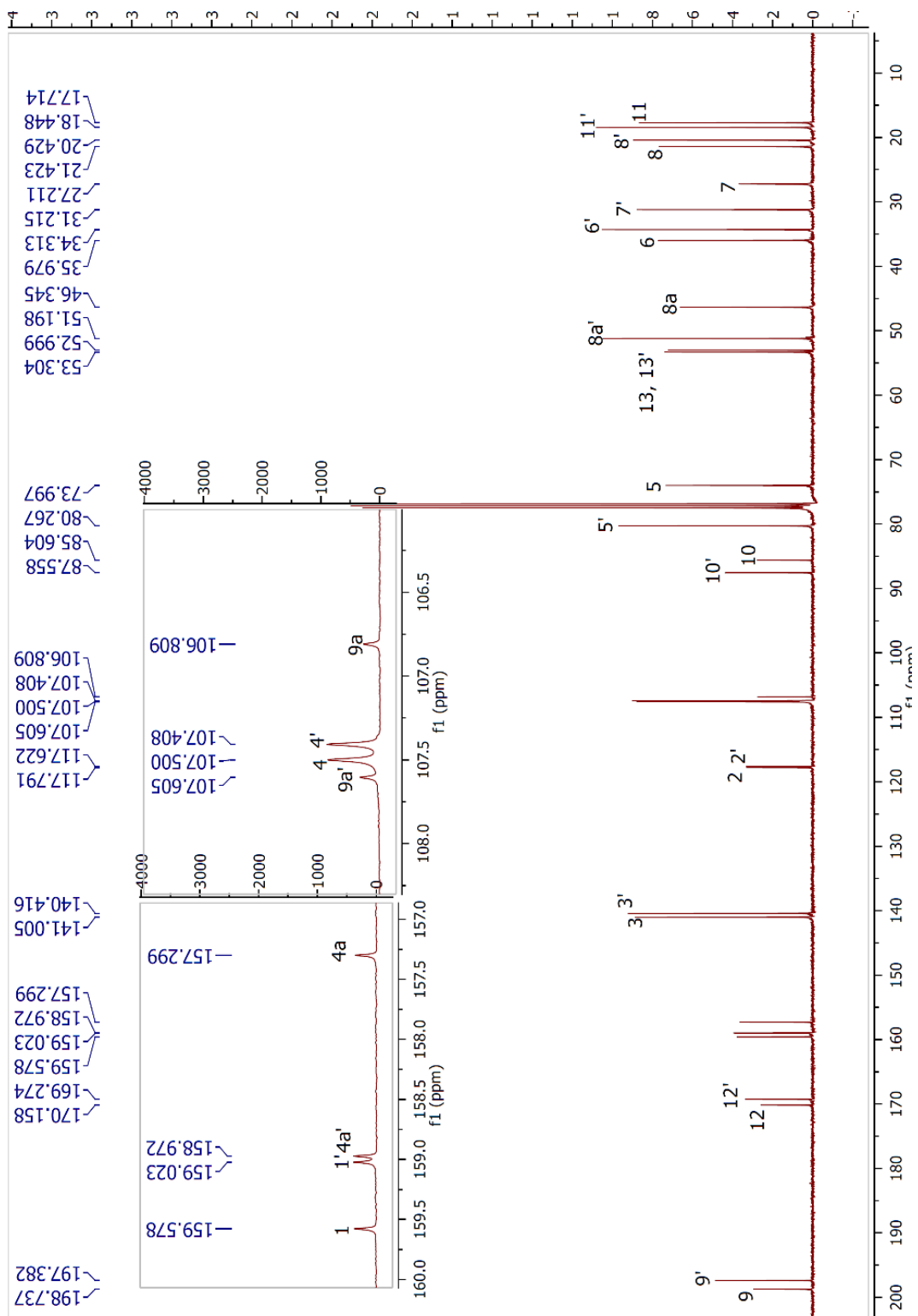


Figure A. 44 The ^{13}C NMR (CDCl_3 , 100 MHz) spectrum of US6

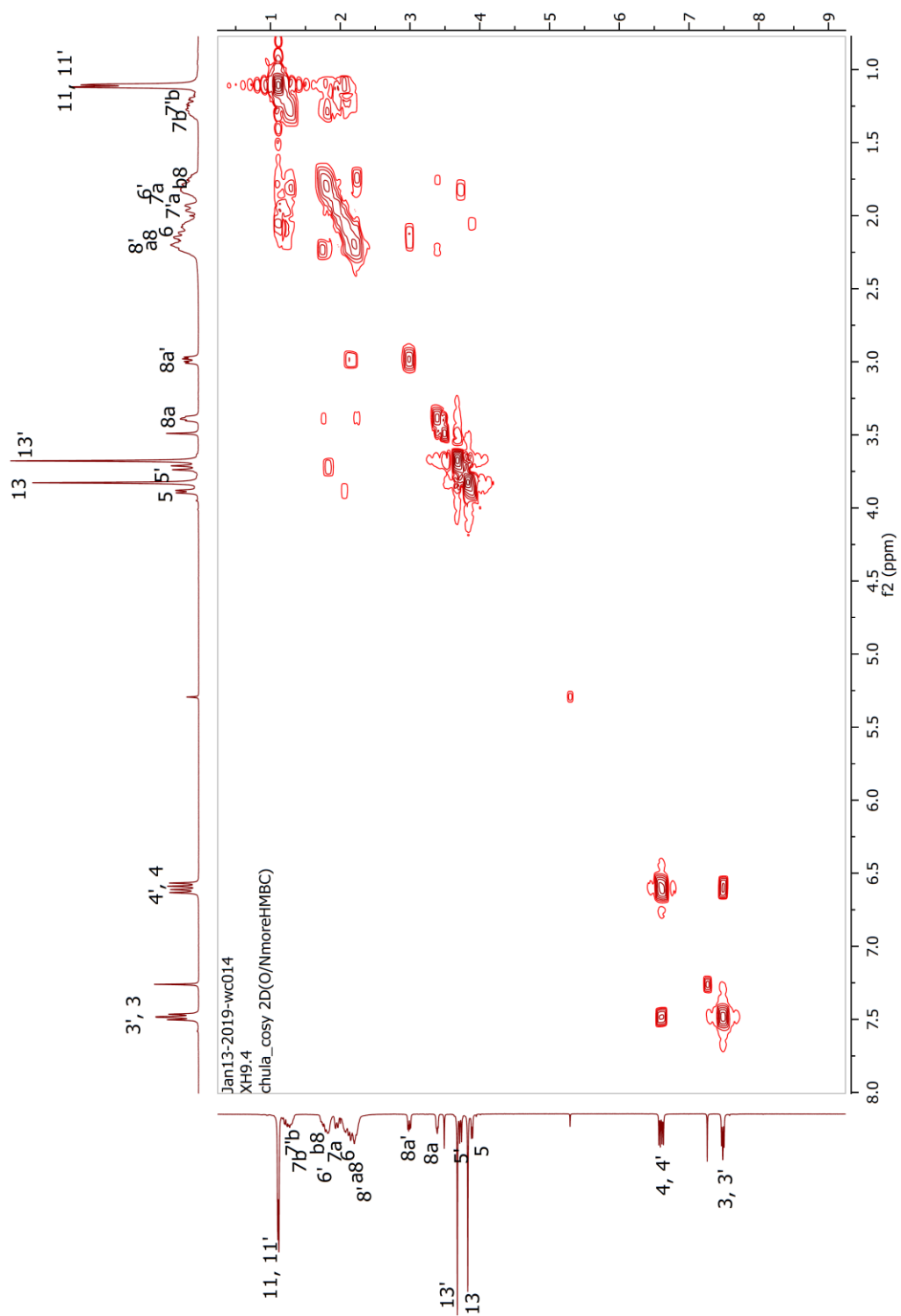


Figure A. 45 The COSY (CDCl₃, 400 MHz) spectrum of US6

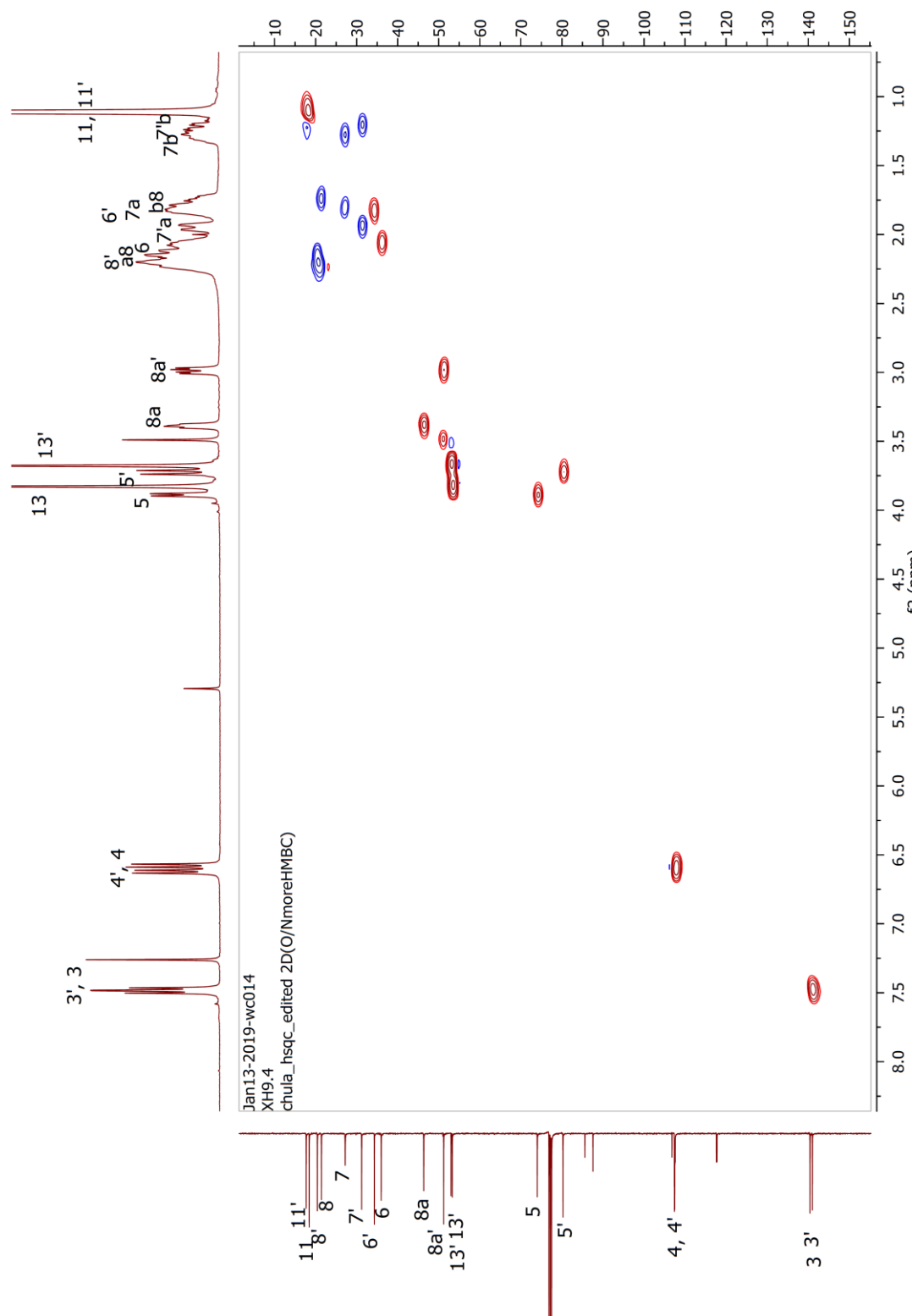


Figure A. 46 The HSQC (CDCl_3 , 400 MHz) spectrum of US6

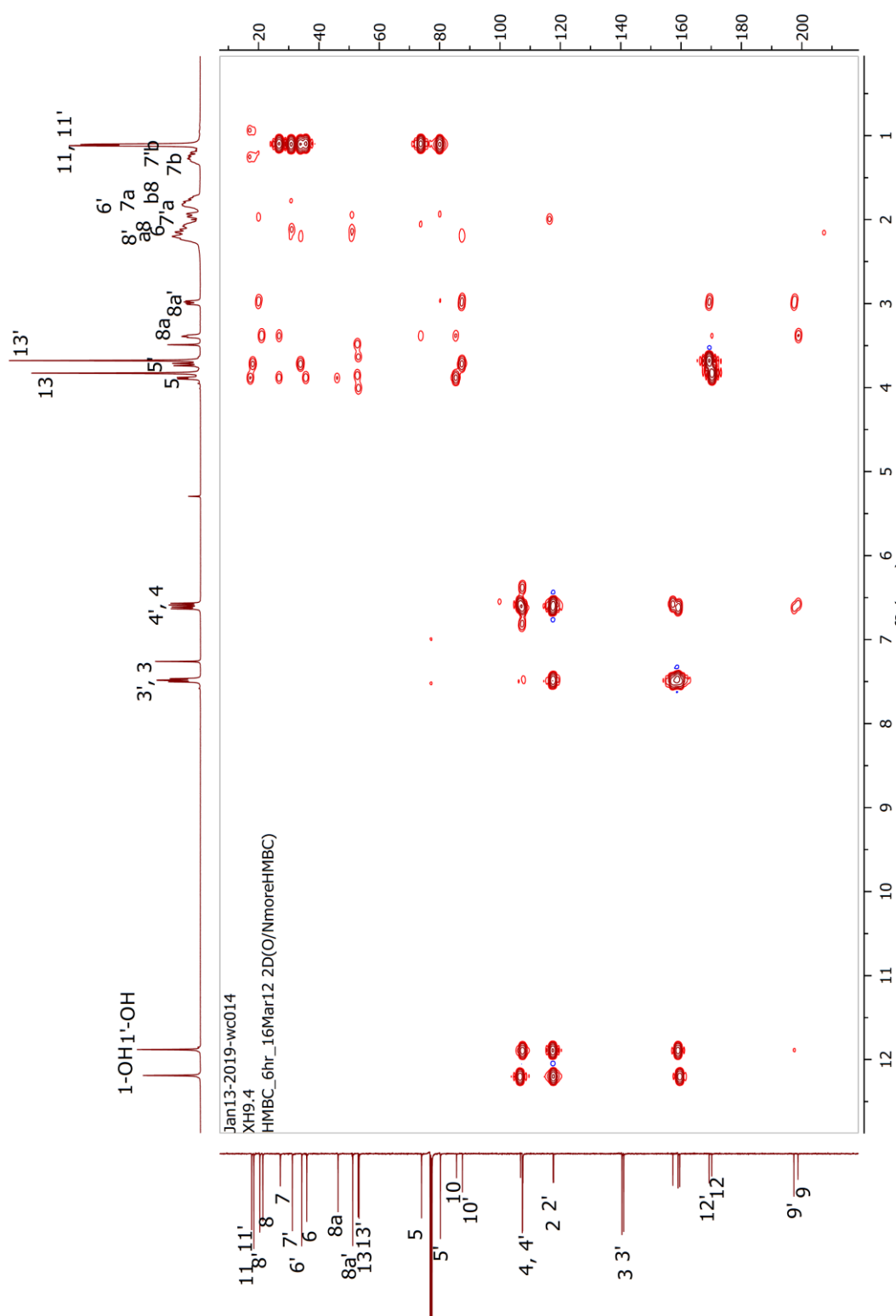


Figure A. 47 The HMBC (CDCl₃, 400 MHz) spectrum of US6

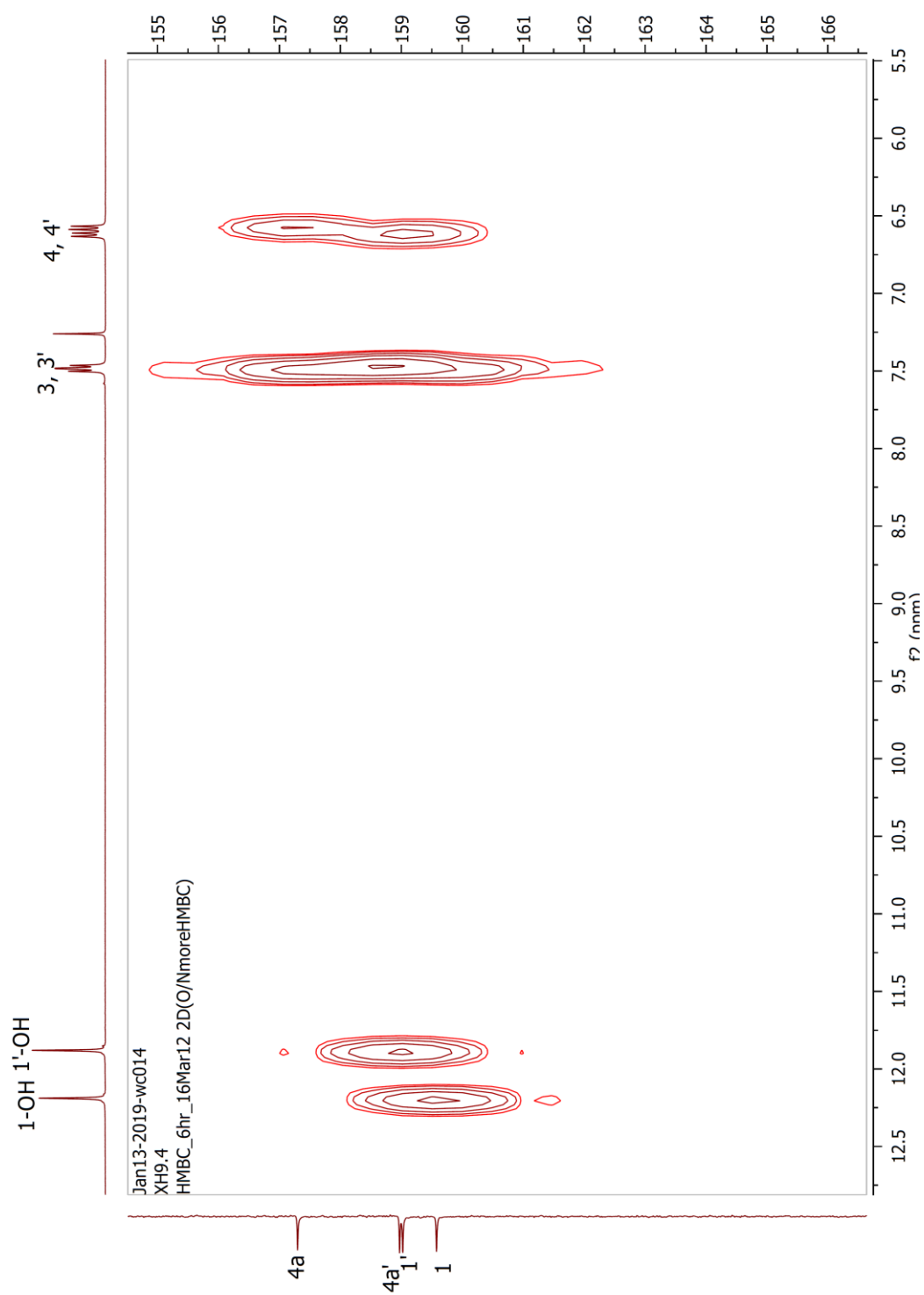


Figure A. 48 The HMBC (CDCl_3 , 400 MHz) spectrum of US6

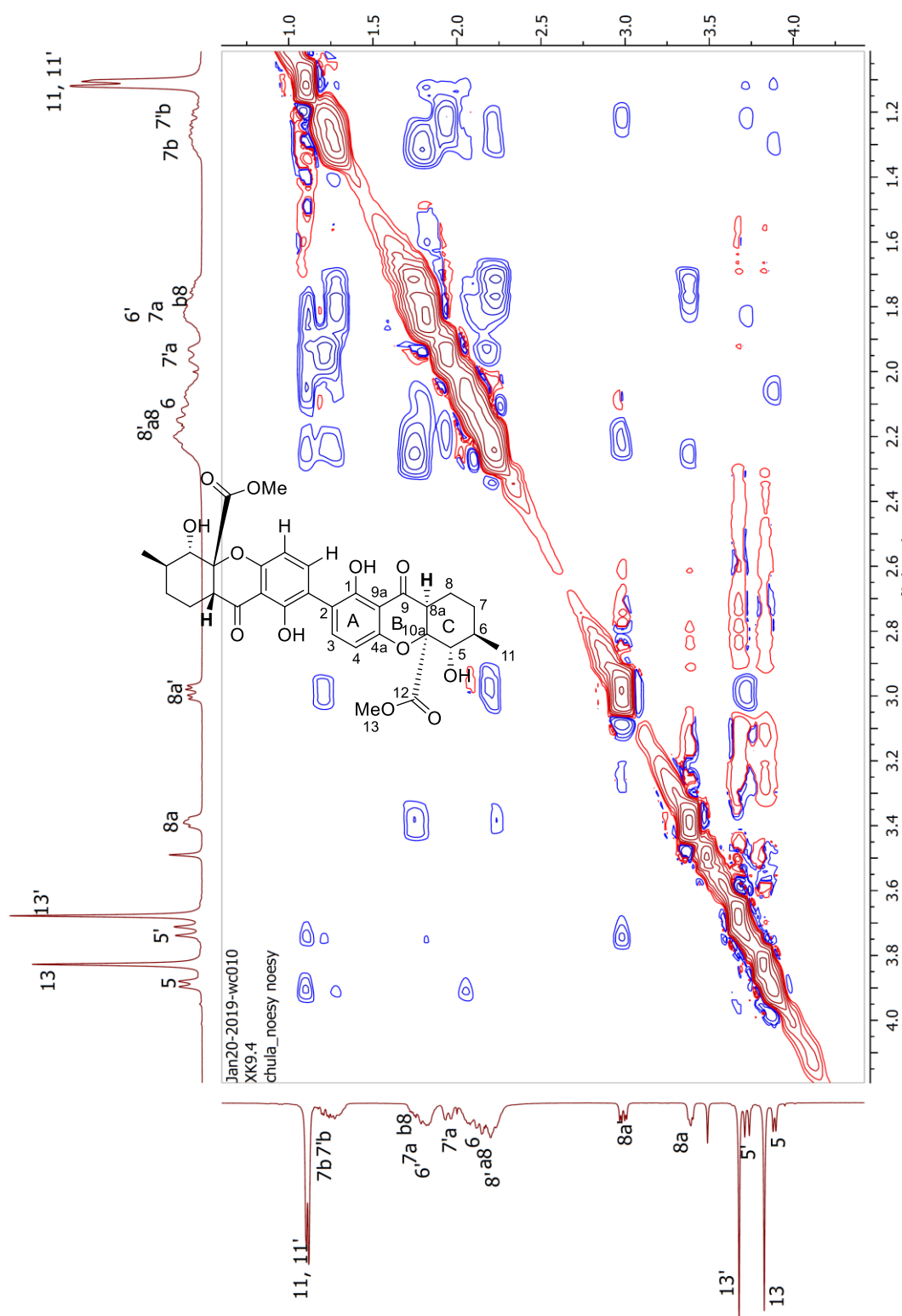


Figure A. 49 The NOESY (CDCl₃, 400 MHz) spectrum of US6

Generic Display Report

Analysis Info

Analysis Name D:\Data\Data Service\190325\XKGX5_RB2_01_2364.d
Method nv_pos_5min_profile_190214.m
Sample Name XKGX5
Comment

Acquisition Date 3/25/2019 5:00:45 PM

Operator CU.
Instrument micrOTOF-Q II

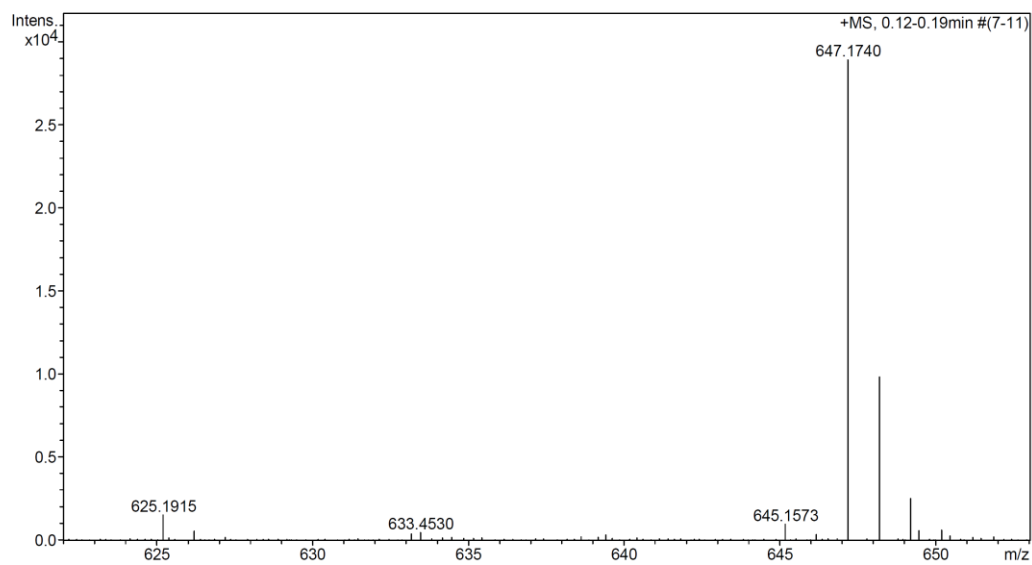
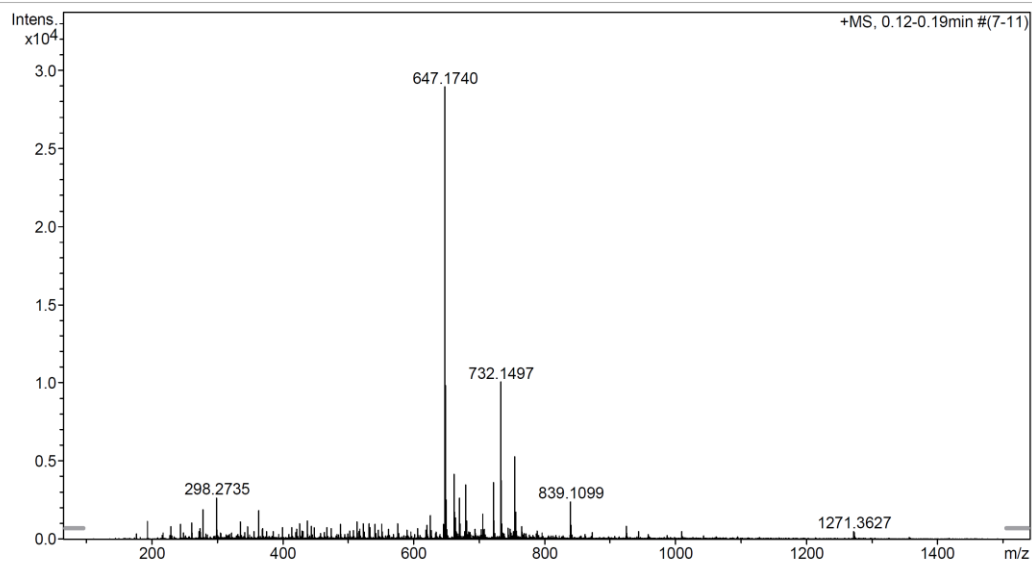


Figure A. 50 The HRESIMS spectrum of US7

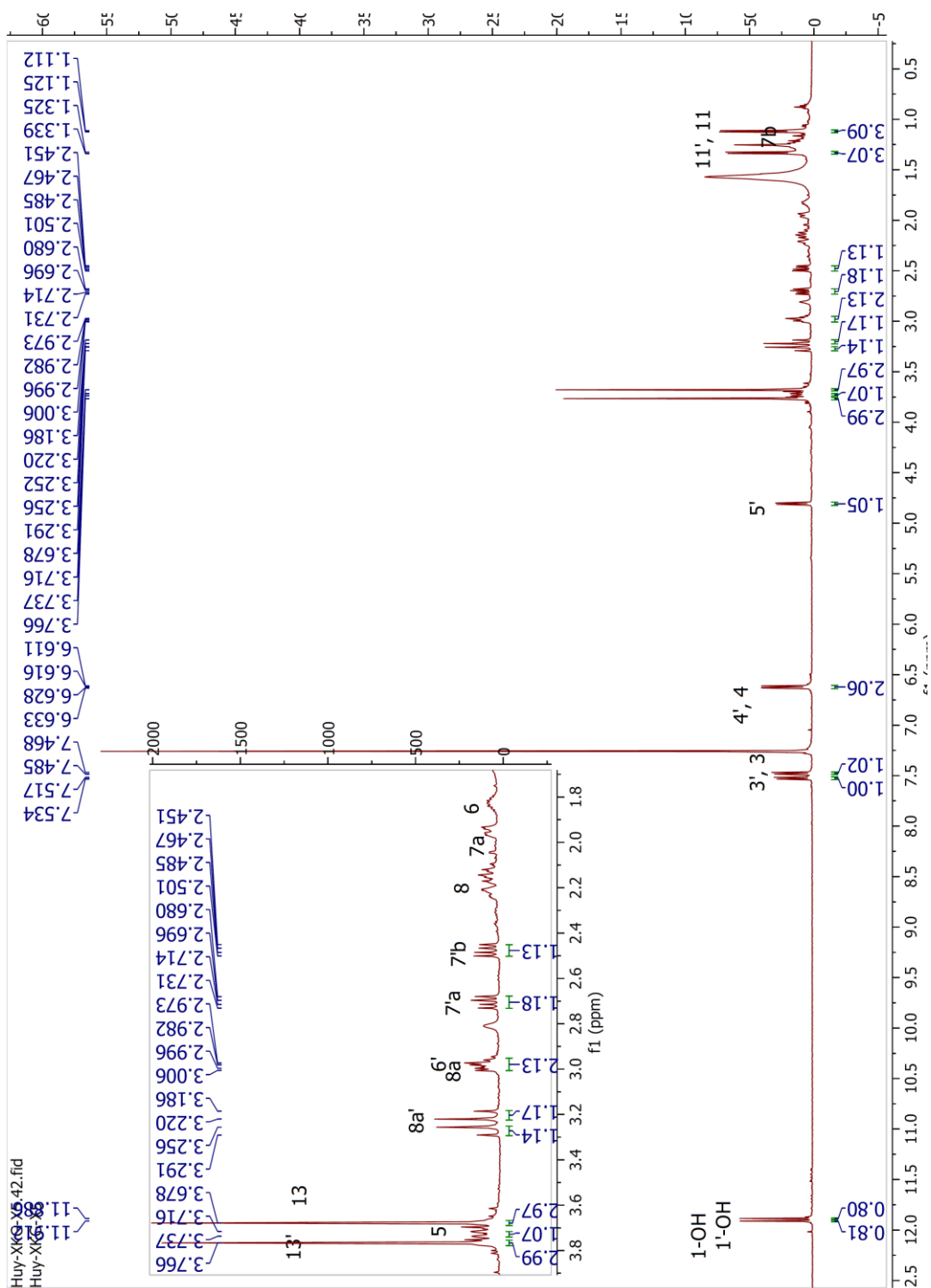


Figure A. 51 The ^1H NMR (CDCl_3 , 500 MHz) spectrum of **US7**

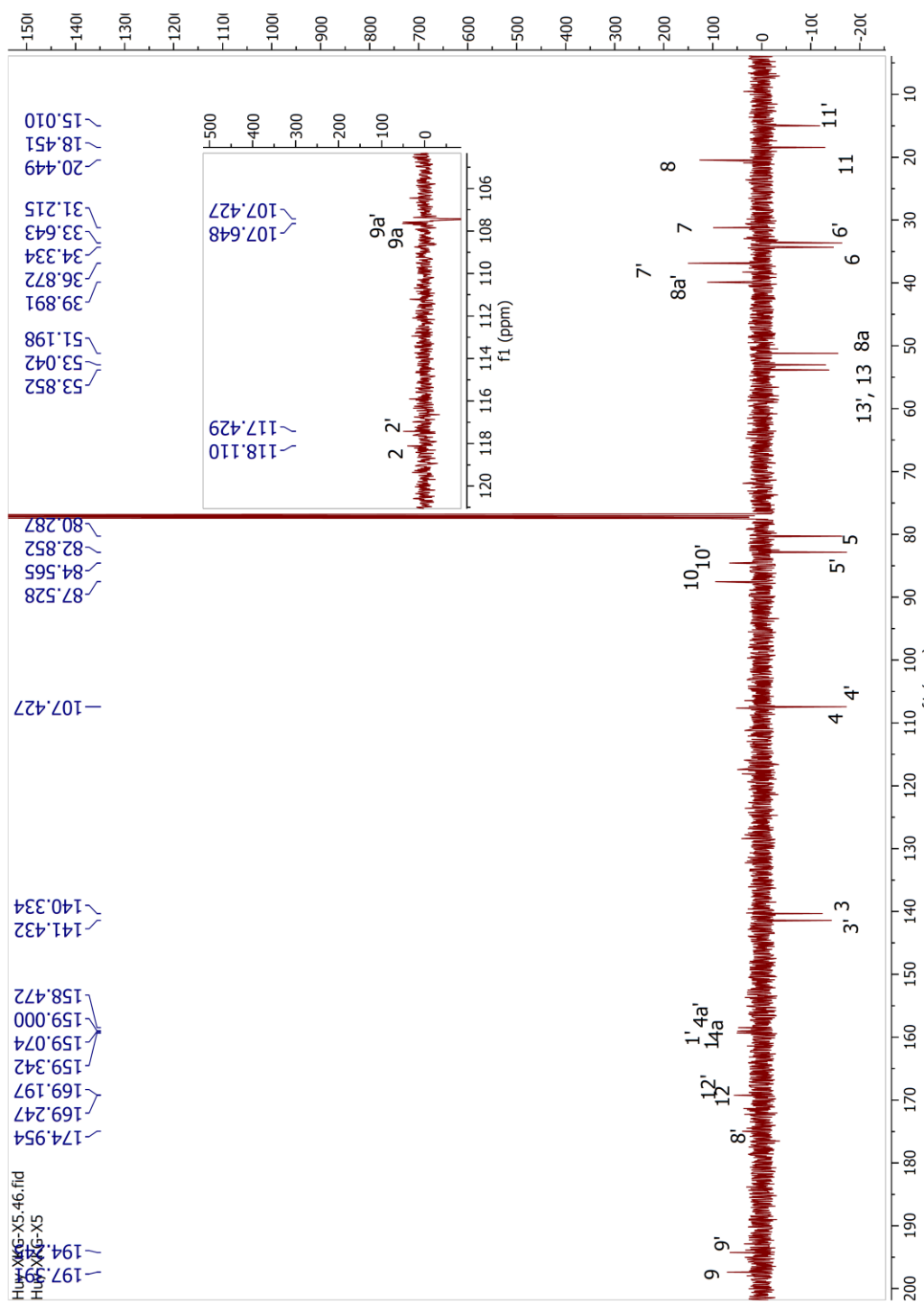


Figure A. 52 The ¹³C NMR (CDCl₃, 125 MHz) spectrum of US7

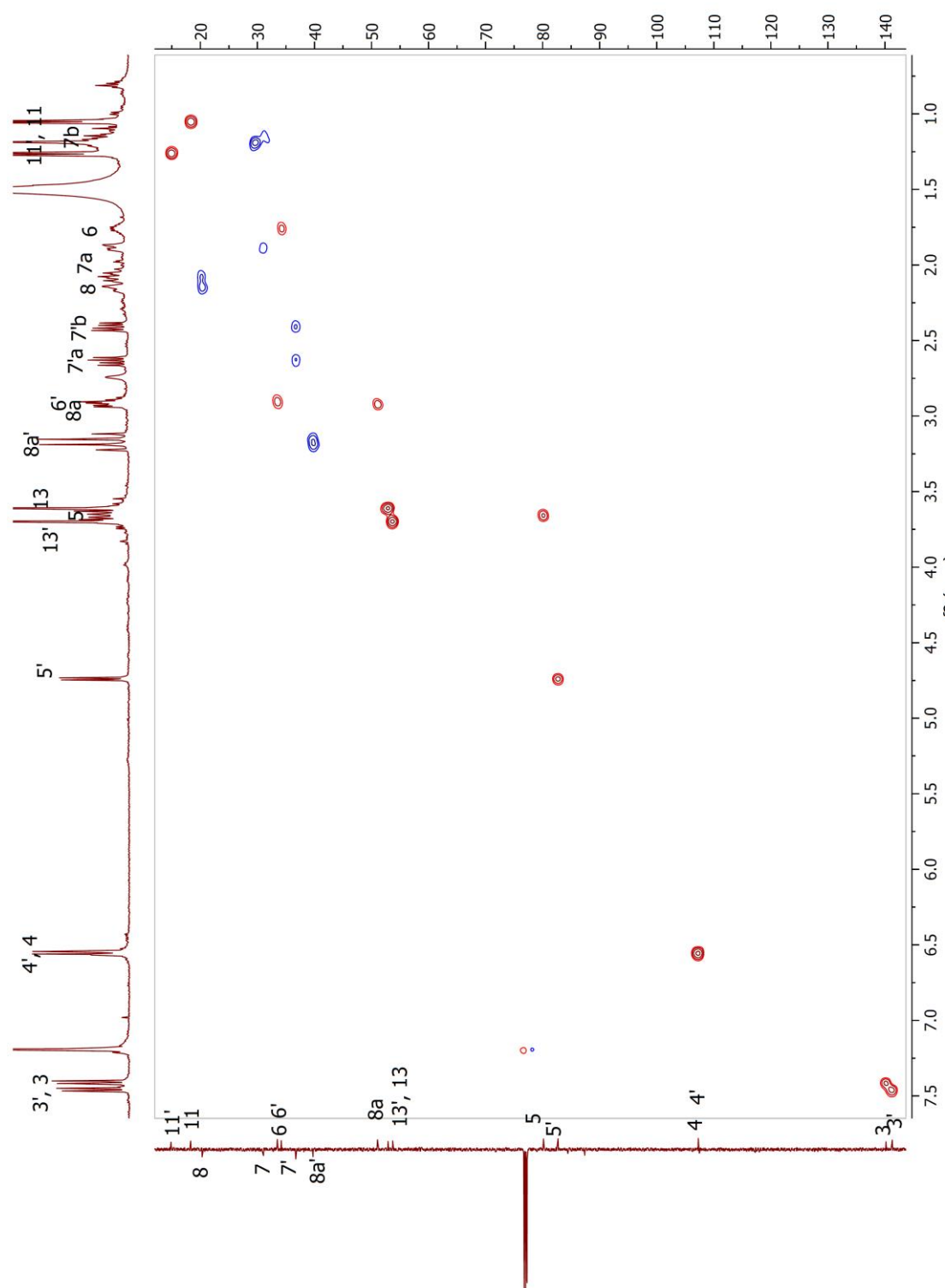


Figure A. 53 The HSQC (CDCl_3 , 500 MHz) spectrum of US7

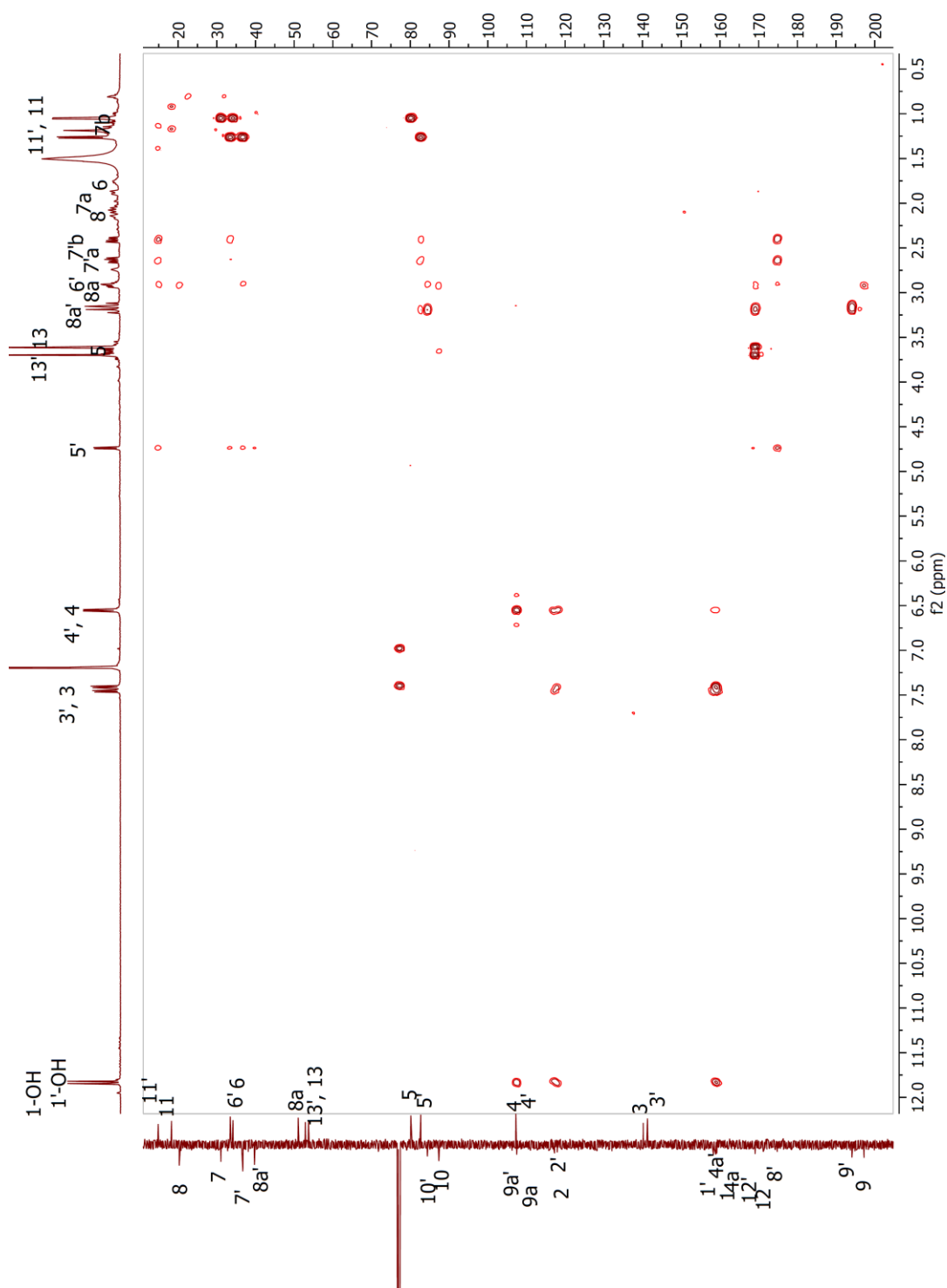


Figure A. 54 The HMBC (CDCl_3 , 500 MHz) spectrum of US7

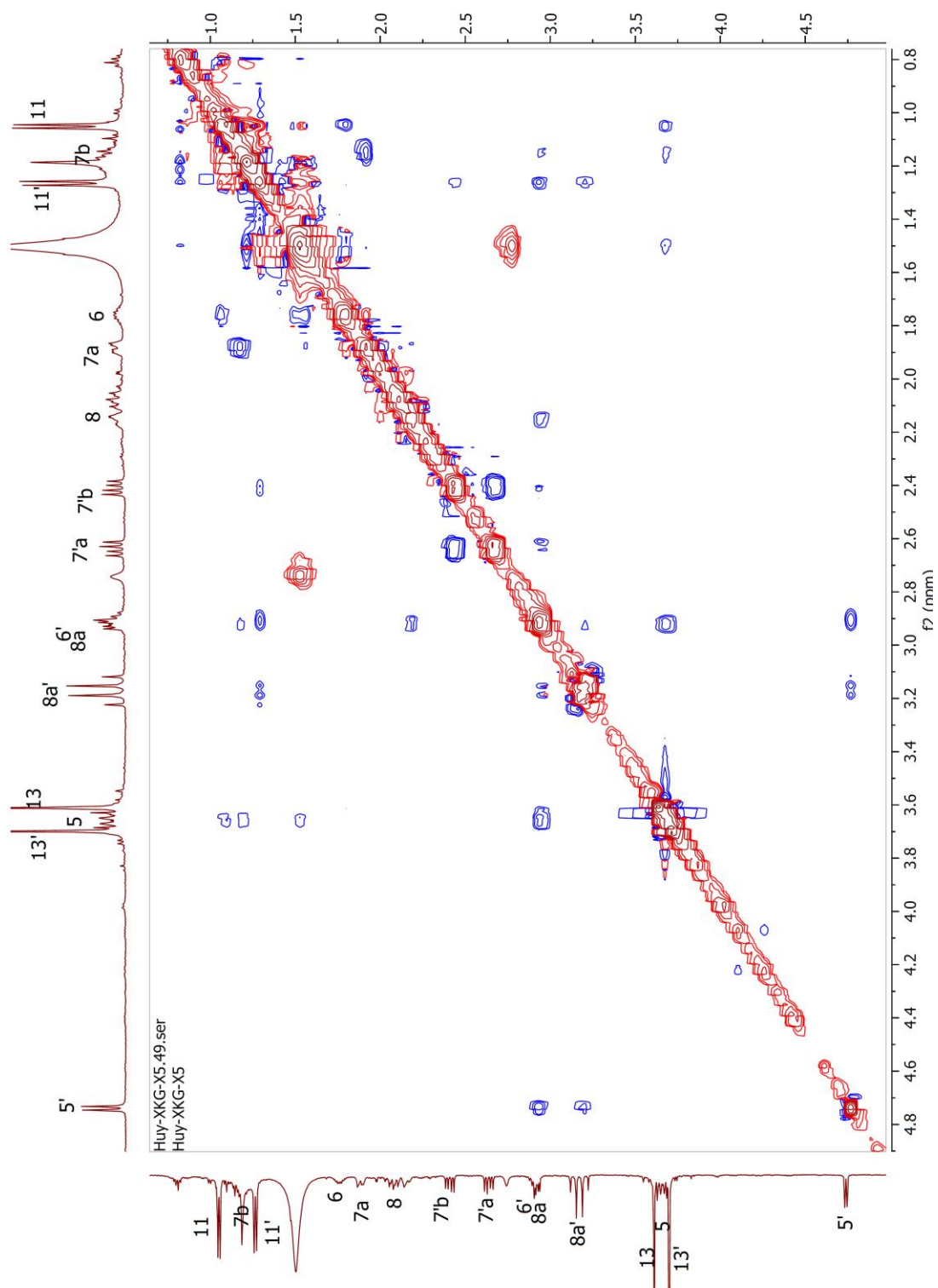


Figure A. 55 The NOESY (CDCl_3 , 500 MHz) spectrum of US7

Data: xkgx6_0001.N3[c] 22 Aug 2019 19:03 Cal: 23 Aug 2019 10:36
Shimadzu Biotech Axima Resonance 2.9.1.20100121: Mode positive, Low 300+, Power: 110

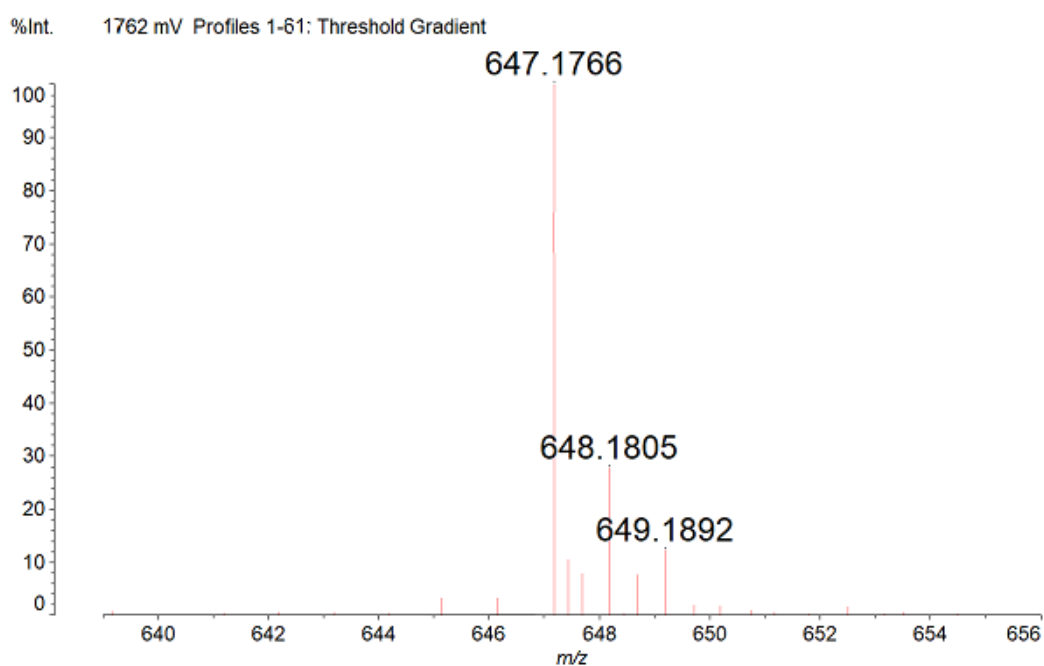
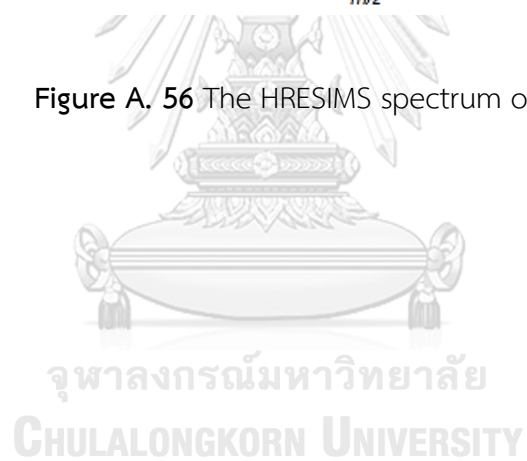
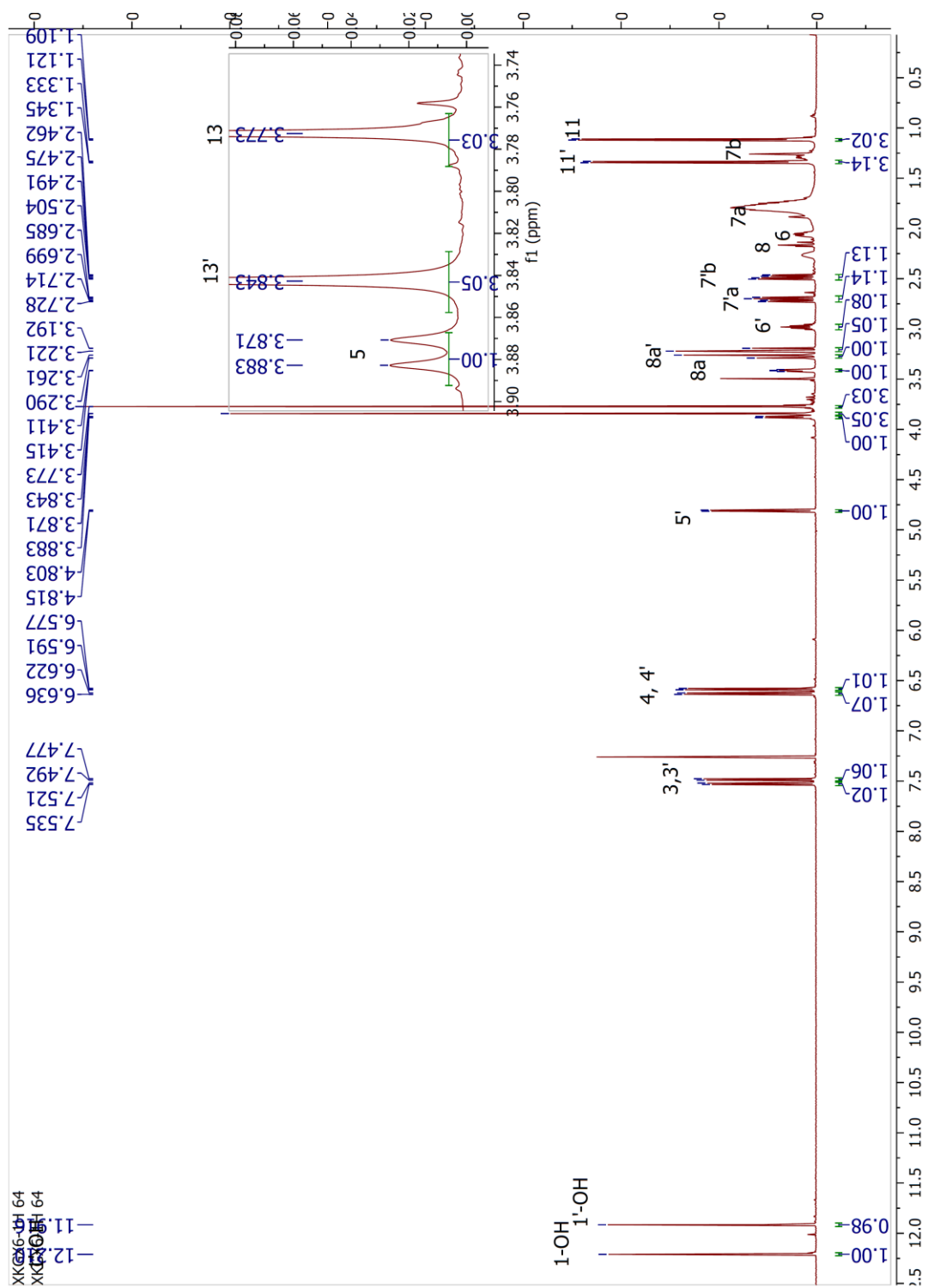


Figure A. 56 The HRESIMS spectrum of US8



Figure A. 57 The ^1H NMR (CDCl_3 , 600 MHz) spectrum of US8

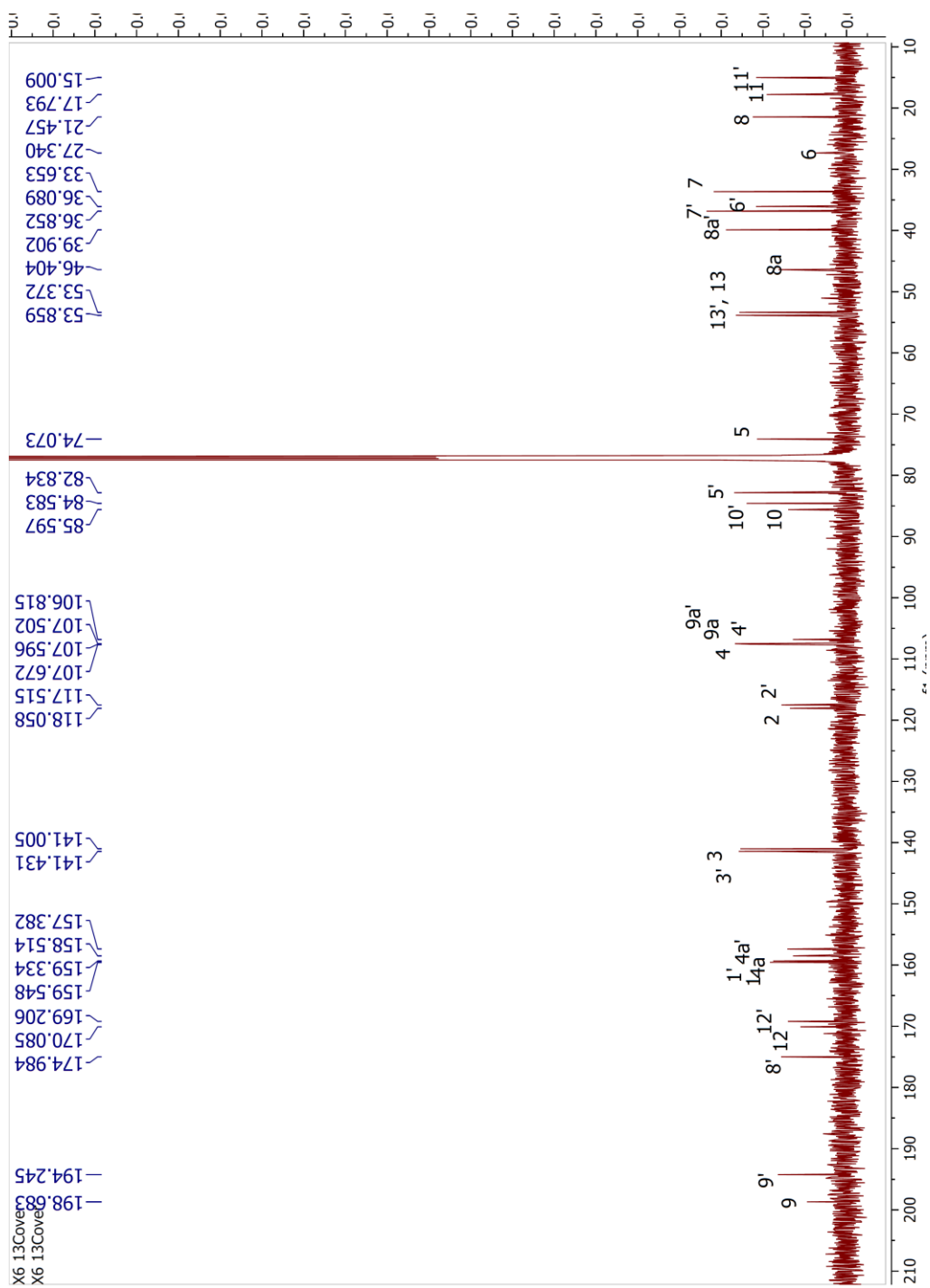


Figure A. 58 The ^{13}C NMR (CDCl_3 , 150 MHz) spectrum of US8

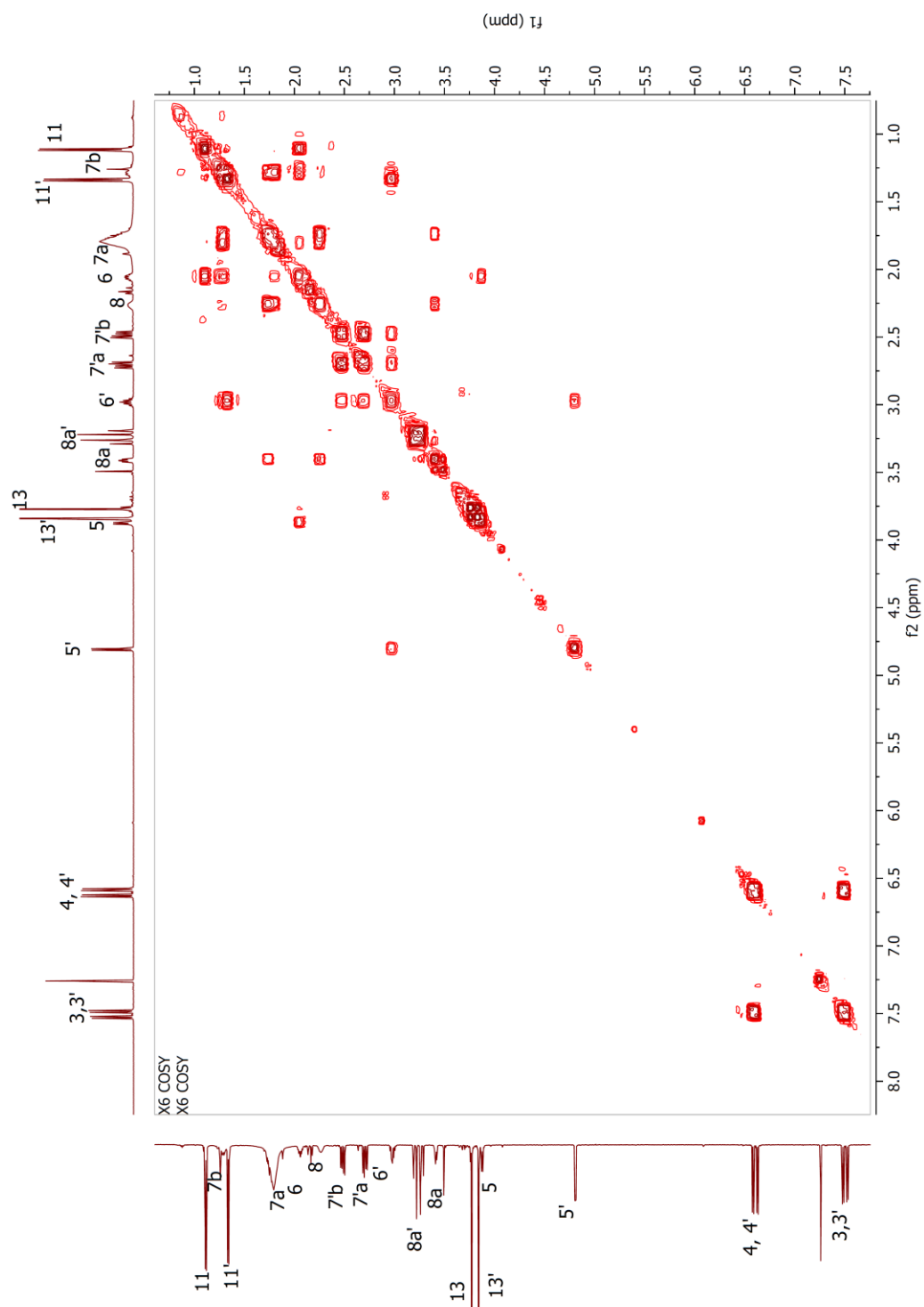


Figure A. 59 The COSY (CDCl_3 , 600 MHz) spectrum of US8

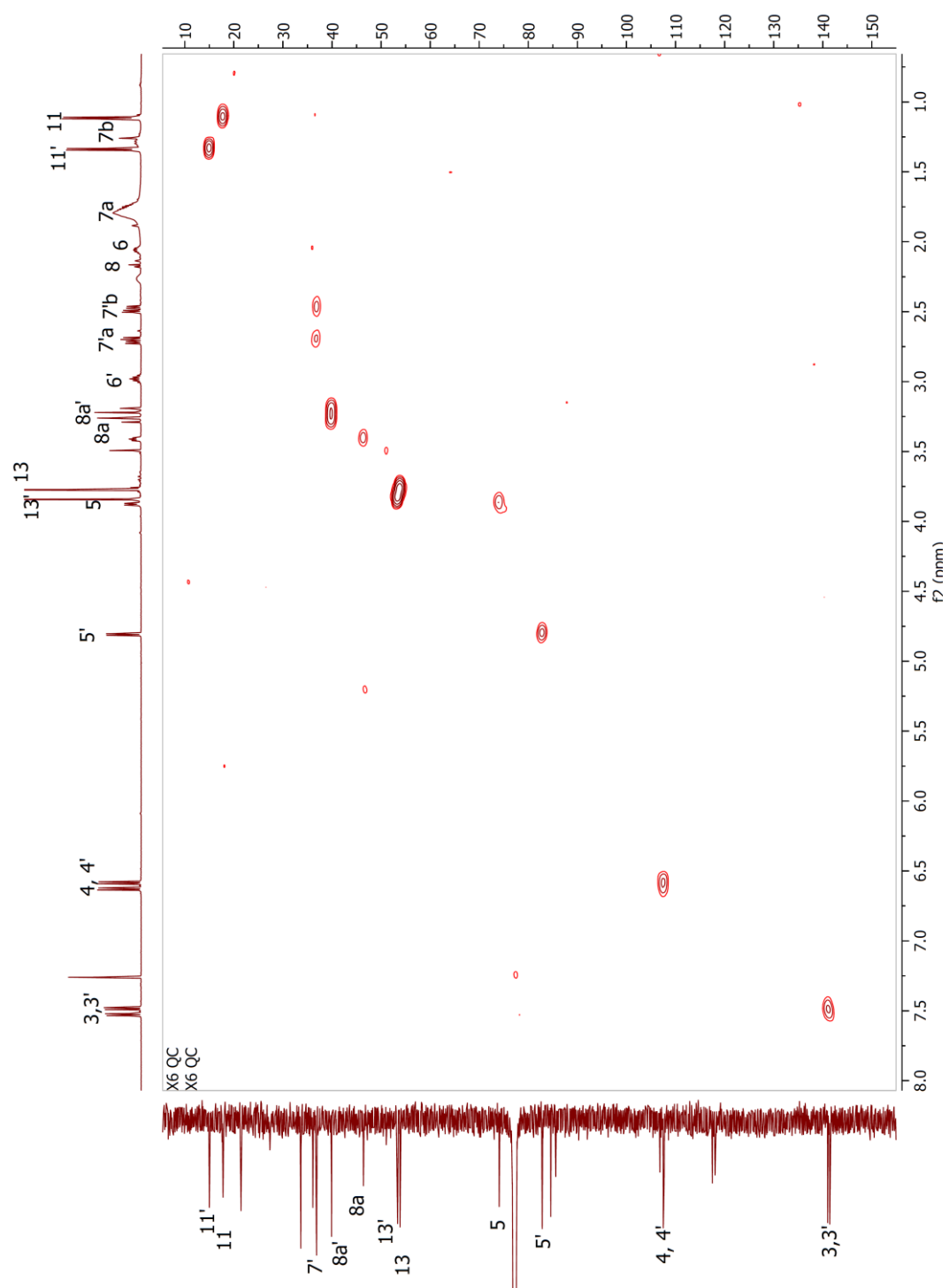


Figure A. 60 The HSQC (CDCl_3 , 600 MHz) spectrum of US8

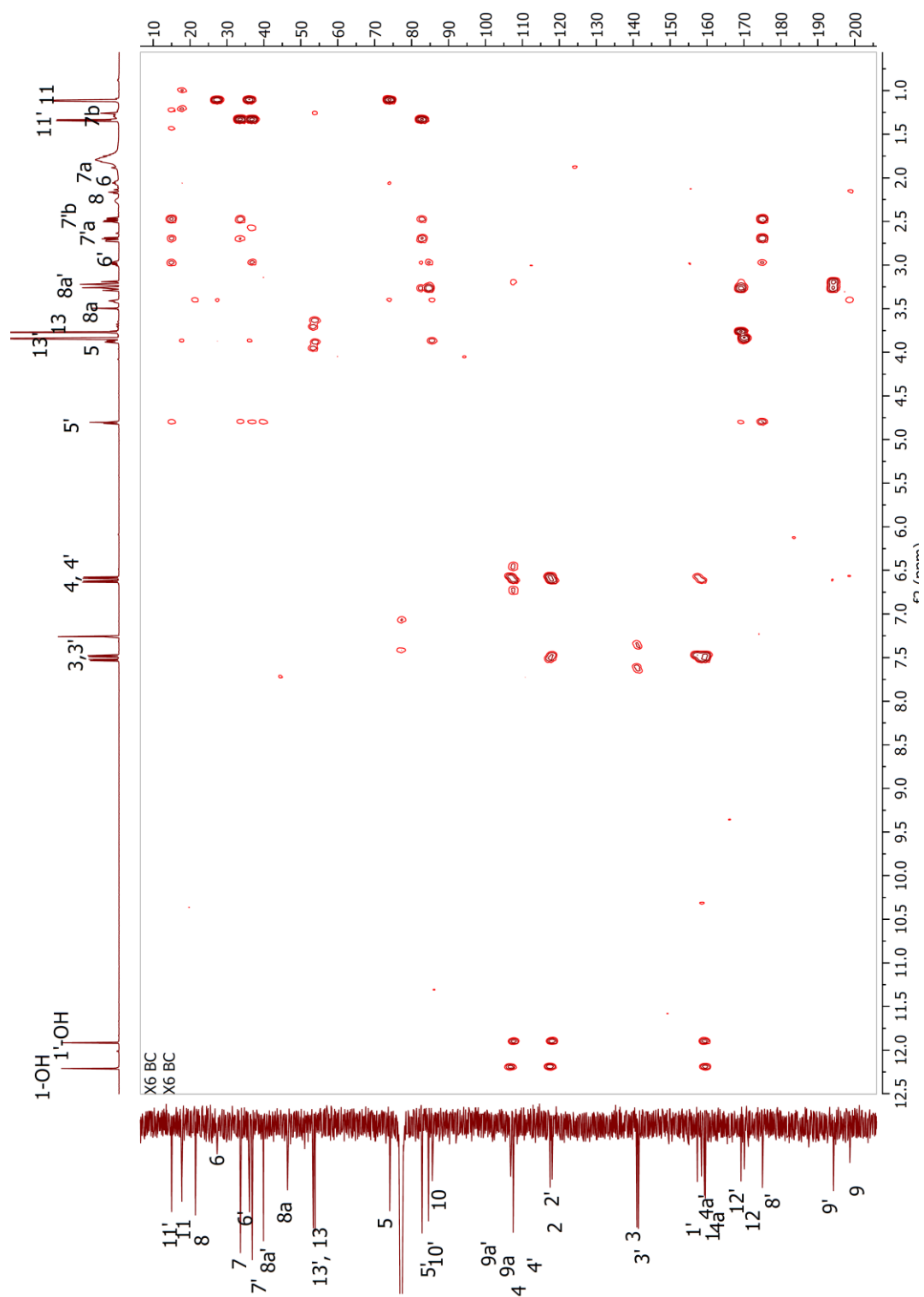


Figure A. 61 The HMBC (CDCl₃, 600 MHz) spectrum of US8

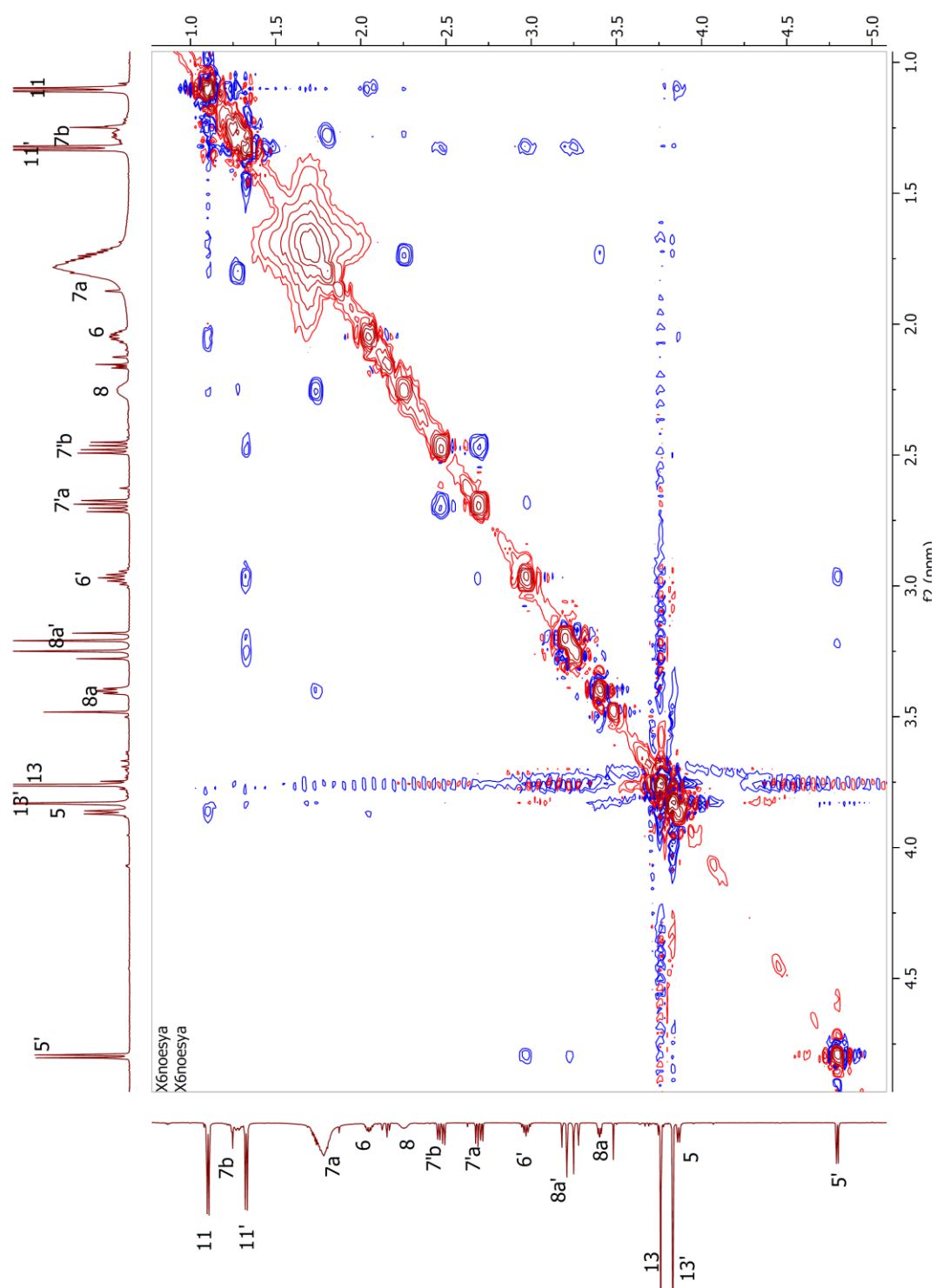


Figure A. 62 The NOESY (CDCl_3 , 600 MHz) spectrum of US8

Generic Display Report

Analysis Info

Analysis Name D:\Data\Data Service\190325\XKGX7_RB1_01_2363.d
Method nv_pos_5min_profile_190214.m
Sample Name XKGX7
Comment

Acquisition Date 3/25/2019 4:54:17 PM

Operator CU.
Instrument micrOTOF-Q II

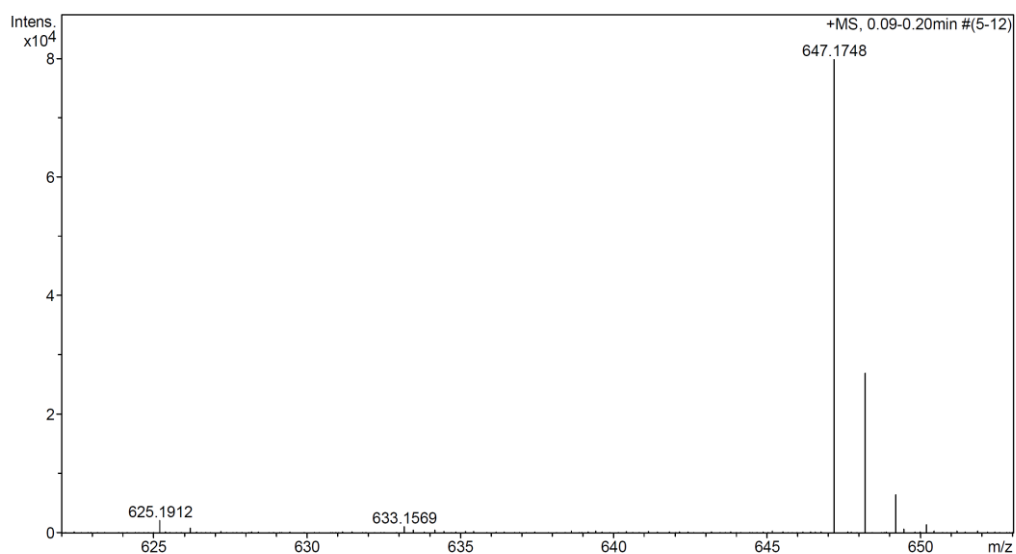
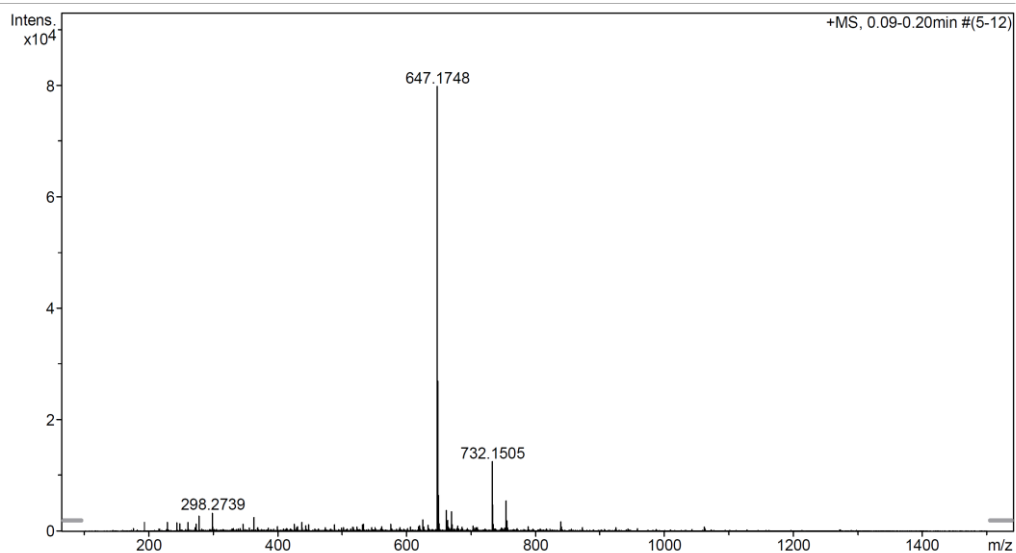


Figure A. 63 The HRESIMS spectrum of US9

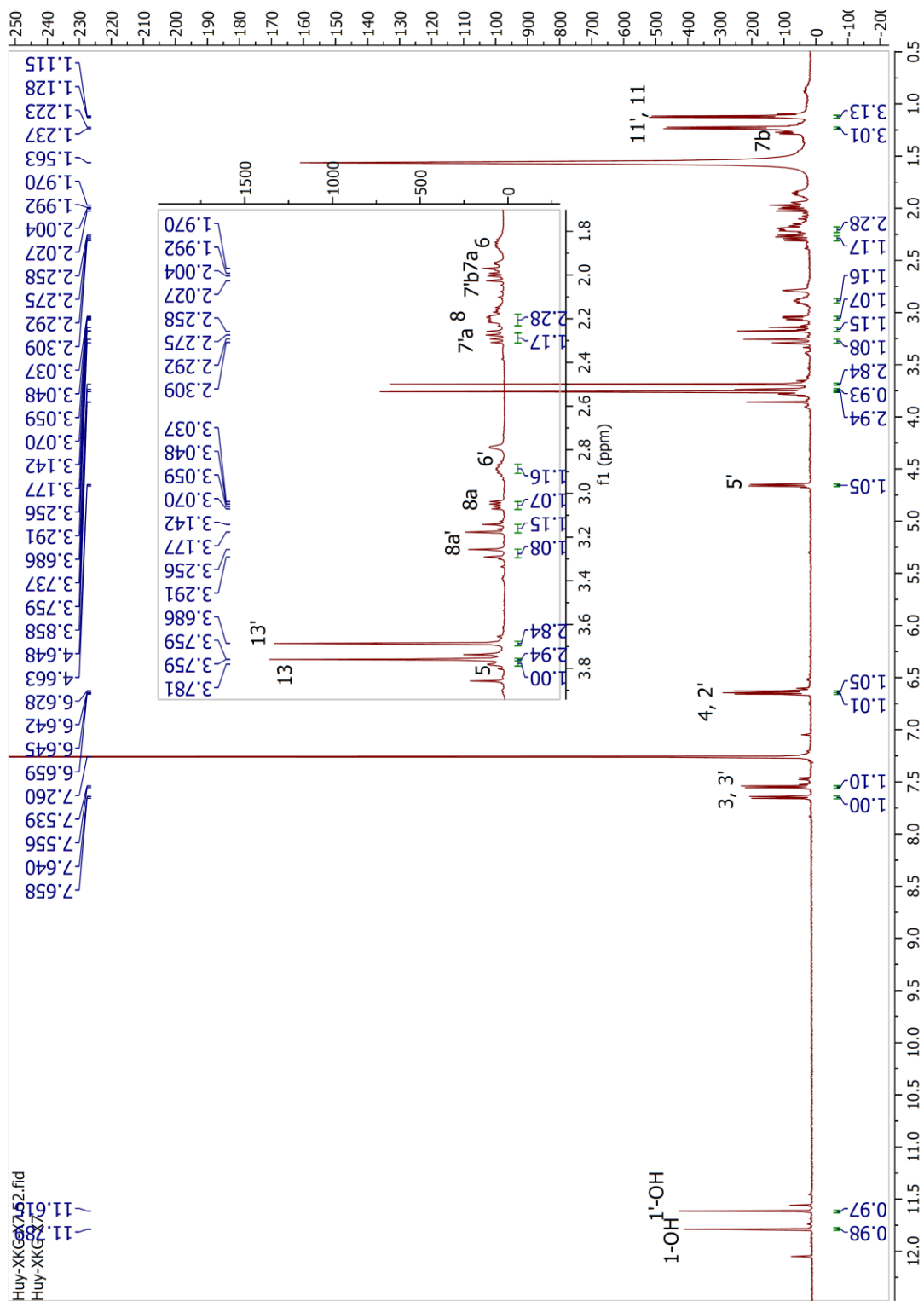


Figure A. 64 The ¹H NMR (CDCl₃, 500 MHz) spectrum of US9

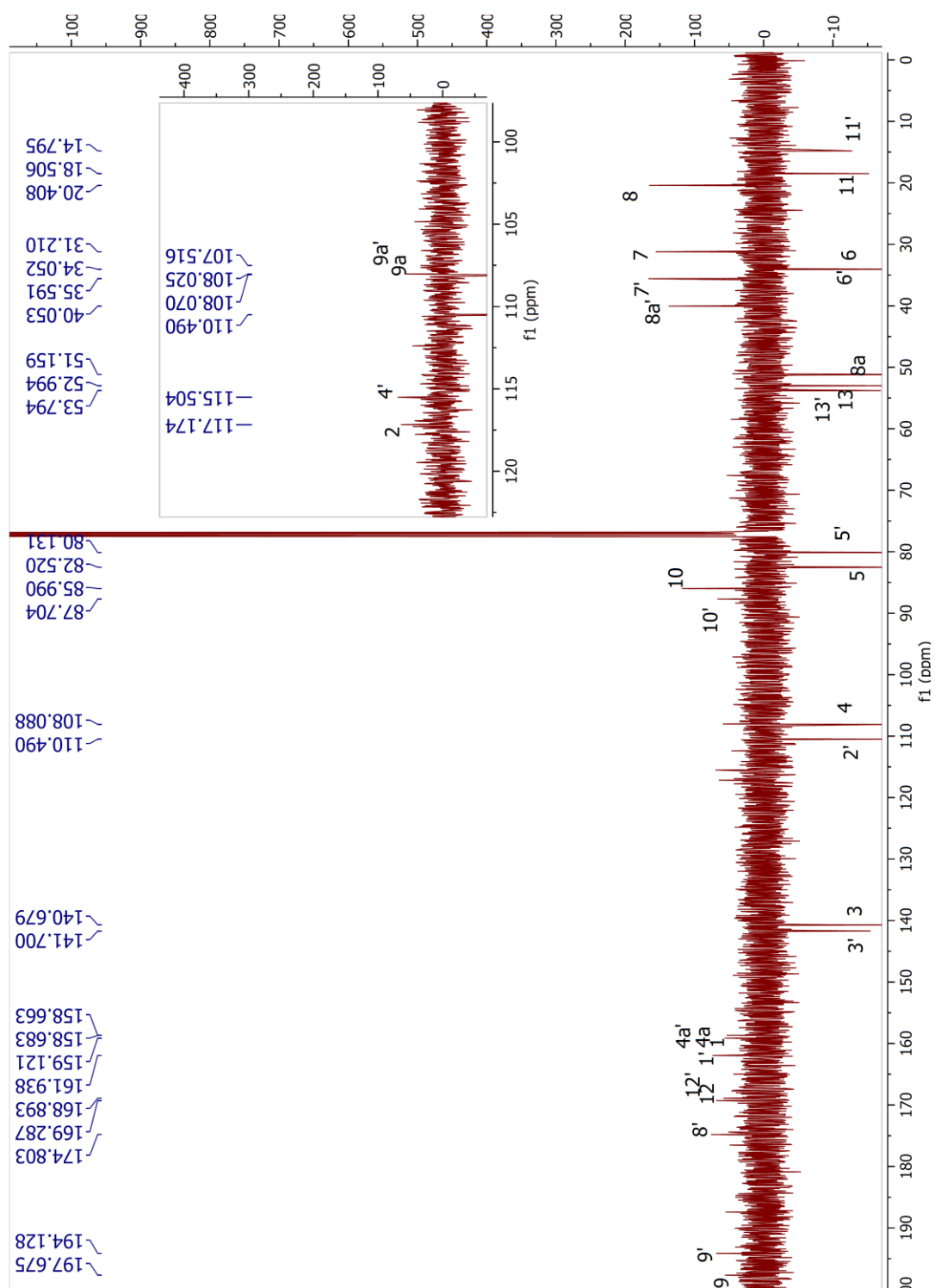


Figure A. 65 The ^{13}C NMR (CDCl_3 , 125 MHz) spectrum of US9

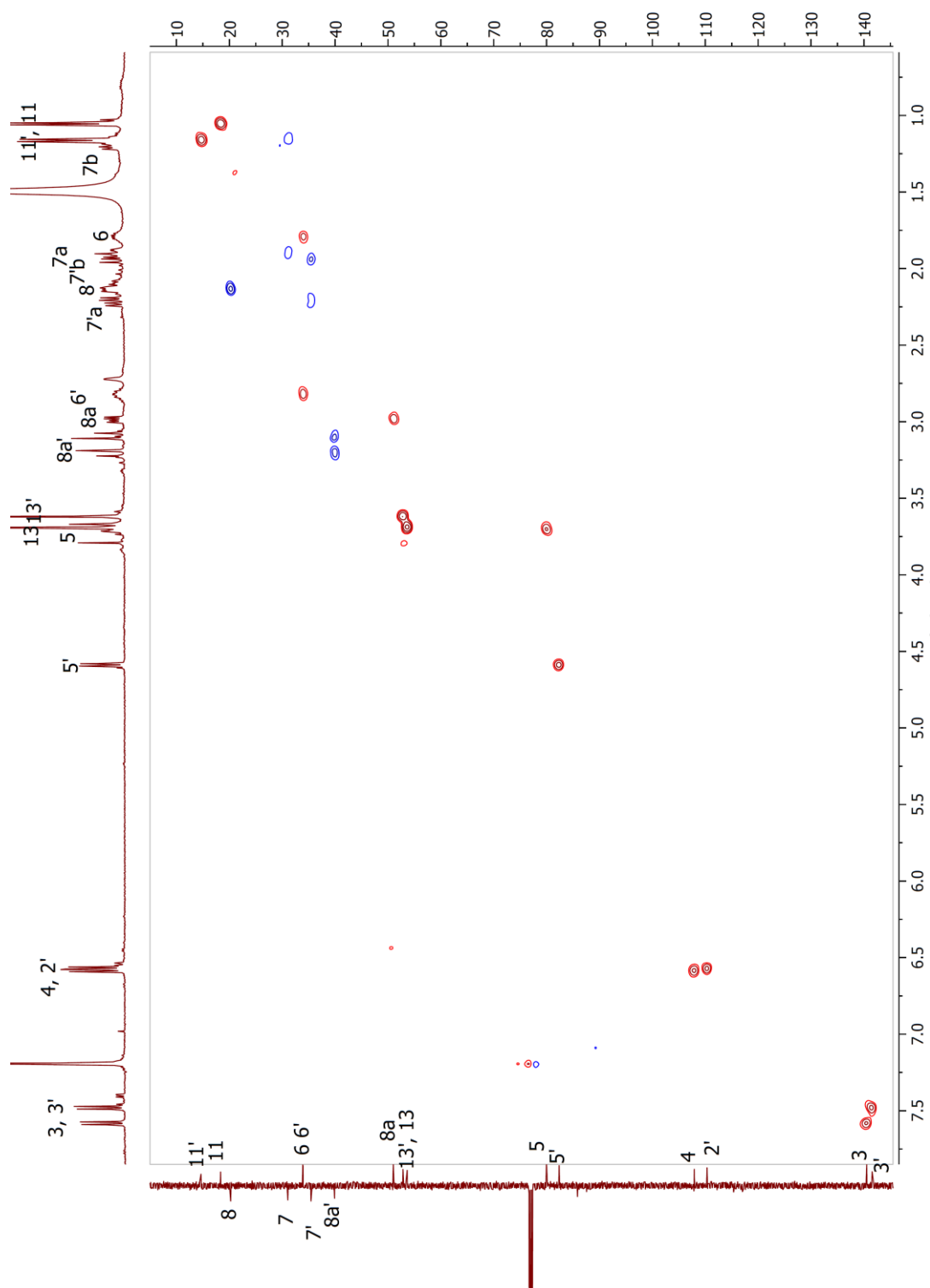


Figure A. 66 The HSQC (CDCl_3 , 500 MHz) spectrum of US9

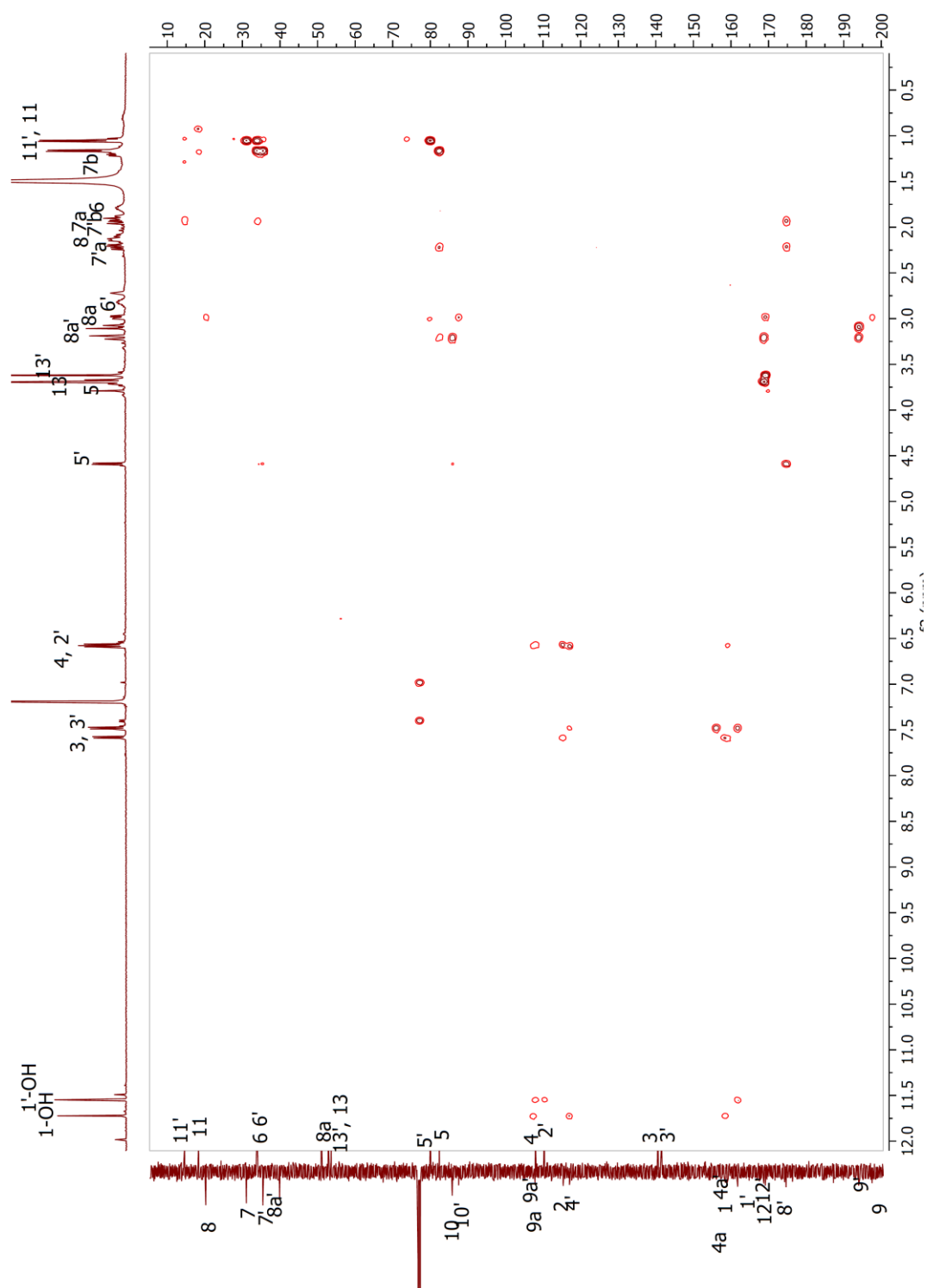


Figure A. 67 The HMBC (CDCl_3 , 500 MHz) spectrum of US9

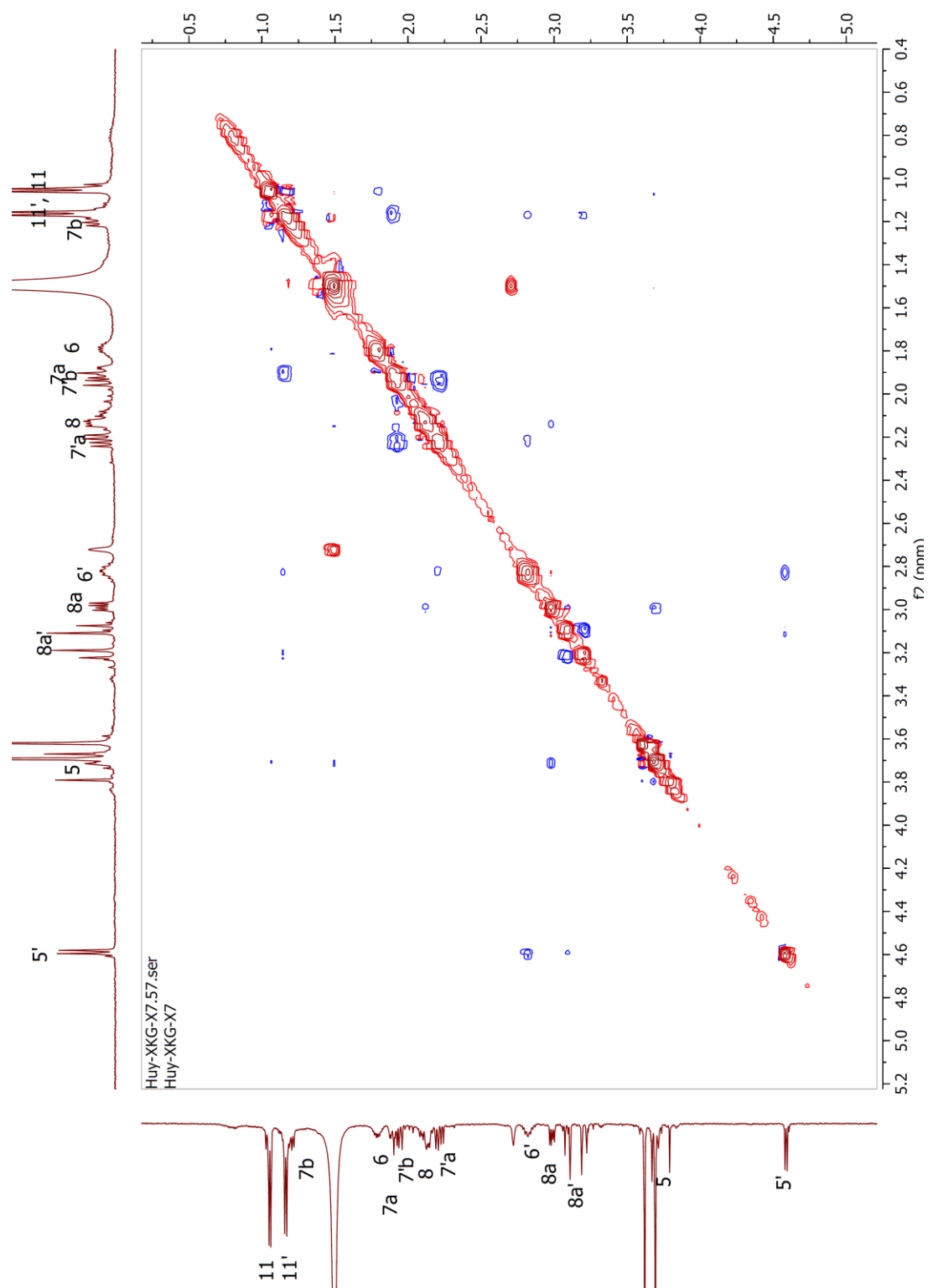


Figure A. 68 The NOESY (CDCl₃, 500 MHz) spectrum of US9

Generic Display Report

Analysis Info

Analysis Name D:\Data\Data Service\190325\T6_RA6_01_2360.d
Method nv_pos_5min_profile_190214.m
Sample Name T6
Comment

Acquisition Date 3/25/2019 4:35:22 PM

Operator CU.
Instrument micrOTOF-Q II

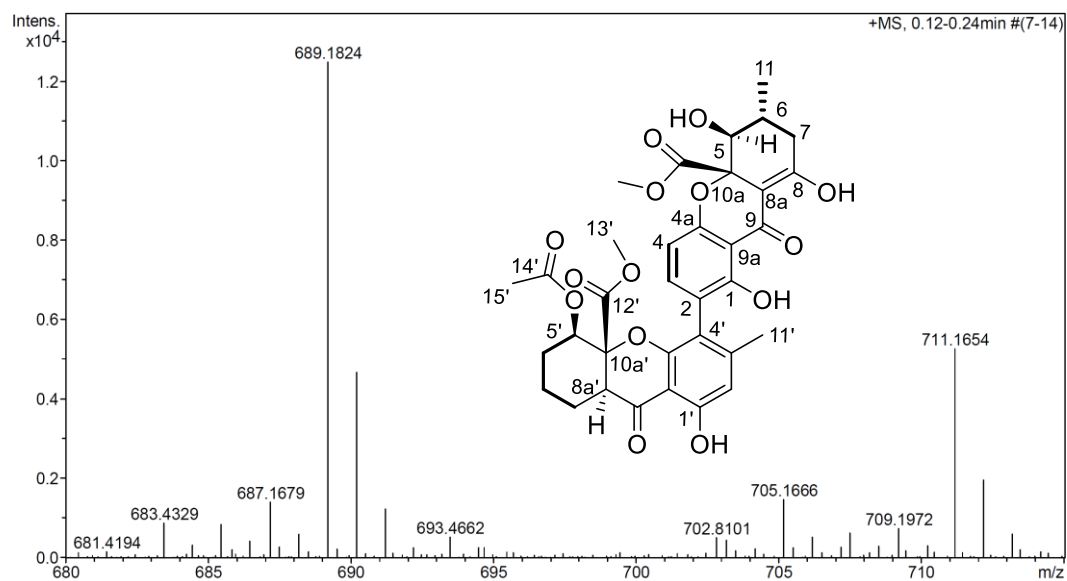
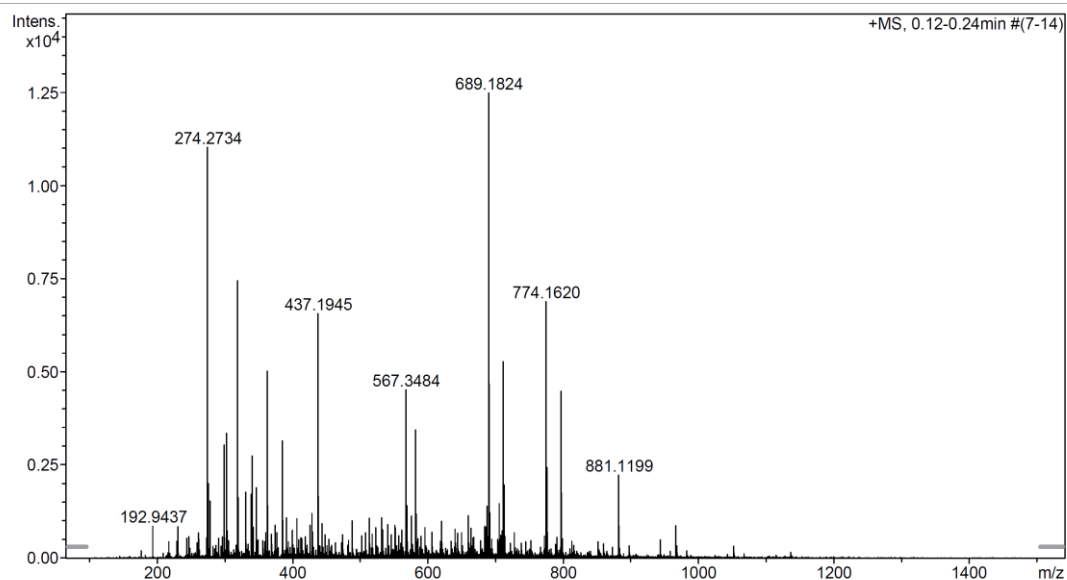


Figure A. 69 The HRESIMS spectrum of US10

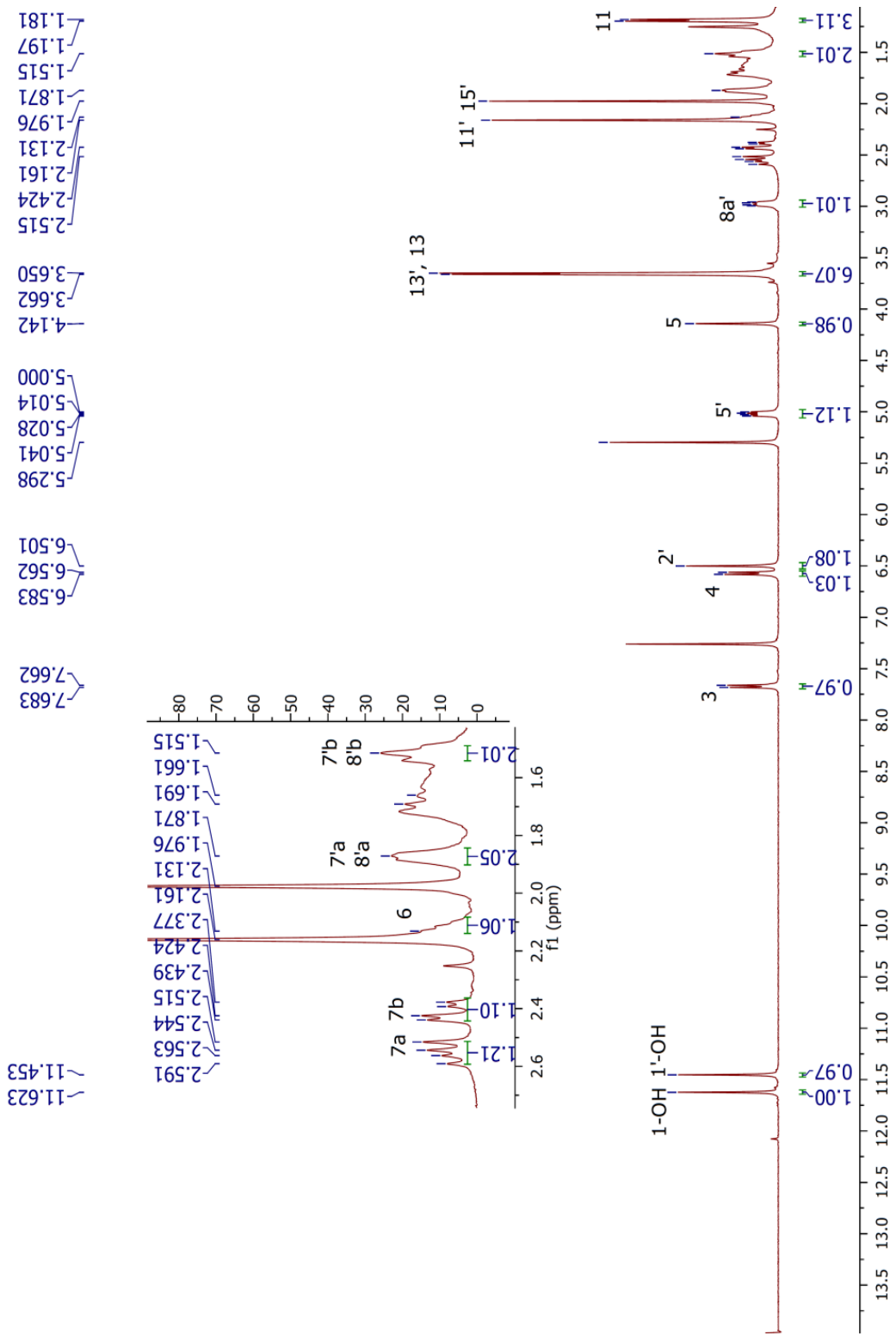


Figure A. 70 The ^1H NMR (CDCl_3 , 400 MHz) spectrum of US10

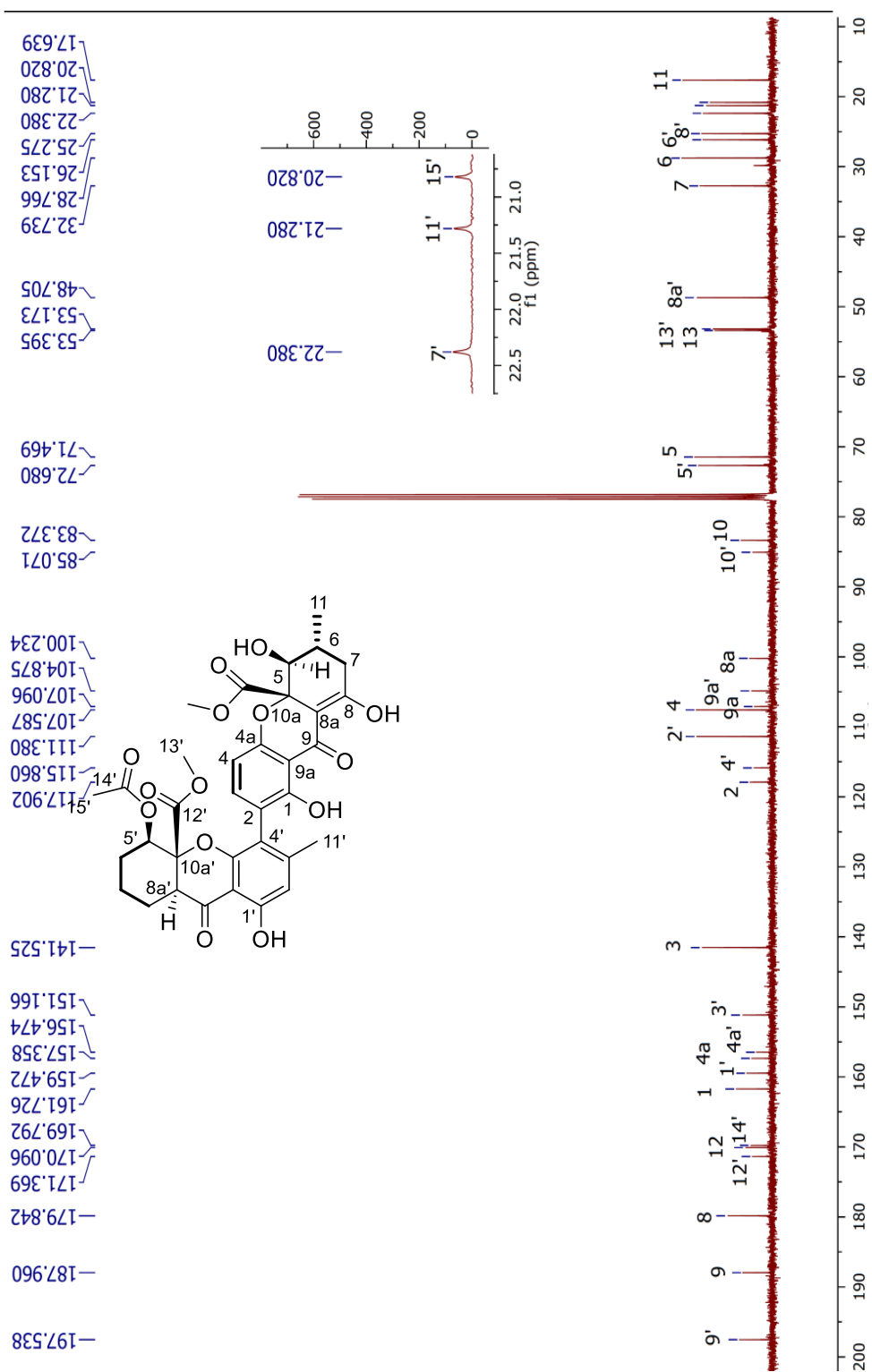


Figure A. 71 The ^{13}C NMR (CDCl_3 , 100 MHz) spectrum of US10

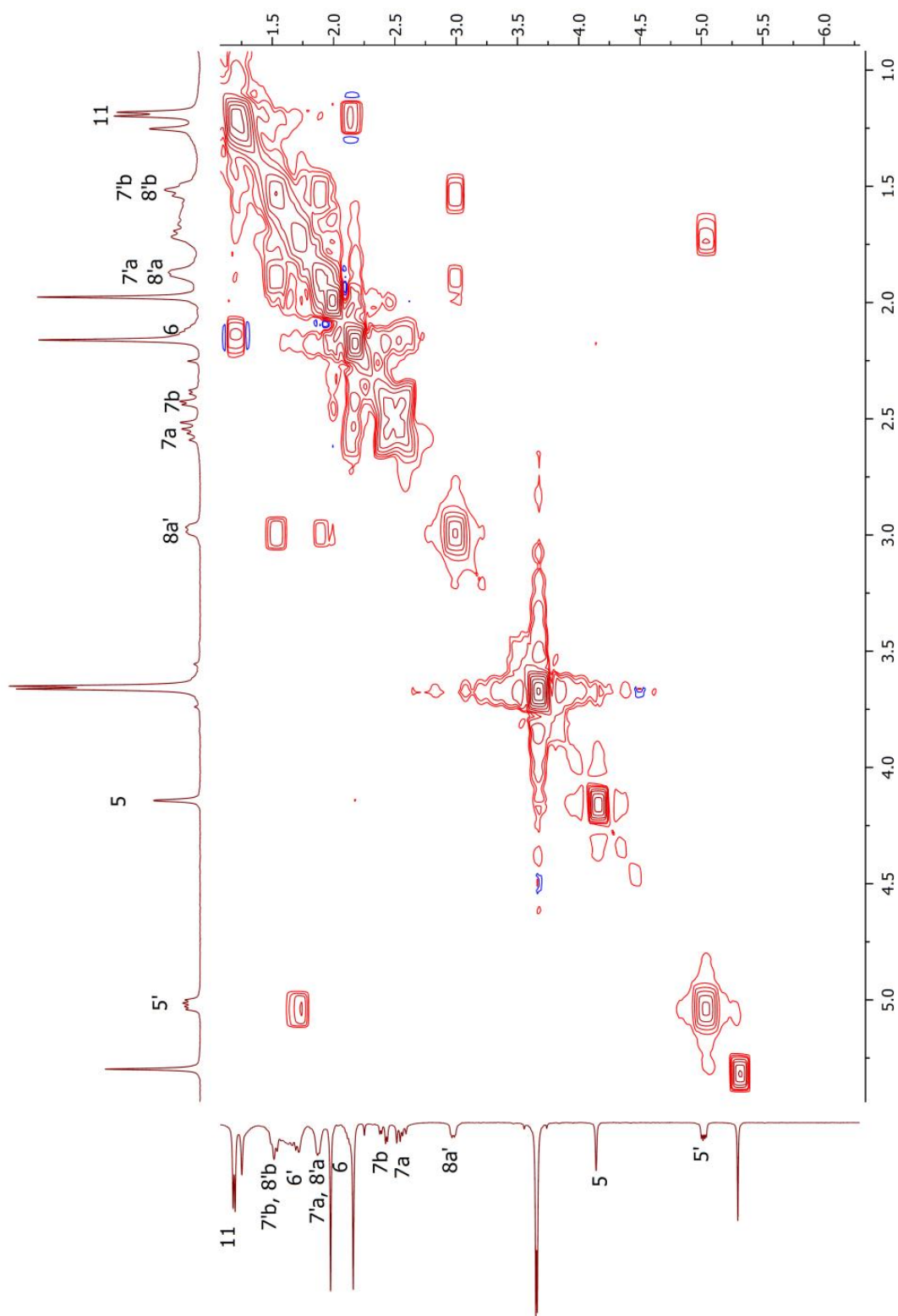


Figure A. 72 The COSY (CDCl₃, 400 MHz) spectrum of US10

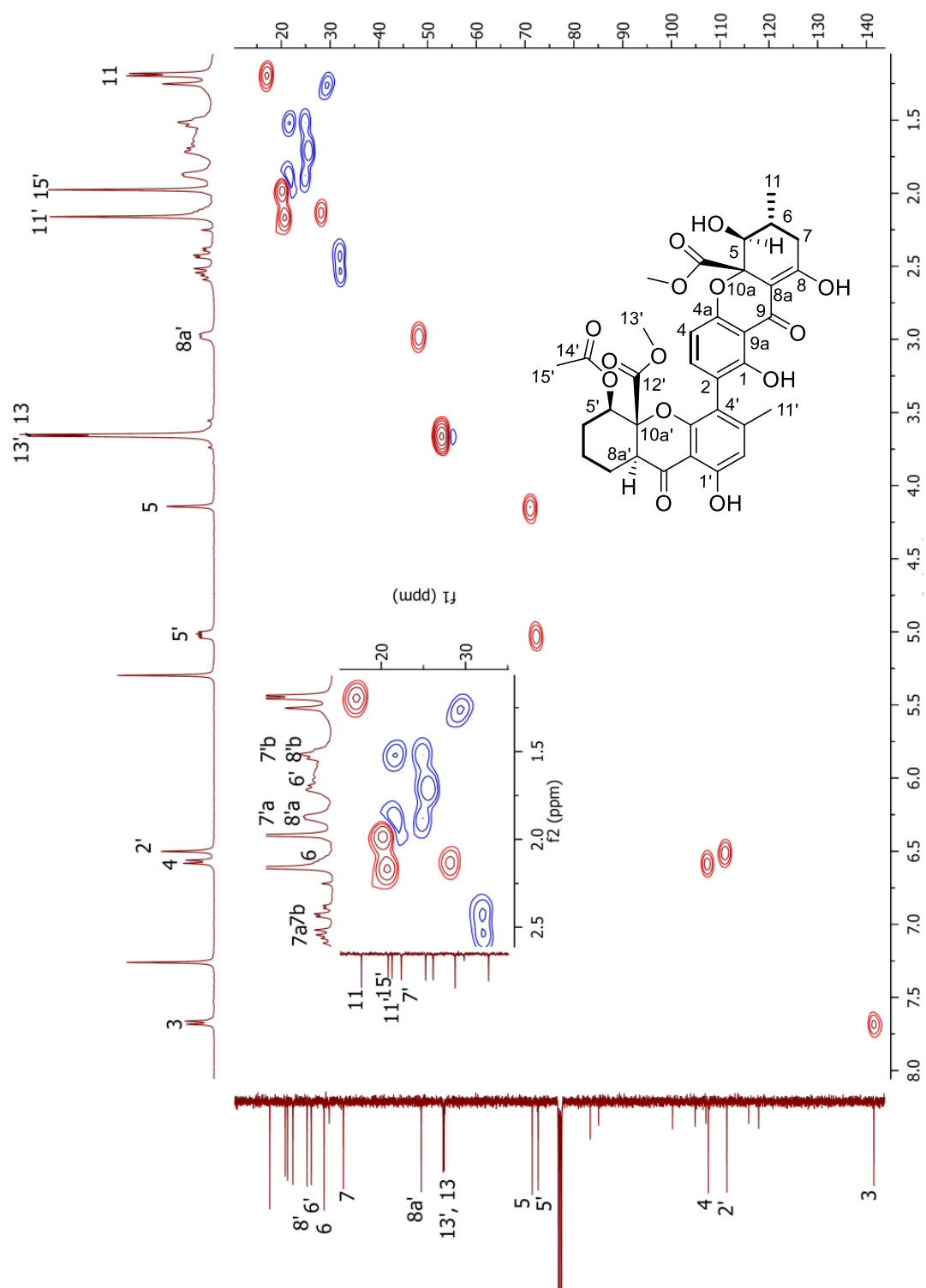


Figure A. 73 The HSQC (CDCl₃, 400 MHz) spectrum of US10

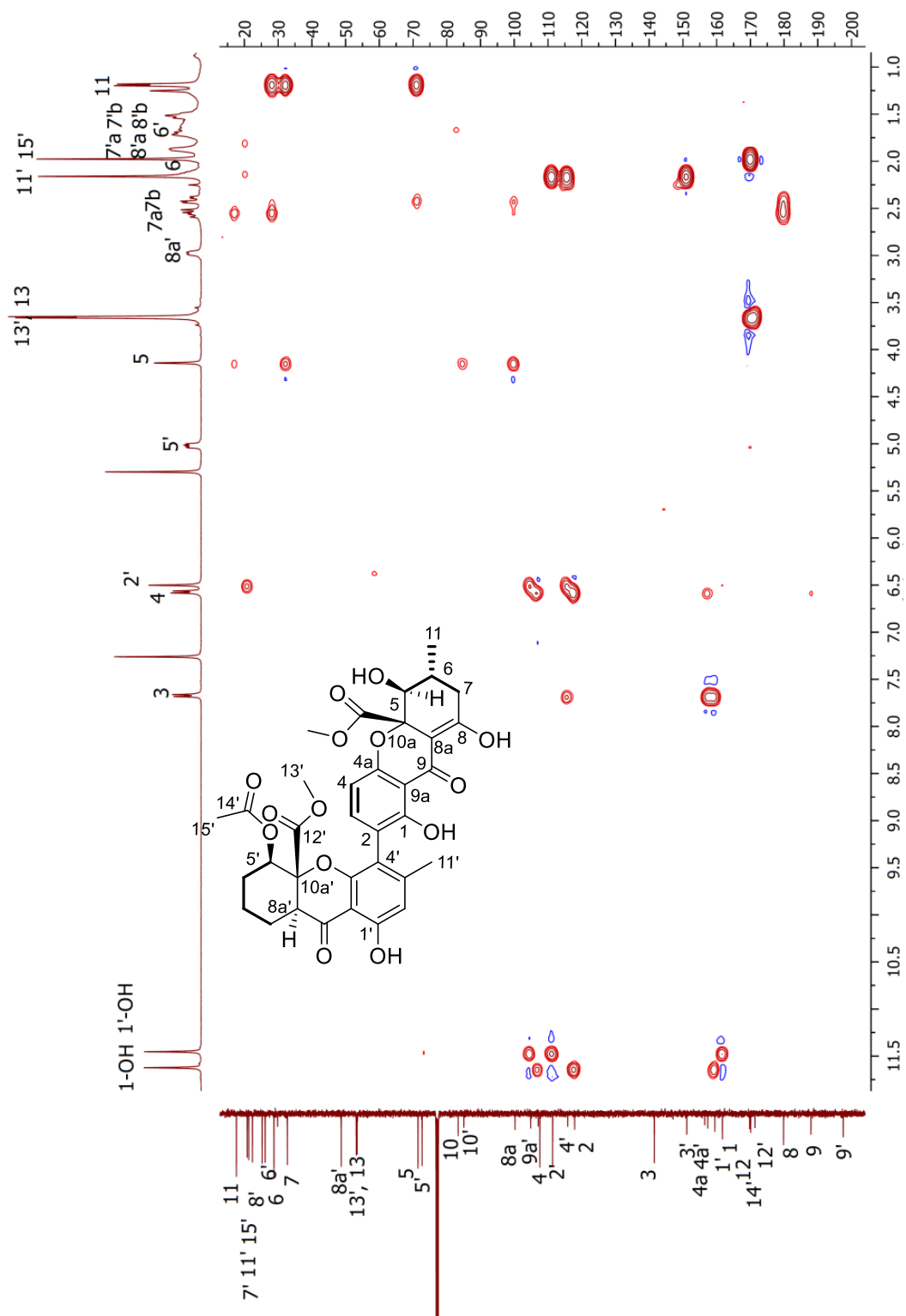


Figure A. 74 The HMBC (CDCl_3 , 400 MHz) spectrum of US10

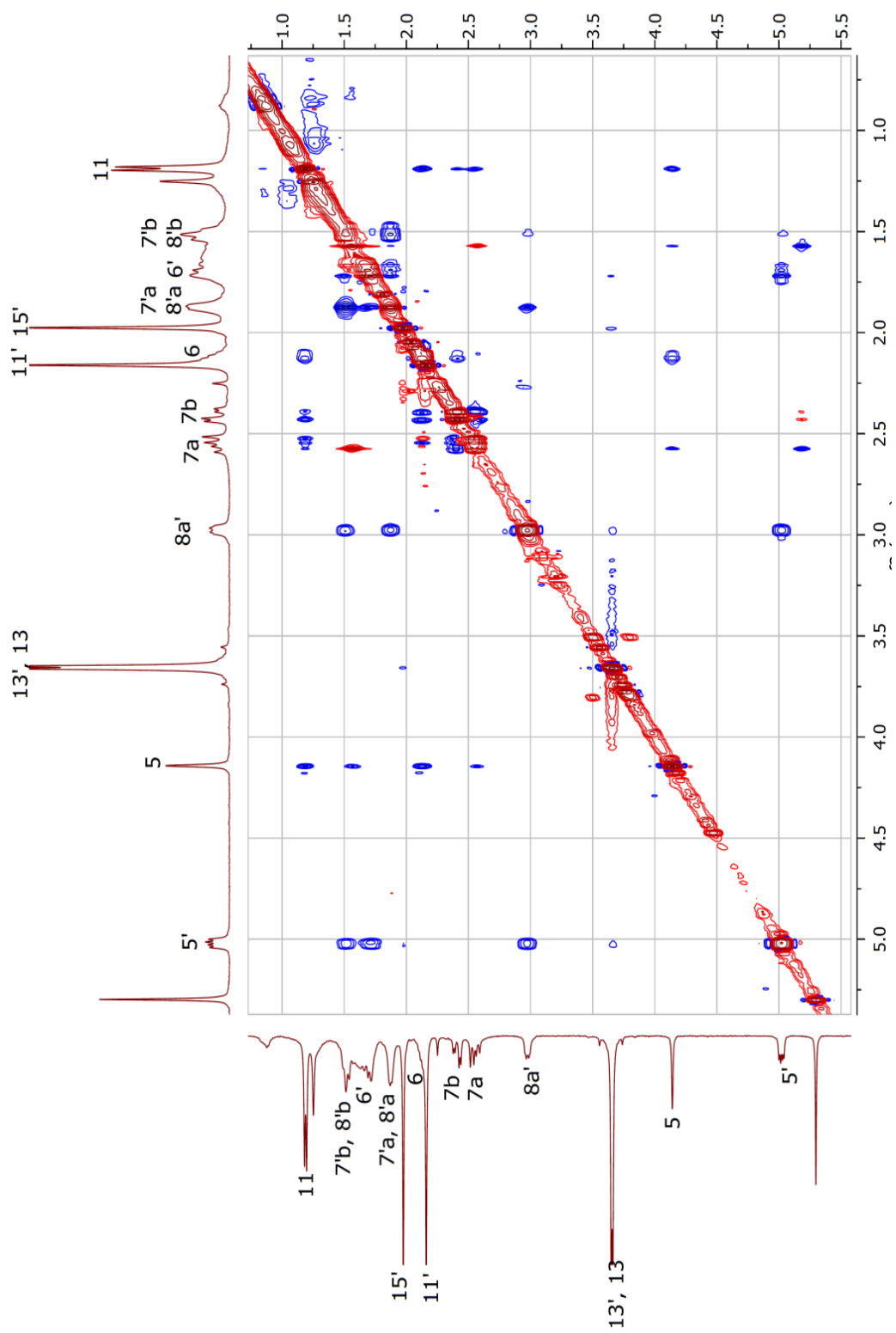


Figure A. 75 The NOESY (CDCl_3 , 400 MHz) spectrum of US10

Data: A6_0001.B3[c] 22 Aug 2019 18:38 Cal: naka 8 Aug 2019 19:32
Shimadzu Biotech Axima Resonance 2.9.1.20100121: Mode positive, Low 300+, Power: 110

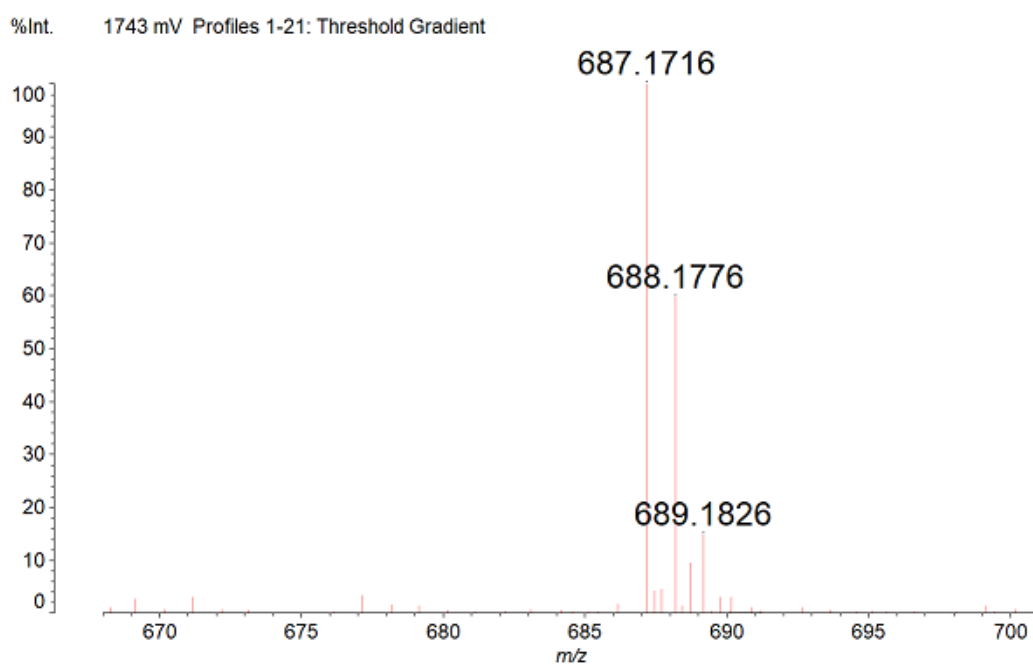


Figure A. 76 The HRESIMS spectrum of US11



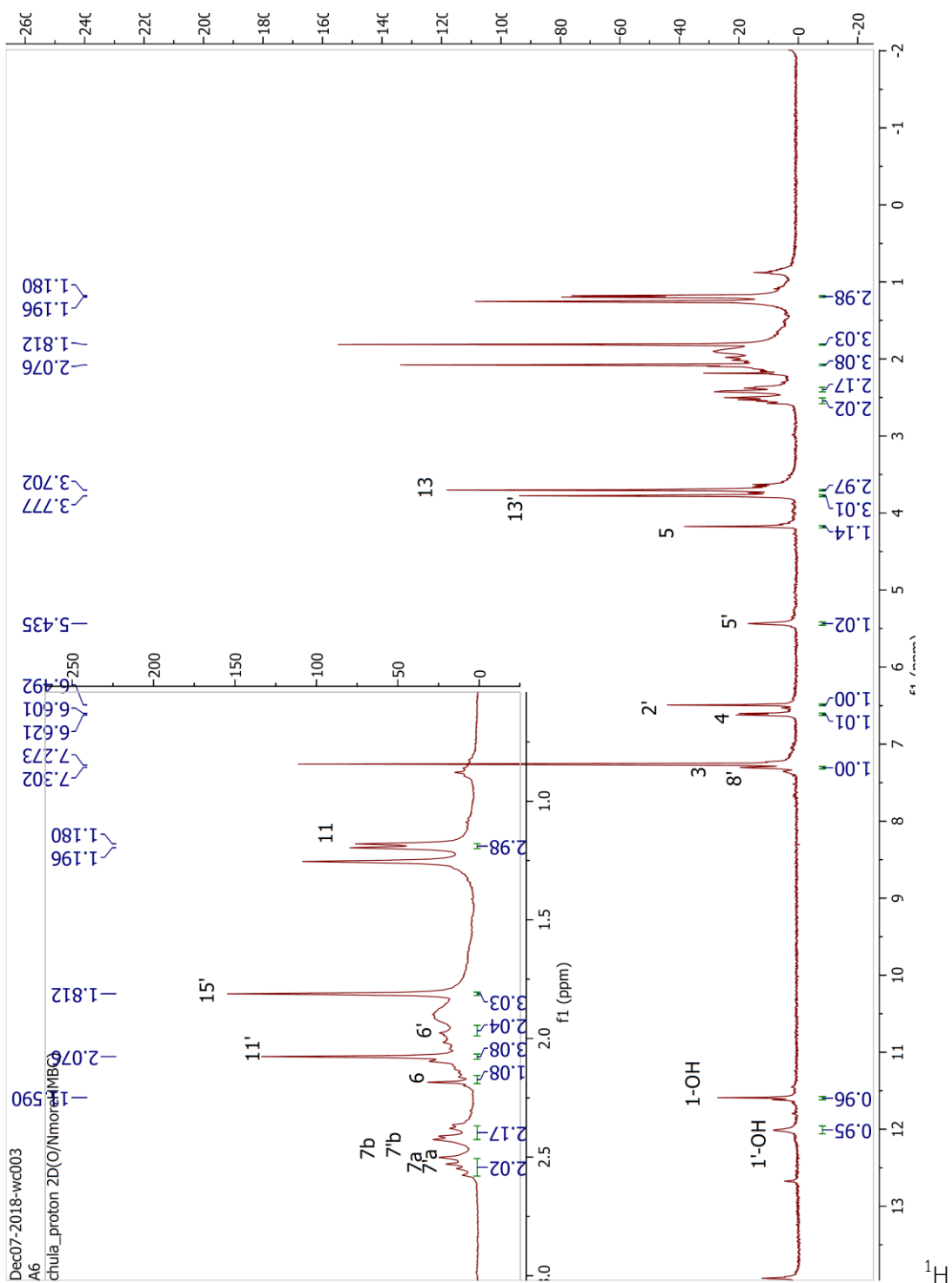


Figure A. 77 The NMR (CDCl_3 , 400 MHz) spectrum of US11

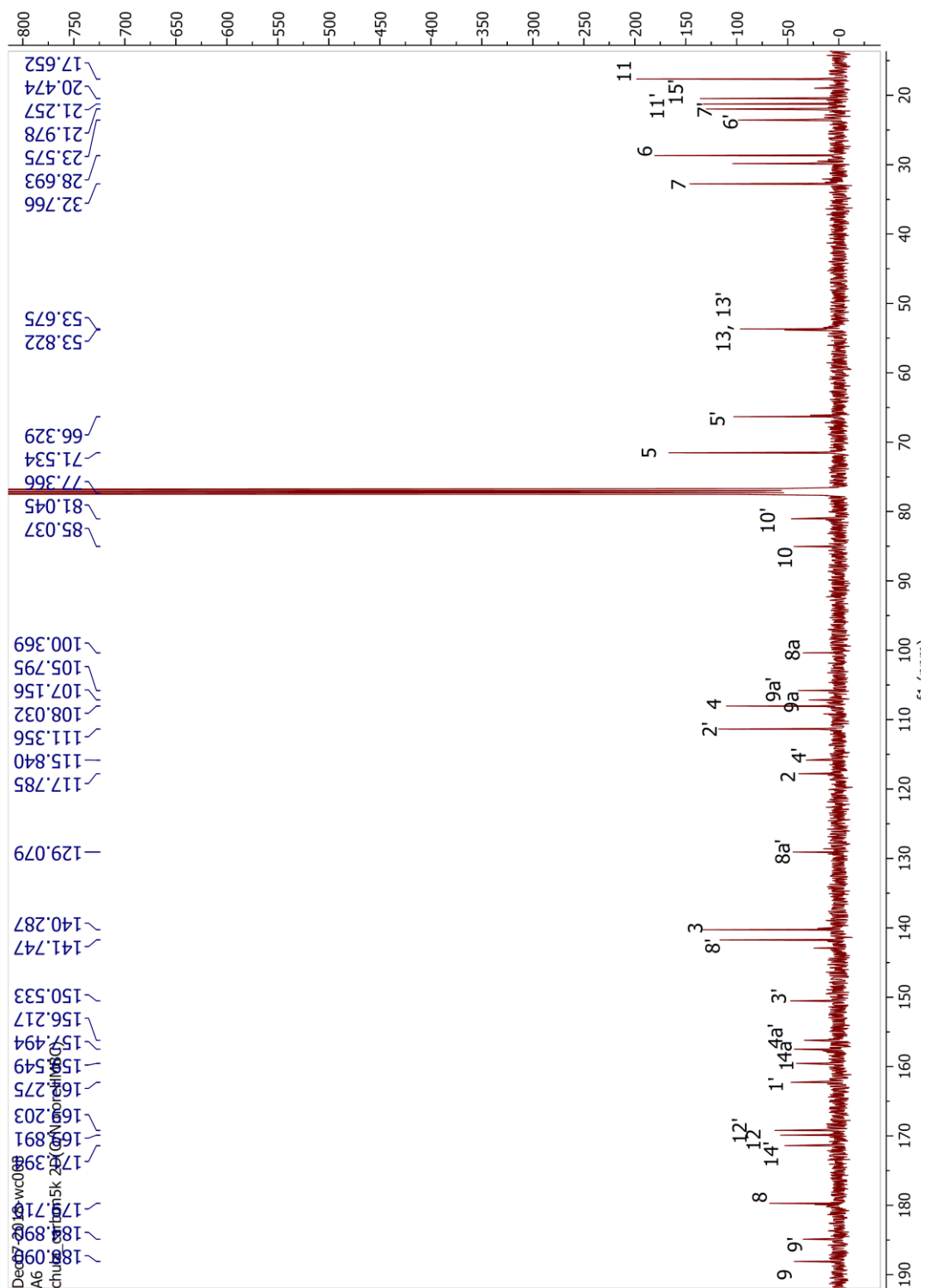


Figure A. 78 The ^{13}C NMR (CDCl_3 , 100 MHz) spectrum of US11

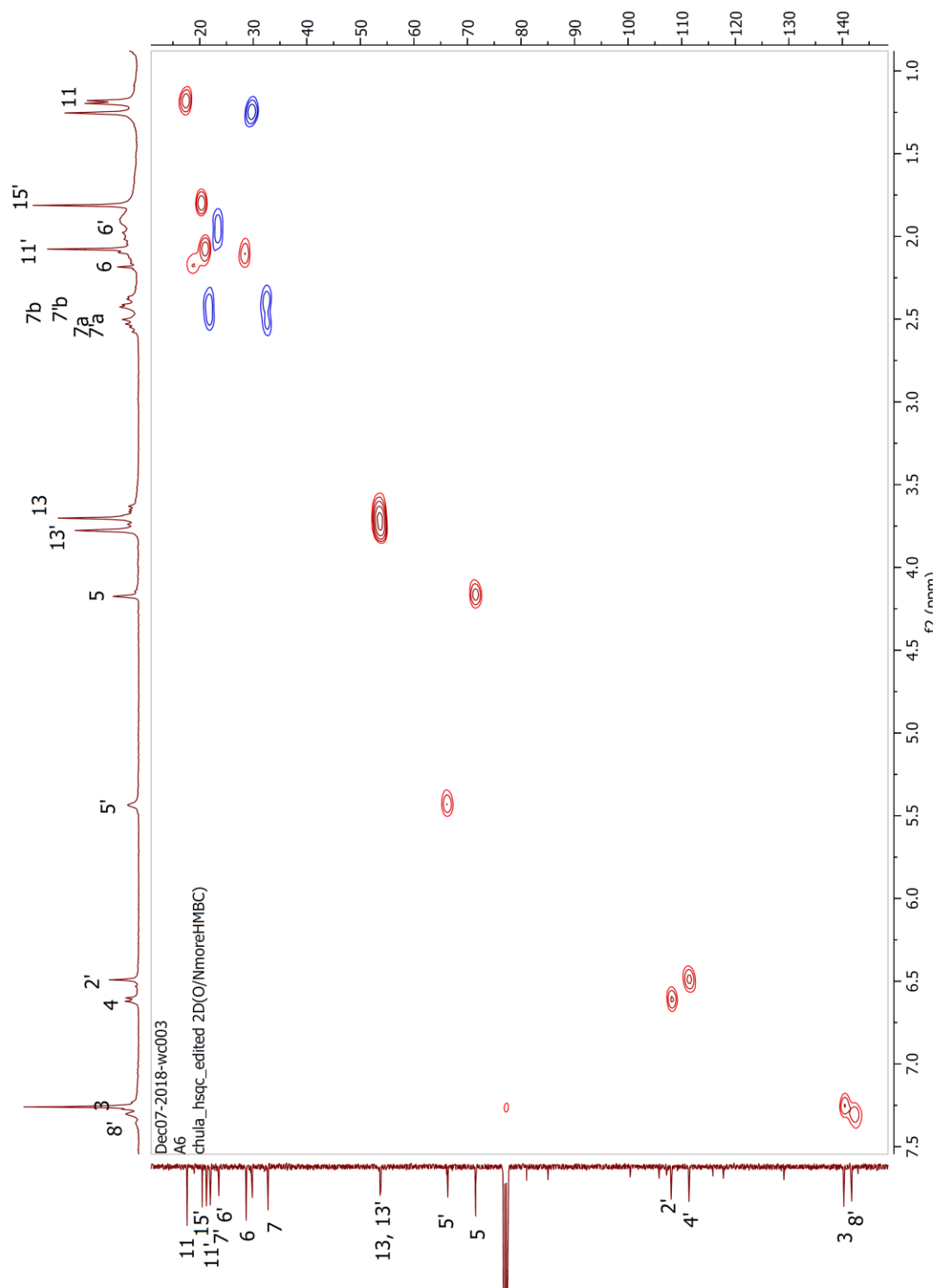


Figure A. 79 The HSQC (CDCl_3 , 400 MHz) spectrum of US11

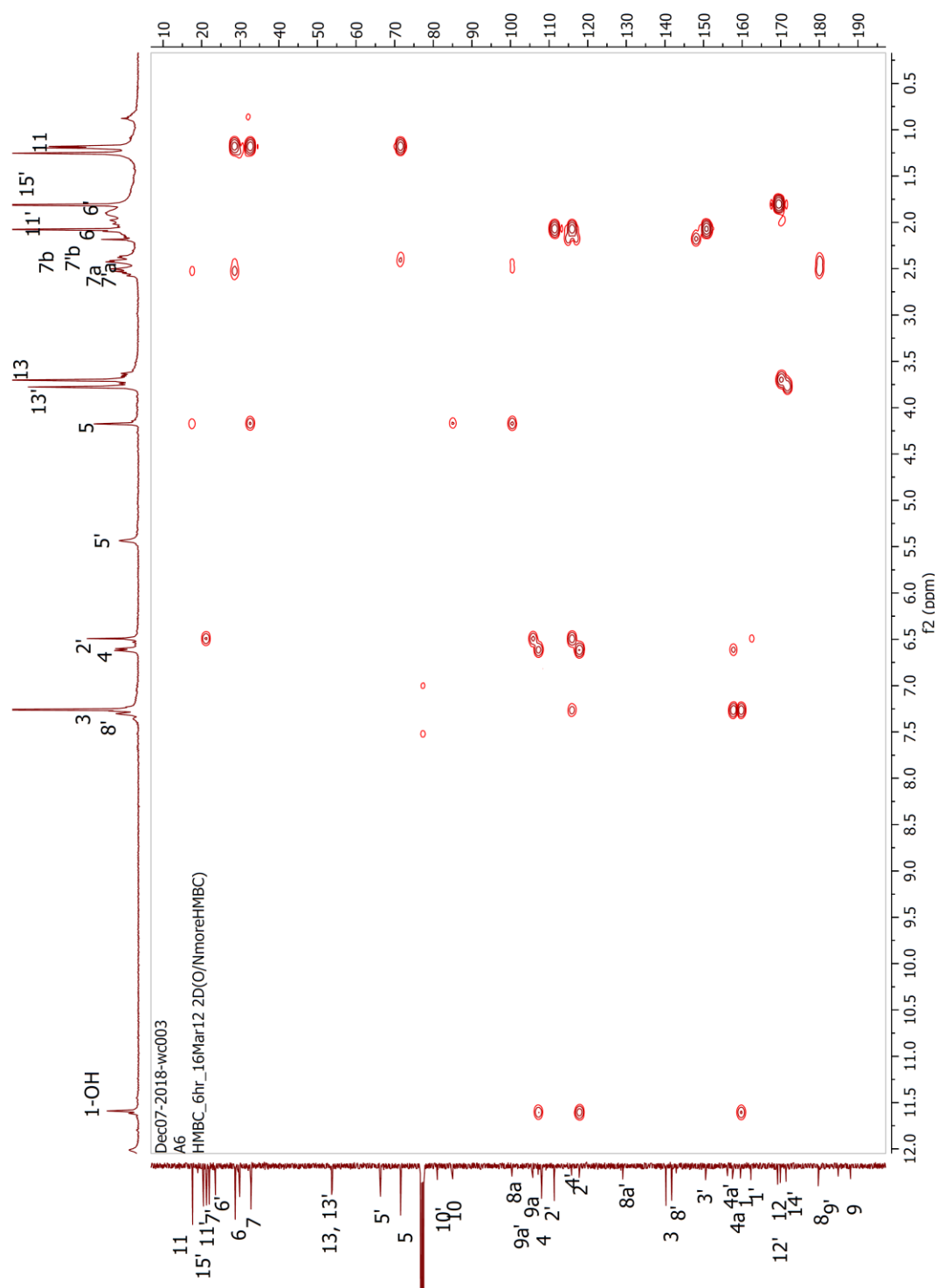


Figure A. 80 The HMBC (CDCl₃, 400 MHz) spectrum of US11

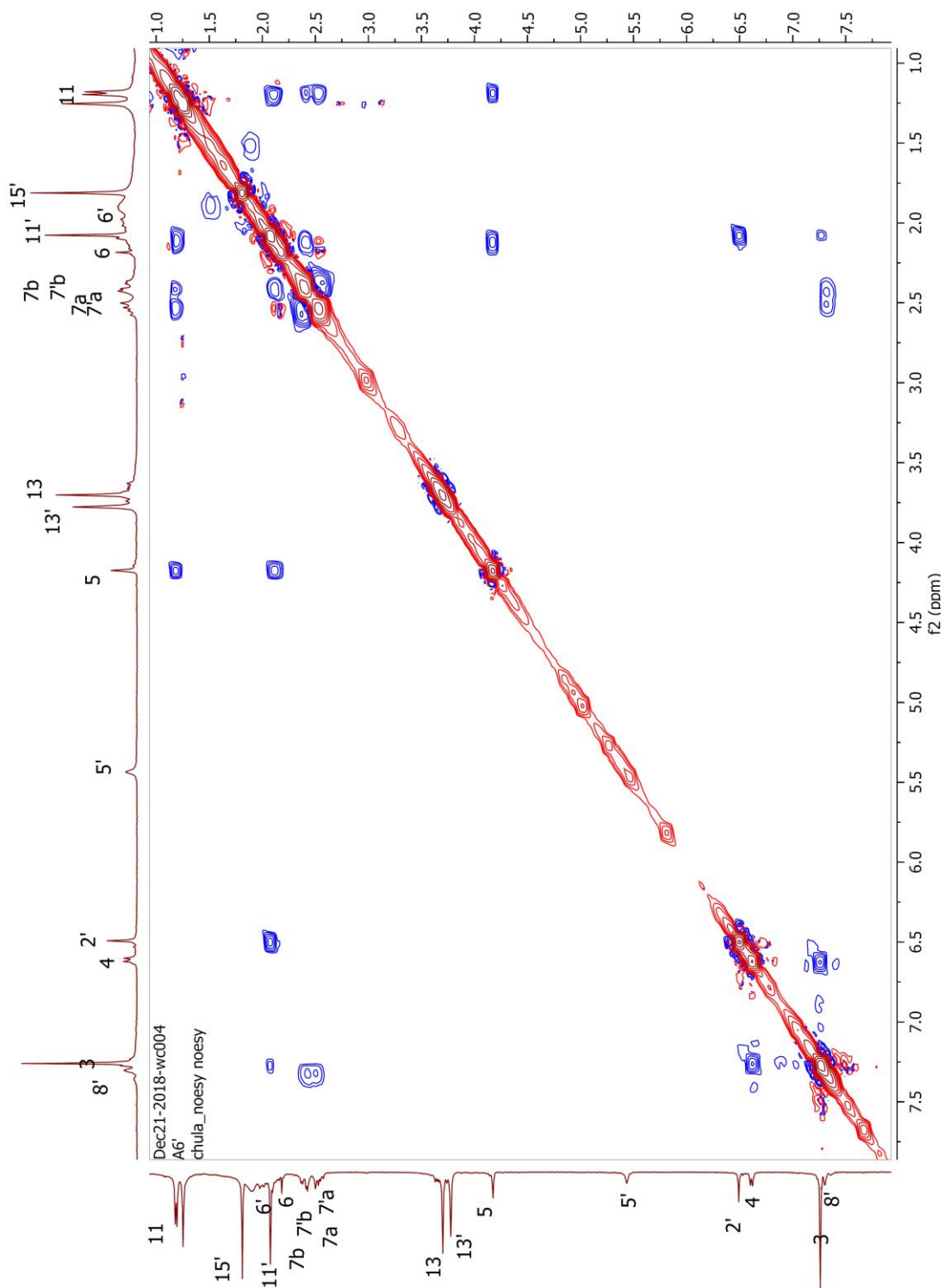


Figure A. 81 The NOESY (CDCl₃, 400 MHz) spectrum of US11

Generic Display Report

Analysis Info

Analysis Name	D:\Data\Data Service\180118_neg_UG1.d	Acquisition Date	1/18/2018 4:05:31 PM
Method	NV_neg_0.3min_profile_1segment_lowNubulizerDrygas(2).m	Operator	CU.
Sample Name	180118_neg_UG1	Instrument	micrOTOF-Q II
Comment			

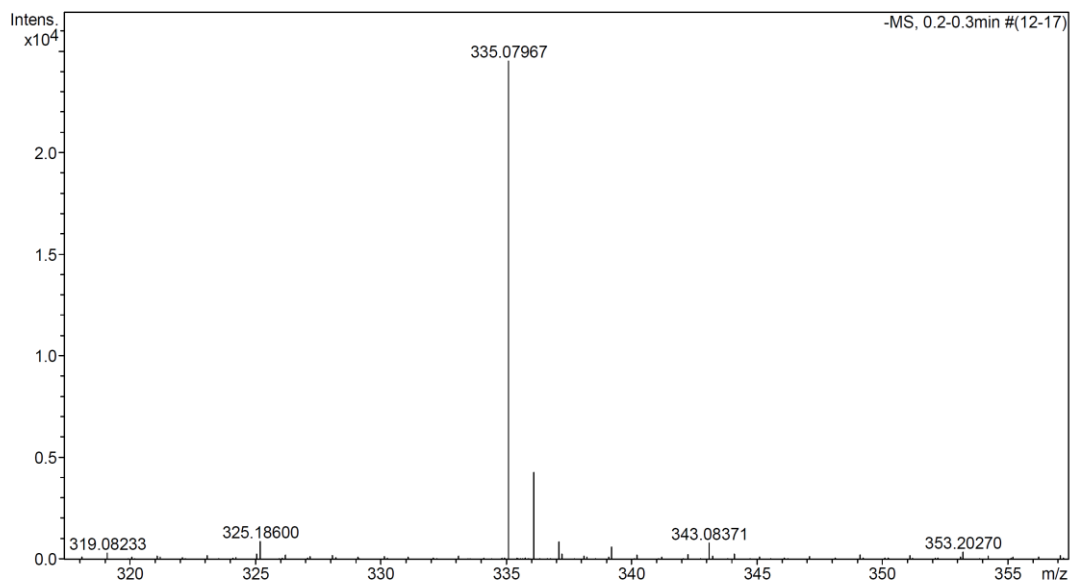
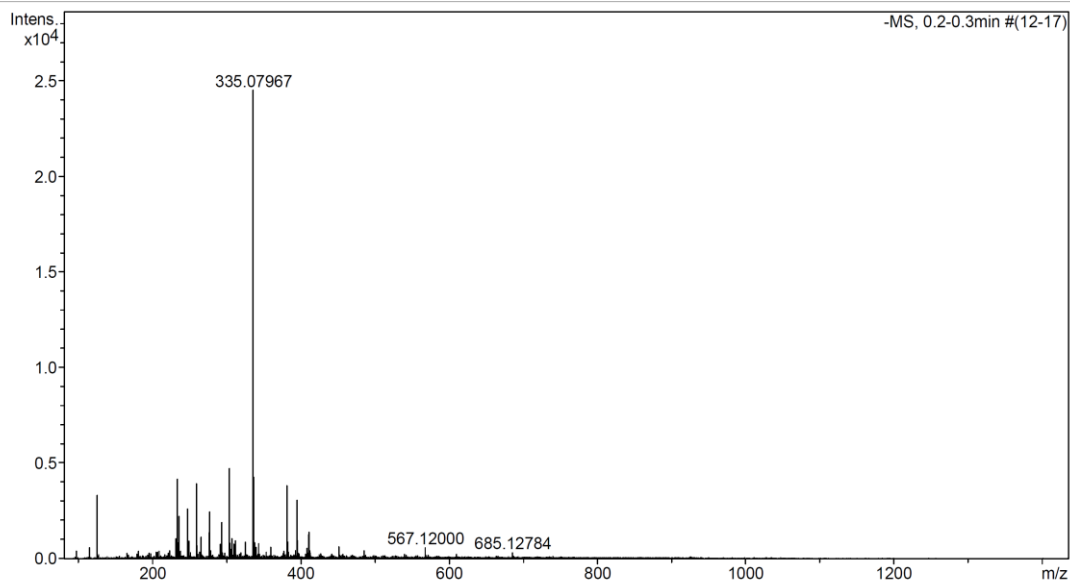


Figure A. 82 The HRESIMS spectrum of UD1

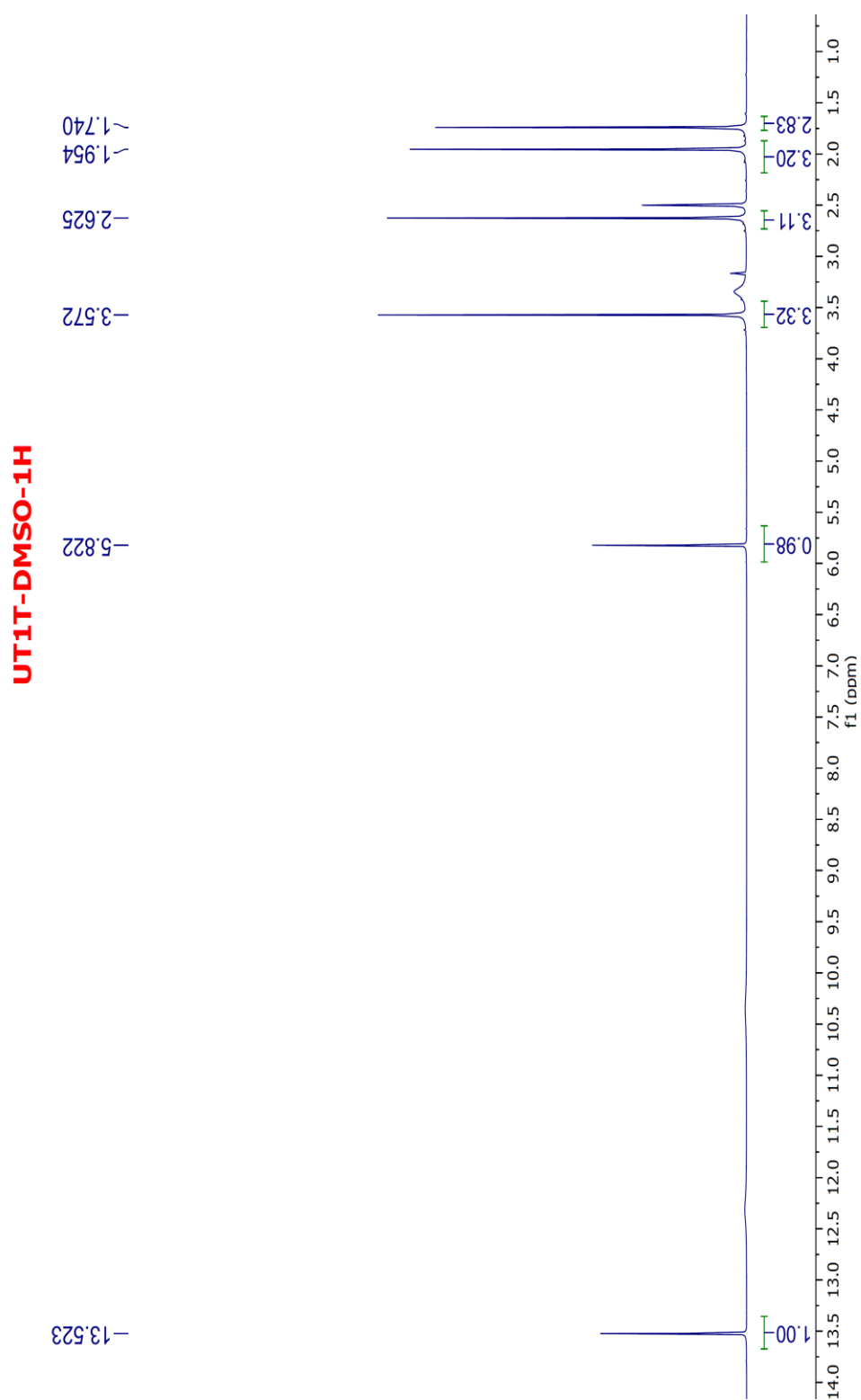


Figure A. 83 The ^1H NMR (CDCl_3 , 500 MHz) spectrum of UD1

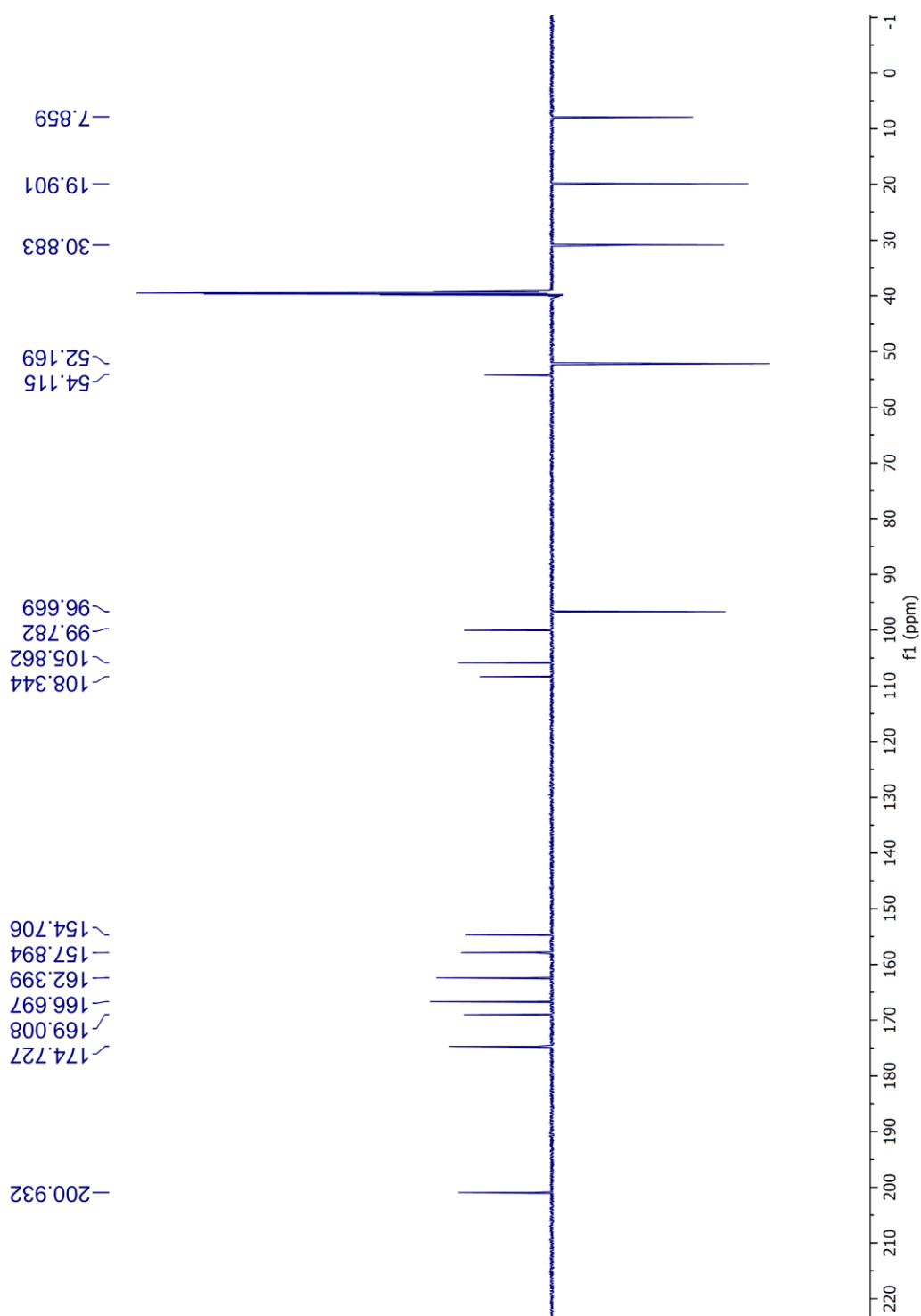


Figure A. 84 The ^{13}C NMR (CDCl_3 , 500 MHz) spectrum of UD1

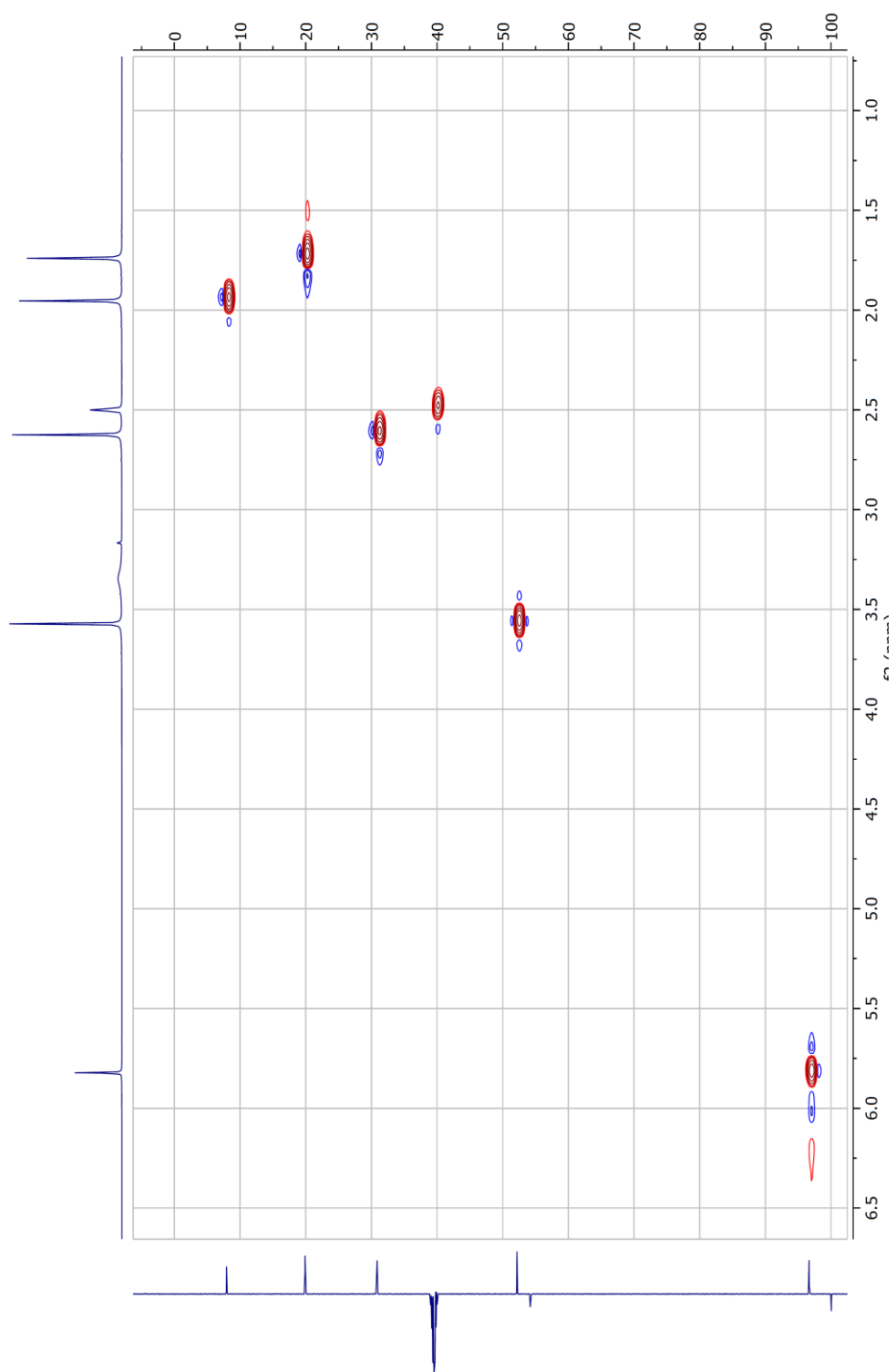


Figure A. 85 The HSQC (CDCl_3 , 500 MHz) spectrum of UD1

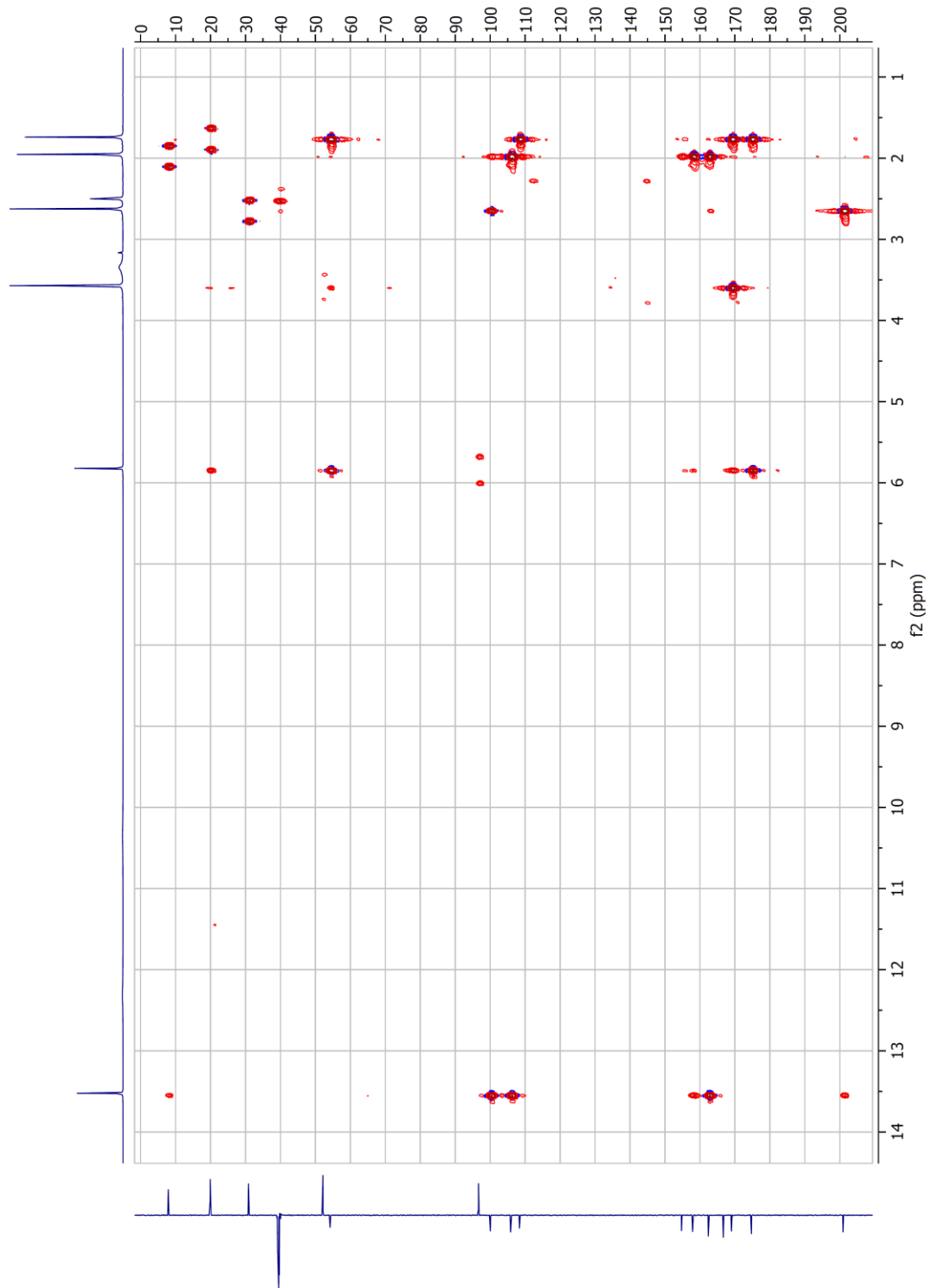


Figure A. 86 The HMBC (CDCl_3 , 500 MHz) spectrum of UD1

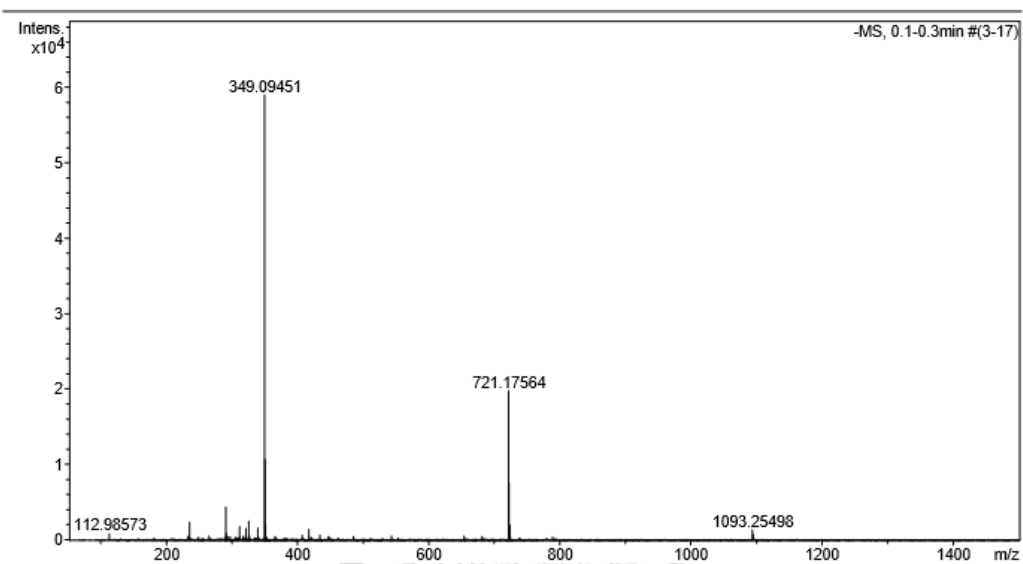
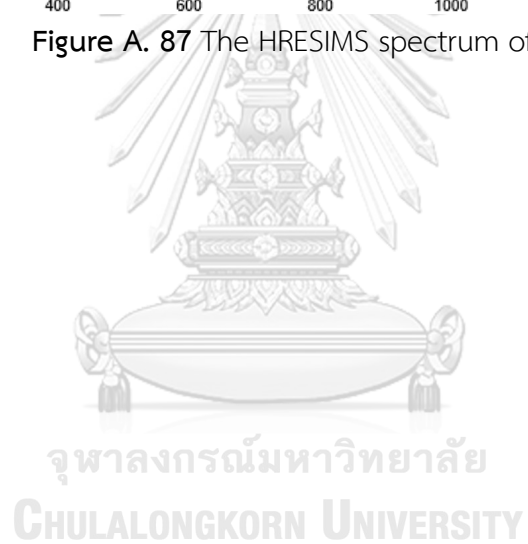


Figure A. 87 The HRESIMS spectrum of UD2



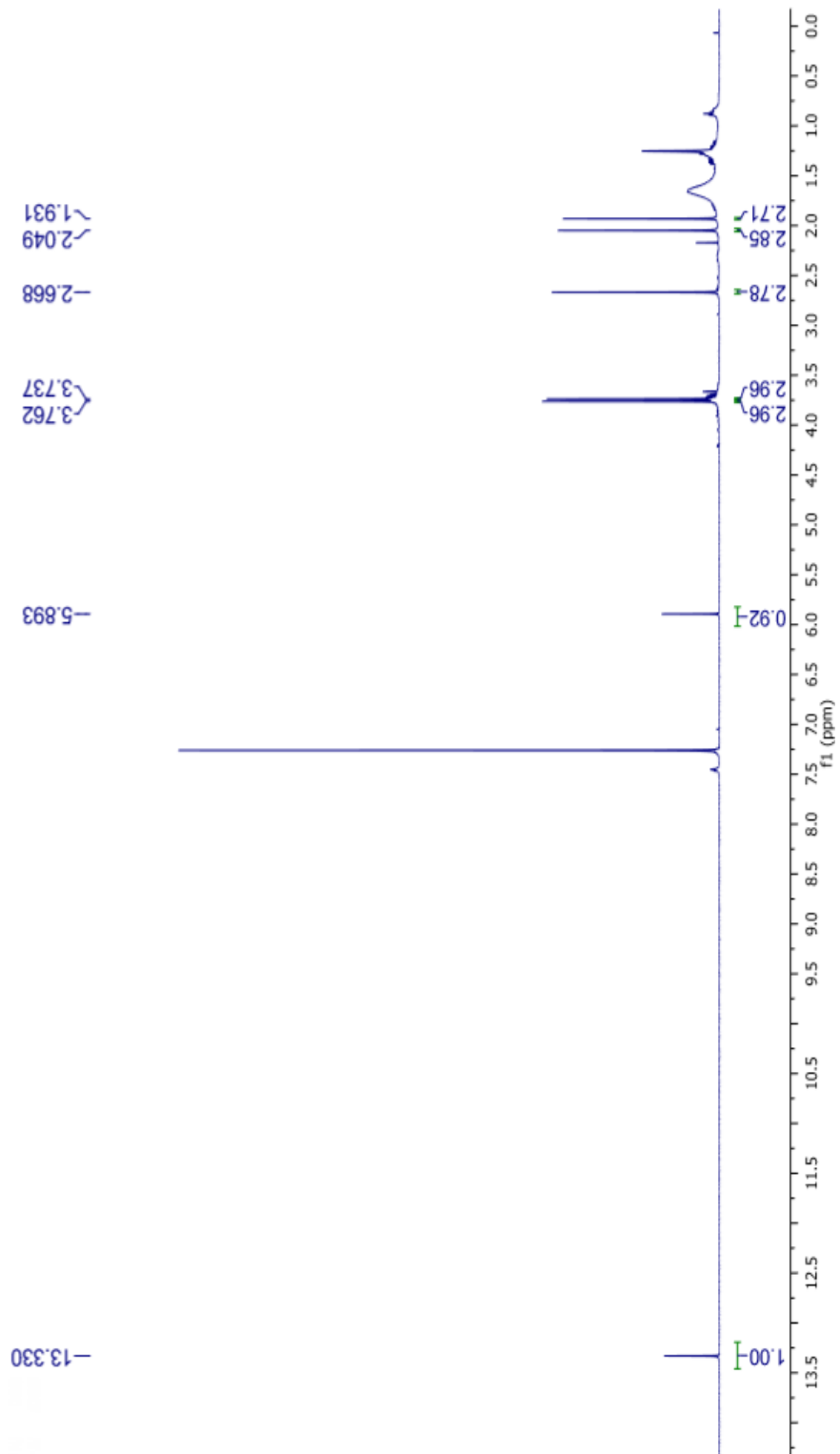


Figure A. 88 The ^1H NMR (CDCl_3 , 500 MHz) spectrum of UD2

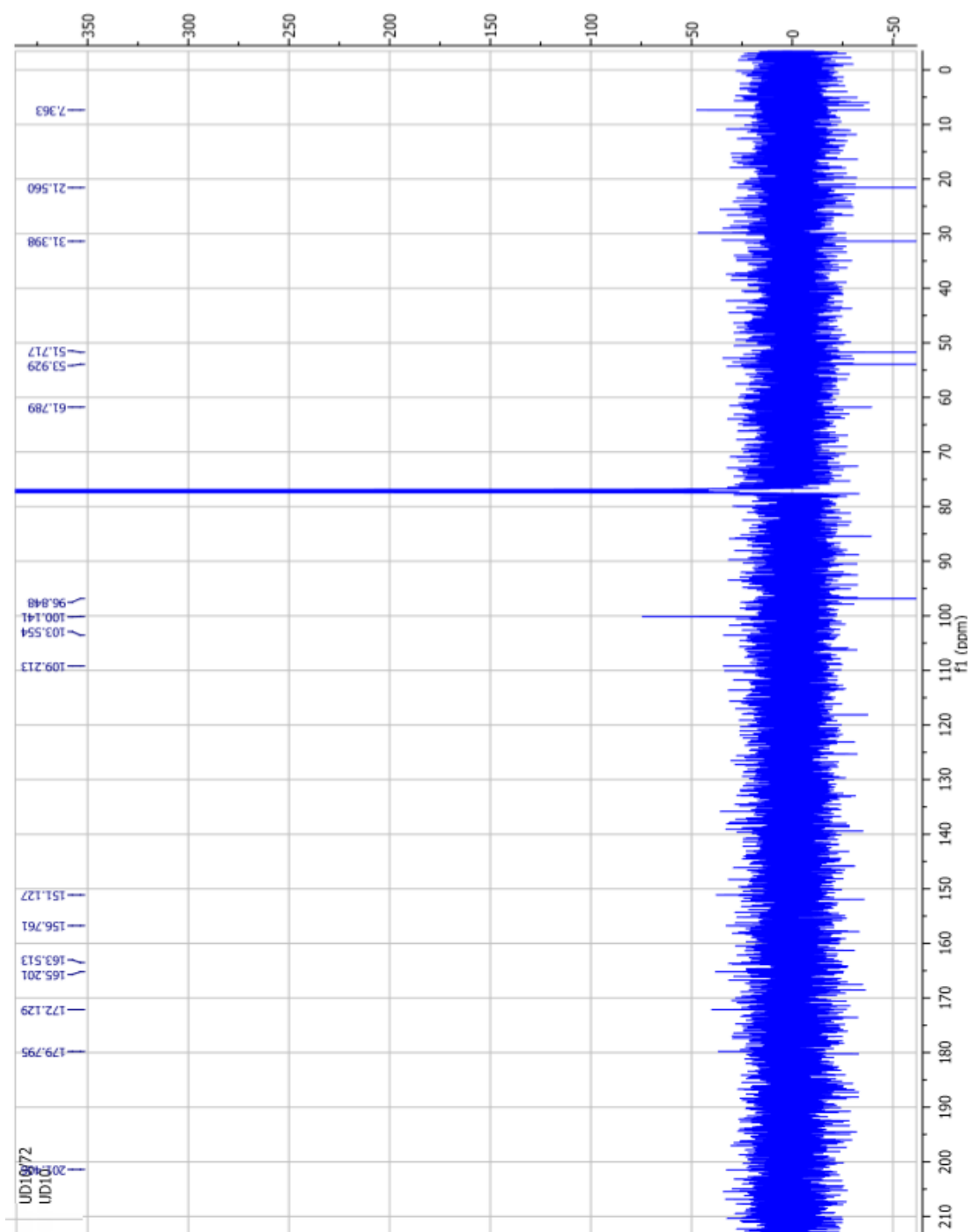


Figure A. 89 The ^{13}C NMR (CDCl_3 , 125 MHz) spectrum of UD2

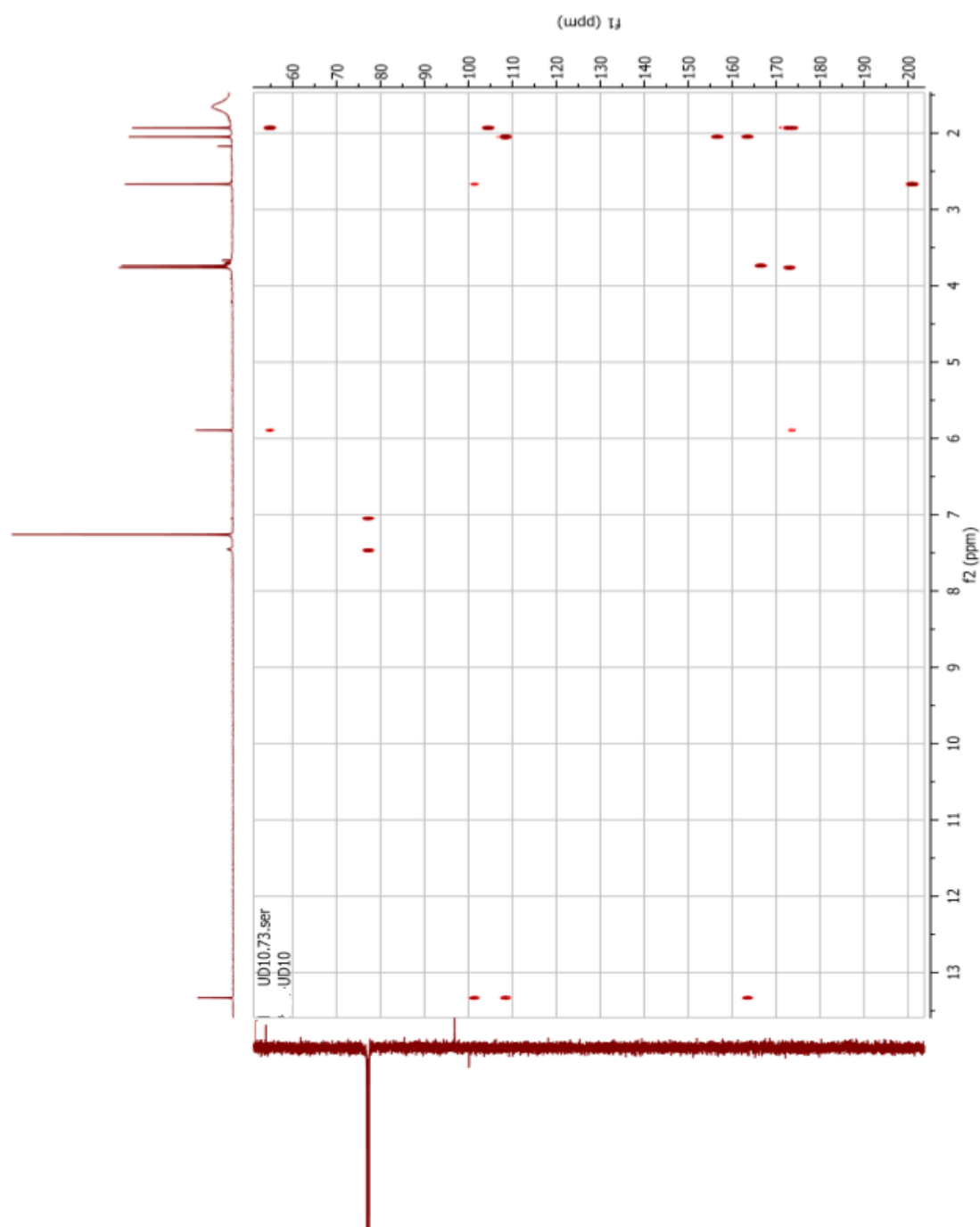


Figure A. 90 The HMBC (CDCl_3 , 500 MHz) spectrum of UD2

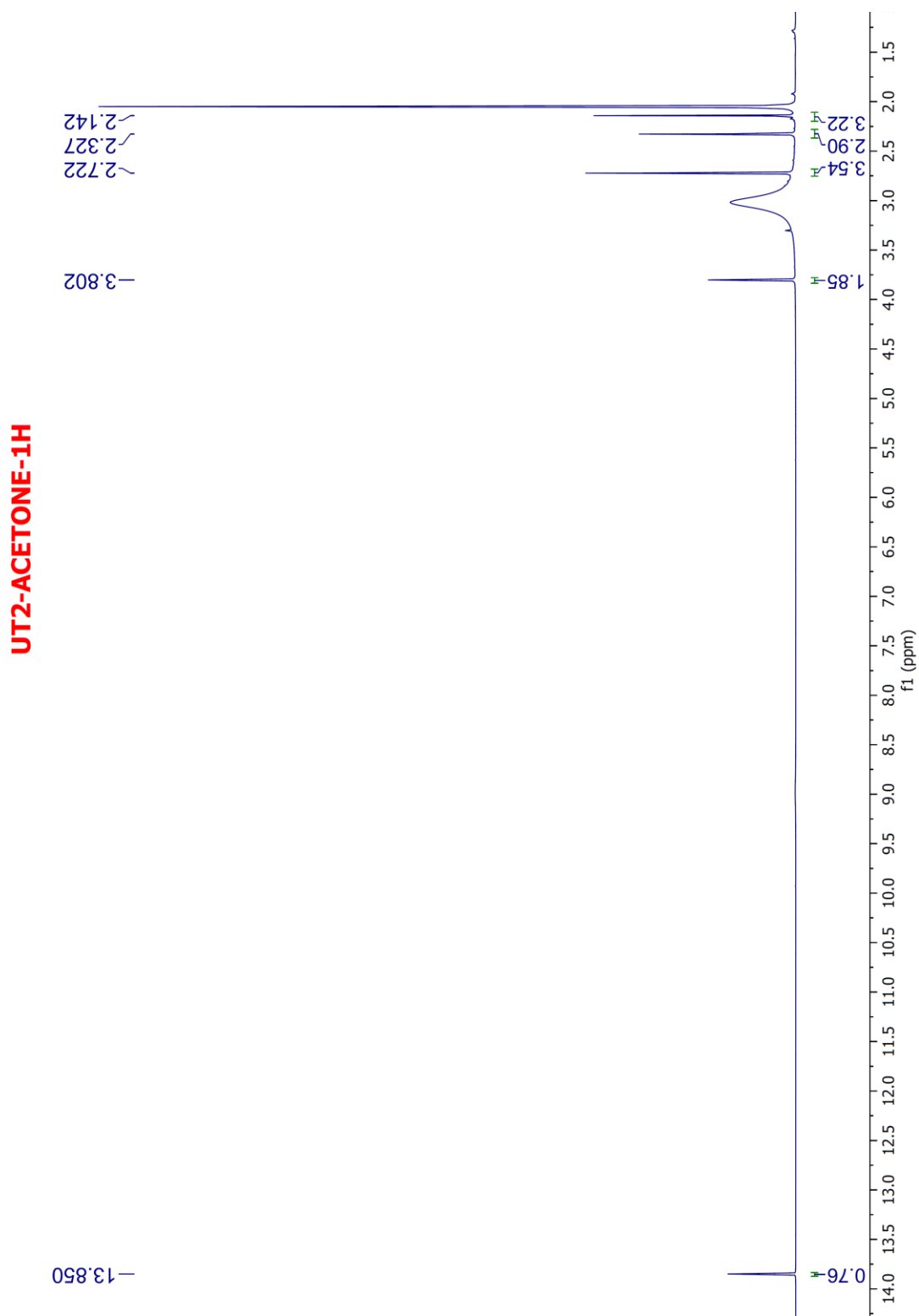


Figure A. 91 The ^1H NMR (CDCl_3 , 500 MHz) spectrum of UD3

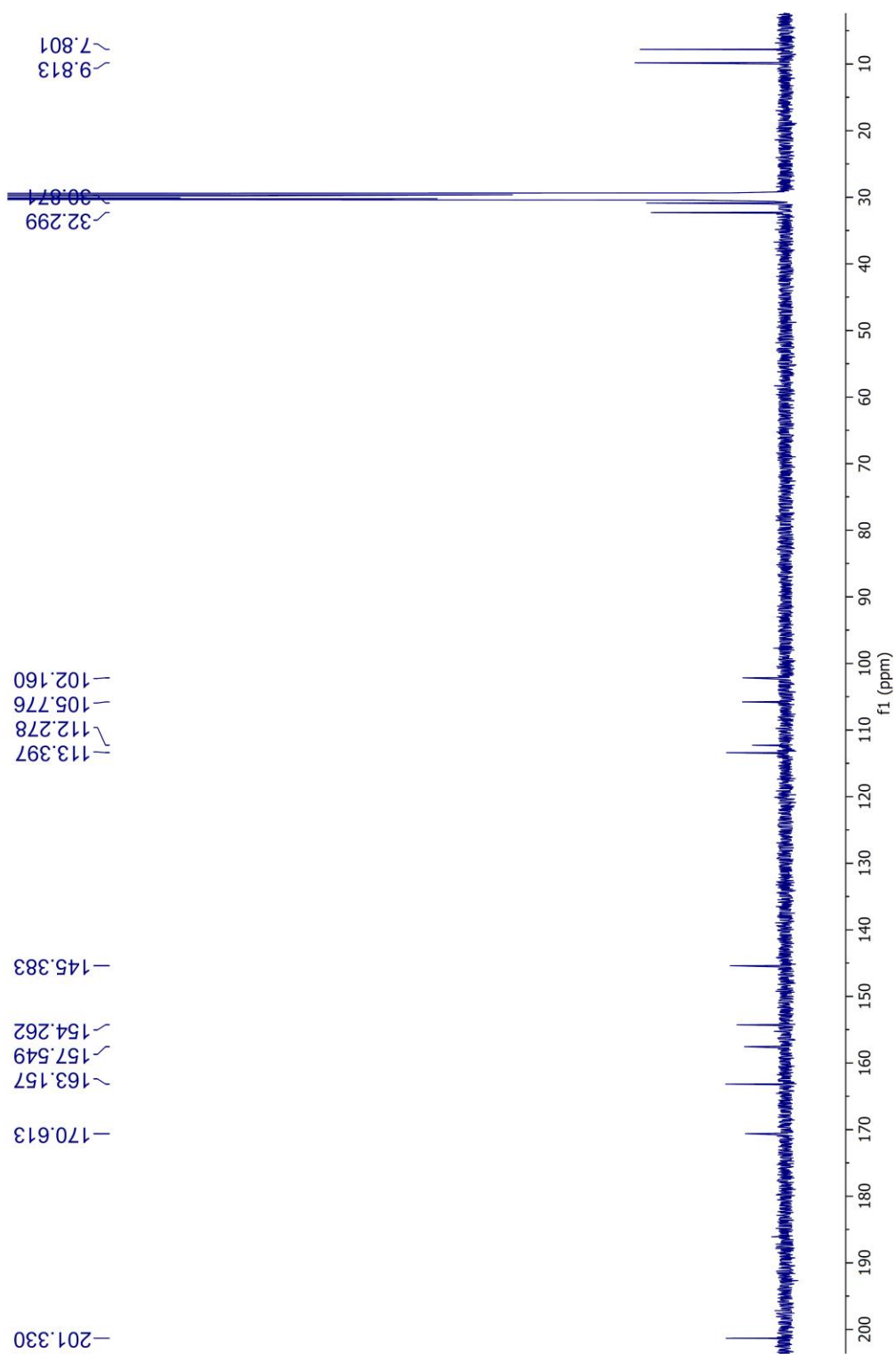


Figure A. 92 The ^{13}C NMR (CDCl_3 , 125 MHz) spectrum of UD3

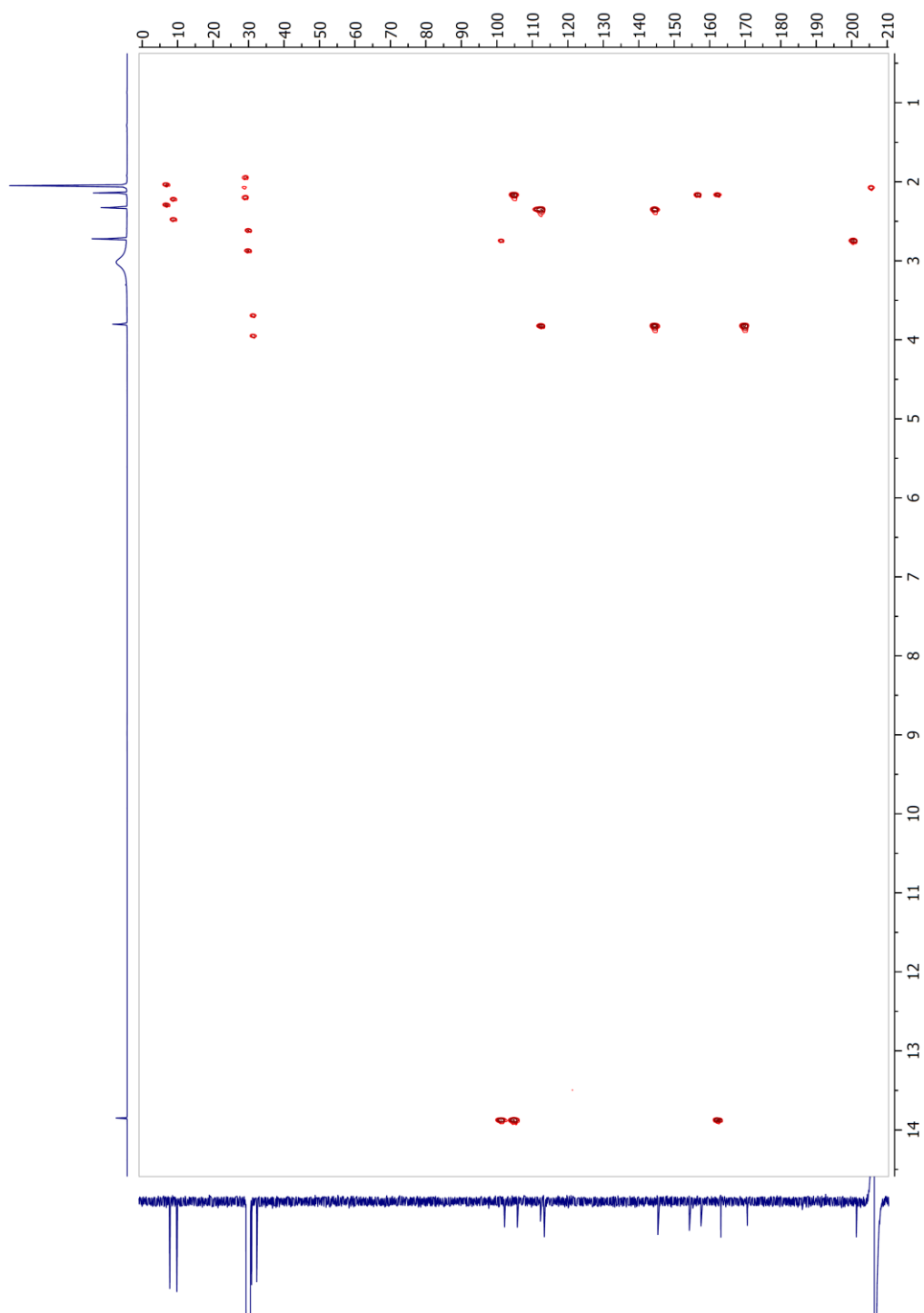


Figure A. 93 The HMBC (CDCl_3 , 500 MHz) spectrum of UD3

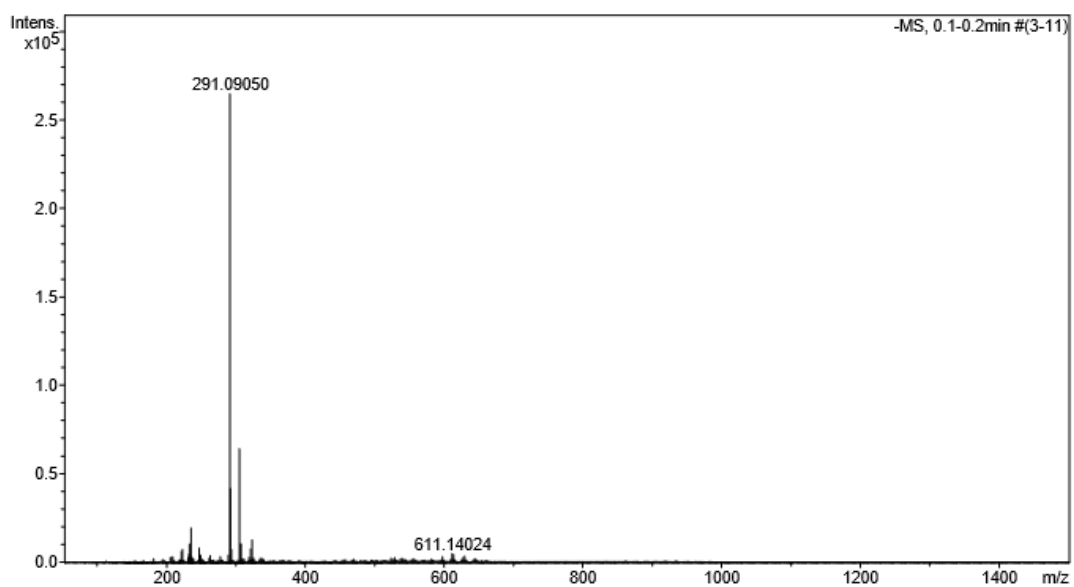


Figure A. 94 The HRESIMS spectrum of UD4



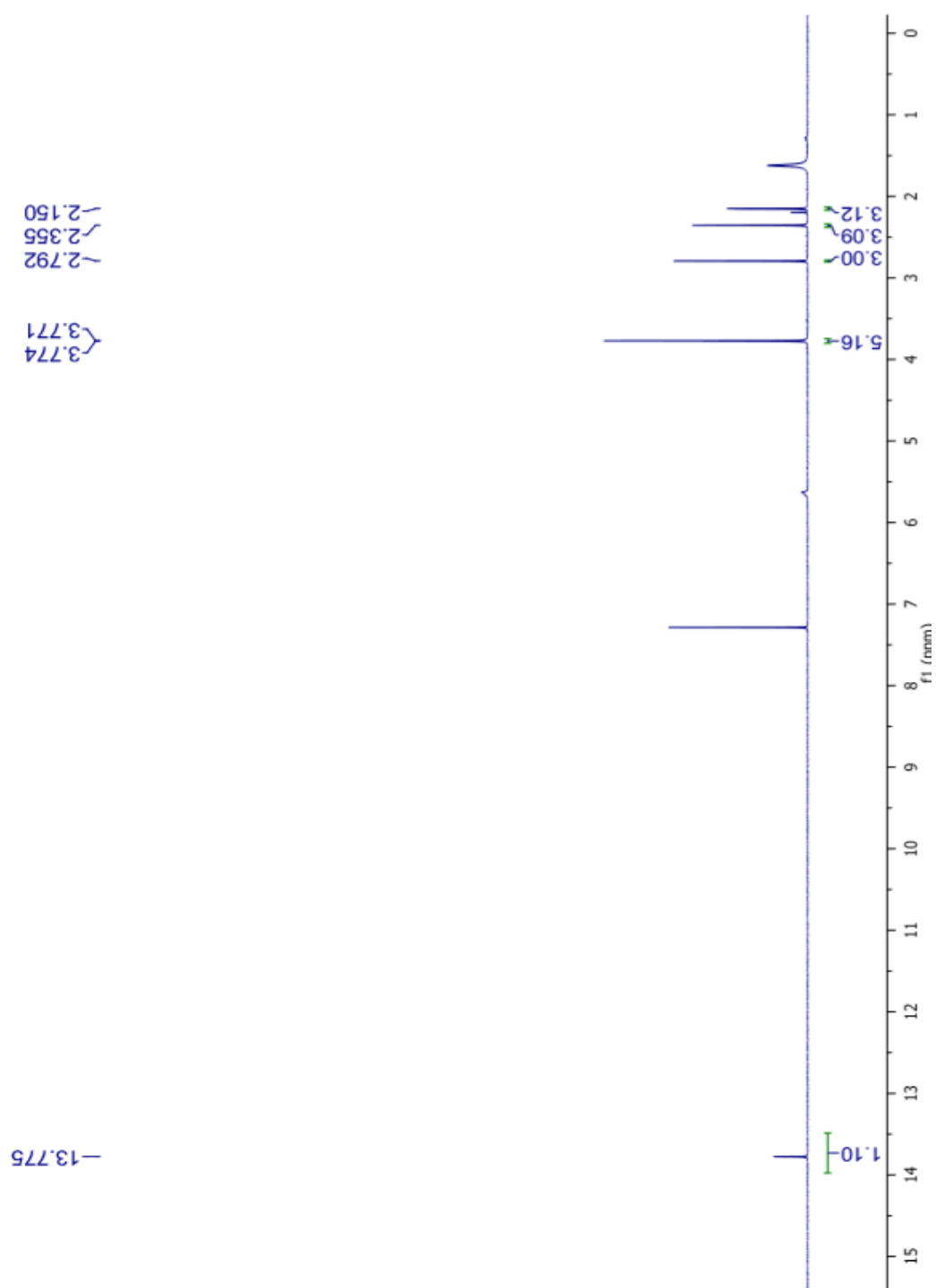


Figure A. 95 The ^1H NMR (CDCl_3 , 500 MHz) spectrum of UD4

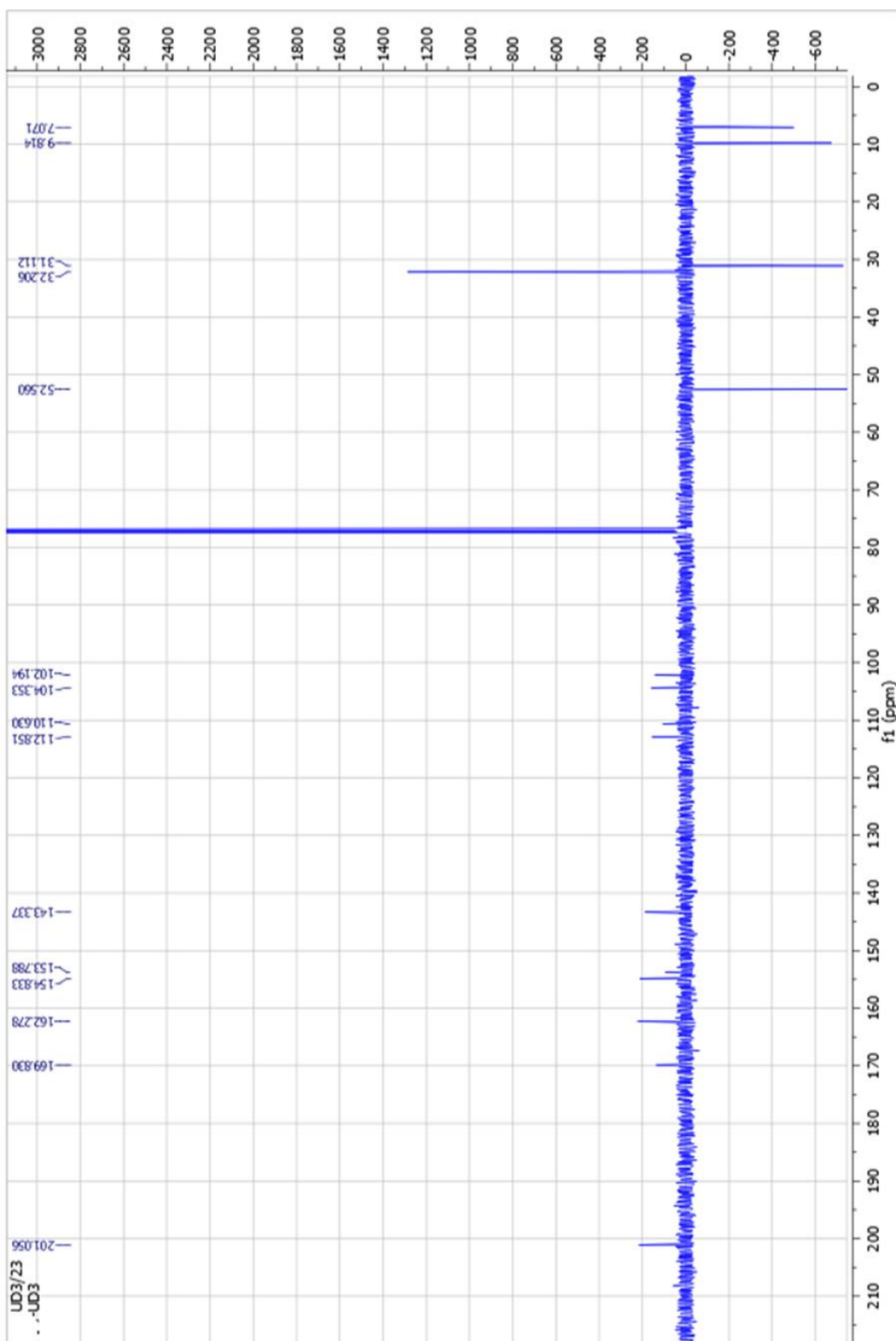


Figure A. 96 The ^{13}C NMR (CDCl_3 , 125 MHz) spectrum of UD4

Generic Display Report

Analysis Info	Acquisition Date	4/20/2018 10:28:34 AM	
Analysis Name	D:\Data\Data Service\180420_neg_UD5.d		
Method	NV_neg_0.3min_profile_1segment_lowNbulizerDrygas(2).m	Operator	CU.
Sample Name	180420_neg_UD5	Instrument	micrOTOF-Q II
Comment			

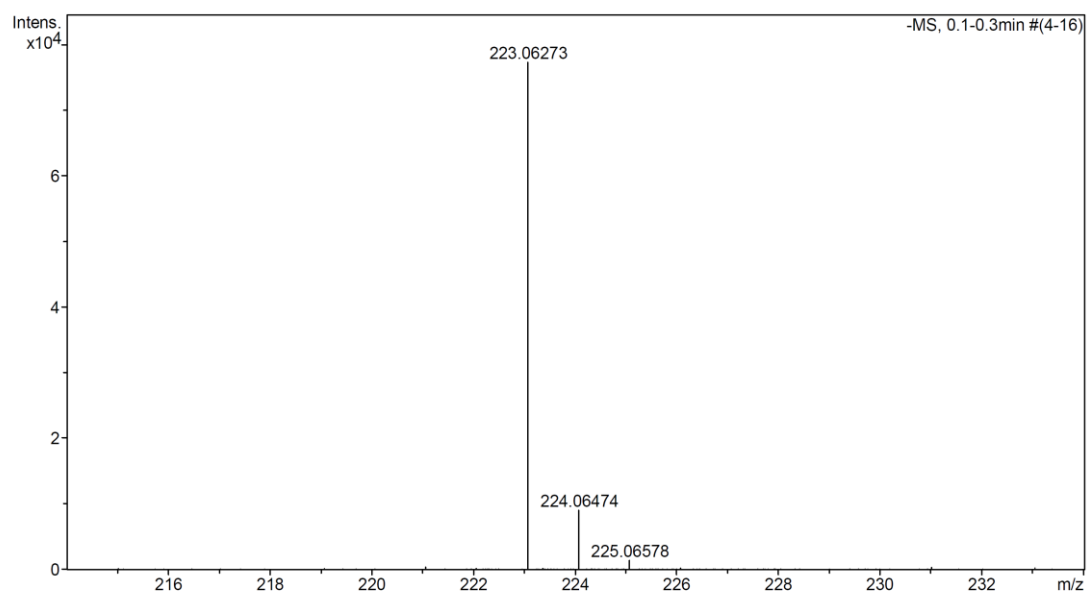
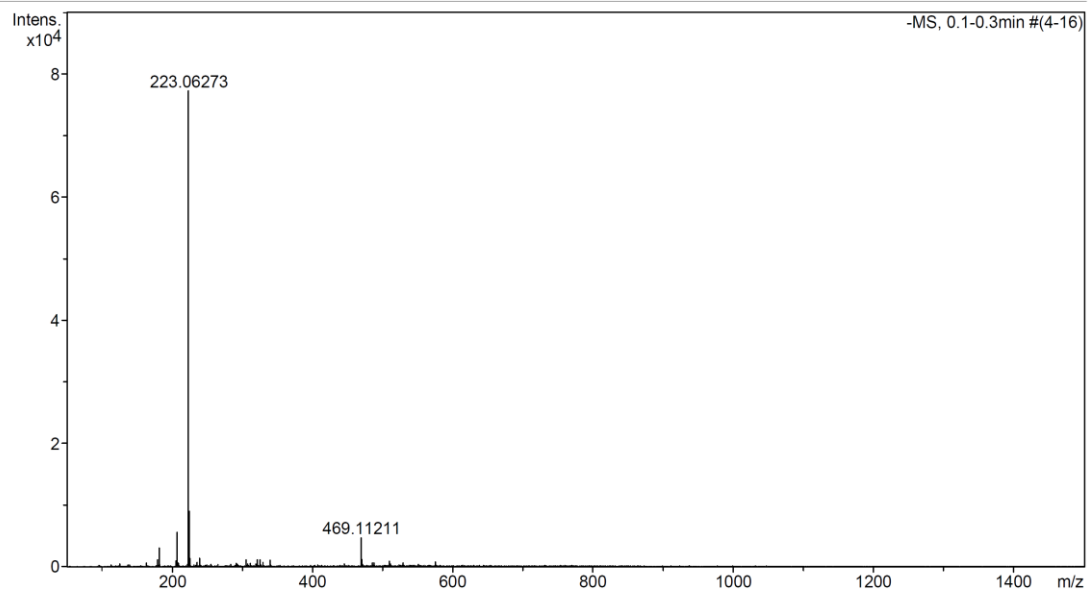


Figure A. 97 The HRESIMS spectrum of UD5

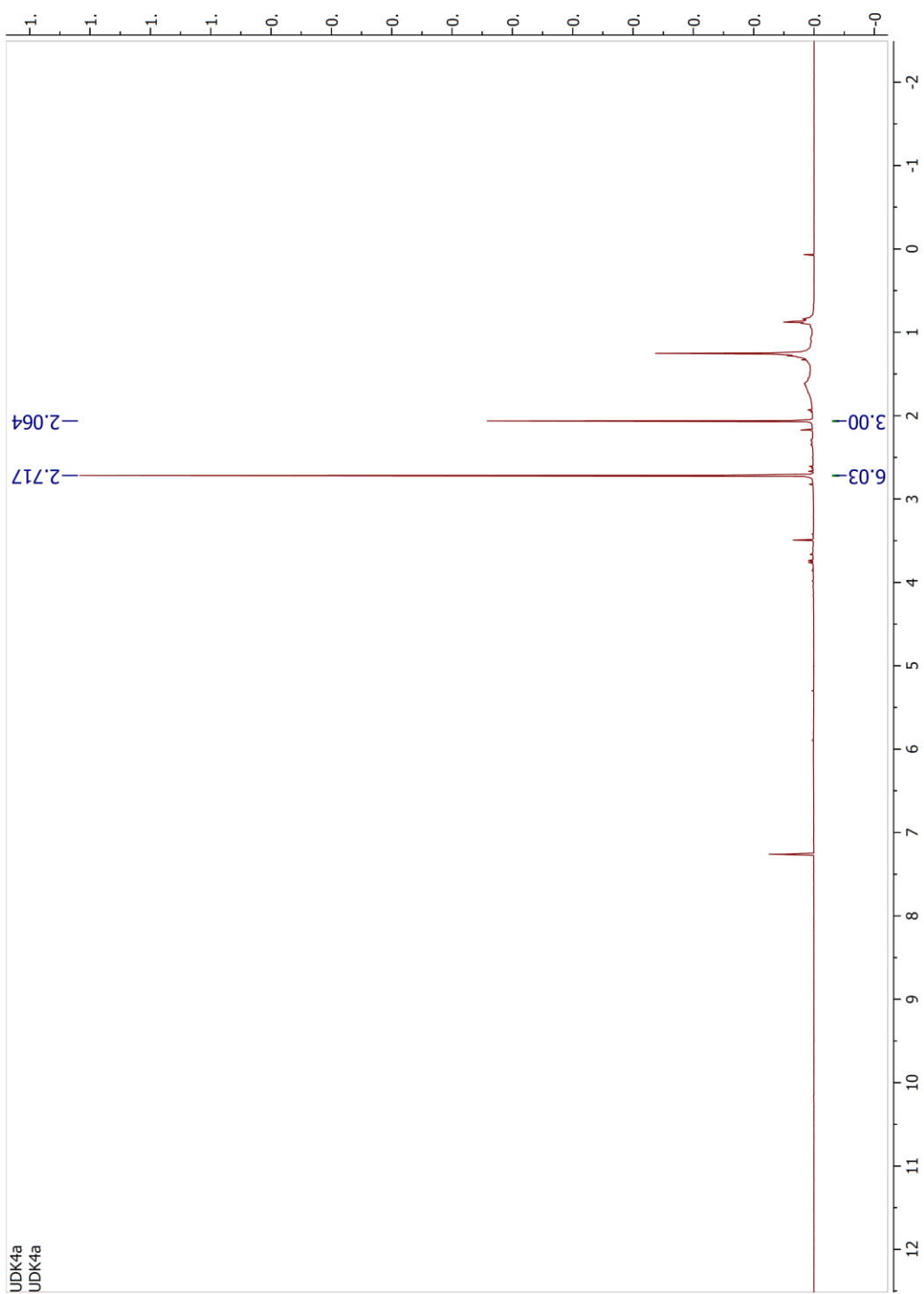


Figure A. 98 The ^1H NMR (CDCl_3 , 500 MHz) spectrum of UD5

Shimadzu Biotech Axima Resonance 2.9.1.ZU1001Z1: Mode positive, Low JU0+, Power: 110

%Int. 824 mV Profiles 1-52: Threshold Gradient

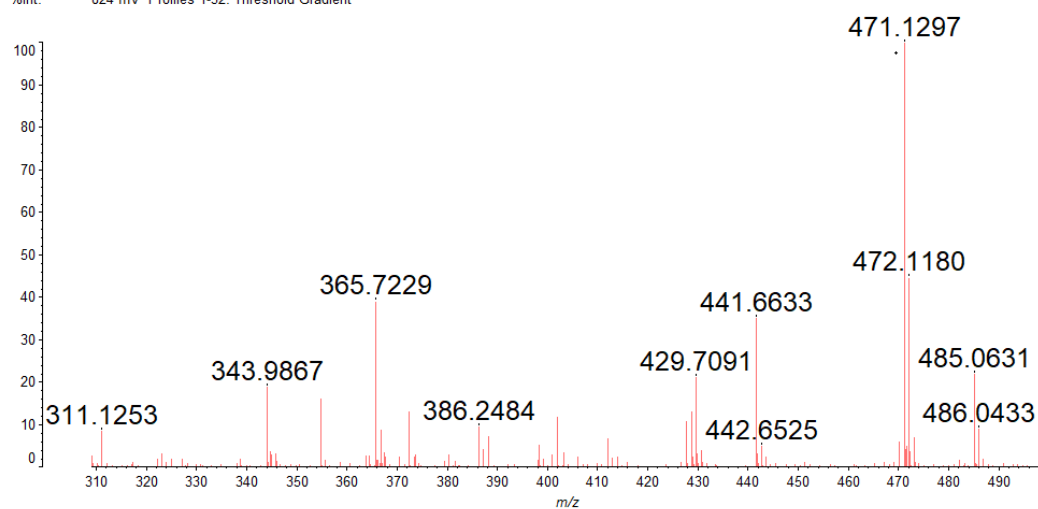
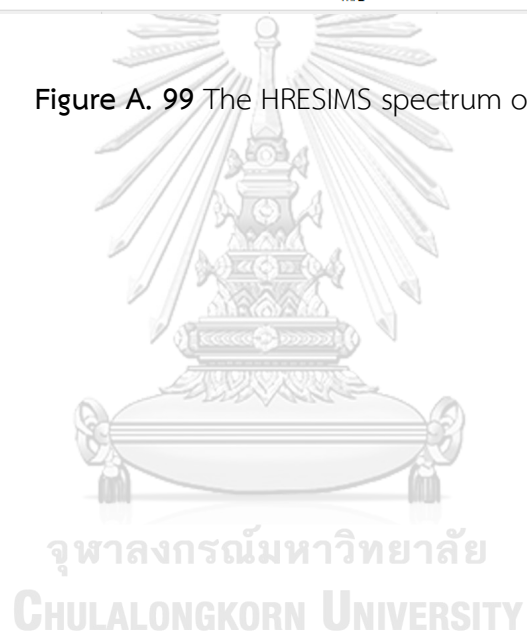


Figure A. 99 The HRESIMS spectrum of UE1



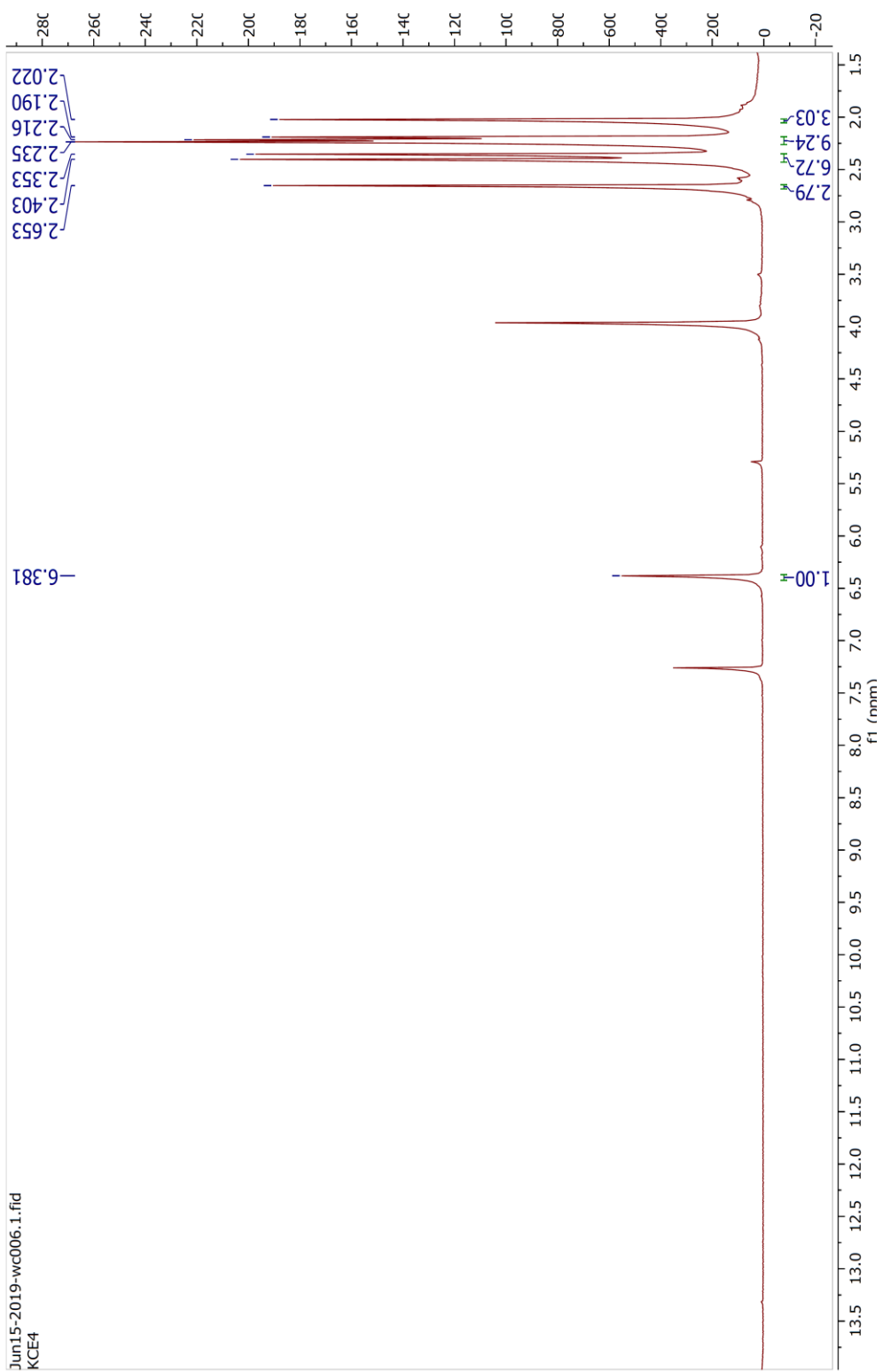


Figure A. 100 The ^1H NMR (CDCl_3 , 400 MHz) spectrum of UE1

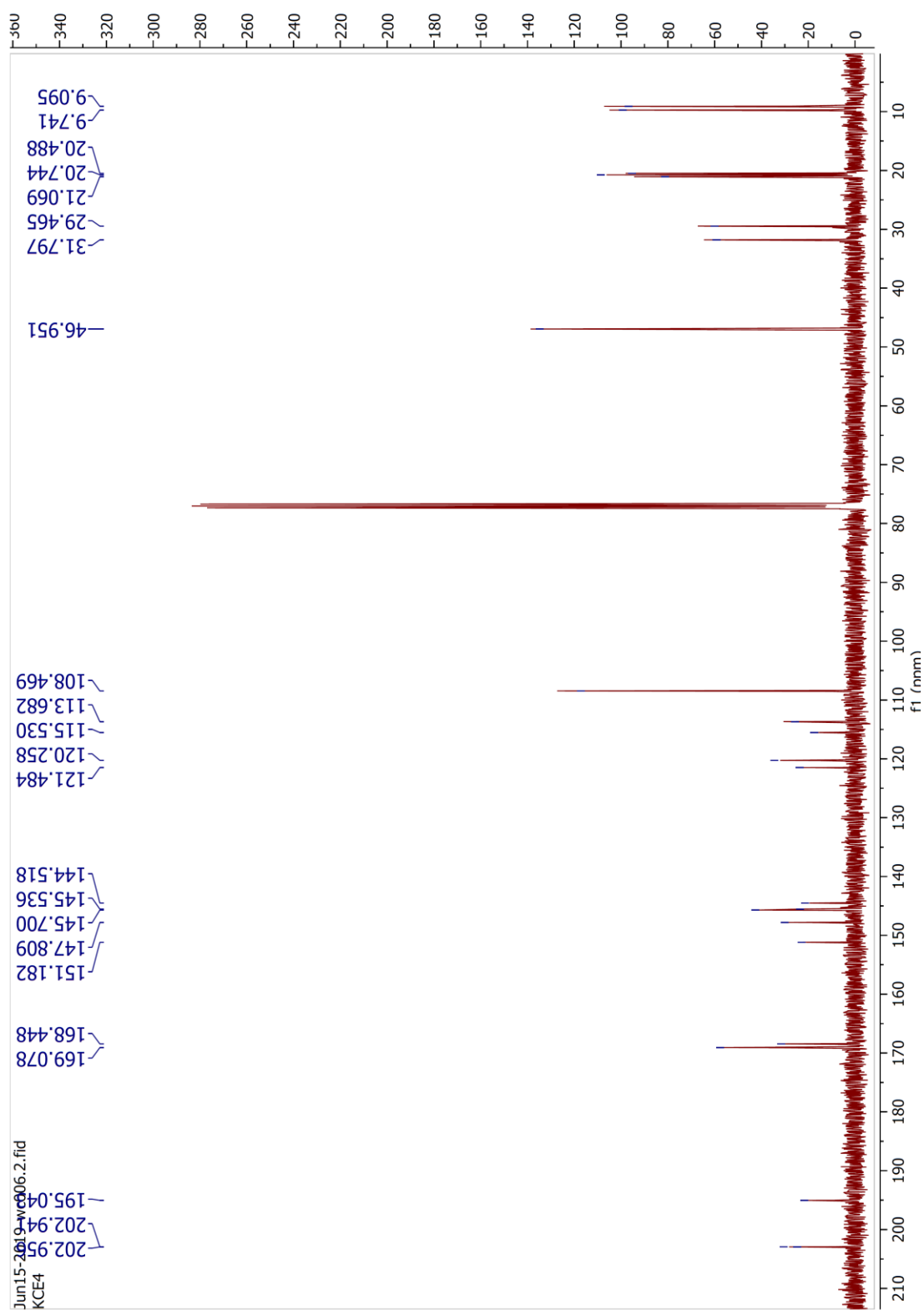


Figure A. 101 The ^{13}C NMR (CDCl_3 , 100 MHz) spectrum of UE1

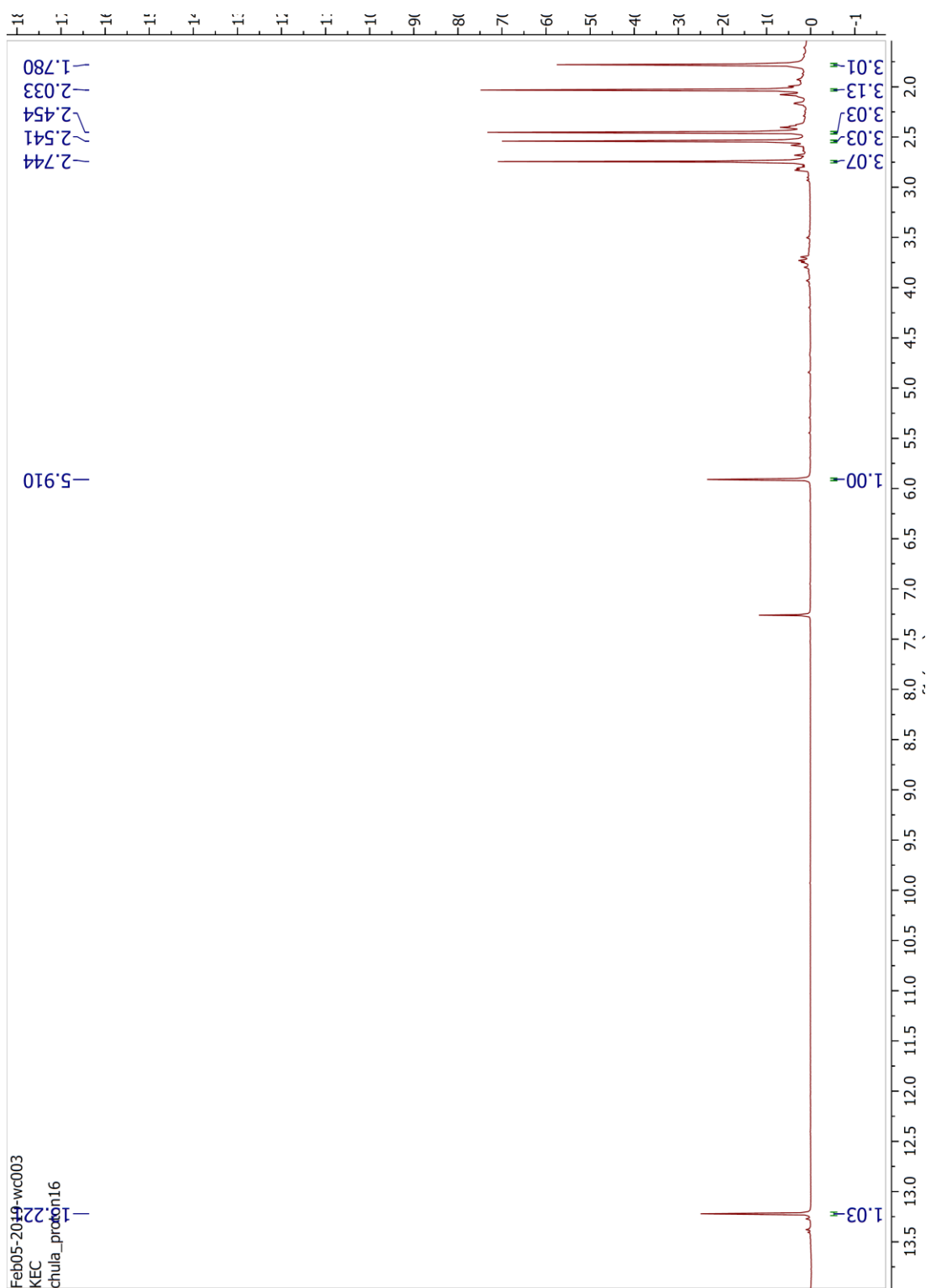


Figure A. 102 The ^1H NMR (CDCl_3 , 400 MHz) spectrum of UE2

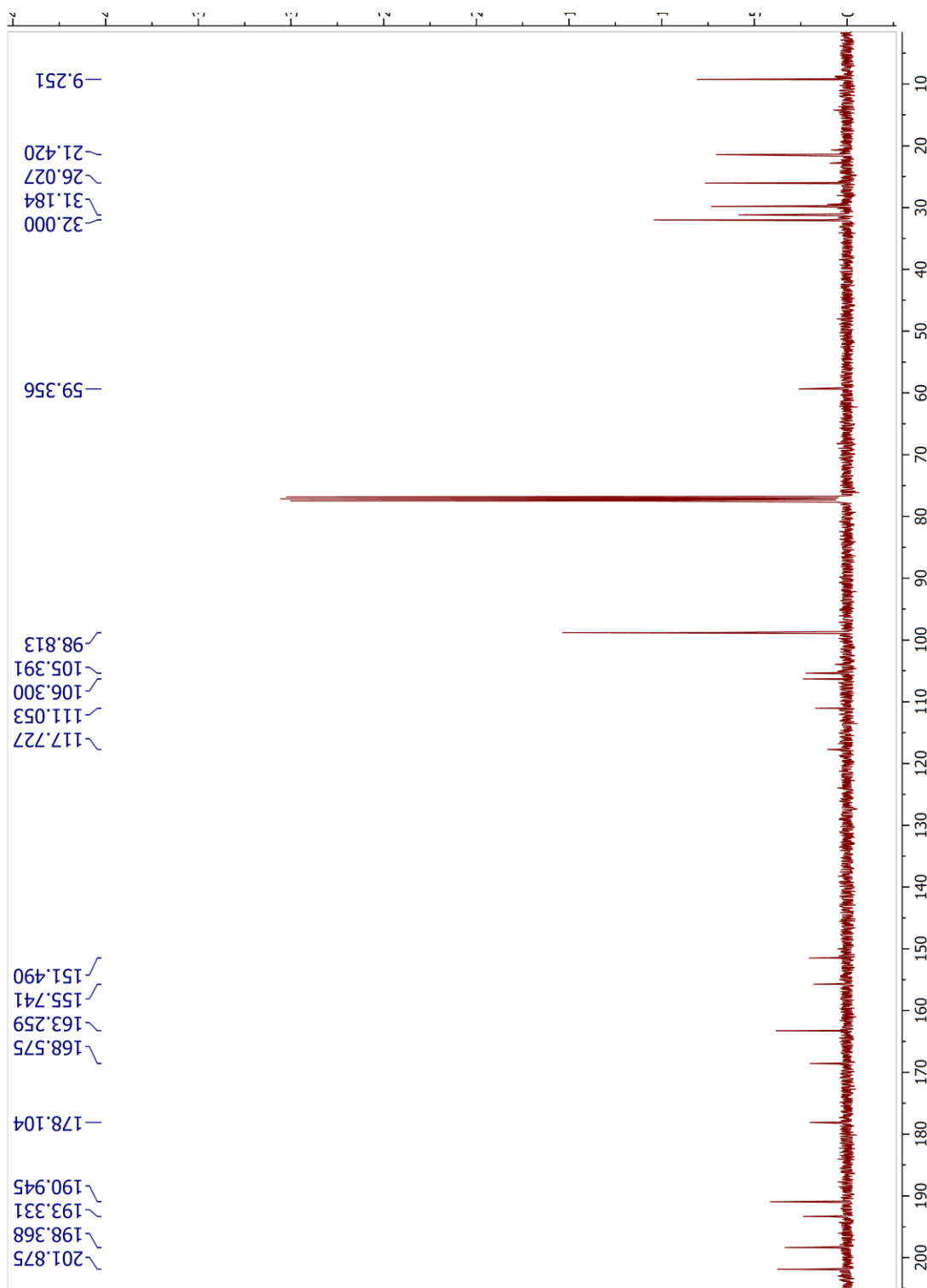


Figure A. 103 The ^{13}C NMR (CDCl_3 , 100 MHz) spectrum of UE2

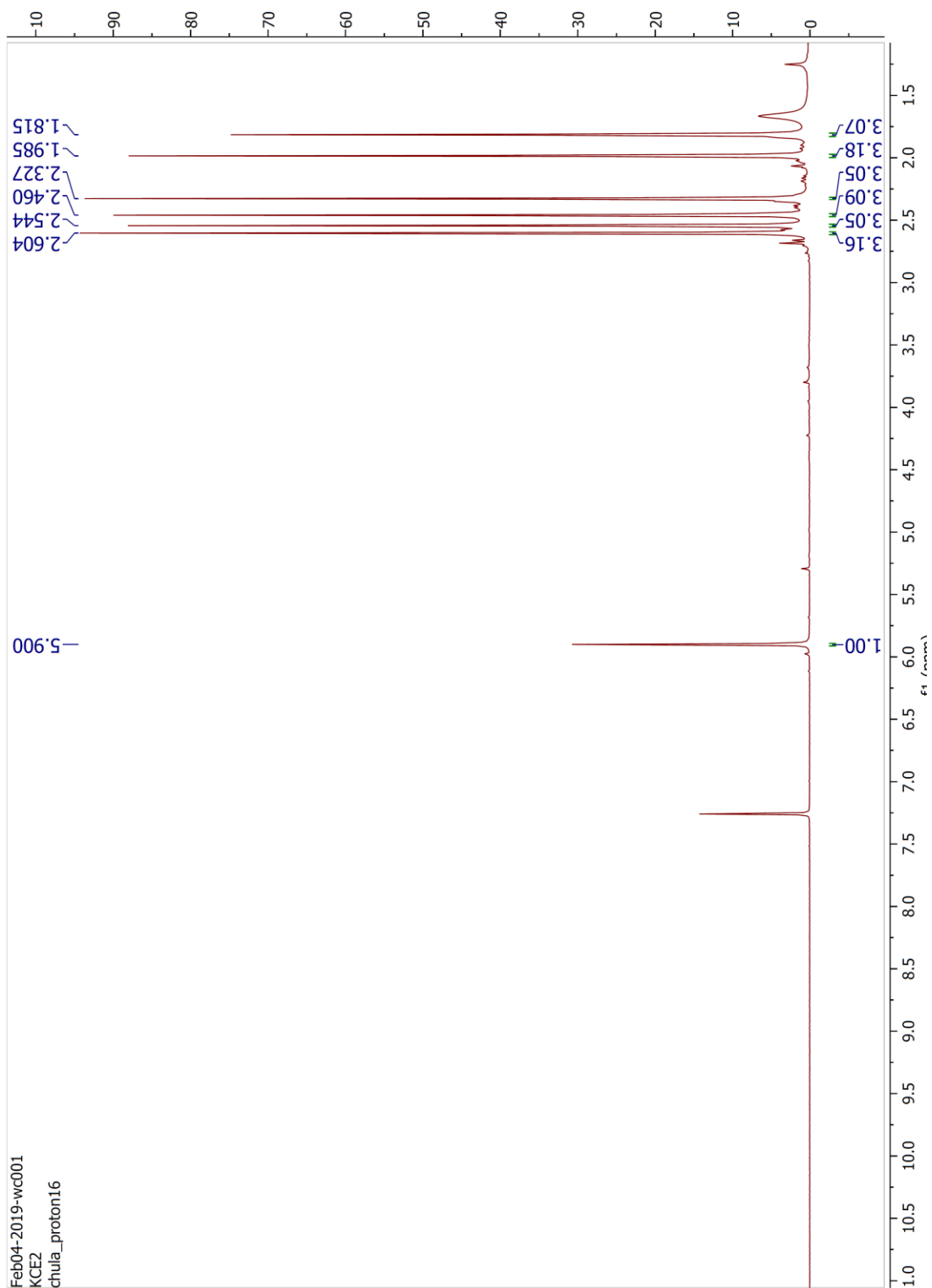


Figure A. 104 The ^1H NMR (CDCl_3 , 400 MHz) spectrum of UE3

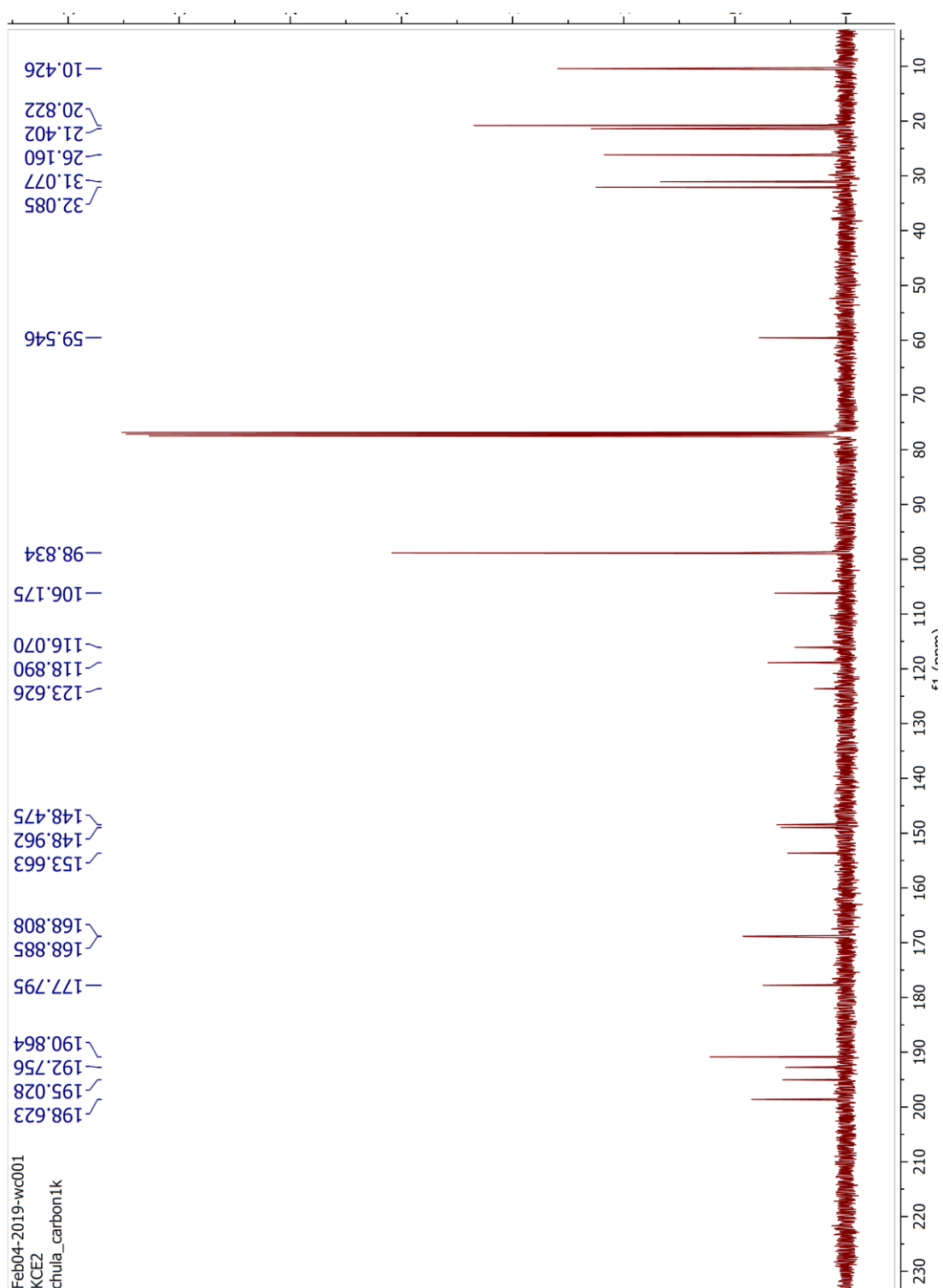


Figure A. 105 The ^{13}C NMR (CDCl_3 , 100 MHz) spectrum of UE3

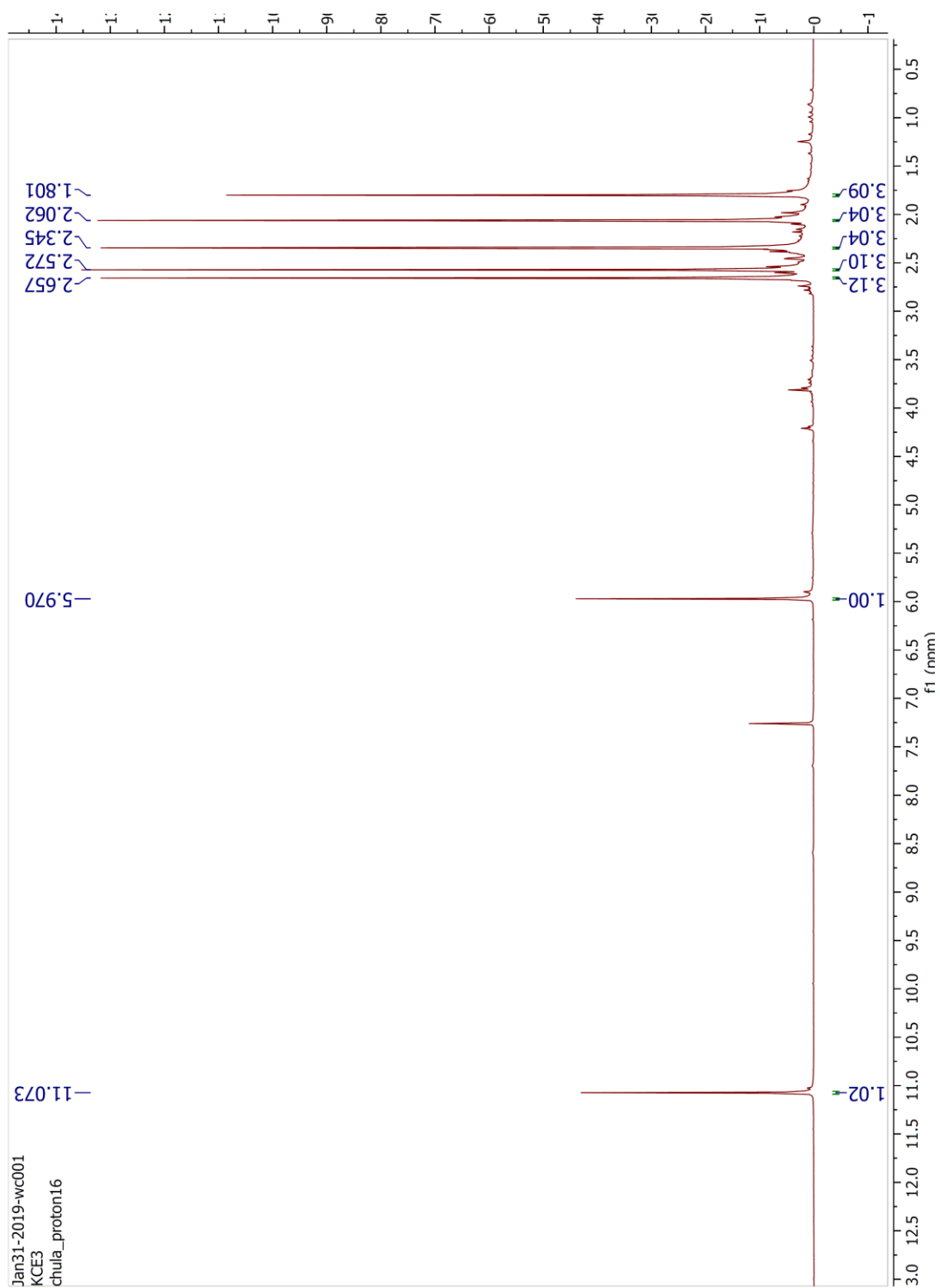


Figure A. 106 The ^1H NMR (CDCl_3 , 400 MHz) spectrum of UE4

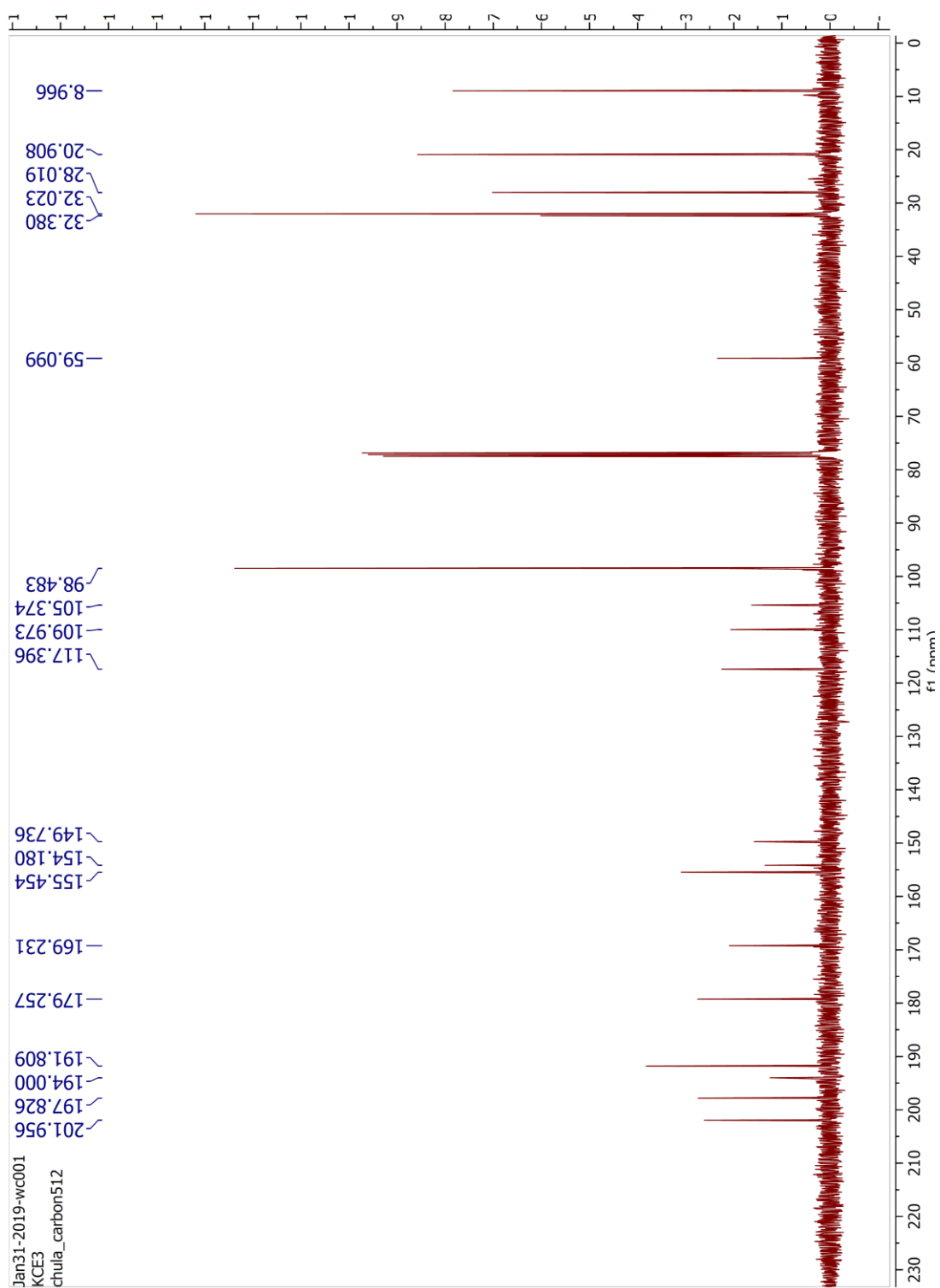


Figure A. 107 The ^{13}C NMR (CDCl_3 , 100 MHz) spectrum of UE4

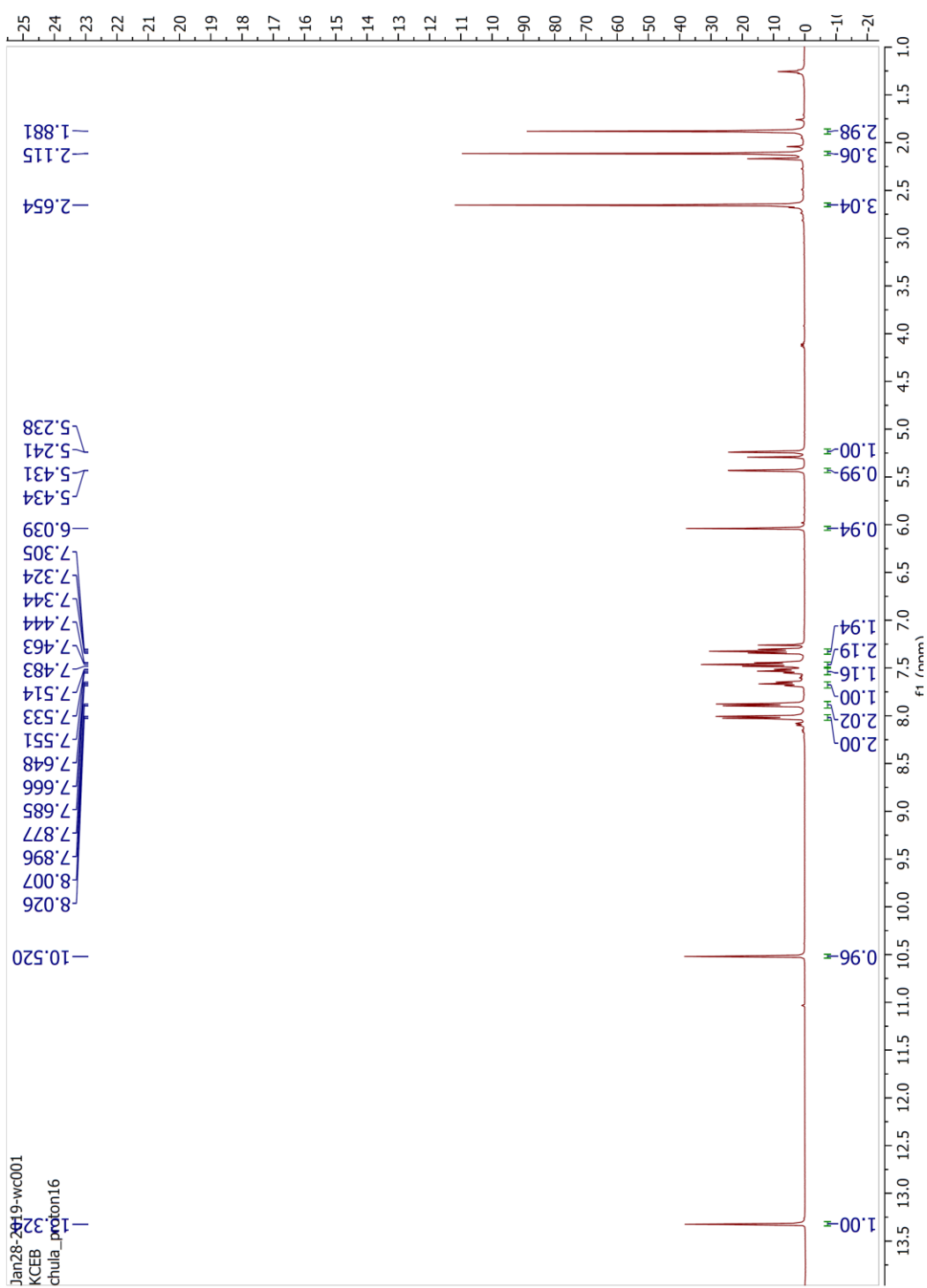


Figure A. 108 The ^1H NMR (CDCl_3 , 400 MHz) spectrum of UE5

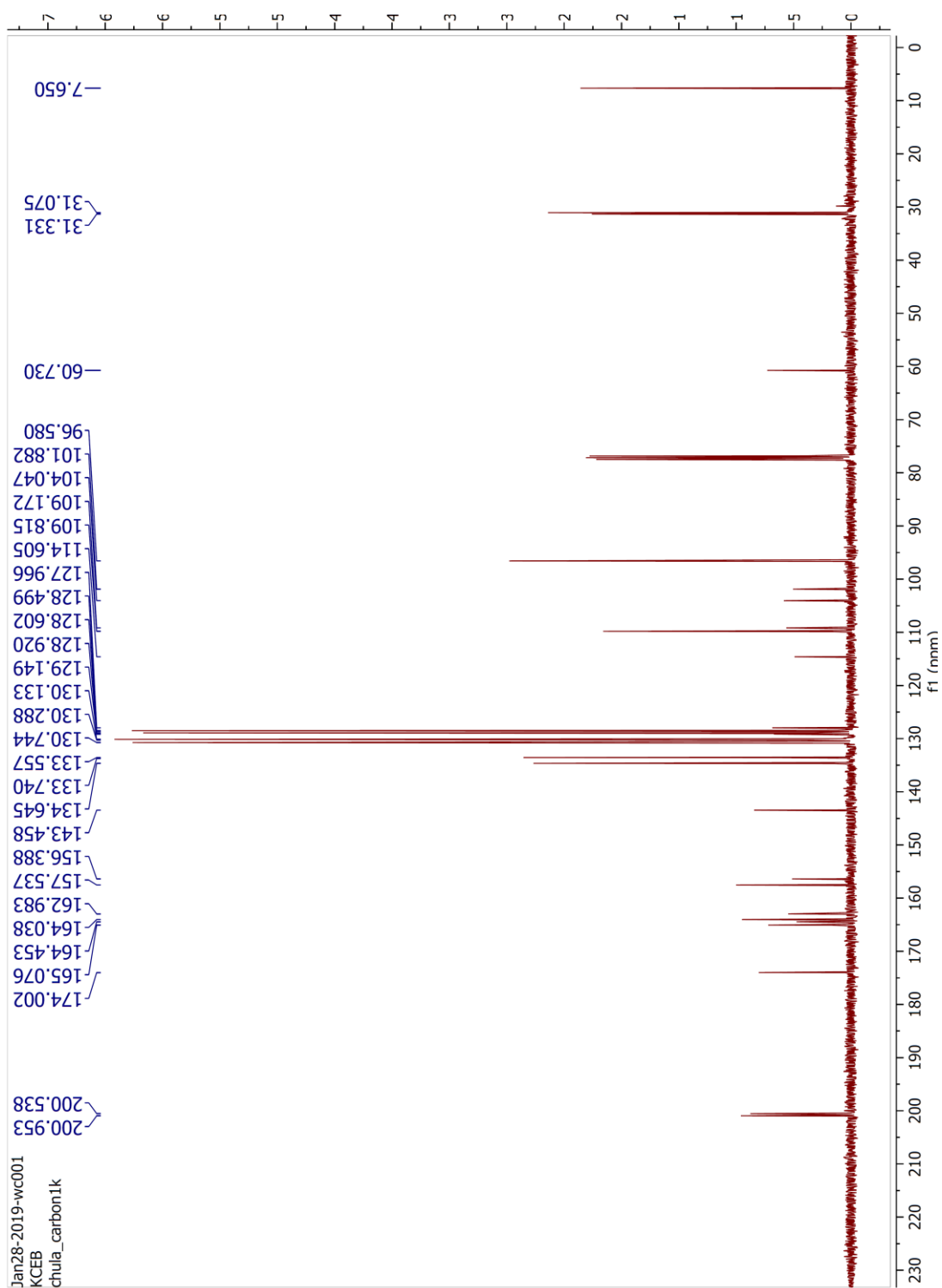


Figure A. 109 The ^{13}C NMR (CDCl_3 , 100 MHz) spectrum of UE5

Data: KECA2a_0001.P5[c] 22 Aug 2019 19:08 Cal: 23 Aug 2019 11:33
Shimadzu Biotech Axima Resonance 2.9.1.20100121: Mode positive, Low 300+, Power: 120

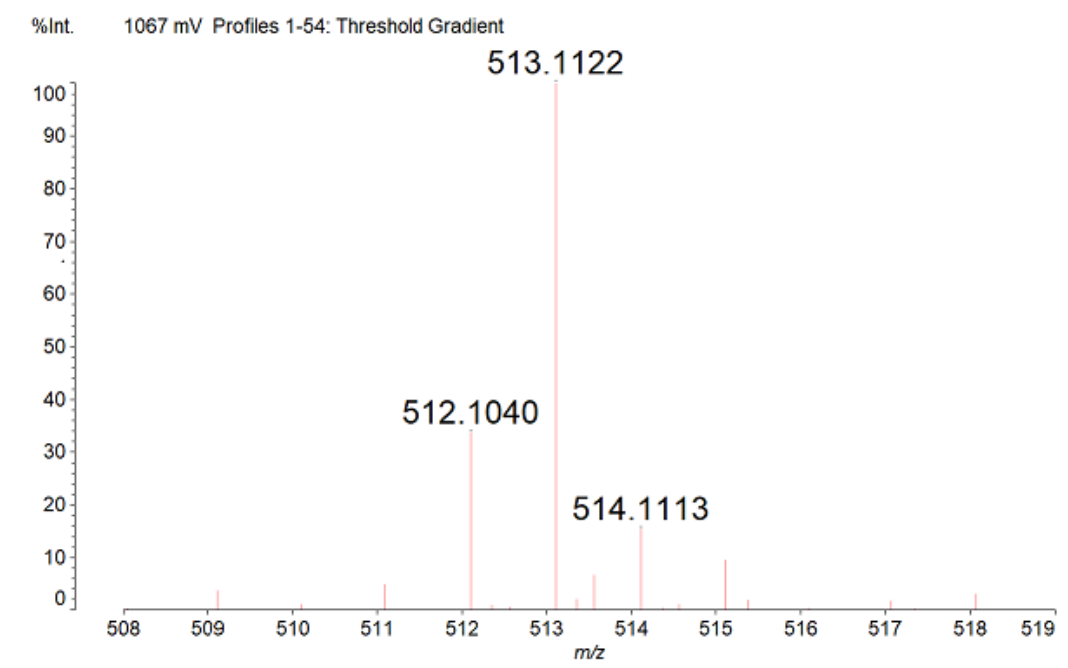
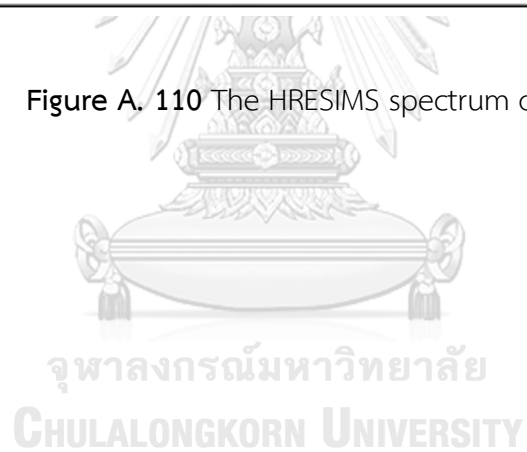


Figure A. 110 The HRESIMS spectrum of UE6



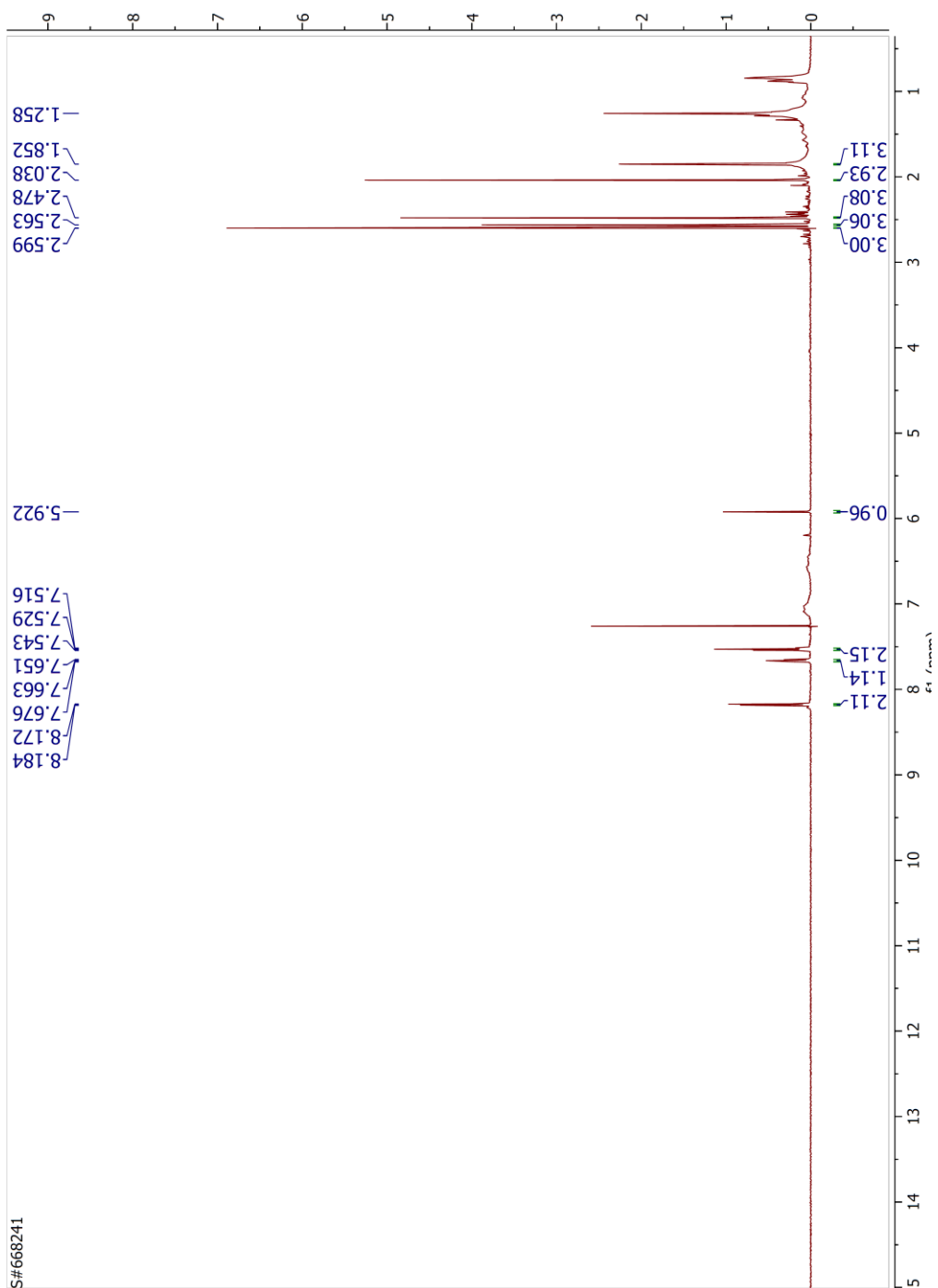


Figure A. 111 The ^1H NMR (CDCl_3 , 400 MHz) spectrum of UE6

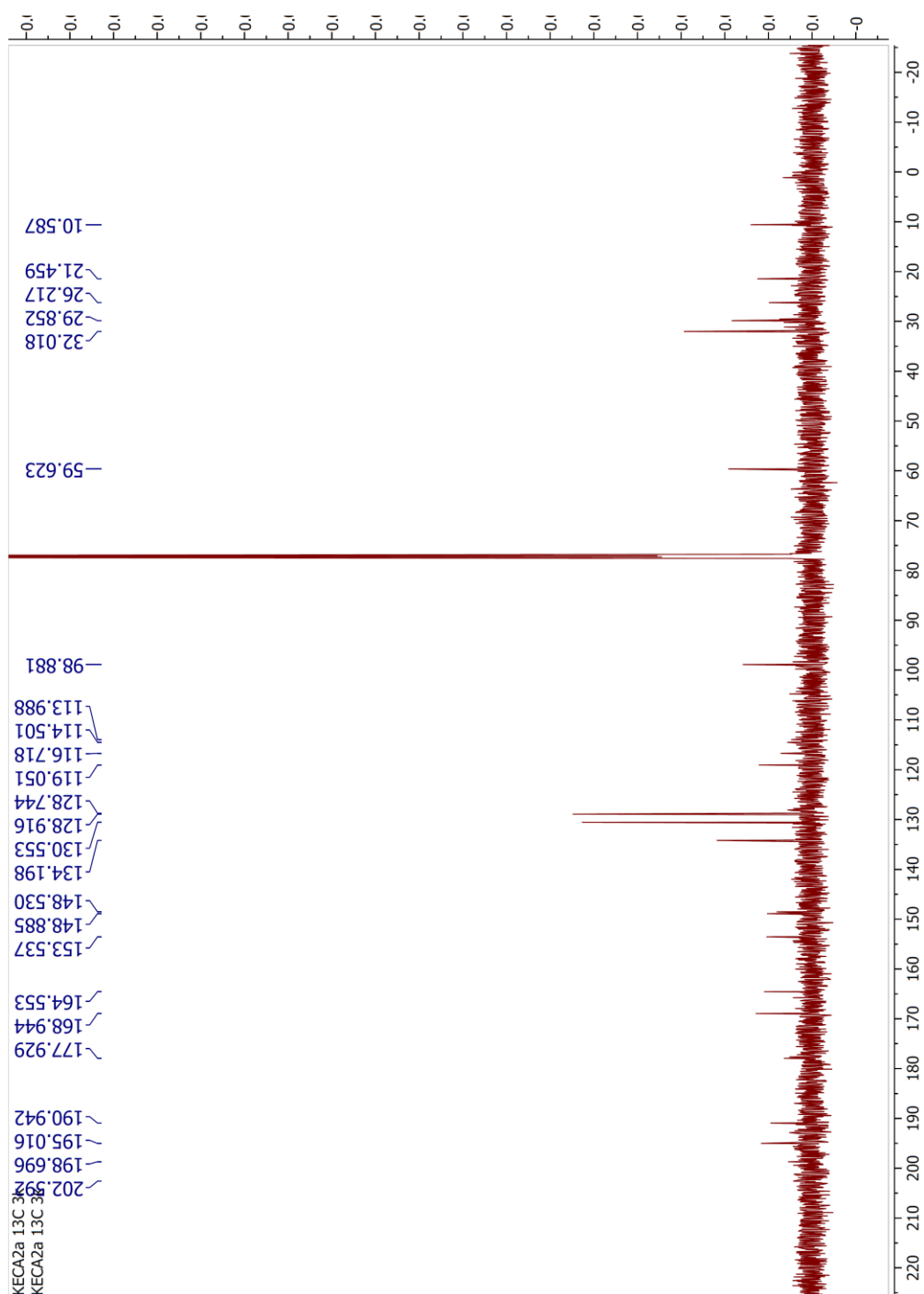


Figure A. 112 The ^{13}C NMR (CDCl_3 , 100 MHz) spectrum of UE6

VITA

NAME Kieu Van Nguyen

DATE OF BIRTH 10 October 1991

PLACE OF BIRTH Binh Dinh, Vietnam

INSTITUTIONS ATTENDED - Ho Chi Minh City University of Science, Vietnam
- Chulalongkorn University, Thailand
- Gifu University, Japan

HOME ADDRESS Tam Quan Bac, Hoai Nhon district, Binh Dinh province, Vietnam

PUBLICATION

1. Nguyen, V.K., Duong, T.H. Phenolic compounds from *Usnea baileyi* (Stirt.) Zahlbr growing in Lam Dong province. Vietnam Journal of Science, Technology and Engineering. 2019, 61, 12-15.
2. Nguyen, V.K., Sichaem, J., Nguyen, H.H., Nguyen, X.H., Huynh, T.T.L., Nguyen, T.P., Niamnontd, N., Mac, D.H., Pham, D.D., Chavasiri, W., Nguyen, K.P.P., Duong, T.H. Synthesis and cytotoxic evaluation of usnic acid benzylidene derivatives as potential anticancer agents. Nat Prod Res. 2019, 1-10.
3. Tran, T.N.M., Bernadat, G., Mai, D.T., Nguyen, V.K., Sichaem, J., Nguyen, T.P., Tran, C.L., Do, P.V., Tran, N.M.A., Nguyen, H.H., Beniddir, M.A., Duong, T.H., Le Pogam, P. Nervisides I–J: Unconventional Side-Chain-Bearing Cycloartane Glycosides from *Nervilia concolor*. Molecules. 2019, 24, 2599.
4. Tran, T.N., Sichaem, J., Nguyen, V.K., Chavasiri, W., Niamnontd, N., Jongaramruonge, J., Duong, T.H. A new ent-atisane diterpenoid from the aerial parts of *Euphorbia*

antiquorum L. Nat Prod Res. 2019, 1-6.

5. Nguyen, H.D., Nguyen, V.K., Pham, N.K.T., Sichaem, J., Duong, T.H. Lindermyrrhin, a novel 3,4-dihydroisocoumarin from *Lindera myrrha* roots. Nat Prod Res. 2019, 1-6.

6. Huynh, N.D., Le, H.T.T., Nguyen, T.M.D., Nguyen, V.K., Duong, T.H., Nguyen, T.A.T., Nguyen, K.P.P. Chemical constituents of *Ficus consociata* Blume (Moraceae). Vietnam Journal of Chemistry. 2019, 57, 202-207.

7. Nguyen, V.K., Duong, T.H., Nguyen, K.P.P., Sangvichien E., Wonganan, P., Chavasiri, W. Chemical constituents of the lichen *Usnea baileyi* (Stirt.) Zahlbr. Tet Lett. 2018, 59, 1348-1351.

8. Nguyen, V.K., Duong, T.H. Extraction, isolation and characterization of depsidones from *Usnea baileyi* (Stirt.) Zahlbr collected from tree barks in Tam Bo Mountain of Di Linh, Lam Dong Province, Viet Nam. Science and Technology Development Journal. 2018, 21, 24-31.

9. Duong, T.H., Beniddir, M.A., Nguyen, V.K., Aree, T., Gallard, J.F., Mac, D.H., Nguyen, H.H., Bui, X.H., Boustie, J., Nguyen, K.P.P., Chavasiri, W., Le Pogam, P. Sulfonic Acid-Containing Flavonoids from the Roots of *Phyllanthus acidus*. J. Nat. Prod. 2018, 81, 2026-2031.

10. Duong, T.H., Huynh, B.L.C., Chavasiri, W., Chollet-Krugler, M., Nguyen, V.K., Nguyen, T.H.T, Hansen, P.E., Le Pogam, P., Thüs, H., Boustie, J., Nguyen, K.P.P. New erythritol derivatives from the fertile form of *Roccella montagnei*. Phytochemistry. 2017, 137, 156-164.

AWARD RECEIVED

- H.M. the King Bhumibhol Adulyadej's 72nd Birthday Anniversary Scholarship

- THE 90th Anniversary of Chulalongkorn University

Scholarship

- Overseas Research Experience Scholarship for Graduate Student

- The 100th Anniversary Chulalongkorn University for Doctoral Scholarship

